Durham E-Theses

Analysis of Low Pressure Steam Turbine Diffuser and Exhaust Hood Systems

BURTON, ZOE

How to cite:

Use policy

School of Engineering
and Computing Sciences

Analysis of Low Pressure Steam Turbine Diffuser and Exhaust Hood Systems

by

Zoe Burton

Submitted to Durham University
as part of the degree of
Doctor of Philosophy

Supervisor: Dr Grant Ingram & Dr Simon Hogg

School of Engineering and Computing Sciences
March 2014

Abstract

This thesis concerns the computational modelling of low pressure (LP) steam turbine exhaust hood flows. A test case for LP last stage blades (LSBs) with a full aerodynamic definition and an accompanying exhaust hood was developed which is representative of current industrial practice. The test case geometry is freely available allowing other researchers to build on this work and is the first of its kind. Studies on this Durham Stage and Exhaust Hood Test Case showed the geometry produces a representative flow pattern and performance metrics comparable to other published research. Using the test case, the effect of condenser cooling water pressure gradient on the hood flow was computed for the first time. A generic boundary condition was developed to represent the transverse condenser cooling water flow and, when applied to the test case, was shown to have a larger influence on the flow asymmetry within the hood than the tip leakage jet. This thesis describes the first application of the non-linear harmonic (NLH) method to couple the LSBs to the exhaust hood. This method enabled the circumferential non-uniformity which develops in the exhaust hood to be transferred across the interface to the stage, in half the computational demand of the full annulus frozen rotor approach. The first review of the influence of inlet circumferential asymmetry on the hood flow field highlighted that modelling its effect is not as crucial as indicated in the literature, unless the diffuser axial length is very compact or if off-design flows are to be studied. A series of recommendations and guidelines for the CFD modelling of steam turbine exhaust hood flows based on this work are supplied. Experimental validation of the Durham Stage and Exhaust Hood Test Case and a comparison of full unsteady studies with the NLH method should be the next steps in this research.

Declaration

This thesis is based on the work carried out by Zoe Burton, under the supervision of Dr. Grant Ingram and Prof. Simon Hogg as a part of the Energy Group, School of Engineering and Computing Sciences, Durham University. No part of this report has been submitted elsewhere for any other degree or qualification and all research included in this thesis is the author's own work unless referenced otherwise.

Acknowledgements

Publications

Aspects of the work included in this thesis have been been published in the following journals or presented at a conference and included in the associated conference proceedings:

Journal Papers:

- Burton, Z., G. L. Ingram, et al. (2013). "A Literature Review of Low Pressure Steam Turbine Exhaust Hood and Diffuser Studies." Journal of Engineering for Gas Turbines and Power 135(6): 1-10.

- Burton, Z., G. L. Ingram, et al. (2013). "Influence of Inlet Asymmetry on Steam Turbine Exhaust Hood Flows." Journal of Engineering for Gas Turbines and Power 136(4): 1-11.

- Burton, Z., G. L. Ingram, et al. (2013). "The Influence of Condenser Pressure Variation and Tip Leakage on LP Steam Turbine Exhaust Hood Flows." Proceedings of the Institution of Mechanical Engineers, Part A Journal of Power and Energy *(accepted for publication)*

Conference Proceedings:

- Burton, Z., G. L. Ingram, et al. (2012). A Generic Low Pressure Exhaust Diffuser for Steam Turbine Research. ASME Turbo Expo, Copenhagen, Denmark, GT2012-68485.

- Burton, Z., G. L. Ingram, et al. (2013). A Generic Steam Turbine Exhaust Diffuser with Tip Leakage Modelling and Non-Uniform Hood Outlet. 11th European Turbomachinery Conference, Lappeenranta, Finland, ETC10-P38.

- Burton, Z., G. L. Ingram, et al. (2013). A Novel Method of Coupling the Steam Turbine Exhaust Hood and the Last Stage Blades Using the Non-Linear Harmonic Method. ASME Turbo Expo, San Antonio, Texas, GT2013-94184.

Nomenclature

English	
Symbol	Definition
a	Diffuser Kink Angle [°]
A_{inlet}	Diffuser/Hood Inlet Area [m^2]
$A_{diffout}$	Diffuser Outlet Area [m^2]
A_{HJ}	Exhaust Half Joint Plane Area [m^2]
A_{hood}	Upper Exhaust Hood Area [m^2]
C_p	Static Pressure Recovery Coefficient [-]
C_P	Heat Capacity at Constant Pressure [$Jkg^{-1}K^{-1}$]
d	Diffuser/Exhaust Hood Inlet Height [mm]
d_1	Diffuser Outlet Axial Length [mm]
d^*	Displacement Thickness [mm]
D	Axial Distance between Hood Back Wall and the Flow Guide Tip [mm]
H	Shape Factor [-]
L	Diffuser/Hood Inlet to Back Wall Distance [mm]
M	Number of Perturbations [-]
m	Number of Multi-Grid Levels [-]
N	Number of Frequencies per Perturbation [-]
n	Number of Blades per Row [-]
P	Static Pressure [bar]
P_t	Total/Stagnation Pressure [bar]
$\vec{r}$	Position Vector [-]
U	Conservative Flow Variable [-]
$\vec{U}$	Frame Velocity [m·s^{-1}]
$\vec{V}$	Absolute Velocity [m·s^{-1}]
V_r	Radial Velocity [m·s^{-1}]
V_t	Tangential Velocity [m·s^{-1}]
V_x	Axial Velocity Velocity [m·s^{-1}]
V_z	Velocity Perpendicular to X-Y Plane from Liu et al. (2003) [m·s^{-1}]
$\vec{W}$	Relative Velocity [m·s^{-1}]

x	Back Wall Position Relative to Flow Guide Tip [mm]
y	Rotor Axial Chord Length [mm]
z	Stator Axial Chord Length [mm]

Greek	
Symbol	Definition
α	Swirl Angle [°]
γ	Ratio of Specific Heats [-]
Δ	Difference Between Values [Pa/°]
η	Stage Efficiency [-]
Ω	Angular Velocity [m·s^{-1}]
θ	Momentum Thickness [mm]
Θ	Cell Count in Theta Direction [-]

Subscripts	
Subscript	Definition
d	Downstream
k	Periodic Fluctuation Index
$T-S$	Total to Static
t	Time Index
u	Upstream
1	Hood Inlet/Rotor Outlet
2	Hood Outlet/Condenser Inlet

Superscripts	
Subscript	Definition
⁻	Time Mean
′	Periodic Perturbation
~	Complex Harmonic Amplitude

Abbreviation	
Abbreviation	Definition
BPF	Blade Passing Frequency
BSDA	Back Surface Deflection Angle
CFD	Computational Fluid Dynamics
CFL	Courant Freidrichs Levy
DOE	Design of Experiments
DSEHTC	Durham Stage and Exhaust Hood Test Case
DSTC	Durham Stage Test Case
DEDHTC	Durham Exhaust Diffuser and Hood Test Case
EDS	Exhaust Design System
FFT	Fast Fourier Transform

HP	High Pressure
IP	Intellectual Property
LP	Low Pressure
LSB	Last Stage Blade
LSBs	Last Stage Blades
MFR	Mass Flow Rate
MFRM	Multiple Frame of Reference Model
NLH	Non-Linear Harmonic
OEM	Original Equipment Manufacturer
RANS	Reynolds Average Navier Stokes

Contents

List of Figures

List of Tables

1

Introduction

1.1 Background

Steam turbines generate 60% of the global supply of electricity [58] in fossil fuel and nuclear power plants in both developing and developed countries. With rising energy demand it is anticipated that this will increase by a factor of 1.7 by 2035 [58]. Meeting this demand whilst mitigating its environmental impact requires more efficient steam turbines.

Figure 1.1 shows an example of a steam turbine power plant. This thesis focuses on the exhaust hood of a steam turbine, which guides flow exiting the low pressure (LP) turbine last stage blades (LSBs) to the condenser. A cross section of the LP cylinder is also given in Figure 1.1 and indicates the trajectory of the flow passing through the last stages of the LP turbine, exiting the LSBs and, guided by the exhaust hood casing, discharges down to the condenser below. The example given is a LP cylinder of *double-flow* configuration, which is symmetrical about section A-A. It is therefore typical to only consider half the LP cylinder, as highlighted in grey in the cross-sectional view. This region can be mapped onto the detailed exhaust hood diagram in Figure 1.2. Throughout this thesis, when referring to the steam turbine exhaust hood, this applies to only half the LP cylinder, as included in Figure 1.2.

Of the exhaust hood system shown in Figure 1.2, the upper exhaust hood has been enlarged in Figure 1.3 to highlight the primary features. The exhaust hood can be subdivided into two main elements: the diffuser and the collector/outer casing. The exhaust diffuser comprises of the flow guide and bearing cone; the purpose of which is to decelerate the flow exiting the last stage steam turbine blades which, given the fixed condenser pressure, generates a lower static pressure at turbine exit and a subsequently higher power output. The flow exiting the diffuser is guided by the collector and exhaust hood outer casing to the condenser.

Large scale steam turbines up to around 1400MW, typically adopt an axial-radial (also known as down-flow) configuration of exhaust diffuser [58], as shown in Figures 1.2 and 1.3, where the condenser is situated beneath the turbine. This is advantageous as it reduces the axial length of the diffuser, one of the primary restrictions in exhaust hood design. As high capacity steam turbines can be 30-40m in length with four low pressure cylinders; the large amount of space required by the diffuser increases the cost, weight and size of the plant [57]. However, this down-flow configuration leads to very compact diffusers, with the axial length only twice that (or less) of the blade height [64]. The short distance over which the axial
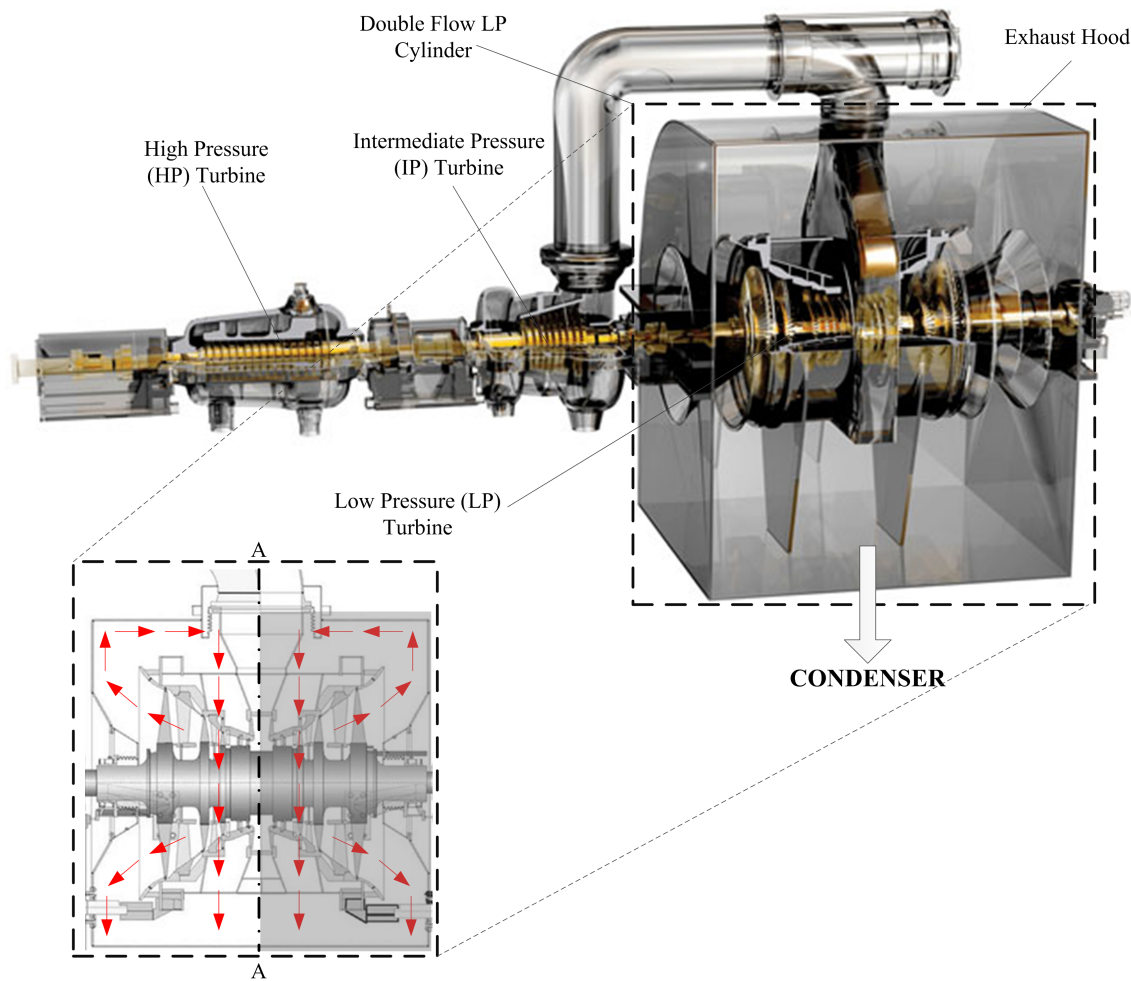
Figure 1.1: Steam Turbine Power Plant [22]

to radial turning takes places generates a highly rotational flow structure within the diffuser and exhaust hood outer casing. The vortices which form cause aerodynamic blockages which are detrimental to diffuser performance.

The amount by which the static pressure at exit from the last stage of a LP steam turbine differs from the condenser pressure is a function of the static pressure recovery in the diffuser (C_p, given in equation 1.1) and the losses in the exhaust hood. Under ideal conditions, all of the kinetic energy in the flow leaving the LSBs would be recovered as an increase in static pressure through the diffuser and all exhaust hood losses would be negligible. These conditions correspond to an exhaust hood static pressure recovery coefficient of unity ($C_p = 1$), resulting in the minimum static pressure at exit from the last stage (plane 1 in Figure 1.3 and 1.2) and therefore maximum turbine power output. In reality, only part of the kinetic energy in the flow leaving the last stage is recovered in the diffuser and there will be some losses in the exhaust hood. A positive pressure recovery in the diffuser, such as the case shown in red in Figure 1.4, will give a higher turbine power output as P_1 is lower as there is a greater pressure (enthalpy) drop across the turbine [2]. C_p values for real LP exhausts are less than unity and often negative in value, such as the case shown in blue in Figure 1.4, e.g.
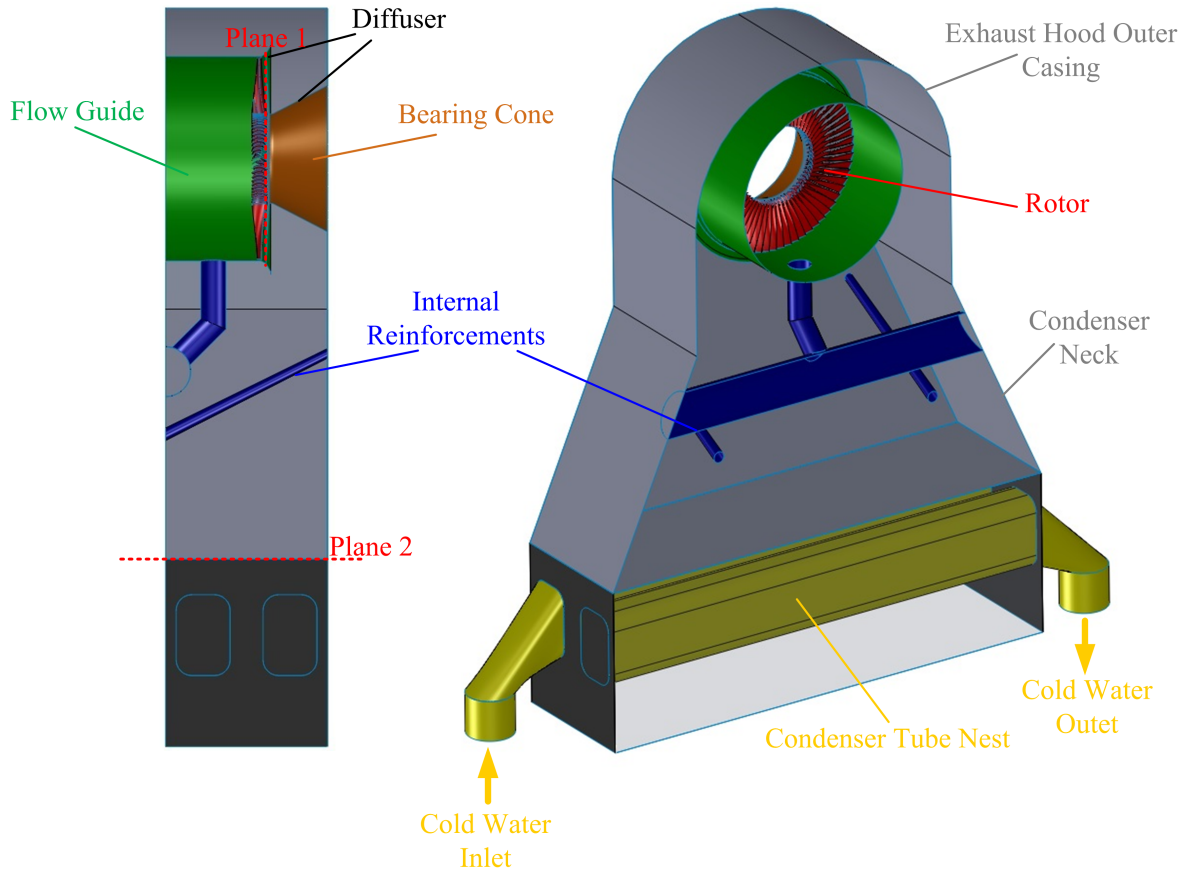
Figure 1.2: Diagram of the Steam Turbine Exhaust Diffuser and Hood

[35] where C_p = -0.25. In a comparatively small scale turbine of 30MW, the leaving energy can be as much as 750MW at nominal load [64] and recovering only a third of this kinetic energy can lead to a 2.5% increase in LP turbine power.

$$C_p = \frac{P_2 - P_1}{P_{01} - P_1} = \frac{P_2 - P_1}{P_{dyn_1}} \tag{1.1}$$

Over the last two decades, both academic and industrial research in the steam turbine exhaust hood field has increased due to the high potential performance gains in the LSBs of the low pressure turbine and the accompanying exhaust diffuser and hood. Figure 1.5 summarises the relative fractions of loss attributed to the main components of the power plant, from Tanuma et al. [59].

In the 1950's and 60's turbine blades were designed using simple radial equilibrium theory resulting in an aerodynamically inefficient design for both LSBs and exhaust hood [1]. Although retrofitting (installing modern blading into an existing exhaust hood casing) can substantially improve the efficiency of the last stage turbine, the exhaust hood is typically not optimised for the retrofitted blades and subsequently the aerodynamic shortcomings are primarily found in the exhaust hood system. As the exhaust hood casing and condenser can rarely be modified in retrofits, it is the exhaust *diffuser* which has the most potential for improvement. Even in new equipment designs, the trend for down-flow exhaust hoods to
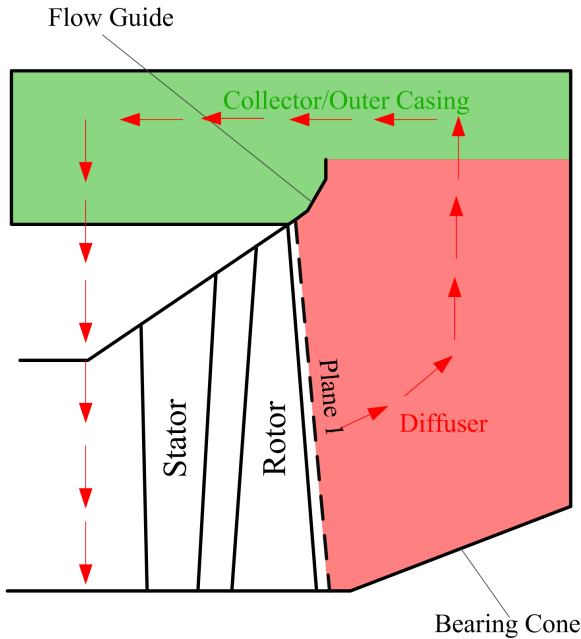
Figure 1.3: Schematic of a Cross Section of Upper Exhaust Hood and its Primary Components
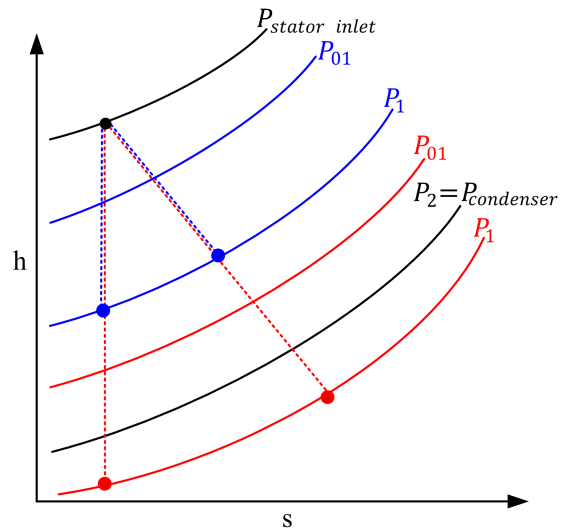
Figure 1.4: h-s Diagram of High C_p (red) and Low C_p (blue)

reduce the turbine shaft axial length, typically leads to exhaust hoods of poor aerodynamic performance because of the vortices which develop due to the sharp axial-radial turning.

With the potential for large performance gains, the accurate prediction of LP exhaust hood flows is vital. In the early 1990's the "usefulness of Computational Fluid Dynamics (CFD) for accurately assessing the performance of low-pressure steam turbine exhaust hoods" [60] was first highlighted. CFD tools have become "increasingly important" in industry [2] as the diffuser is often the subject of optimisation studies which would be prohibitively expensive with experimental testing. However, the study of steam turbine exhaust diffuser flows "is [still] considered very challenging" [64].

Aside from the highly rotational flow structure which forms from the 90° turn from the axial to radial direction in the diffuser shown in Figures 1.1 and 1.3; the flow is further complicated by wet steam effects and the transonic nature of the flow. The steam expansion through the latter LP stages leads to wetness which affect the flow angle into the diffuser [2]. The rotor tip jet is supersonic which can cause shock induced separations around the flow guide due to the shockwaves and expansion fans which form in this region. In addition, the wakes of the upstream rotor which pass through the diffuser generate unsteadiness. The flow exiting from the turbine is highly radially non-uniform which develops a circumferential asymmetry when interacting with the exhaust hood due to the non-axisymmetric hood geometry and swirl from the rotation of the turbine blades. This asymmetry which develops is considered by some to be one of the "most challenging problems with fluid dynamics" [21]. The complex flow regime in the upper exhaust hood progresses down to the condenser, interacting with the hood reinforcing elements (such as splitter plates e.t.c.) and generating
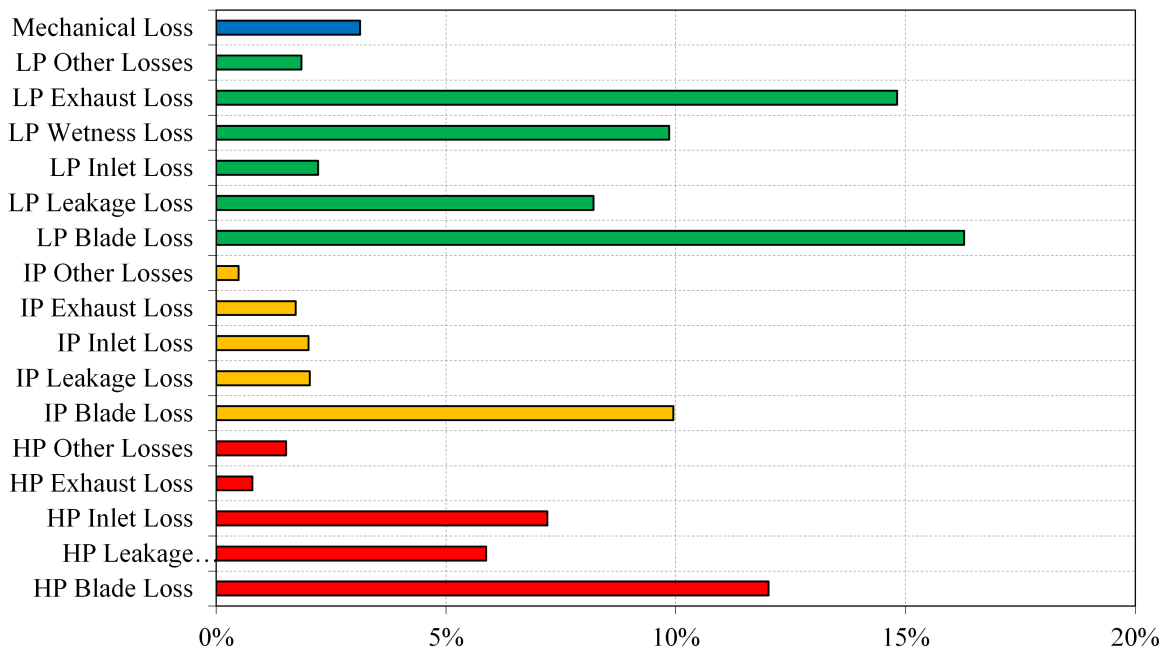
Figure 1.5: Diagram of the Relative Fraction of Losses in the Steam Turbine [59]

further losses.

Despite the technological advances leading to significant developments in the availability of computational power; modelling highly rotational, asymmetric, transonic, unsteady wet steam exhaust hood flows with full internal 'furniture' is still almost impossible. Mizumi and Ishibashi in 2013 summarised the problem of computational modelling of turbine exhaust hood flows [40]:

> *"Ideally it would be preferable to take all those influential factors into consideration in designing an exhaust hood. However, it is neither cost effective nor practical to take everything into consideration at the same time. For this reason it is necessary to reach a compromise to some extent between the ideal and the realistic design methods."*

Despite comprehensive CFD research, particularly over the last decade, addressing methods of simplification and "compromise", there is at present no single best-practice approach for computational modelling steam turbine exhaust hood flows. Some aspects of the flow field, such as the rotor tip leakage jet, are unanimously considered vital to include in the exhaust hood calculation. It is also universally accepted that the radial variations of the turbine flow field are critical to impart on the exhaust hood, as using a uniform inlet boundary condition to an exhaust hood calculation has been shown to give unrepresentative results.

Early flow calculations solve the exhaust hood and turbine flow structure independent of each other; with radial variations of the turbine outlet flow applied to the exhaust hood inlet and solved in a separate CFD calculation, known as a *sequentially coupled* approach. Typically, the most sophisticated modern exhaust hood models solve the last stage turbine

and exhaust hood flow fields simultaneously in a, so called, *bi-directional coupled* approach. However, the flow field which results is still "highly dependent on [...] the interface treatment used" [2] between the exhaust hood inlet and the last stage rotor outlet.

The treatment of the exhaust hood inlet and rotor outlet interface is the subject of much debate and a range of methods are still considered valid by researchers. The relative merits of each method is typically argued on two criteria: whether the circumferential variations in exhaust hood flow are captured, and whether unsteady effects are considered. The quasi-steady, single passage, mixing plane approach is a computationally efficient method of capturing the interaction between the turbine and exhaust hood, but the circumferential averaging at the hood/rotor interface means the asymmetry of the exhaust hood is neglected. Modelling the full turbine annulus in a steady frozen rotor calculation enables the circumferential non-uniformity of the exhaust hood inlet flow to be simulated, but the high cell counts arising from modelling all the blade passages lead to a high computational power requirement. Full annulus unsteady calculations are now possible with modern computing, but are typically rare due to the prohibitively high computational demand.

Despite the range of methods and simplification strategies currently in use in the field, there is no set of recommendations or guidelines of the best approach for computational modelling of steam turbine exhaust hood flows.

1.2   Thesis Scope and Overview

This thesis explores a range computational modelling strategies for computing steam turbine exhaust hood flows using commercial CFD software. From this work, the outcome has been four novel contributions to the field.

Firstly, the first open source, generic, last stage steam turbine blade and exhaust diffuser with outer casing test case has been developed: the *Durham Stage and Exhaust Hood Test Case* (DSEHTC). A comprehensive literature review (Chapter 2) highlighted that despite the rapidly increasing interest in the steam turbine exhaust hood field, no representative geometry for both LP blading and exhaust hood existed which was free to use. The high level of secrecy associated with the commercial IP of turbomachinery manufacturers means that for those in academia, research in this field is difficult without an industrial backer as no published test geometries are available. To facilitate research in this rapidly expanding field, an IP restriction free geometry for LSBs and accompanying exhaust hood was generated which is representative of current industrial practice.

Secondly, the effect of *condenser cooling water flow* on steam turbine exhaust hood flow fields has been studied for the first time using the DSEHTC. A generic, pressure gradient boundary condition was produced to represent the temperature change as a function of the condenser cooling water flow. This was shown to have a larger influence on the exhaust hood flow asymmetry than the tip leakage jet, the importance of which is universally acknowledged.

Thirdly, this thesis documents the first application of the *non-linear harmonic* (NLH) method to steam turbine exhaust hood flows. Analysis and evaluation of bi-directional/fully

coupled turbine and exhaust hood calculations highlighted that with the current methods (mixing plane or frozen rotor) a sacrifice must be made; either generating computationally efficient results where the circumferential asymmetry is neglected, or computationally intensive results where the hood inlet non-uniformity is captured. This highlighted the potential for a method which achieves a compromise between computational efficiency and the accurate modelling of the exhaust hood inlet boundary conditions. The NLH method was shown to transfer the circumferential asymmetry at the exhaust hood inlet plane across the interface to the stage, in only half the computational demand of the current, widely used, full annulus methods.

Finally, following this body of work, a set of recommendations is provided to guide researchers, in both industry and academia, as to the current state-of-the-art simplification strategy for CFD simulations. The research highlights a set of *minimum requirements* for the computational set-up (inlet and outlet boundary conditions and rotor/hood interface treatment) which should be considered mandatory for modelling of the exhaust hood flow structure and for determining loss coefficients. The guidelines are universal and apply to computations carried out with commercial CFD codes or with custom software.

Research in this thesis can be divided into four distinct sections:

1. In the first two chapters, the research presented in the thesis is contextualised and work by other researchers is described. This comprises of:

   (a) This introduction which places the research in a wider context.

   (b) Chapter 2 is a comprehensive literature review which summarises the current knowledge in the field. The present understanding of the exhaust hood flow physics and complex flow field are outlined. Two decades of computational and experimental simulation methods are discussed and the current state of the art knowledge is summarised.

2. The next chapter describes the development an open source test geometry for a last stage LP steam turbine and accompanying exhaust hood. This test geometry is the subject of the computational studies later in this thesis.

   (a) Chapter 3 outlines the development of the *Durham Stage and Exhaust Hood Test Case*. Specifically, the modification to a 20 year old, industry developed LP last stage blade (LSB) geometry which was adapted in collaboration with a leading turbine manufacturer to remove commercial IP restrictions and to ensure that the outlet profiles of the blade are representative of modern blading. Also, this chapter describes the process behind the generation of a generic exhaust diffuser and hood from the amalgamation of designs published in the literature.

3. The main body of work explores the effect of computational modelling strategy on the flow structure and loss predicted for the DSEHTC. This is broadly considered in two parts; the effect of inlet and outlet boundary conditions, and the effect of the interface treatment between rotor and exhaust hood.

(a) Chapter 4 summarises the computational methods used in this thesis in the calculation of the exhaust hood flow structure. The interface treatment and computational set-up for both sequential and bi-directional coupled calculations is described; specifically the mixing plane, frozen rotor and non-linear harmonic fully coupled approaches. The purpose of this thesis is not to develop custom coded methods but instead to evaluate their relative merits and subsequently all methods described are incorporated into commercial CFD software.

(b) Chapter 5 compares the DSEHTC against other computational studies using commercial CFD software and a sequential coupling approach. The flow profiles exiting the LSBs are compared with examples from the literature, confirming that the open source blading produces a representative inlet boundary condition to an exhaust hood CFD calculation. The complex flow structure within the exhaust hood is compared with the vortex categorisation by other researchers in Chapter 2 to confirm that the magnitude and location of the recirculations are similar to those previously published in the literature.

(c) Chapter 6 explores the influence of the bulk inlet and outlet boundary conditions on the exhaust hood flow structure. The tip leakage effect, which is widely accepted as mandatory to include in flow calculations to predict a accurate flow structure in the exhaust hood flow guide region. The test case is shown to predict performance trends similar to those published in the literature. This thesis also presents the first study of the effect the condenser cooling water flow pressure gradient on the exhaust hood flow structure and pressure recovery. An additional outcome of this study is the generation of a 'generic' condenser pressure gradient outlet boundary condition, produced from field data which can be easily incorporated into other researchers' models.

(d) Chapter 7 considers the treatment of the rotor/hood interface when only a single LSB passage is modelled. This specifically compares two approaches; the widely adopted mixing plane approach and the novel, non-linear harmonic approach; the first application of which to exhaust hood flows can be found in this thesis. The loss coefficient, flow structure and circumferential asymmetry predicted by the two methods is compared. The NLH method is shown to transfer the circumferentially asymmetric flow within the hood to the rotor, an effect not previously achievable when modelling only a single blade passage. In addition, the effect of reducing the diffuser axial length is also explored, along with the effect the rotor/hood interface treatment has on the results.

(e) Chapter 8 compares the current state-of-the-art for capturing the circumferential asymmetry at rotor outlet, the frozen rotor approach, with the newly applied method in this thesis, the non-linear harmonic method. The loss coefficient, flow structure and circumferential non-uniformity predicted by both approaches are compared. As the NLH method is suggested as a computationally efficient alternative to full annulus methods for calculating the inlet asymmetry, the memory

requirement of each method is compared. In addition, the effect of running at off-design condition is considered for the range of bi-directional coupled interface treatments described in Chapter 4.

4. Given the computational studies of bulk boundary conditions and interface treatments described in the main body of work, a set of recommendations and guidelines for the CFD modelling of steam turbine exhaust hood flows is provided in Chapter 9 along with overall conclusions and recommendations for future work.

2

Literature Review

2.1 Introduction

Research focusing specifically on steam turbine exhaust hoods has stretched over the last 30 years but currently the "understanding of the flow physics in the exhaust hood is not yet mature" [68]. Small scale experimental tests in the 1980's highlighted the potential improvements possible with the exhaust hood design, but it is only since the rise of CFD simulations from the mid-1990's that a more detailed understanding of the complexities of the flow has been gained.

At present, the key challenge faced is efficiently numerically modelling the 3D, unsteady, transonic wet steam exhaust hood flow given the impractically high computational power requirement. Multiple calculation simplifications to reduce the computational demand have been successfully verified with experimental data, but at present there is no 'best-practice' approach to reduce the computation time for routine design exercises.

This chapter outlines the complexity of the flow regime in the steam turbine exhaust hood and summarises the current understanding of the source of vortices and separations within the system. The evolution of CFD practices over the past two decades is discussed and the present state-of-the-art simulation is outlined. Experimental methods are discussed, as is the role scaled testing plays in CFD validation. Finally, the current knowledge regarding the influence that the turbine has on the exhaust hood flow field is presented and an indication is given to the primary exhaust hood geometric features which influence loss. This chapter is adapted from a publication in the ASME Journal of Engineering for Gas Turbines and Power [8].

2.2 Flow Structure in the Exhaust Hood

The three-dimensional, highly complex, exhaust hood flow structure, shown in Figure 2.1, can be categorised into two distinct regions of importance:

1. Separations in the diffuser

2. Down-flow to the condenser
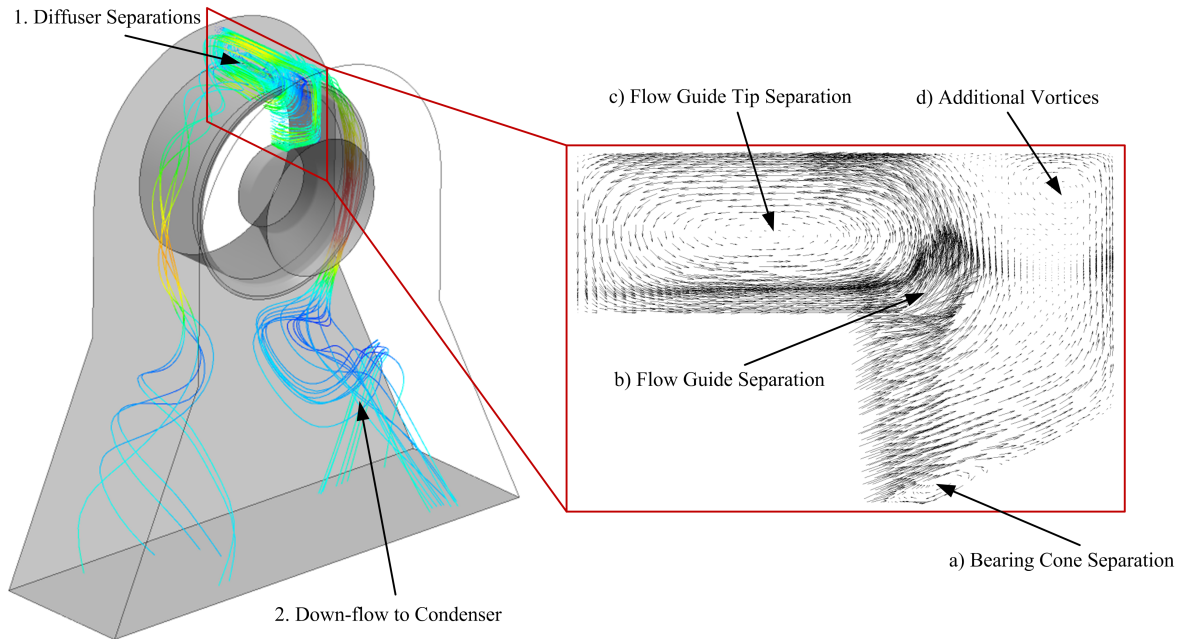
Figure 2.1: CFD Generated Steamtraces and Velocity Vectors Detailing the Complex Flow Structure Present in the Exhaust Hood from Burton et al. [9]

The rotational flow downstream of the LSBs has non-uniform distributions of pressure, velocity and temperature. This, combined with the high flow turning of the compact axial-radial diffuser results in the formation of a series of vortices and separations within the diffuser, shown in detail in Figure 2.1. The diffuser separations and vortices have been explored and categorised in research over the last 15 years, notably in the work of Xu et al. and Zhang et al. [67, 70], as follows:

(a) Bearing cone separation

(b) Flow guide separation

(c) Flow guide tip separation

(d) Additional vortices

The vortices formed within the diffuser (labelled 1 in Figure 2.1) merge with progression downstream, to form a single vortex stretching downstream into the condenser (labelled 2 in Figure 2.1). This flow structure reverses across the meridional plane, so two counter-rotating vortices are present in the condenser neck. However, despite the vertical symmetry of the hood geometry, the flow structure is asymmetric because of the direction of rotation of the turbine and horizontal asymmetry of the hood casing.

2.2.1 Separation along the Bearing Cone

Owczarek et al. in 1990 [44], using the lampblack oil flow visualisation technique, was the first researcher to observe a separation along the bearing cone in the form of a horseshoe

vortex. The flow was attached at the diffuser inlet but separated along the bearing cone, with the separation continuing into the collector. Numerical simulations by Tindell et al. in 1996 [61] attributed the horseshoe vortex which forms from this separation to be one of the major contributors 15-20% of the loss found typically in exhaust hoods. The significance of the horseshoe vortex within the diffuser has been highlighted by many researchers over the past two decades, including Xu et al. in 2001 [67] and Fan et al. in 2007 [15].

Zhang et al. in 2007 [70] highlighted that the very nature of a diffuser leaves it susceptible to separation, with the adverse pressure gradient increasing the potential for the low kinetic energy boundary layer fluid to separate from the bearing cone wall as the flow velocity decreases. The steam turbine exhaust diffuser is particularly susceptible due to the large swirl of the inlet flow, highlighted by Fan et al. in 2007 [15]. The components of inlet velocity in the axial and tangential directions, act against the curvature of the bearing cone, facilitating boundary layer separation. This was corroborated by Fu and Liu in 2008 [18] who found that a large swirl angle at the hub resulted in the separation along the bearing cone, with the magnitude of the separation reducing with decreasing swirl.

Numerical analysis by Tindell et al. in 1996 [61] with representative inlet conditions showed the separation point was dependent upon the operating point of the turbine. Accurate prediction of the separation point is vital, as Beevers et al. observed in 2010 [2]; the earlier the separation the less pressure the diffuser can recover. Liu et al. in 2003 [36] investigated the effect of hood inlet conditions, comparing uniform with distorted inflow, and found the bearing cone separation was only present with non-uniform distributions at inlet to the diffuser. This was corroborated by Fan et al. in 2007 [15].

The losses resulting from this vortex can be large because of its magnitude. Xu et al. [67] estimated the vortex can occupy up to $\frac{2}{3}$ of the diffuser height. The blockage effect (and subsequent reduction of the effective area) reduces the diffuser's ability to recover pressure. The bearing cone separation is absent in Fig. 2.1 as for this calculation the swirl angle was small at the hub of the rotor blade [4].

Based on the current knowledge the susceptibility of the bearing cone of the diffuser to separation is increased by high swirl in the LSB hub exit flow and by non-uniformity of the flow at inlet to the diffuser.

2.2.2   Flow Guide Separations

"The general form of the static pressure distribution along the [flow guide] is essential to the prediction of the pressure recovery" within an exhaust diffuser simulation [2]. This region is of particular importance in exhaust hood studies as it is the most likely to have boundary layer separation where "the effects of flow deceleration due to flow area expansion and streamline curvature are superimposed" [43]. Typically, two separations are present in the flow guide region, as shown in Figure 2.1.

1. Flow guide tip separation

2. Separation along length of the flow guide

Owczarek et al. [44] was the first to note the separation in the step region behind the tip of the flow guide, labelled c) in Fig. 2.1. This separation was attributed by Zhang et al. [70] to be due to the "backward-facing step expansion" phenomena. With progression downstream, the magnitude of the of the vortex increases, as the pressure decreases when approaching the condenser neck.

The separation along the length of the flow guide, labelled b) in Fig. 2.1, is highly dependent on the flow guide geometry and the modelling of the tip leakage jet. A sharp kink angle (such as that shown in the geometry in Fig 2.1) changing the flow from the axial direction to 30°, was found by Yoon et al. [68] to result in separation along the flow guide. Previous research has shown optimisation of the flow guide geometry can suppress this separation [66, 68, 64]. Research has also indicated [56, 27, 16] the positive influence of modelling the tip leakage jet, discussed in detail in Section 2.5.3.

2.2.3   Additional Vortices

There has been little research on additional vortices which form within the diffuser due to the comparatively small losses associated with them. Xu et al. in 2001 and Fu and Liu in 2008 [67, 18] have attempted to categorise the vortices, with Xu et al. observing an endwall vortex in the collector and a separation vortex on the outer guide wall. Both noted that with progression downstream, the magnitude of the vortices decreases and by inlet to the condenser neck all vortices, including those described in Sections 2.2.1 and 2.2.2, combine to form the outlet vortex loop discussed earlier.

2.2.4   Downflow to the Condenser

The counter-rotating outlet vortices in the condenser neck have a detrimental effect on condenser efficiency, as it is desirable to have a uniform distribution of steam across the heat transfer surface. Reverse flow at the core of each vortex has been noted by multiple researchers including Stastny et al. in 2000 [54]. The low energy at the core drives the main flow outwards to the walls of the condenser neck, resulting in high velocities in this region and the bulk of the flow discharging down the endwalls in a highly non-uniform flow, shown in the V_z contours in Figure 2.2 from Liu et al. [36]. Positive V_z denotes a region of reverse flow, re-entering the exhaust hood. Zhang et al. also observed that the core of the vortex is not at the geometric centre of the condenser neck half plane, and found it to be situated towards the backwall, a characteristic which was found by Zhou et al. to be dependent upon the flow coefficient. Increasing the flow coefficient caused the vortex to move towards the back wall. Fan et al. in 2007 noted the asymmetry of the flow decreases throughout the condenser neck because the complexity of the flow rotation weakens the non-uniformities [15].

2.2.5   Flow Asymmetry

One key aspect characterising the exhaust hood flow structure is its asymmetry. This asymmetry is present between both the radial and meridional planes of the exhaust hood due to
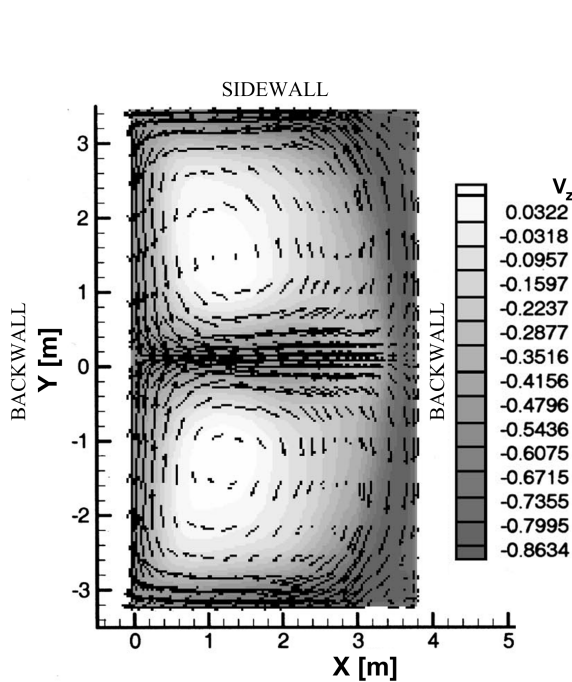
Figure 2.2: V_z Contours and Velocity Vectors at the Hood Outlet/Condenser Inlet Plane from Liu et al. [36]
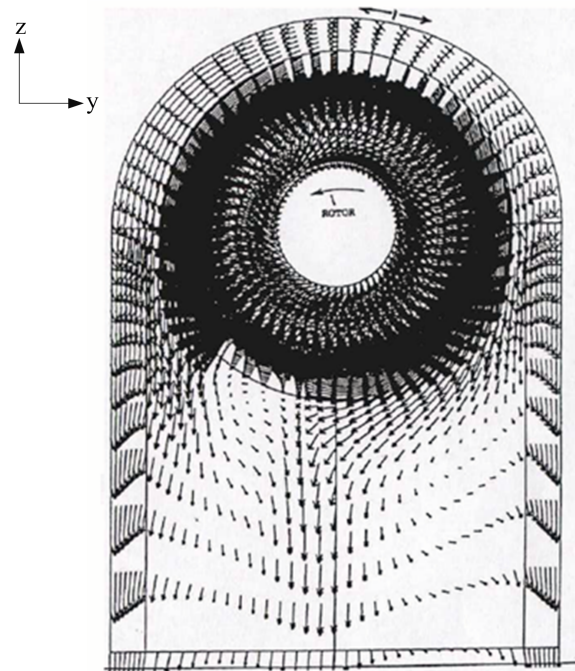
Figure 2.3: Velocity Vectors of Flow Asymmetry in the Front Plane from Benim et al. [3]

two different mechanisms.

The asymmetry of the exhaust hood geometry in the radial plane results in a flow asymmetry between the top and bottom of the exhaust hood. This characteristic, according to Benim et al. in 1995 [3], plays an important role in the formation of vortices in the diffuser. The geometry causes the flow downstream of the rotor to develop a circumferentially non-uniform distribution, which couples the exhaust hood to the last stage. This important observation adds to the complexity of any exhaust hood numerical simulation.

Researchers in the past 15 years have observed this two plane asymmetry [3, 67]. Benim et al. [3] found prominent meridional flow asymmetry between the left and right hand sides of the exhaust hood, Figure 2.3. This was attributed by Xu et al. [67] to be due to the swirl at inlet to the exhaust hood due to the rotation of the turbine.

2.3   Computational Fluid Dynamics Methods

Tindell et al. in 1992 [60] "highlighted the usefulness of CFD for accurately assessing the performance of low-pressure steam turbine exhaust hoods." However, the complexity of the unsteady, transonic, wet steam flow regime within the exhaust hood is too time-consuming for currently available computational power. Although Moore's Law anticipates the doubling of computational power approximately every 18 months, at present, various simplification methodologies must be adopted to reduce the computational demand of the problem to a manageable level. Primarily, the simplification strategies focus on the method of modelling

the exhaust hood inlet boundary condition, and specifically the coupling of the exhaust hood to the last stage turbine blades. Broadly the stage/hood interface treatment can be divided into two main categories:

1. Sequential Coupling

2. Bi-Directional Coupling

2.3.1   Sequential Coupling

Sequential coupling methodologies involve solving the exhaust hood flow structure isolated from the LSBs. The predicted exhaust hood flow structure is governed by the complexity of the inlet boundary condition to the exhaust calculation. Throughout the mid 1990s and early into the new millennium, 3D viscous flow models with uniform flow at exhaust diffuser inlet were used. However these were quickly shown to not produce a representative flow structure in the exhaust hood [34, 61].

Application of radially non-uniform flow profiles taken downstream of the last stage turbine blades were shown by many researchers to be useful for producing representative flow field results at a reduced computational cost [21, 30, 36]. Early calculations featured experimentally determined turbine outlet flow profiles applied at hood inlet. With the development of computational modelling methods, these later progressed to turbine outlet profiles extracted from a separate LSB CFD calculation.

Sequential coupling approaches are useful for establishing 'ball-park' flow regime predictions at a low computational cost. However, the significant drawback of the method is that only the influence the turbine has on the exhaust hood is captured and the effect the exhaust hood has on the turbine is ignored. It has become increasingly clear that the most accurate numerical simulations are achieved when the turbine is fully coupled to the exhaust hood, capturing the interaction between the two. However, modelling this interaction is significantly more computationally demanding and "many researchers have focused on numerical methods to reduce the computational burden" [64] for these, so called, *bi-directionally coupled* approaches. Despite nearly two decades of research in this area, no single, 'best-practice', approach for modelling the fully coupled exhaust hood flow structure has come to the forefront.

2.3.2   Bi-Directional Coupling

Bi-Directional methods of coupling concern the modelling of the interaction between the last stage turbine blades and the exhaust hood, the significance of which researchers have been aware of since 1995 [3]. This is "essential" [34] as the turbine affects the flow structure and performance of the exhaust hood, but conversely the operating point and efficiency of the turbine is governed by the flow regime in the diffuser. The accurate modelling of this interaction however is still considered "the biggest challenge in simulating an exhaust hood by CFD" [64].

The range of bi-directional coupling modelling strategies focus on the treatment of the interface between the last stage blade rotor outlet domain and the inlet to the exhaust hood. The strategies range from steady models incorporated into commercial CFD software to custom and industrially developed tools. Unsteady simulations of the full coupled exhaust hood system is now possible with current computational power resources, at present is not common place.

Mixing Plane

The Mixing Plane approach, developed by Denton and Singh [14] is the industry standard for single passage multi-stage turbine calculations. Fan et al. in 2007 [15] successfully applied the mixing plane method to couple the turbine to the exhaust hood and produced a representative flow structure. Modelling only a single blade passage keeps the computational demands low for a fully coupled method. However, at the interface between the rotor and the exhaust hood, the flow variables are circumferentially averaged. In multi-stage calculations this is a valid simplification as the circumferential flow variations are small, however, the exhaust hood flow structure is highly circumferentially non-uniform because of the asymmetric hood geometry and the swirl from the turbine. The circumferential averaging at the interface removes this asymmetry contributing to inaccuracies in the inlet boundary condition as only the radial flow variations are maintained.

Frozen Rotor

Zhou et al. [71] advises that in order to capture the circumferential asymmetry, all blade passages should be modelled . The increase in computational power availability in the new millennium led to more frequently used full annulus models with the frozen rotor approach [30, 71, 33, 64]. This widely adopted method involves the simulation of all rotor passages, enabling both the radial *and* circumferential variations at the hood inlet to be captured. The resulting turbine flow structure is dependant on rotor positioning as the simulation is carried out with the rotor in a fixed location, but allows the interaction of the exhaust hood and LSBs to be captured, along with the non-axial symmetry of the flow. In isolated stage calculations, frozen rotor calculations are typically run for a series of rotor clocking positions to assess the sensitivity of the solution to the relative positioning of the rotor to the stator. However, no examples exist for this study being carried out for bi-directionally coupled frozen rotor exhaust hood simulations.

The frozen rotor calculation is still highly computationally demanding due to the large cell counts (over 54 million [64]) and the subsequently long computation times (267 hours on 3 parallel computers, each with 8GB of memory and 4 CPU [33]) and it is recommended that the method should be used as a "validation tool, rather than a design tool" [64].
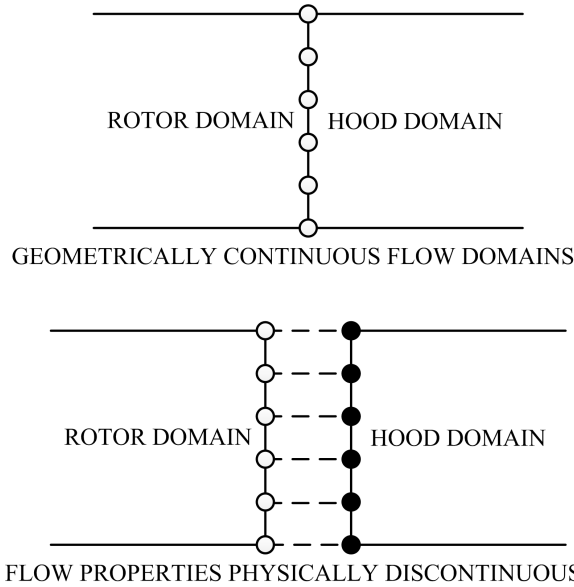
Figure 2.4: Diagram of the Actuator Disc Model by Liu and Hynes [34]
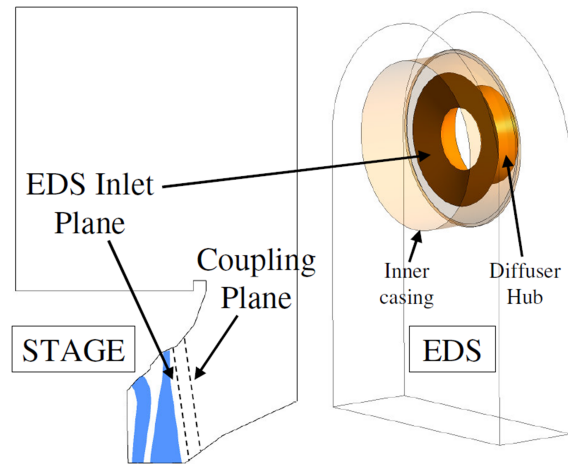
Figure 2.5: Diagram of the EDS Calculation Method from Beevers et al. [2]

Actuator Disc Model

Despite the relative drawbacks of both the mixing plane and the frozen rotor approach, each method has the advantage of being widely incorporated into commercially available CFD software. A few custom code CFD methodologies have been developed and published but have not been widely adopted. Liu and Hynes custom coded the Actuator Disc CFD Model in 2002 [34] as an alternative for simulating asymmetric flows, developing the method from an existing blade model by Hynes [28]. The method models the blade row as a zero thickness disc where flow properties take a physically discontinuous jump, preserving the conservation of mass flow, momentum and energy whilst capturing flow turning and entropy generation across a blade row, Figure 2.4 gives an illustration of the calculation domains in the model at the rotor/hood interface. Two discs were applied at stator and rotor trailing edges and the simulations successfully captured the asymmetry of the flow at condenser inlet and diffuser separations. However, this method has not been widely adopted with the only evidence of its use in the paper in which it was developed. This is likely due to the fact that the rotor tip leakage jet and choking in the LSB nozzle cannot be simulated: both of which significantly influence the exhaust hood flows [68].

Industry Developed Tools

Benim et al. in 1995 [3] presented the first comprehensive model of the interaction between the exhaust hood and the turbine, known as the Exhaust Design System (EDS). This method is not incorporated into commercial available CFD codes but has proven to be one of the most robust, with the methodology integrated with state-of-the-art in-house CFD codes, which are still used by a leading industrial supplier over 15 years later [2, 68].

Firstly, a set of single passage stage calculations are performed coupled to a section of

diffuser the width of a single blade passage, for a range of operational conditions. This forms a database of the variation of stage flow properties with operational condition for the rotor trailing edge/EDS inlet plane and the exhaust hood coupling plane, shown in Figure 2.5. In a separate calculation the full exhaust hood geometry is modelled with the EDS Inlet Plane circumferentially divided into segments, the number of which can be increased to anything up to the grid resolution in the circumferential direction. The exhaust hood flow field is initially calculated for a circumferentially uniform inlet boundary condition. The circumferentially non-uniform flow field which develops at the coupling plane can be referenced to the database of turbine flow fields, updating the segmented exhaust hood coupling plane. The calculation is rerun, the EDS exhaust inlet plane segments updated from the turbine flow field database and calculation repeated, iteratively, until convergence.

Full Unsteady Models

At present "the most advanced [CFD] models take into account the flow unsteadiness" [51] but comparatively few studies are available in the literature due to the high computational demand of the simulation. Sieker and Seume in 2008 [49] acknowledged that "a highly efficient turbine exhaust diffuser cannot be designed without taking into account the unsteady interactions" but, at present, the enormous CPU requirements for a full 3D unsteady CFD calculation (10000 CPU hours on parallel 4 processor machine for 65000 iterations [51]) means this remains a research method rather than a daily design tool.

An early study by Solodov and Gnesin in 1997 [50] investigated the effect of unsteadiness on aerodynamic blade force using a 3D Euler solver. Unsteady analysis by Stanciu et al. [51] of the coupled full stage annulus and exhaust hood system found the turbine blades not only experience high frequency fluctuations due to the stator rotor interaction, but also low frequency forces due to the interaction between the stage and the exhaust hood. This was attributed to the non axis-symmetric turbine outlet pressure boundary due to the presence of the hood geometry. This was corroborated in recent research by Fu et al. [20] who noted that the amplitude of the low frequency fluctuations due to the presence of the exhaust hood were higher than the amplitude of high frequency fluctuations, as shown in Figure 2.6. This indicates that the interaction between rotor and exhaust hood has a significantly larger influence on the unsteady blade force than the interaction between stator and rotor. The CFD studies, verified by test data, confirmed the presence of unsteadiness in the exhaust hood which was found to increase the larger the flow coefficient. Unsteadiness was clearly noted in the hood collector and outer casing, which was thought to be enhanced by the separations which form within the diffuser. Fu et al. also noted the importance of selecting an appropriate time step, as an increase of between 17% and 42% occurred in the amplitude of pressure fluctuations around the blade when moving from a coarse to a fine time step. Although the majority of exhaust hood flow features can be "reasonably well predicted with steady simulations" [52], it is anticipated that many future publications will include a full annulus unsteady CFD hood calculation as computational power increases.

Despite the range of CFD calculations methods currently and simultaneously in use, there
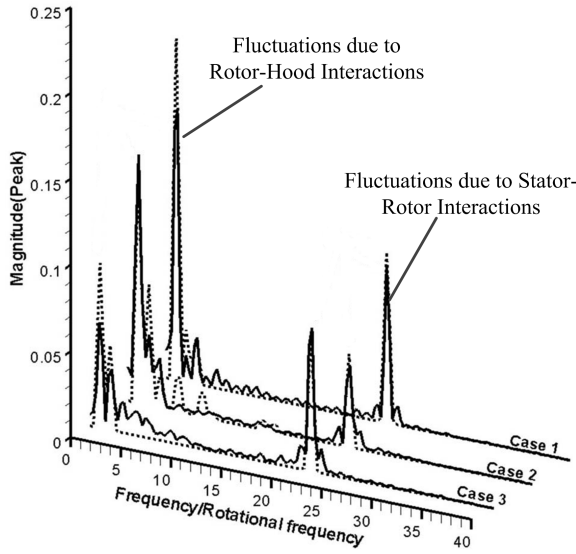
Figure 2.6: FFT of the Unsteady P_t Fluctuations at the Rotor Pressure Surface Trailing Edge from Fu et al. [20]
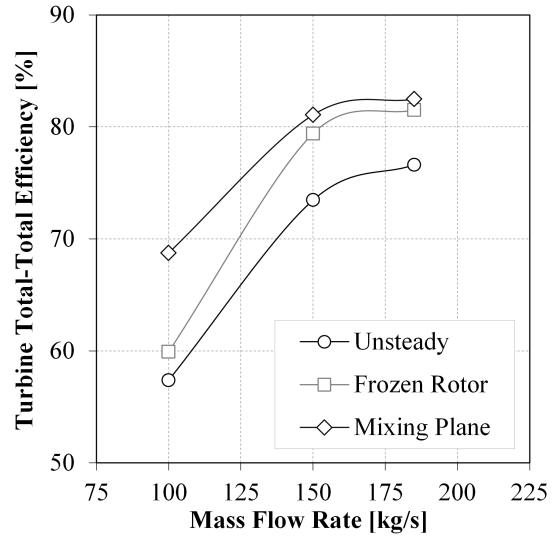
Figure 2.7: Variation of η_{T-T} with Mass Flow Rate for Different Calculation Methods from Stanciu et al. [51]

are relatively few comparative studies available in the literature. Gardzilewicz et al. [21] compared, using experimental conditions at hood inlet, stage/hood coupling via a method similar to the EDS approach described in Benim et al. [3] with direct simulation of the full turbine annulus. The research highlighted the difficulty in obtaining compatible boundary conditions between LSB exit and diffuser inlet in coupled calculations. Stanciu et al. [51] compared three methods of coupling; mixing plane, frozen rotor and full unsteady. The steady models (i.e. mixing plane and frozen rotor) were found to over-predict the performance of the stage compared to unsteady calculation, by as much as 8%. The research highlighted the importance of examining the flow characteristics at off design conditions, as the accuracy of the efficiency prediction varies with load, as shown in Figure 2.7. Due to the uniform back pressure generated by the mixing plane approach, the effect of the exhaust hood is not fully experienced by the stage and this method subsequently over-predicts the stage efficiency, particularly at low load. As the frozen rotor method enables the asymmetric hood inlet pressure to be applied to the stage, this method is more accurate at predicting stage efficiency.

2.3.3   Turbulence Modelling

By far, the most widely adopted turbulence model for exhaust hood flow simulations is the k-ϵ turbulence model [12, 30, 47, 53, 67, 71], despite its poor performance in predicting highly separated flows. Both SST [58] and k-ω [52] models are also used, although infrequently. Few turbulence model studies have been carried out for the exhaust hood system, although all predict a small difference in diffuser performance between different models used. A study by Cordova and Stoffel in 2006 [10] of six turbulence models in a channel diffuser found an "acceptable" level of accuracy for all models examined. In 2009, Ris et al. [47] found a
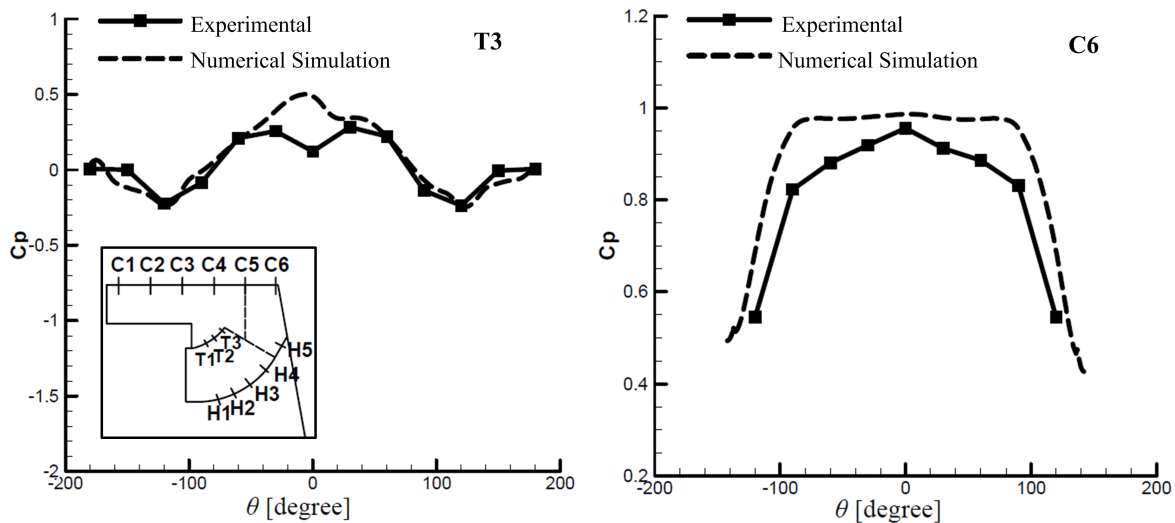
Figure 2.8: C_p Predicted by Experiments and CFD around two Circumferential Locations from Fu and Liu [19]

change of no more than 5% in hood losses was observed when varying the turbulence models. Industry studies by Beevers et al. in 2010 [2] revealed that "no significant difference was shown between the k-ϵ and the k-ω SST turbulence models." The Reynolds Stress model predicted a larger separation region in the diffuser, but the turbine efficiency calculated was less than 0.1% lower than the alternative, less computationally expensive turbulence models. This produced "no large appreciable differences" in the diffuser and exhaust hood flow field.

Regardless of CFD methodology or turbulence model, one common shortcoming of numerical simulations is the over-prediction of the hood static pressure recovery coefficient compared with experimental data, as shown in Figure 2.8 from Fu and Liu [19]. This can sometimes vary by up to 7% [36], with the discrepancy increasing with increasing vortex size. Typical values of exhaust hood C_p are around 0.2-0.4 [35, 36, 15, 19, 66, 16]. Discrepancies between experimental and numerical results are primarily attributed to unrepresentative boundary conditions [54], inaccuracies in turbulence and transitional modelling [13] and simplification of the exhaust hood geometry [2].

2.4   Experimental Techniques

The majority of experimental testing focuses around scaled models, due to the financial constraints of full-scale testing. Gray et al. stated in 1989 that "typical scale factors used in such models range from 1:20 to 1:30 depending on the length of the last row blade in the actual turbine" however, over the past 20 years the scale of models has increased to between $\frac{1}{15}$ [36, 70] and $\frac{1}{10}$ [2, 68] more closely matching the Reynolds Number to that of the actual turbine. To attempt true dynamic simulation, Beevers' facility in 2010 [2] used R134a gas mixed with air (the latter of which is typically used by most researchers) to match the γ in the $\frac{1}{10}$ scale models with full-scale turbine.

Experimental testing does have drawbacks compared with CFD as creating representative

inlet conditions is also difficult for scaled testing. In LP exhaust hood tests, two distinct approaches are adopted for creating representative pressure, swirl and velocity distributions at inlet:

1. Static Devices

2. Rotating Devices

Static devices have remained relatively unchanged over the past 30 years with the multiple wire mesh screens and stationary vane used by Gray et al. in 1989 [23] to generate radial distributions of pressure and swirl angle adopted right up until testing from Liu et al. in 2003 [36]. Alternative methods include a row of narrow plates and stationary row of blades used by Tajc et al. in 2007 [56]. Static devices are a simple way of giving representative conditions at inlet but fail to capture the unsteady effects, which have recently [20] been highlighted as important.

Rotating devices have scarcely been explored in scaled experimental testing of exhaust hoods. Application of even a large $\frac{1}{4}$ scaling to a 50Hz machine increases the rpm from 3000 to 12000, introducing issues concerning structural integrity and absorbing the generated power. Typically rotating devices have taken two forms: wheels with varying diameter spokes or scaled rotating blades. Spoked wheels were used by Sieker and Seume in 2008 [49] to generate the high level of turbulence, energizing the boundary layer. A larger diameter spoke was used to reduce the diffuser separation region because of the increased turbulence from the wakes. Zhou et al. in 2008 has been one of the few researchers to include a scaled model of rotating blades, using resistors to absorb the power generated by the $\frac{1}{15}$ scale turbine. The majority of published work using rotating devices has been carried out by large industrial suppliers with custom test facilities such as those used by Beevers et al. in 2010 and Yoon et al. in 2011 [2, 68]. Rotating devices have been found to challenge experimental instrumentation due to the unsteady flow, with both Xu et al. and Sieker and Seume [67, 49] finding repeatable experimental results difficult to achieve with a 5-hole probe because of instabilities from the flow unsteadiness.

Probe traverses may enable the validation of CFD results but usually "cannot provide enough information in order to understand the flow details and finally improve the design approaches [34]". Particle Image Velocimetry (PIV) offers an alternative; a reliable method for capturing instantaneous whole field velocity measurements which can be used to determine the kinetic energy loss, turbulence characteristics and the performance of the hood [71]. Although this approach allows a more detailed flow structure to be measured, common seeders such as oil require regular cleaning from the clear acrylic hood models and there can be restrictions in the size of the flow field which can be captured in a single traverse. In 2008, Sieker and Seume [49] recommended Laser Doppler Velocimetry (LDV) as a method for recording velocity profiles as it is non-intrusive, requires no calibration and allows stagnant and reverse flow (such as in vortices) to be accurately captured.

2.5   Influence of the Turbine

Regardless of the experimental or computational methodology, the aim is to accurately simulate the inflow conditions to the exhaust diffuser generated by the LP turbine. It has been shown that uniform hood inlet flow does not produce a flow structure in the exhaust hood representative of that found in reality and "actual and accurate inlet flow conditions are critical" [58]. As such, it is important that the radial and circumferential flow variations "such as flow swirl and total pressure distortion which are set-up by the operation of the last stage turbine" are applied to any exhaust hood simulation.

The literature indicates that the following features are the most influential (first order effects) in generating a representative hood flow structure:

1. Total pressure distribution downstream of the turbine

2. Swirl angle distribution

3. Rotor tip leakage jet

2.5.1   Pressure Distribution Downstream of the Turbine

The total pressure distribution at inlet to the exhaust hood has been shown by Fu et al. [18] to have a significant influence on the flow structure and vortex formation in the exhaust diffuser. Ideally, the total pressure distribution downstream of the LSBs would be uniform however, in reality, this is not the case, as shown in the example total pressure distribution (based on data from Beevers et al. [2]) shown in Figure 2.10. A uniform total pressure profile would mean that the leaving energy, which is potentially lost, exiting the last stage turbine blades is at a minimum. As leaving energy is a function of velocity squared ($\frac{1}{2}\rho V^2$), a more uniform outlet velocity profile results in lower V^2 losses as shown in Figure 2.9.

The high total pressure region in the top 5% of the blade span, shown in Figure 2.10, represents the tip leakage jet. The elevated region at the blade hub is due to the tangential lean applied in the blade design process. Liu et al. in 2002 [34] were the first to observed that high pressure region at the hub of the blade has a positive effect on the diffuser performance as it can help suppress the separation region along the bearing cone. Fu and Liu in 2008 [18] carried out an comprehensive evaluation of the effect of the total pressure gradient and magnitude on exhaust hood flows. An adverse pressure gradient, as expected, facilitated bearing cone separation whereas a favourable pressure gradient helped suppress the separation region.

2.5.2   Swirl Angle Distribution Downstream of the Turbine

In 2010, Fu and Liu [19] were confident in concluding that "inlet swirl angle [was] a primary factor governing losses in the exhaust hood." The effect of swirl angle on the pressure recovery of annular diffusers has been widely explored in the works of Kumar et al. and McDonald et al. [38, 31]. Swirl was proven to have a positive effect on the performance of a separated
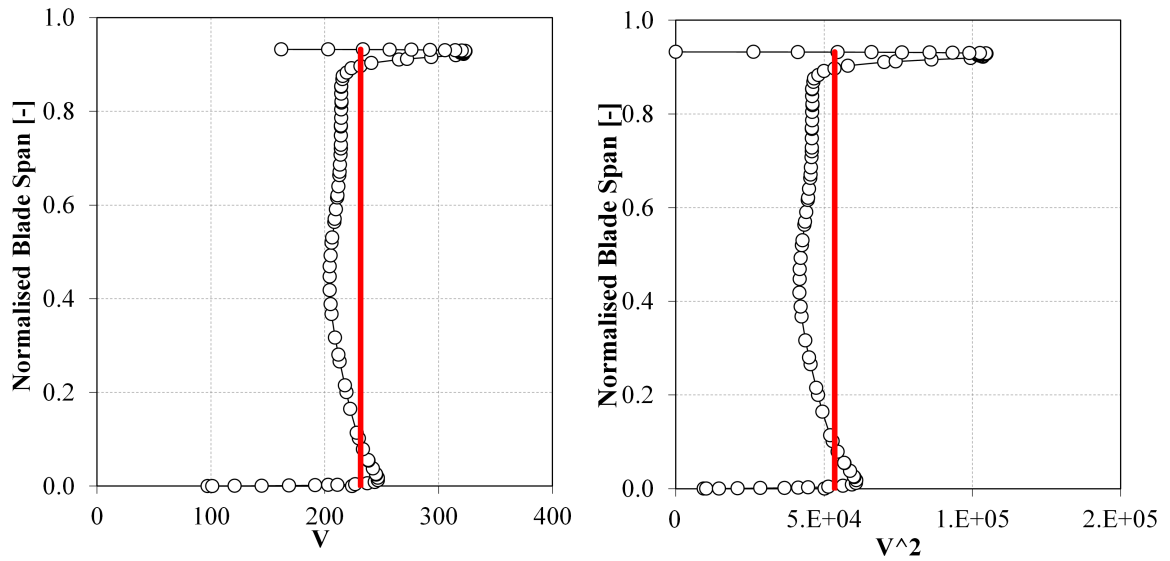
Figure 2.9: V and V^2 Distributions at Last Stage Blade Outlet

diffuser by suppressing the separation, compared with the axial case, however, this positive effect deteriorates at high swirl angles. There has been no comparable research on the effect of swirl angle in axial-radial diffusers, where the effect of flow deceleration due to flow area expansion and streamline curvature are superimposed [43]. Research has shown it is also difficult to translate the early annular diffuser work to the steam turbine exhaust hood, due to the highly non-uniform flow structure downstream of the turbine blade [62]. Typically, swirl downstream of the rotor should be small, indicating the turbine has effectively converted the angular momentum of the flow to usable power. Fu and Liu carried out extensive studies [18, 19] on the effect of swirl angle distribution on the separations forming within the exhaust diffuser and concluded that the swirl angle at the hub has the greatest influence on losses. A high swirl angle at the hub of the blade facilitates the formation of a large vortex along the bearing cone, reducing the effective area of the diffuser and hindering the pressure recovery potential. Tajc et al. in 2006 [56] noted that although flow swirl can act to stabilise the boundary layer in some regions, high swirl at the hub can cause separation along the bearing cone. Although the flow mechanisms behind this separation were not considered in depth by either researcher, Fan et al. in 2007 [15] attributed this to the tangential component of velocity acting against the curvature of the bearing cone.

2.5.3 Tip Leakage Jet

Analysis of a range of studies by Musch et al. [43] have lead to the conclusion that the "main effects (first order effects) on the diffuser flow field are the tip jet and the swirl of the last stage." Benim et al. was one of the first researchers in 1995 [3] to acknowledge the favourable effect that the rotor tip leakage jet has on the boundary layer along the flow guide in the exhaust hood. This has since been investigated in a variety of published work [56, 27, 16]. The rotor tip typically has a shrouded cover with a seal segment on top. The jet which results
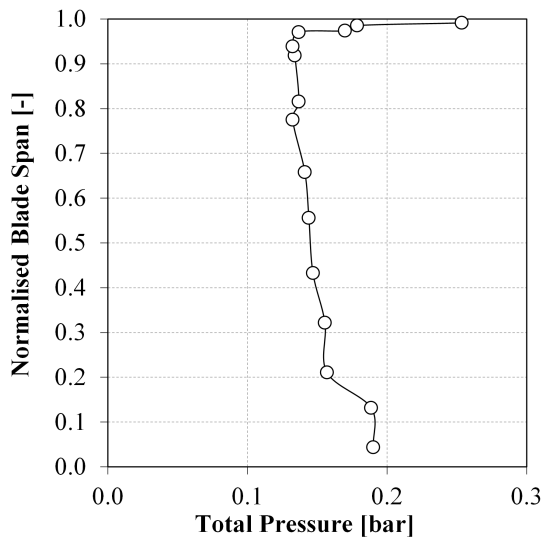
Figure 2.10: P_t Distribution at LSB Outlet from Beevers et al. [2]
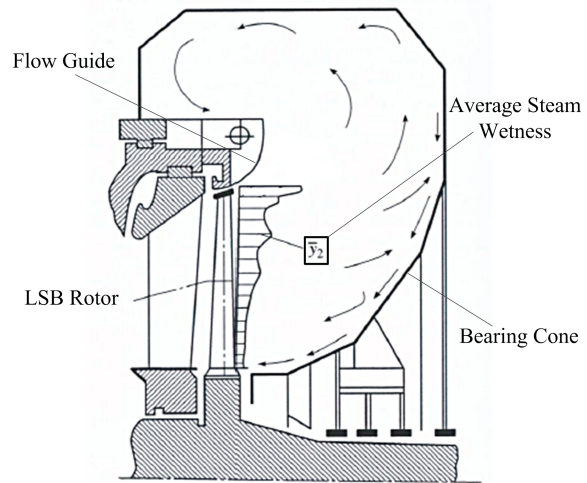
Figure 2.11: Diagram of Wetness Distribution at LSB Exit from Kasilov et al. [29]

from the seal clearance gives kinetic energy to the flow near the flow guide wall helping to prevent flow separation [40]. Experimental work by Tajc et al. in 2006 and 2009 [56, 27] successfully suppressed the separation along the flow guide, and reduced losses by up to 20% by using a synthetic jet to tangentially blow in steam, simulating the tip jet.

The high adverse pressure gradient in the flow guide region can lead to flow separation but the leakage jet adds momentum to the boundary layer suppressing or reducing the separation region. The separation point was shown by Finzel et al. in 2011 [16] to move further downstream with increasing jet strength until completely suppressed.

Despite the widely accepted positives of the tip leakage jet on the diffuser flow field, there are also disadvantages. The presence of the tip jet results in turbine leakage losses and a lower turbine efficiency; an effect which increases with increased jet strength [16]. Maier and Wachter in 1988 [37] studied the effect of the unsteady shock induced separations which can form at the flow guide as a result of the supersonic tip jet. The self-excited nature of this effect within the diffuser was found to induce potentially dangerous oscillations in the rotor blade itself.

2.5.4   Wetness Effects

The expansion of steam through a steam turbine LP cylinder rear stages, and the associated enthalpy decrease, leads to steam becoming wet in the latter turbine stages. Flow exiting the LSBs typically has a moisture content of 6-14% [29] which decreases the sound velocity and changes Mach number which dictates the flow patterns in the supersonic and transonic flow observed in a steam turbine. The spontaneous formation of condensation when steam is in a non-equilibrium state affects the incident angle of the flow and influences the flow structure in the exhaust hood. Within the hood casing, the distribution of large moisture

droplets is highly non-uniform both along the hood inlet and throughout the casing, shown in Figure 2.11, due to the high flow swirl and boundary layers at the casing walls. The droplet distribution is also stratified due to the high circumferential forces from the turbine rotation.

Despite the wide acceptance that wetness in steam turbines of nuclear and thermal power stations affects both efficiency and reliability, there is very little published work on the effect of wetness on LP exhaust hoods. Hood wetness research is restricted by the difficulty in obtaining reliable field data [29] and the effects are at present primarily studied using test facilities with custom instrumentation for wet steam flow measurements and computational models. Early experimental results showed an increase in hood losses with increased wetness at turbine inlet [69]. Later research corroborated this claim with scaled experimental test models, and developed correction factors for the exhaust hood total pressure loss coefficient to account for the effect of wetness [29]. It was also found that the wetness effect is dependent on the performance of the exhaust hood itself. For high performance exhaust hoods $(1 > C_p > 0)$ the effect of wetness on hood losses was greater than for a poor performance exhaust hood $(C_p < 0)$. It is advised that improving the aerodynamic performance of the poorly performing exhaust hoods should be the priority, and that investigating the effect of wetness should only be attempted for high performance hoods [29].

With the high expense of experimental wet steam studies, recent research by Tanuma et al. [57] has shown that test data can be reliably reproduced using computational models, integrating mathematical models for non-equilibrium condensation into 3D unsteady CFD codes. The computational results revealed that in the large vortex structures formed along the flow guide, the wetness decreases due to the entropy generated by the separation. Further research by the same authors [58] has shown that increasing the percentage inlet wetness from 3.5% to 8.2% effects both the size and circumferential distribution of the vortices within the hood. This echoes findings from Fu et al. in 2010 [19], studying the effect of two-phase wet steam by modelling its thermodynamic properties using the Redlich-Kwong equation. The flow guide tip vortex and additional vortices in the diffuser are shown to be marginally larger when wet steam effects are included under moderate inlet swirl.

A study by Fu and Liu [19] made direct comparison to the perfect gas air model and showed that the pressure recovery coefficient and circumferential non-uniformity predicted with wet steam models are very similar to that in air, across a range of inlet swirl intensities. Although it is acknowledged in many exhaust hood studies that the wet steam flows in the exhaust hood affects the losses; it is generally accepted that the flow structure can be studied using CFD with a "reasonable degree of confidence and with less computational cost on perfect gas models" [51]. Subsequently the majority of studies are carried out "using air or equilibrium wet steam approximations" [58] typically using an ideal gas model with a specific heat ratio (γ) for wet steam [47, 42, 68, 52]. As research on the accurate modelling of wet steam flows is a substantial research area in itself, in exhaust hood flows it "seems to be of secondary order for reasonable flow predictions" [52].

2.5.5   Off-Design Operation

The operating point of a turbine is influenced by two factors related to the flow through the exhaust hood. These are:

1. Flow rate through the system from turbine inlet

2. The condenser pressure at hood outlet

Despite the fact that majority of the time the turbine operates under conditions "quite different from the nominal design point" [52], there has been very little research, until recently, regarding the exhaust hood and turbine performance at off design conditions.

Early experimental studies at a range of flow rates by Stastny et al. [53, 54] showed that the swirl downstream of the turbine blades was dependent upon the volumetric flow rate through the system. At off-design the inlet swirl angle increases and separation regions in the diffuser were shown to expand. Shao et al. [48] explored the effect of running at off-design conditions on a fully coupled exhaust hood and steam turbine system using CFD. As the mass flow rate through the system decreases, the power output of the turbine decreases. The static pressure recovery performance of the exhaust hood also decreases because of growth of vortices within the diffuser at low flow rates. At very low volume flows (less than 20% of nominal operating mass flow rate), the reaction at the root of the rotor blade can be negative and the turbine operates under the windage condition which could potentially introduce damaging asynchronous blade loading [48]. However, in this study, the use of the mixing plane approach means that the effect of the circumferential flow asymmetry was not taken into account. A full unsteady computation by Megerle et al. [39] found that at low volume flows during start up, the observed rotating instabilities were analogous to rotating stall found in axial compressors. The importance of CFD calculation methodology when computing off design conditions was highlighted by Stanciu et al. [51] as large discrepancies in the predicted turbine efficiency between methods was found when using full unsteady, frozen rotor and mixing plane interface treatment between rotor and exhaust hood. This was discussed in Section 2.3.2.

Although the inflow conditions to the turbine are fixed by the plant operation, condenser pressure varies seasonally due to atmospheric and/or sea water temperature variations leading to changes in both efficiency and mass flow rate through the LSBs. This annual variation has been shown to be as large as 0.2 bar (from 0.23 bar to 0.52 bar) for a sea water cooled plant in Finland [45]. At present, only one study exists exploring the effect of condenser pressure variation on exhaust hood flows. Stanciu et al. [52] noted that large, potentially unsafe vibrations in the turbine shaft bearings are present at critical condenser pressures due to a shift in exhaust hood recirculations which drive water films down the bearing cone causing a thermal imbalance in the shaft. This paper revealed that exhaust hood flows can be clearly categorised depending on the condenser operating point. At nominal conditions, the turbine is most efficient and both sub and supersonic flows occur. At lower pressures the recirculations move upstream and the stage is choked. At higher pressures the recirculations

move further upstream until reaching the LSBs. All these studies were carried out at uniform outlet pressures and no account was taken of the large pressure gradient which in reality occurs in water cooled steam turbine condensers.

It is anticipated that off-design studies, particularly at low mass flow rates, will become more prominent as the need for a more flexible plant operation is required with the rise of renewable energy production.

2.6   Influence of the Exhaust Hood Geometry

As early as 1990 the sensitivity of the exhaust hood performance to the size of the exhaust, the length and shape of the diffuser and the nature of the internal reinforcing elements was acknowledged [44]. Early diffuser geometry studies focused on a single component, comparing the relative performance of two individual designs [61, 34]. With the improvement in the accuracy of numerical simulations, since 2003, geometry studies have become more detailed, with optimisations of a single component for a given performance variable, typically loss coefficient, widely adopted [30, 66, 42, 68]. Tajc et al. [55] made the important observation in 2001 that "flow in all parts [is] mutually interdependent" and that "making one part of the hood work more effectively may cause another segment to be less effective." In the last five years there has been an increase in the number of integrated studies, comparing the effect of multiple geometry changes on the exhaust hood performance [15, 27, 16].

The current knowledge indicates that the following variables have the largest influence on loss coefficient:

1. Flow guide and bearing cone geometry

2. Diffuser divergence ratio

3. Axial length of the diffuser

4. Change in area from inlet to the half-joint plane

2.6.1   Flow Guide and Bearing Cone Geometry

The first comprehensive flow guide study was carried out by Tindell et al. in 1996 [61], comparing the relative merits of two flow guide geometries. A shorter flow guide was found to have a positive impact on pressure recovery, as a reduction in diffuser performance was outweighed by an improvement in mixing from an increased flow area, from the diffuser into the hood. Seven years later, Liu et al. [36] considered the benefits of locally trimming an axisymmetric diffuser and concluded that trimming the flow guide reduced the blockage caused by the separation in the diffuser, reducing flow acceleration and subsequently improving pressure recovery. Yoon et al. in 2011 [68] conducted a full numerical study with a range of asymmetric cut-backs and found locally trimming the flow guide to accommodate mechanical struts and to increase the flow area in the top of a retrofit exhaust hood, enhanced performance.
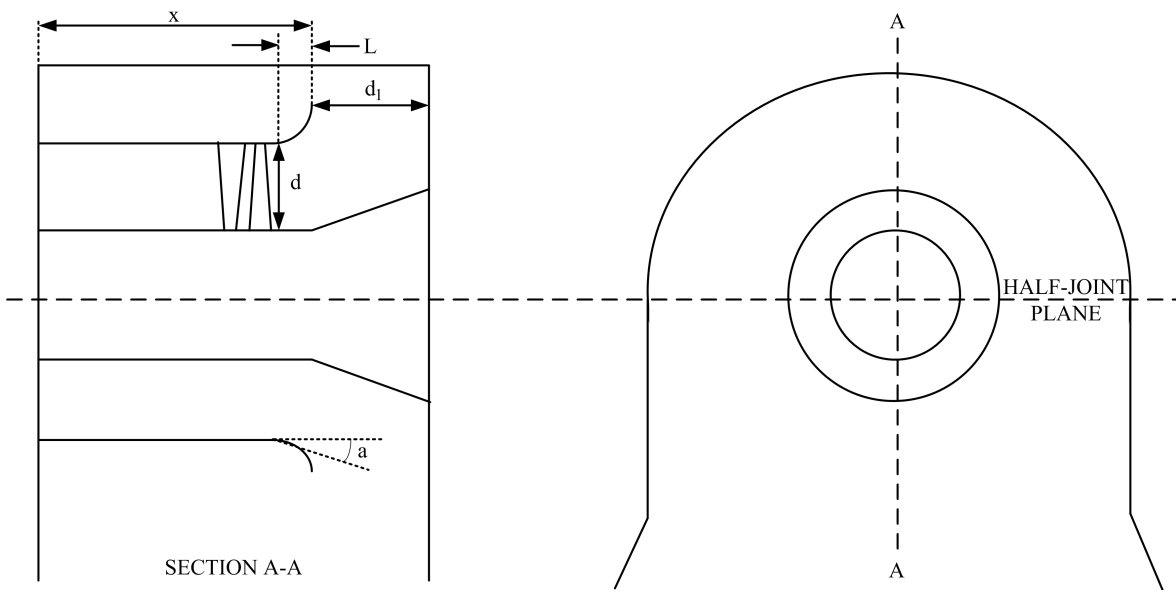
Figure 2.12: Diagram of the Influential Geometric Features of the Exhaust Hood

Mizumi and Ishibashi in 2013 [40] found that the highest vorticity flow was located in the upper exhaust hood and isolating this flow with a novel, double flow guide design as it is guided downstream, led to an increase in pressure recovery.

The shape of the flow guide as well as its length is highly influential on the pressure recovery in the diffuser. Kreitmeier and Greim [30] described controlling the kink angle along the flow guide is of "extreme importance", as a sharp kink angle can facilitate separation. A comprehensive geometric study by Fan et al. [15] using the Taguchi methodology found statistically the expansion (kink) angle at the inner annulus of the diffuser, a in Figure 2.12, to have the most significant influence on diffuser pressure recovery. A diffuser constructed of a series of kinks is easier to manufacture and such a design is common industry. Wang et al., Yoon et al. and Musch et al. [66, 68, 42] have carried out successful shape optimisation on the flow guide geometry, leading to an increase in the pressure recovery within the diffuser by as much as 0.3 by reducing the blockage effect.

2.6.2   Diffuser Geometry

An experimental diffuser geometry study in 2011 by Finzel et al. [16] compared two diffusers of different axial length, and found a longer diffuser resulted in a higher pressure recovery as the flow expansion takes places through a less acute angle, reducing the adverse pressure gradient which encourages separation along the flow guide. Fan et al. [15] statistically argued that the axial length of the diffuser, L in Fig. 2.12 has the second largest influence on pressure recovery, behind the expansion angle of the flow guide.

A geometric study by Hoznedl et al. [27] highlighted dependence of pressure recovery on diffuser divergence ratio, $\frac{d_1}{d}$, found to be optimum at 1.4. A divergence ratio which is too large or too small results in separations which hinder pressure recovery. Hoznedl et al. also found the relative position of the casing with respect to the diffuser, $\frac{x+L}{d}$, to influence
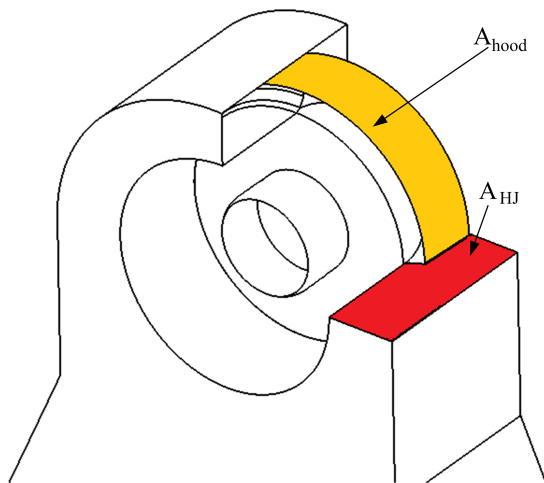
Figure 2.13: Diagram of Hood Area (A_{hood}) and Half-Joint Area (A_{HJ})
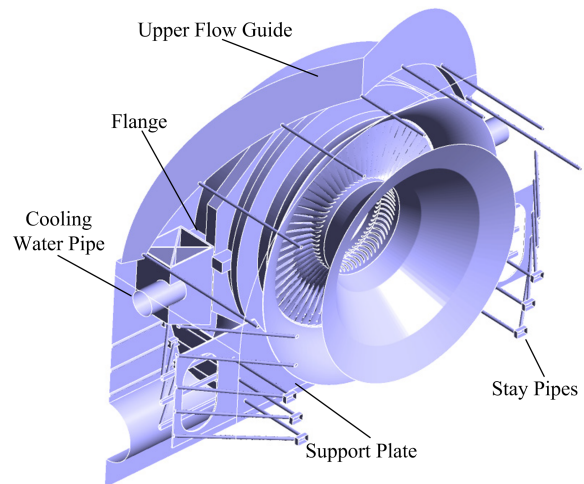
Figure 2.14: Typical Internal Furniture in the Exhaust Hood from Li et al. [32]

pressure recovery, with larger losses when the outer casing is closer to the diffuser.

2.6.3   Change in Cross Sectional Area with Progression Downstream

Liu and Hynes in 2002 [34] compared the two hood geometries, one with a gradually increasing cross sectional area down to the half-joint plane and one which remained constant . The latter, resulted in flow acceleration and a subsequent pressure drop through the exhaust hood and a decreased pressure recovery. This was corroborated by Finzel et al. [16], showing an increased area at the half-joint plane, shown in Figure 2.13, improved the pressure recovery in the diffuser. This highly influential geometric variable and was also shown to be almost independent of the diffuser geometry.

Pressure recovery was shown by Finzel et al. [16] to be relatively insensitive to hood area, A_{hood} in Figure 2.13, when the area was above a critical value. Yoon et al. [68] attributed this to restriction of the flow in the upper hood, resulting in more mixing loss and a reduced pressure recovery.

2.6.4   Internal Furniture

One simplification, common in the vast majority of both numerical and experimental exhaust hood studies, is to neglect the hood internal reinforcements. With the high capital costs of producing the large exhaust hood geometries, the tendency is to restrict their size and reinforce with supporting elements [44], such as struts, baffles and flanges to maintain the structural integrity of the hood, as in the example in Figure 2.14. Although it is widely acknowledged that each structural reinforcement contributes to the loss in the hood due to flow blockage, almost all researchers using CFD models choose to examine the flow structure in an "empty" casing, free of all internal geometry, due to the increased computational power requirement to model them.

Under the bearing cone there are usually 2-4 support plates which affect the flow field, with the flow guide reinforced by multiple supports. The lower exhaust hood is subdivided into a series of smaller paths by various reinforcing plates, which are typically not designed for optimum aerodynamics [40]. At the inlet to the condenser and within the condenser neck there are various structural reinforcements as well as feed-water heaters and extraction pipes [44]. Neglecting these elements contributes to discrepancies between field data and experimental [54].

Tajc et al. in 2007 [56] carried out one of the few internal geometry studies and found "internal reinforcements considerably influence the loss coefficient" and "even minimal reinforcements increase losses by 15%" compared with an empty casing. An annular diffuser study by Fric et al. [17] found losses can be reduced by strut shape optimisation for a range of load conditions. Increasingly, minimal internal reinforcements are being included in simulations as computational power increases [64, 33, 41, 40].

2.6.5   Insensitivities

Although the pressure recovery has been shown to be highly dependent on certain geometric parameters, there are regions which have been shown to be relatively insensitive. Hoznedl et al. [27] showed loss to be insensitive to the extent the front wall is extended, which is advantageous as this can be designed with ease of accessibility to the bearing cover with minimal aerodynamic penalties. Fan et al. [15] corroborated the insensitivity in this region, observing that the radius of the inner annulus of the diffuser to have little impact on loss.

Finzel et al. [16] investigated the position at which steam enters the hood, either from the top, sides, or current standard position and all were shown to have little influence on loss
.

2.7   Conclusions

The literature has highlighted that it is critically important to model the radial flow variations downstream of the turbine blade at inlet to an exhaust hood simulation, whether experimental or computational. Of the flow properties, the total pressure and swirl angle distributions exiting the turbine, in particular, have been highlighted as of paramount importance to capture accurately. In addition, the rotor tip leakage jet should be simulated in order to generate a representative pressure distribution along the flow guide wall, as significant performance improvements have been predicted with the jet modelled. As a bare minimum, these three factors can be considered of first order importance in exhaust hood simulations.

The circumferential variation in flow properties experienced by the turbine due to the non-axisymmetric exhaust hood geometry is increasingly considered vital to accurately model, typically by means of frozen rotor or full unsteady interface between rotor and exhaust hood in a CFD calculation. However, despite wide acceptance in the literature of the importance of the circumferential non-uniformity, the magnitude of its influence on exhaust hood flows has yet to be quantified.

With the rise in computational power, full unsteady CFD simulations are becoming increasingly common. Similarly, CFD modelling of two-phase wet steam is more frequent, however studies have shown that accurate results can be achieved using ideal gas approximations. Turbulence model studies have also shown little difference in predicted flow structure or loss coefficient. Hence, full unsteady, wet steam and high order turbulence models should be considered, at present, of secondary importance in exhaust hood CFD simulations.

Experimental and computational geometric studies have highlighted a set of parameters which are known to have the most significant influence on exhaust hood pressure recovery: primarily the shape, length and area ratios of the diffusing region of the hood casing. The internal furniture within the exhaust hood has been widely shown to have a significant influence on loss and with increasing computational power, studies with minimal reinforcements are becoming more common. However, the high cell counts required to accurately resolve the boundary layer on each reinforcing element are still prohibitively high and hence modelling internal reinforcements should be considered of second order importance compared to accurate modelling of the turbine.

With a wide variety of computational modelling approaches currently simultaneously in use by researchers, there is currently no 'best-practice' recommendations for modelling exhaust hood flows.

Findings from this literature review provides scope for the following areas of research:

1. A open-source design for an exhaust hood geometry encapsulating the primary geometric features based on current recommendations

2. Evaluation of the effect of modelling the hood inlet circumferential asymmetry

3. Providing a set of guidelines for CFD modelling of exhaust hoods

4. Explore current trend for studies at off-design conditions

3

Development of the Durham Last Stage Blade and Exhaust Hood Test Case

3.1 Introduction

Low pressure steam turbine last stage blading and exhaust hood geometries are highly commercially sensitive, with each manufacturers' designs typically kept secret and protected by commercial IP. As such, the literature review has highlighted an absence of any freely available detailed geometries and test data for LP last stage blades or accompanying exhaust hoods.

Representative profiles of velocity, swirl and pitch angle at the outlet from the LSB are included in some published work [21, 71] but are insufficient to fully define an inlet boundary condition to an exhaust hood CFD calculation. Profiles typical of current industrial blading are either plotted on a graph without a scale [2] or normalised by an undefined quantity [56].

Exhaust hood designs, including some dimensions, are available in the literature [61, 67, 66, 15, 70] but are all insufficiently detailed to be able to recreate the design in CAD.

To address this, this chapter includes a proposed design for a generic, IP restriction free, low pressure steam turbine LSB and accompanying exhaust hood. The steps taken to produce these designs are described below.

3.2 Generation of a Generic Last Stage Blade

A generic last stage blade was generated in conjunction with Alstom Power in Rugby, Warwickshire, known as the *Durham Stage Test Case* (DSTC). The blade design originated from a 20 year old, 50Hz, last stage stator and rotor, which, although no longer in use, is still protected by Alstom IP. This original design is denoted as the *baseline* blade throughout this chapter. Using Alstom's in-house design tools, the original blade was sufficiently modified to remove IP restrictions on the geometry and also to ensure that the outlet flow field and efficiency were in line with modern blading. The primary objective of the DSTC design was to produce representative inlet flow boundary conditions to a modern exhaust hood calculation. As such, modifications were made focusing purely on the aerodynamics of the blade, and not the mechanical design and structural integrity. The blade in its current form could not be used in a real turbine but is aerodynamically representative of modern designs.

The focuses of the aerodynamic design exercise include:

- Improving uniformity of the static pressure distributions at the rotor exit

- Reducing the elevated outlet total pressure at the hub of the rotor

- Reducing the stator losses

- Improving blade efficiency

Geometry modifications were made manually on individual, stacked blade sections using in-house blade design software. Each design iteration was rapidly analysed using the blade to blade solver, MISES, where S1 stream-surface calculations computed the Mach number distributions, stream-tube thickness and profile losses for a given blade section on a specified blade. At the end of each phase of the design process, the optimum design iteration predicted by the blade to blade solver was input into the custom in-house 3D CFD multi-stage flow solver for axial flow turbomachines for further analysis, before proceeding with the next step of the design phase.

3.2.1   Fixed Blade Modifications

Modifications were initially made to the fixed blade. The blade was subdivided into three equally spaced sections, at the tip, midspan and hub, and modifications were made on each span-wise profile individually.

Typically, the design of older blades tended to focus more on the mechanical integrity and manufacturability of the blade rather than the aerodynamics. As such, the back surface deflection angle (BSDA) tends to be larger than modern blading by around 10°. This adds a greater curvature to the blade to offer greater resistance against axial loading. However, with the progression of material science and the subsequent improved strength of modern blading, it is desirable to reduce the BSDA to control the acceleration on the suction surface of the blade. This reduces the Mach number on the suction surface to closer in line with that of the suction side, reducing the strength of the shock structure (and associated shock losses) formed at the trailing edge when the two flow streams combine, as shown in the diagram in Figure 3.1.

Additionally, a larger BSDA can lead to separations at the trailing edge of the suction surface of the blade due to the increased adverse pressure gradient in this region. Flattening the BSDA can suppress these separations, contributing to an improved fixed blade efficiency. To assess the magnitude of separation the shape factor, H, was calculated, Equation 3.1.

$$H = \frac{d^*}{\theta} \tag{3.1}$$

where d^* is the displacement thickness and θ is the momentum thickness. From industrial cascade tests, flat plate experiments and experience, the recommended maximum shape factor is 1.9. By reducing the back surface deflection angle, the primary aim was to reduce the shape

factor for each of the three stator sections to below this level. This was carried out iteratively for each of the three blade sections.

Figure 3.2 shows the hub blade profile (in black) for the baseline blade on the left and the modified blade on the right. The streamlines are over the blade are shown as red lines, indicating a separation at the trailing edge of the baseline blade. For each reduction in back surface deflection angle, the software automatically increased the axial chord of the blade to maintain the same curvature of the original blade. Due to the high sensitivity of blades to chord/pitch ratio, it was important to maintain the same axial chord compared with baseline design. This was done by manually scaling the blade with each BSDA reduction to ensure the same axial chord, which led to an increased blade chord in the modified blade in Figure 3.2. However, with large reductions in BSDA it was not possible to scale the blade sufficiently to maintain the same axial chord whilst eliminating the stator trailing edge separation. With this restriction, the minimum achievable back surface deflection angle at the blade hub was 6°, giving a shape factor of 2.576, above the recommended 1.9, shown in Figure 3.2. However, this still provided a significant reduction in the separation region compared with the baseline blade and was carried forward to the final design.

The suppression of the separations by reducing the BSDA significantly increased the fixed blade efficiency relative to the baseline blade. However, the rotor root reaction reduced by 8% and the mass flow rate through the stage increased relative to the baseline as the stator flow passage area has increased as a result of the reduction in BSDA, as shown in Figure 3.3 and 3.4.

To make valid comparisons between design iterations, it was important to maintain a consistent mass flow rate throughout the design process. Increasing the stagger angle of the blade to close up the blade passage, decreased the mass flow rate back to within 1% of the baseline blade.

In addition, the modifications to the stator lowered the root reaction. The change in throat width compared with the baseline blade is larger at the root than at the tip, resulting in non-linear change in reaction along the blade span. It is desirable to keep the root reaction in line with the design conditions as a low root reaction may result in negative reaction at low exit static pressures (i.e. cold days) and a subsequent separation at the root. If the root reaction is too high, the pressure drop increases, resulting in a higher Mach number and the blade may reach limit loading sooner.

Two options were considered for raising the root reaction of the blade; addition of tangential lean on the stator and re-staggering the blade. Tangential lean is a simple method of raising the root reaction, but as the body forces are redistributed, forcing the flow down towards the root of the blade, the leaving energy tends to increase because of the existing high velocity in this region. Re-stagger has a less detrimental effect on leaving energy but as the inlet angle to the rotor changes, separation can be introduced on the leading edge of the moving blade because of its high incidence sensitivity. To evaluate the two approaches; +10° and +5° of tangential lean were added to the stator. Re-stagger was added by twisting the root section of the stator by -0.5° and the tip by +0.5°.

Common Pt and V

SHOCK

STRONGER SHOCK

M_1

$M_2 >> M_1$

LARGE BACK SURFACE DEFLECTION ANGLE

Common Pt and V

SHOCK

WEAKER SHOCK

M_1

$M_2 \approx M_1$

SMALL BACK SURFACE DEFLECTION ANGLE
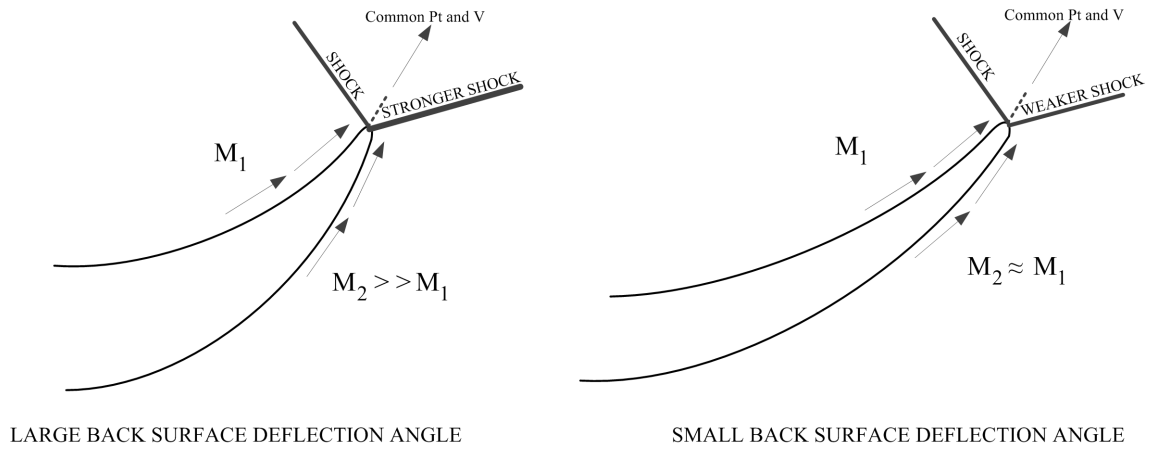
Figure 3.1: Influence of BSDA On Shock Structure at Trailing Edge

Shape Factor: 19.149

Shape Factor: 2.576
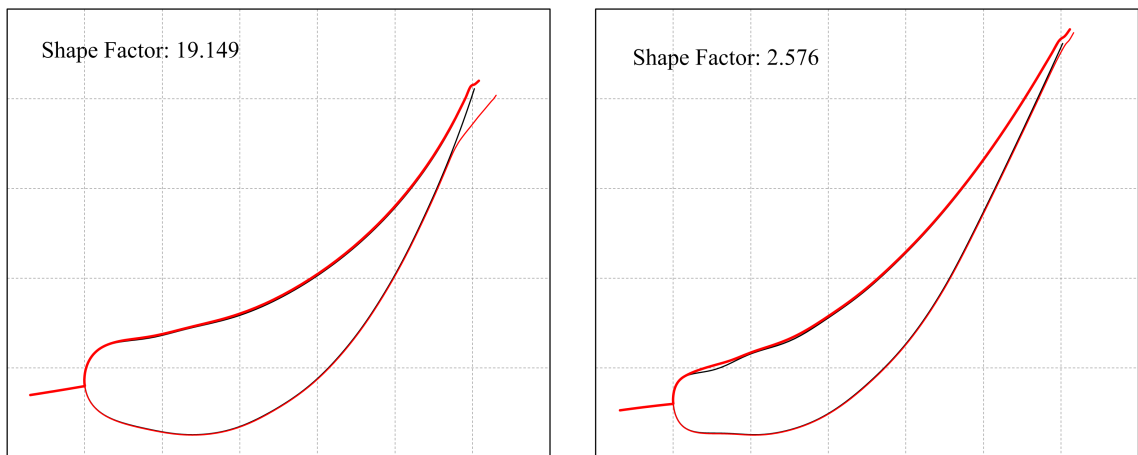
Figure 3.2: Streamlines of Separations at the Stator Hub on Baseline (left) and Modified (right) Blades

Both approaches successfully raised the root reaction, shown in Figure 3.5, but the effect of re-stagger was marginal. Adding +10° of lean gave the best blade efficiency, but the leaving energy was significantly increased which it is important to minimise, Figure 3.6. The root reaction also increased to 35%, which is likely to cause the blade to reach limit loading prematurely, Figure 3.5. Application of +5° of lean offered the best compromise between raising the root reaction and minimising the increase in leaving energy.

The corresponding higher stator hub velocity leads to a higher velocity at inlet to the rotor. This decreases the swirl angle at inlet to the rotor which has the desirable effect of reducing positive incidence, Figure 3.7. High positive incidence may cause a separation to form on the leading edge of the rotor, reducing lift and subsequently blade efficiency. Rotor blades tend to be more resistant to negative incidence as the geometry curvature facilitates flow reattachment.

3.2.2 Moving Blade Modification

Unlike the stator, individual section modifications were not possible with the rotor. Due to the high degree of twist along the blade span, it is highly sensitive to modifications made on a reduced number of sections. As the design exercise was of a short duration, manual modifications on each of the seven sections was not possible given the time scale.

However, improvements were still possible. Examining the rotor geometry with 60 blades per circle, Figure 3.8, revealed that there was a gap between adjacent blades when the rotor row is viewed in the axial direction. Although performance losses associated with this are small, it is generally undesirable to have a region of unguided flow. To address this, the blade count per circle was increased from 60 to 65, closing the gap as shown in Figure 3.8. Although this did not completely eliminate the gap at all blade sections, 65 was the maximum achievable blade count without compromising the rotor root section by creating a divergent passage. It is important that the rotor hub sections remain convergent to decelerate the supersonic inlet flow exiting the fixed blade.

Increasing the blade count decreases both the blade pitch and the throat area. For the same mass flow rate through the stage, this results in a higher static pressure forming on the leading edge of the rotor and the trailing edge of the stator, as in Figure 3.9, a greater heat drop over the rotor stage and a more reactive blade, Figure 3.10.

To reverse the closing up the flow passage, the stagger angle of the rotor blade was reduced. However, with 65 blades per circle it was not possible to obtain the same throat passage area without compromising the convergent passage at the rotor root. A -1.4° stagger (rotation around the centre of gravity) maintained the convergent passage at the hub, and increased the passage area.

3.2.3 Final Blade Design

The final LSB geometry hub, midspan and tip profiles are shown in Figures 3.11, 3.12 and 3.13. Blade data and nominal operating conditions are tabulated in Figure 3.14. The mach
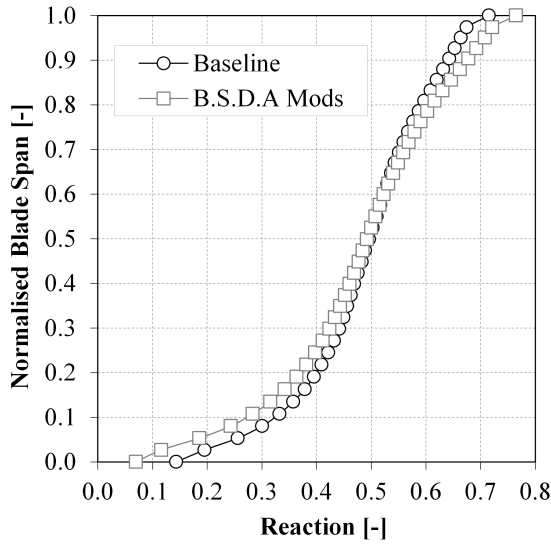
Figure 3.3: Predicted Radial Reaction Distribution for Baseline vs. Modified Blading [-]
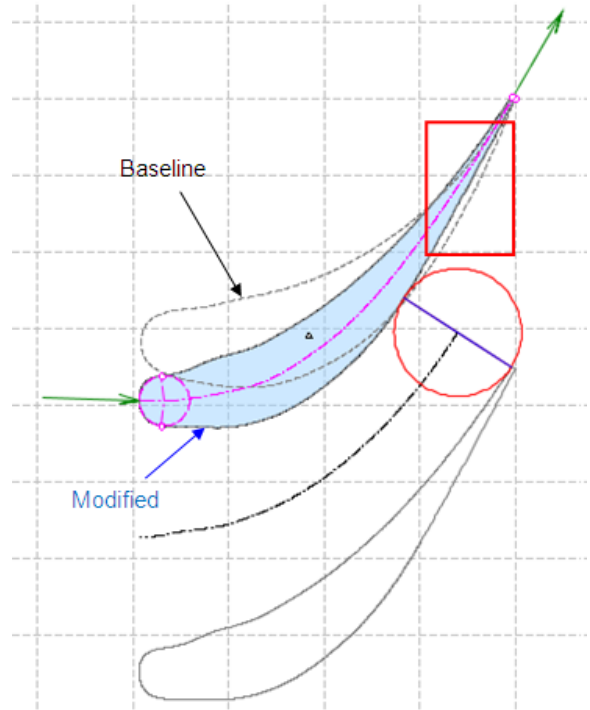
Figure 3.4: Effect of Reducing the BSDA on Stator Hub Geometry
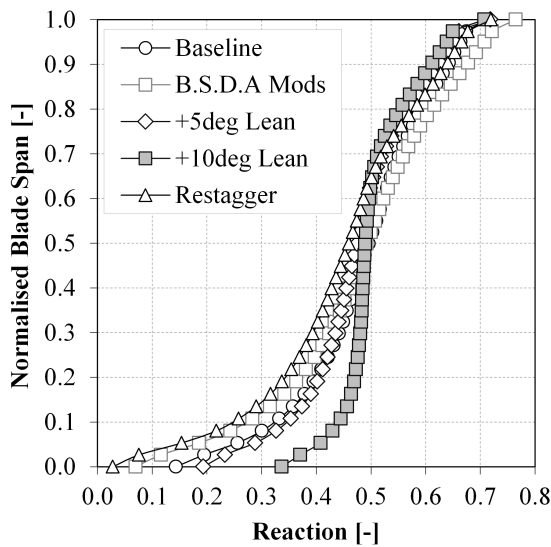
Figure 3.5: Comparing Three Methods of Raising the Predicted Reaction at the Root of the Blade [-]
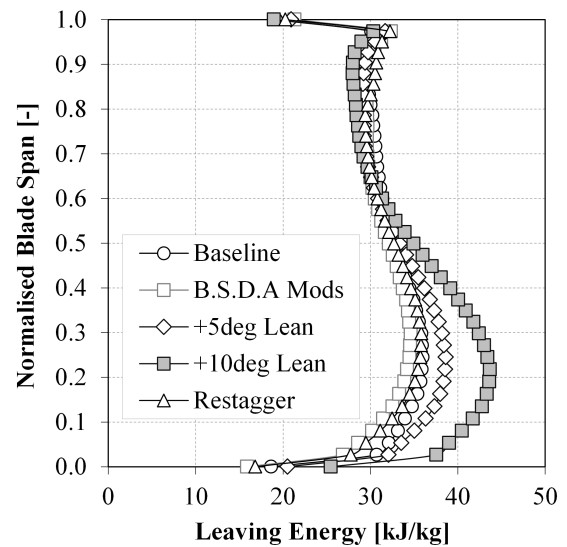
Figure 3.6: Corresponding Predicted Increase in Leaving Energy from Three Methods of Raising Root Reaction [kJ·kg^{-1}]
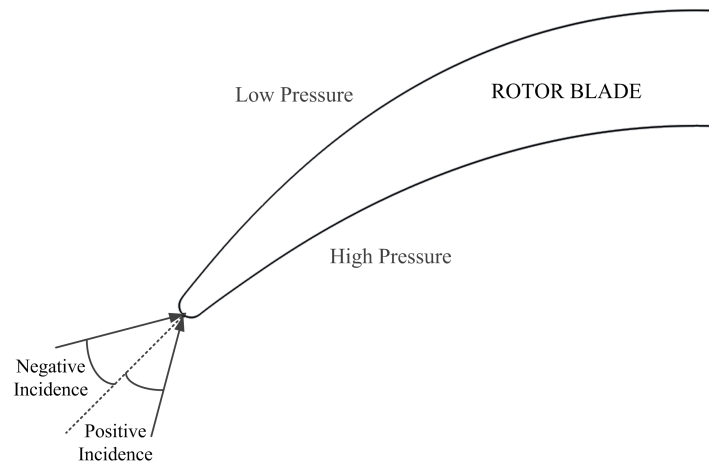
Figure 3.7: Diagram of Rotor Incidence Sensitivity

60 Rotor Blades Per Circle   65 Rotor Blades Per Circle
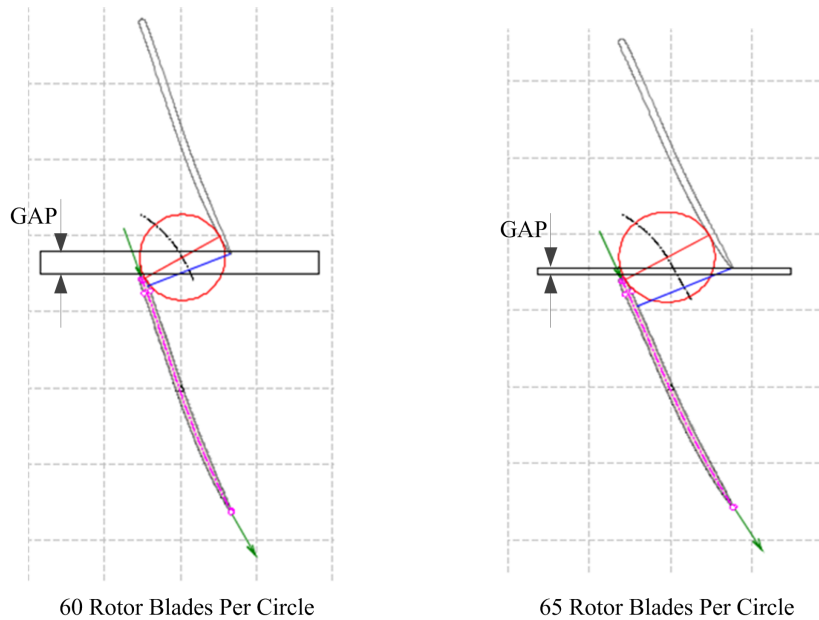
Figure 3.8: Diagram of the Gap Between Adjacent Rotor Blades Dependent Upon the Number of Blades Per Circle

number distributions on the stator and rotor blades at hub, midspan and tip at nominal load are given in Figures 3.15, 3.16, 3.17, 3.18, 3.19 and 3.20.

Compared with the baseline blade at nominal operating conditions of 7500Pa exit static pressure, there is a reduction in fixed blade loss of up to 5%, Figure 3.21, due to suppressing the separations at the trailing edge of the blade when reducing the back surface deflection angle. This should lead to an improved total-static efficiency of the stage, η_{T-S}, Figure 3.22. Although there is a noticeable improvement at the blade midspan, the efficiency is poorer, relative to baseline, at 0.8 fractional height and at the hub. This loss caused by the moving blade, see Figure 3.23.

This high loss at 0.8 fractional height was found only to be evident at static pressures on or below the nominal load. Raising the exit static pressure to 8800Pa eliminated this high loss region, Figure 3.23, and produced a more consistent η_{T-S} along the blade span, Figure 3.25.

Running at the off design condition of 8800Pa outlet pressure is viable, provided the root reaction does not go negative. The application of tangential lean to the fixed blade in the design process raised the root reaction above that of the baseline case, *Durham @ 7500Pa* compared with *Baseline* in Figure 3.26. When running at the off-design condition of 8800Pa, *Durham @ 8800Pa* in Figure 3.26, the root reaction is still positive.

The primary objective of the blade design exercise was to produce a blade which would provide representative inlet boundary conditions to an exhaust hood CFD calculation. It was therefore desirable to generate a uniform static pressure at rotor outlet and reduce the high total pressure at the hub of the blade. Figures 3.27 and 3.28 compare the static and total distributions at rotor outlet of the generic LSB with the baseline. No data is available for the baseline blade at 8800Pa outlet static pressure and therefore comparison can only be made between the shape of the distributions and not their magnitude.

The slight negative static pressure gradient with the baseline blade has been removed in the generic geometry, and the resulting static pressure profile is more uniform. It has not been possible to reduce the high total pressure at the hub of the blade as the application of tangential lean to the stator in the design process drives more flow to the hub of the blade, increasing the total pressure in this region. However, the magnitude of the elevated region remains approximately unchanged from the baseline case. Between 0.3 and 0.9 fractional blade span, the uniformity of the outlet total pressure is improved.

Overall, a LSB design which is representative of current industry practice has been achieved, which produces a exit flow suitable for use as the inlet boundary condition to an exhaust hood CFD calculation.

3.3   Generation of a Generic Exhaust Hood

A generic steam turbine exhaust hood was designed to accompany the LSBs, known as the *Durham Exhaust Diffuser and Hood Test Case* (DEDHTC). The design originated from an amalgamation of existing published designs. The geometry is free of all exhaust hood internal
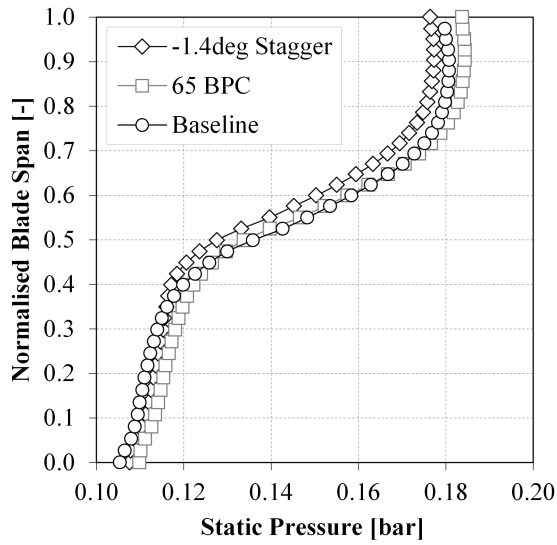
Figure 3.9: P Distribution at the Rotor Leading Edge [bar]
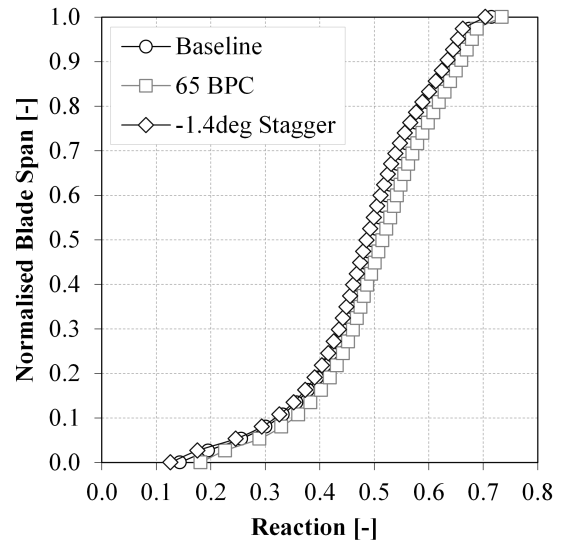
Figure 3.10: Rotor Reaction when Increasing the Blade Count per Circle [-]
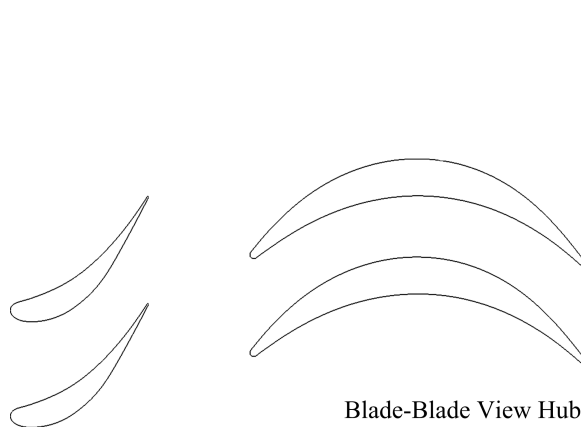
Figure 3.11: DSTC Profiles at Hub
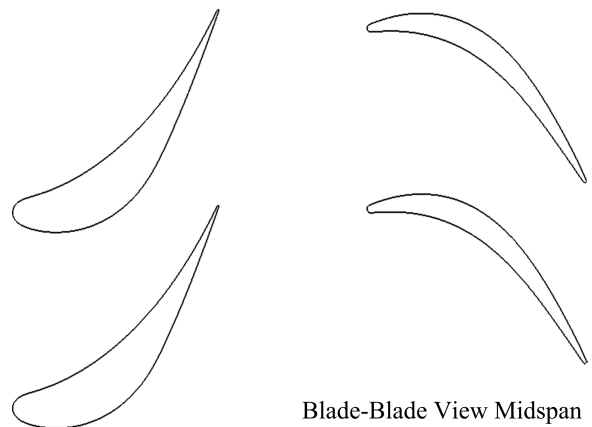
Figure 3.12: DSTC Profiles at Midspan
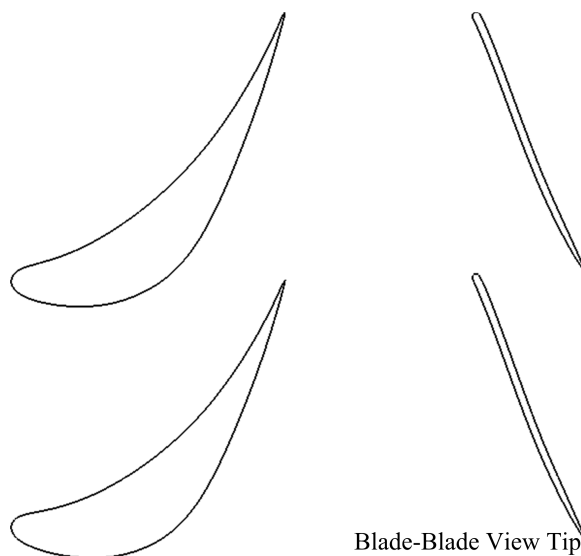
Figure 3.13: DSTC Profiles at Tip

Pressure Ratio	0.292
Mass Flow Rate	88.44 kgs^{-1}
Outlet Mach Number	0.6
Outlet Static Pressure [bar]	0.75

	Stator	Rotor
Blade Count	60	65
RPM	-	3000
Blade Length [m]	0.79	0.92
Hub Diameter [m]	0.77	

Figure 3.14: DSTC Features
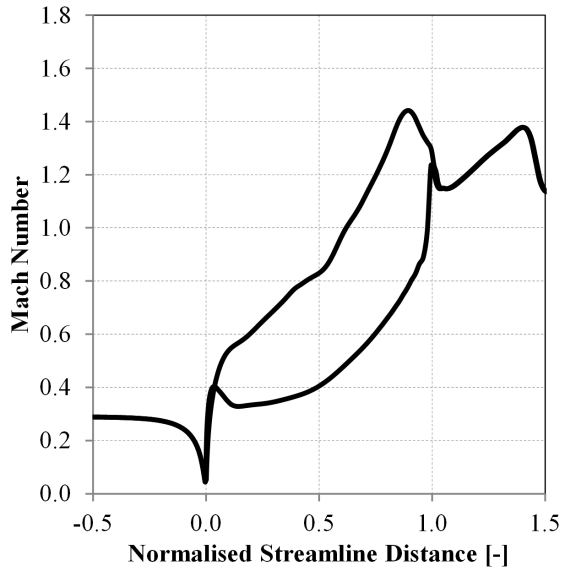
Figure 3.15: Mach Number Distributions at Nominal Load at Stator Blade Hub
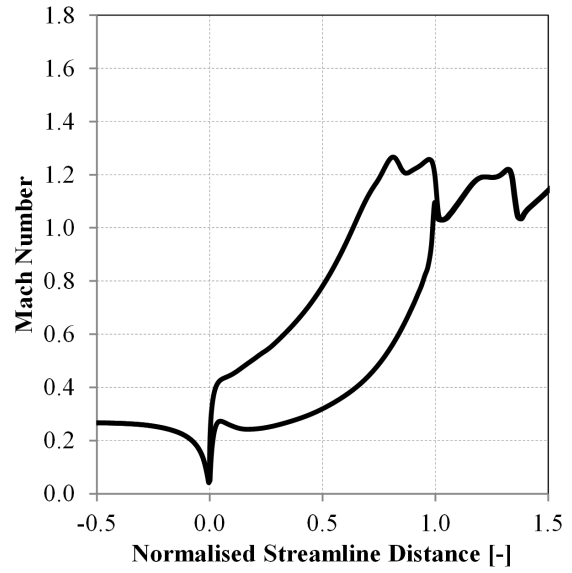
Figure 3.16: Mach Number Distributions at Nominal Load at Stator Blade Midspan
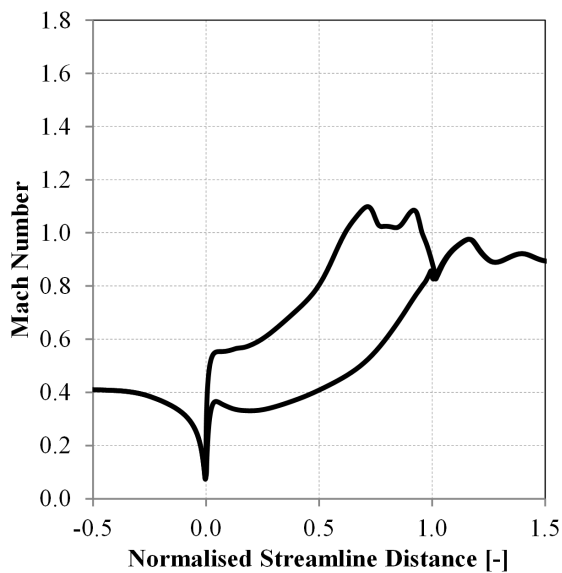
Figure 3.17: Mach Number Distributions at Nominal Load at Stator Blade Tip
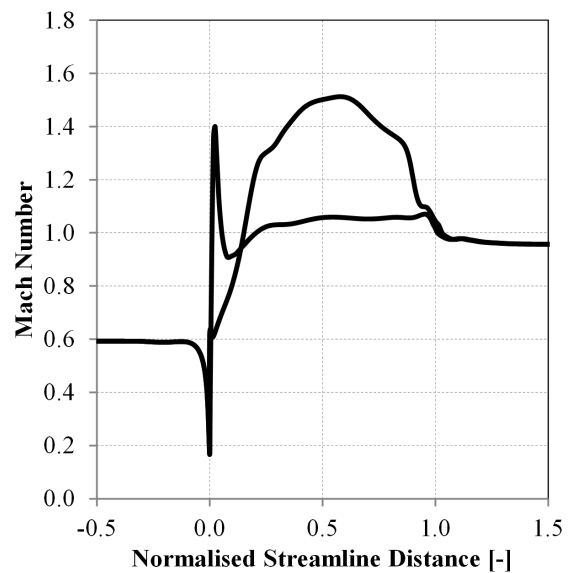
Figure 3.18: Mach Number Distributions at Nominal Load at Rotor Blade Hub
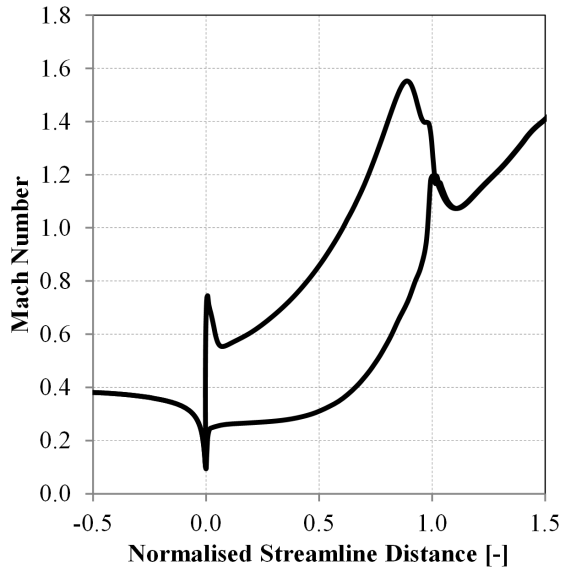
Figure 3.19: Mach Number Distributions at Nominal Load at Rotor Blade Midspan
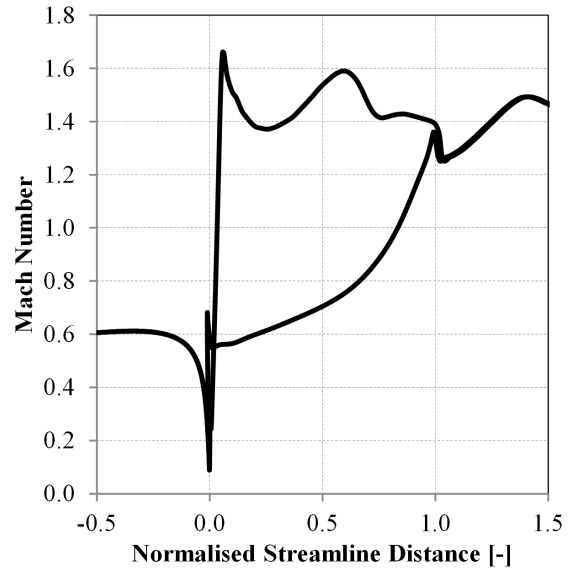
Figure 3.20: Mach Number Distributions at Nominal Load at Rotor Blade Tip
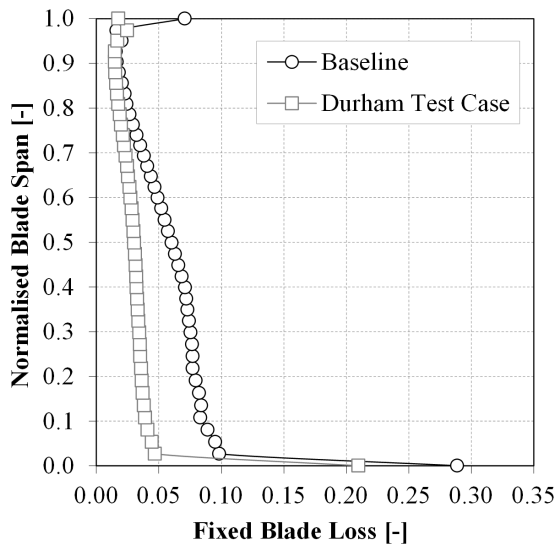
Figure 3.21: Fixed Blade Loss at Nominal Load (Rotor Outlet $P = 7500$Pa) [-]
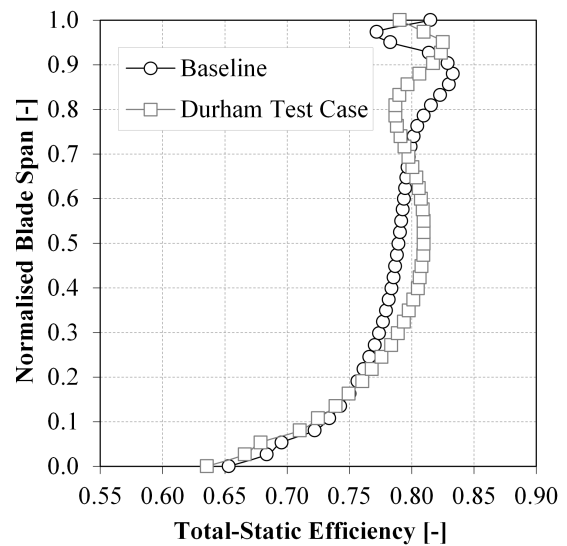
Figure 3.22: η_{T-S} at Nominal Load (Rotor Outlet $P = 7500$Pa) [-]
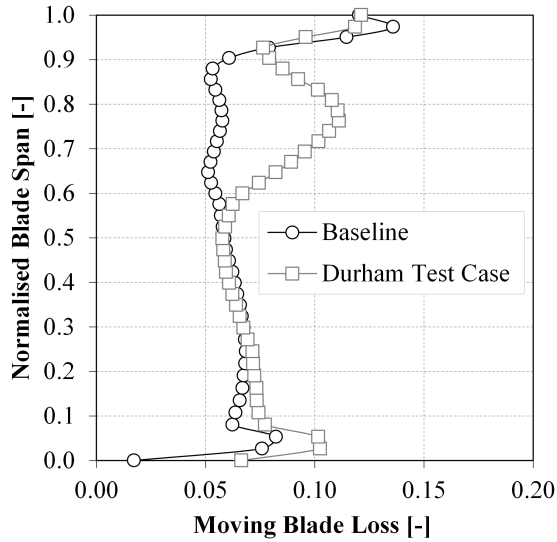
Figure 3.23: Moving Blade Loss at Nominal Load (Rotor Outlet $P = 7500$Pa) [-]
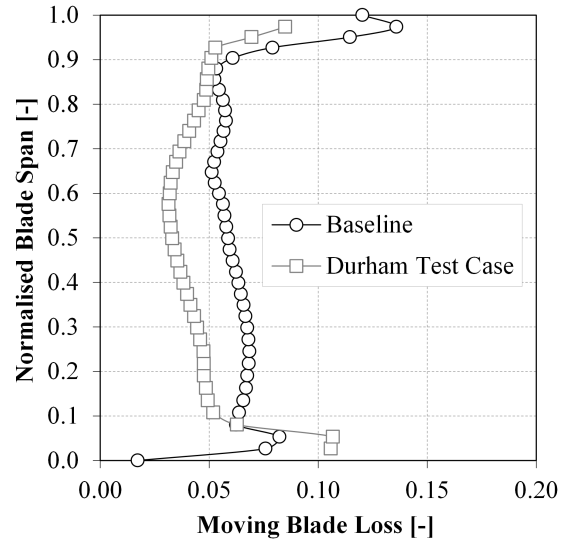
Figure 3.24: Moving Blade Loss at Rotor Outlet $P = 8800$Pa [-]
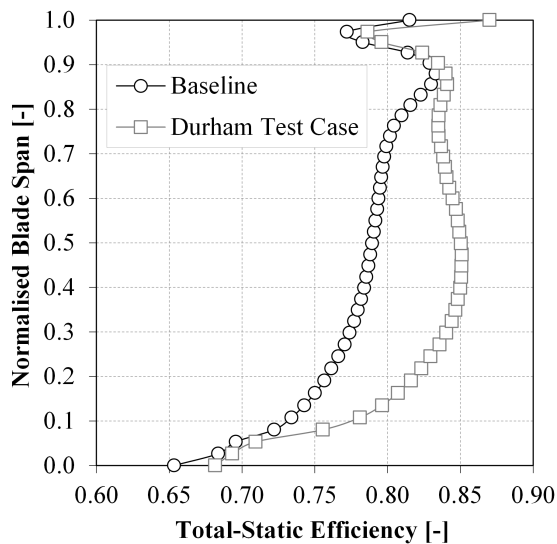
Figure 3.25: η_{T-S} at Rotor Outlet $P = 8800$Pa [-]
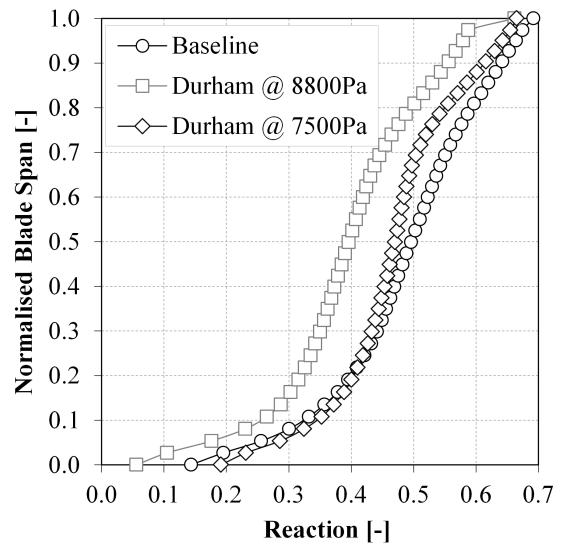
Figure 3.26: The DSTC Predicted Blade Reaction [-]
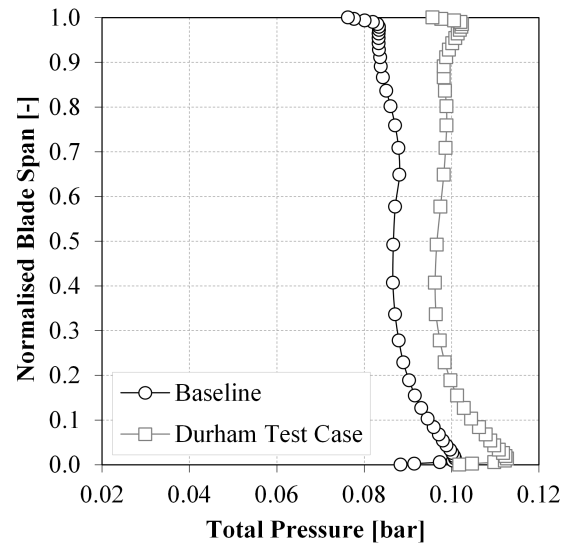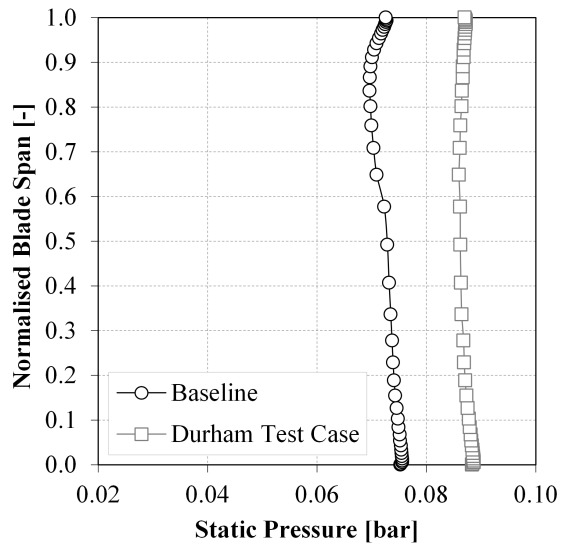
Figure 3.27: P Distribution at Rotor Outlet [bar]

Figure 3.28: P_t Distribution at Rotor Outlet [bar]

furniture, such as struts, baffles and reinforcing elements; a common simplification with the majority of available exhaust hood geometries. These structures are typically specific to the individual exhaust hood and cannot be generalised in a similar manner to the major geometrical parameters.

The design for the DEDHTC started with the definition of the primary governing dimensions, the length of the last stage rotor blade and the corresponding hub to shroud distance. The LSB height was denoted by a vertical line from the rotor hub trailing edge at 0.922m, and this line dictates the exhaust hood inlet boundary.

The LSB geometry from the OEM partner had a corresponding hub and shroud geometry. This hub geometry was extended to form a straight bearing cone, typical in the design published by Yoon et al. [68].

With the bearing cone geometry defined and the location of the exhaust hood inlet specified, it was possible to position the exhaust hood back wall. The ratio of the back wall location to that of the LSB exit, $\frac{L}{d}$, is a vital parameter in industrial exhaust definition. Studies revealed that for straight bearing cones this ratio was typically around 1:1, for curved bearing cones typically larger at 1.5:1. For this generic design an $\frac{L}{d}$ of 1.085:1 was selected, an average of the studied designs.

With the position of the exhaust hood back wall defined, it was possible to specify the depth of the exhaust hood. A study of existing published designs suggested that the ratio of the exhaust hood inlet height to exhaust hood depth, was typically around 3. With the application of this ratio, an exhaust hood depth of 2.59m was selected.

The flow guide geometry was specified by considering the axial and vertical location of the flow guide tip, highlighted by a red cross in Figure 3.29. The axial length of the flow guide is governed by the diffuser divergence ratio $\frac{A_{diffout}}{A_{inlet}}$, where the diffuser outlet area ($A_{diffout}$) can be translated into an axial distance between hood back wall and the flow guide tip, D,
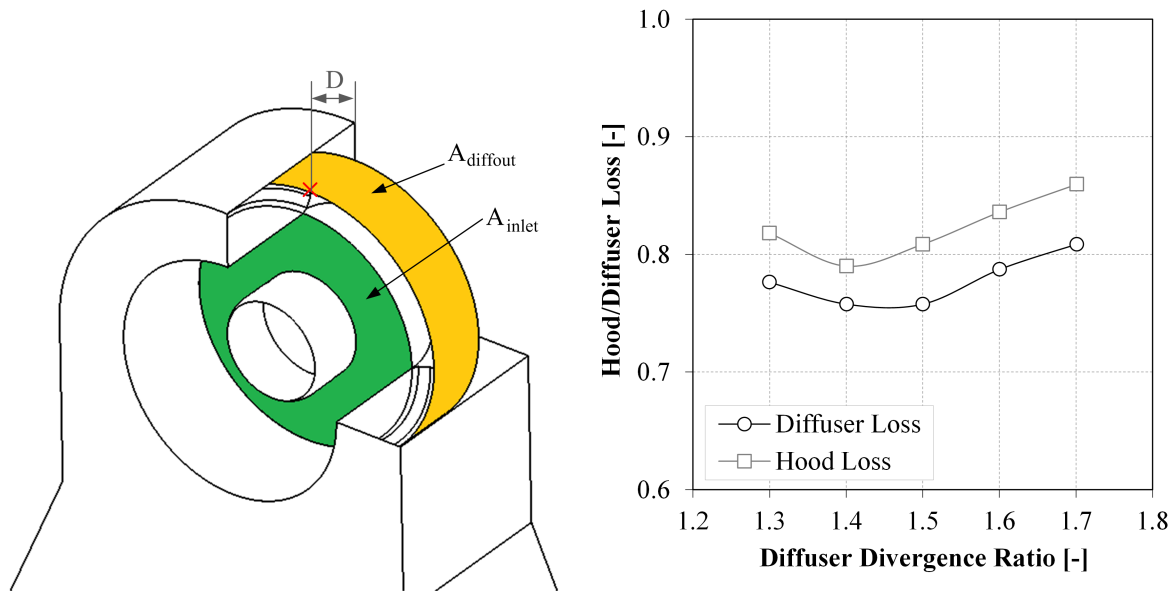
Figure 3.29: Flow Guide Tip Axial Location and $A_{diffout}$ Plane

Figure 3.30: Losses in the Exhaust Hood and Diffuser from Hoznedl et al. [27]

shown in Figure 3.29. A computational study by Hoznedl et al. [27] found that for a given diffuser geometry, both exhaust hood and diffuser losses could be minimised at a diffuser divergence ratio of 1.4, as shown in Figure 3.30. This $\frac{A_{diffout}}{A_{inlet}}$ was subsequently incorporated into the generic geometry.

With the axial length of the flow guide fixed, a vertical height could be defined. A computational and experimental study by Finzel et al. [16] found that the ratio of hood area (A_{hood}) to hood inlet annulus area (A_{inlet}), shown in Figure 3.31, reduced the pressure recovery potential at ratios of less than 1.1:1. Above this ratio, the changes in predicted exhaust hood loss were found to be small. A $\frac{A_{hood}}{A_{inlet}}$ ratio of 1.1:1 gave an exhaust hood height, of 2.4m, shown in Figure 3.32. This is of a similar magnitude to other published exhaust hood heights of 2.83m and 3.05m [15, 67].

With the flow guide tip positioned, the geometry of the outer exhaust diffuser, the flow guide itself could be defined. Extensive optimisation studies of flow guide geometries are widely available in the literature [61, 66, 43]. For the purposes of this design exercise, the flow guide geometry needs to be representative of current industrial practice. A paper published by Alstom Power in 2011 [68] observed that flow guides where the transition from the axial to the radial direction occurs in three angular steps of 30° were common in exhaust hood designs, as shown in Figure 3.33. Although improvements in exhaust hood pressure recovery were shown to be possible by extending and smoothing this flow guide design to control the kink angle, for the purposes of a generic geometry, this design provides a suitable baseline upon which future flow guide optimisation studies can be benchmarked. The final flow guide geometry, including dimensions is shown in Figure 3.34.

With the exhaust hood bearing cone and flow guide geometry fully defined, it was important to verify the characteristics of the diffuser. The diffuser area was plotted for cross
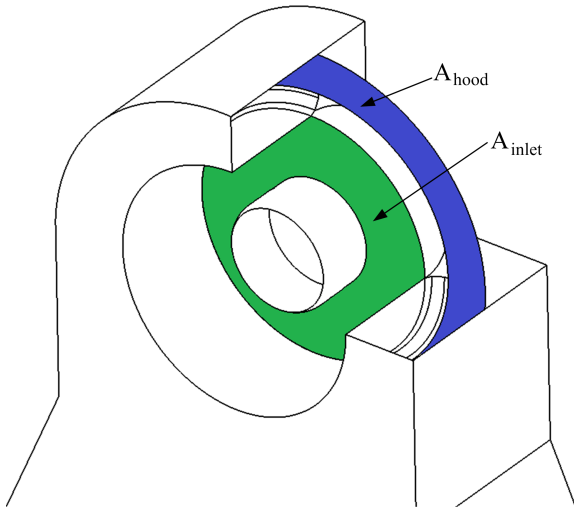
Figure 3.31: Diagram of A_{inlet} and A_{hood} Planes
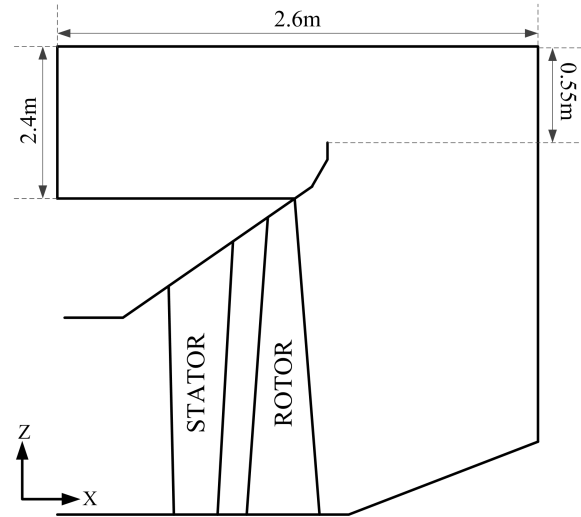
Figure 3.32: Chosen Exhaust Hood and Flow Guide Arrangement
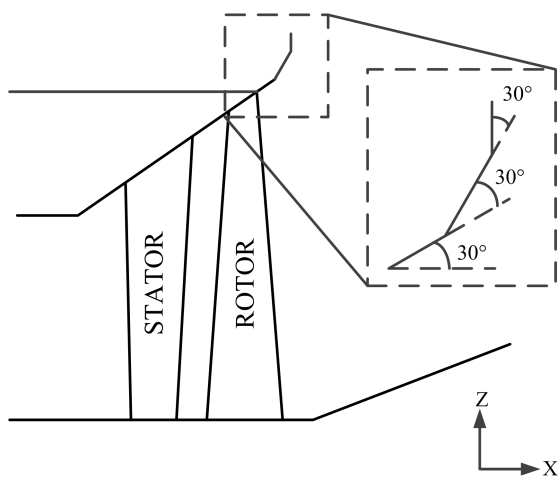
Figure 3.33: Axial to Radial Transition in Three 30° Steps
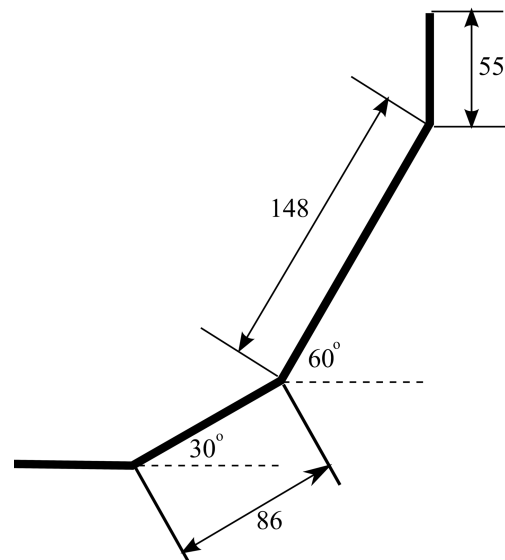
Figure 3.34: Selected Flow Guide Geometry Dimensions [mm]
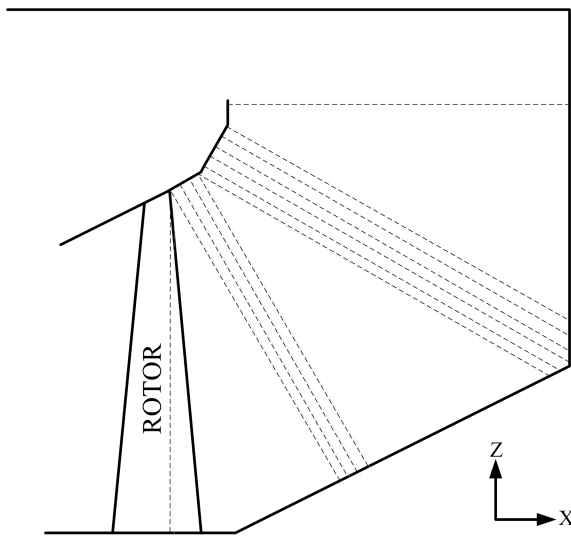
Figure 3.35: Diffuser Cross Sectional Area Measurement Locations
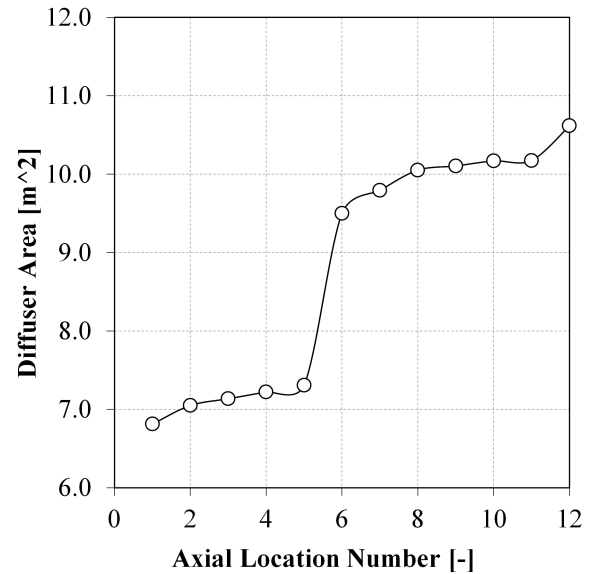
Figure 3.36: Change in Diffuser Area with Axial Location

sections at a series of axial locations, normal to the flow guide wall, as shown in Figure 3.35. Figure 3.36 shows the progressive increase in area from the inlet to the outlet of the diffuser.

Research by Liu and Hynes [34] showed that a constant cross sectional area between the hood inlet (A_{inlet}) and the half-joint plane (A_{HJ}), Figure 3.37, leads to an acceleration into the condenser neck and a large pressure drop with a subsequent poorer pressure recovery. The study carried out by Finzel et al. [16] showed that A_{HJ} should be at least 1.4 times A_{inlet} to maximise the pressure recovery potential of the exhaust hood. Using this area ratio, and the already specified depth of the exhaust hood, it was possible to define the exhaust hood width as 2.63m.

With the upper exhaust hood and diffuser defined, the condenser neck geometry was required to complete the model. An extensive design of experiments study by Fan et al. [15] yielded a recommendation for eight geometrical hood parameters for optimum pressure recovery. From their well defined exhaust hood geometry it was possible to scale the height of the condenser neck in relation to the height of the LSB, giving a height of 4m. To continue to decelerate flow into the condenser, an angle of 66° was included at the walls of the condenser neck.

The final exhaust hood geometry is shown in Figures 3.39 and 3.40.

3.4   Concluding Remarks

The literature review in Chapter 2 highlighted the absence of any freely available designs for an exhaust hood and last stage blade. In order to facilitate additional work in this rapidly expanding area of turbomachinery research, this chapter described the generation of an open source generic geometry which is freely available to all workers.
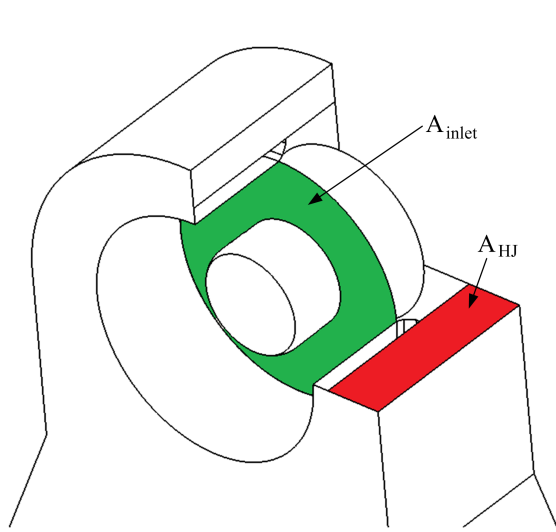
Figure 3.37: Diagram of A_{inlet} and A_{HJ} Planes
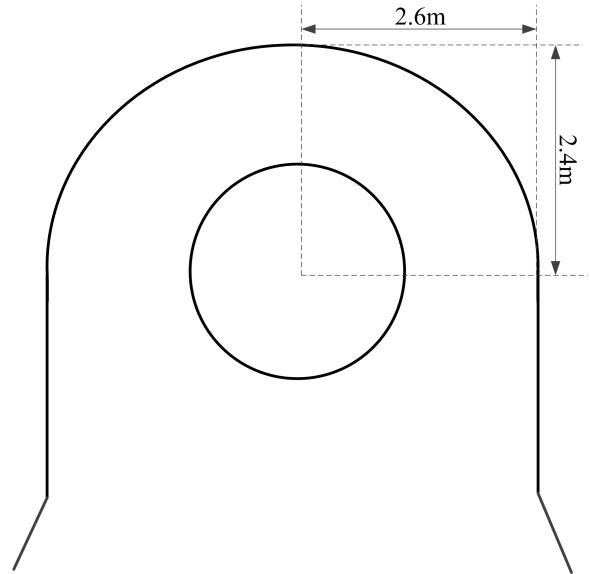
Figure 3.38: Exhaust Hood Width Diagram
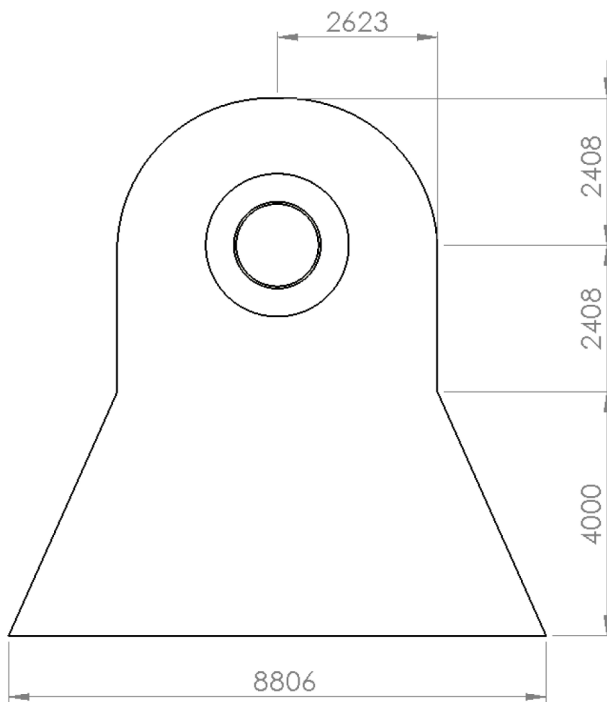
Figure 3.39: Final Hood Geometry Dimensions on Front Plane [mm]
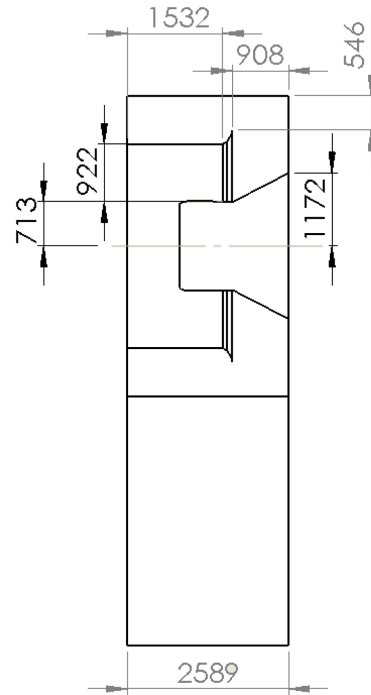
Figure 3.40: Final Hood Geometry Dimensions through Cutplane [mm]

The Durham Stage Test Case has been produced based on a modified, out of use, 20 year old industrially designed blade. The objective of the design exercise was to adapt the original blade to remove any IP restrictions and bring the outlet flow profiles closer in line with modern blading for use as an inlet boundary condition to an exhaust hood CFD calculation. Manual aerodynamic modifications using Alstom Power's in-house tools improved the efficiency of the stage by reducing separation losses on the stator and improving the static and total pressures distributions at outlet. Preliminary studies using the in-house analysis tools indicate the modified blade is an improvement on the original design; but to determine the suitability of the DSTC as an exhaust hood inlet boundary condition, required validation against data in the literature. Chapter 5 describes the evaluation of the rotor outlet flow profiles against other published results.

An accompanying exhaust hood geometry was required which produces vortices of representative magnitude and location based on those published in the literature. The Durham Exhaust Diffuser and Hood Test Case was developed from a comprehensive literature review, incorporating dimensions which are representative of current industrial practice. Particular attention was paid to the design of the flow guide, bearing cone and diffuser region as this was highlighted in Chapter 2 as of strong influence on the loss and vortex formation within the hood. Although the DEDHTC incorporates elements of existing published designs, the flow structure produced by the geometry must be validated against the literature; ensuring that the vortices are of representative magnitude and location. This analysis is carried out in Chapter 5.

4

Numerical Methodology

Computational Fluid Dynamics (CFD) has become the most popular method of predicting steam turbine exhaust diffuser flows as a cost efficient alternative to full experimental testing. With advancing computational resources, the complexity of exhaust hood calculations is increasing, but at present it is still too time consuming to calculate the full 3D, 360° unsteady exhaust hood flows with all internal furniture and wet steam modelling. Subsequently, each CFD simulation employs a method of simplification to reduce the calculation size to within practical computational limits. However, at present, no single accepted method has come to the forefront as the 'best-practice' approach to calculating exhaust hood flows. This chapter describes the range of CFD simplification methodologies used in the calculation of steam turbine exhaust diffuser flows in this thesis.

4.1   Common Calculation Parameters

For each computation in this thesis, carried out with the methods described in the following sections, certain aspects of the calculation set-up remain consistent between each calculation; namely, location of the inlet and outlet boundary conditions, the flow profiles applied at inlet to the stationary blade and working fluid specification.

The stator inlet plane is specified as a total pressure boundary condition in all calculations. This is located 2.5 stator axial chord lengths upstream of the stator leading edge in both isolated stage calculations and in bi-directionally coupled models, shown in Figure 4.1. Representative profiles of total pressure, total temperature and three velocity components were supplied by Alstom Power for use as the stator inlet boundary condition, Figures 4.2 and 4.3. These were generated from a previous multi-stage calculations by the industrial provider.

The stator/rotor interface is situated equidistant between the stator trailing edge and the rotor leading edge in each calculation. The treatment of the interface between adjacent domains is dependent upon the calculation method, to be discussed in forthcoming sections.

The exhaust hood outlet boundary is always specified as a static pressure, at a plane situated at the end of the condenser neck, in Figure 4.4. The axial location hood inlet plane in Figure 4.4 are dependent upon whether the calculation is sequential or bi-directionally coupled and is discussed in each forthcoming section individually.

The wet steam present in the last stage of a steam turbine was approximated as an ideal
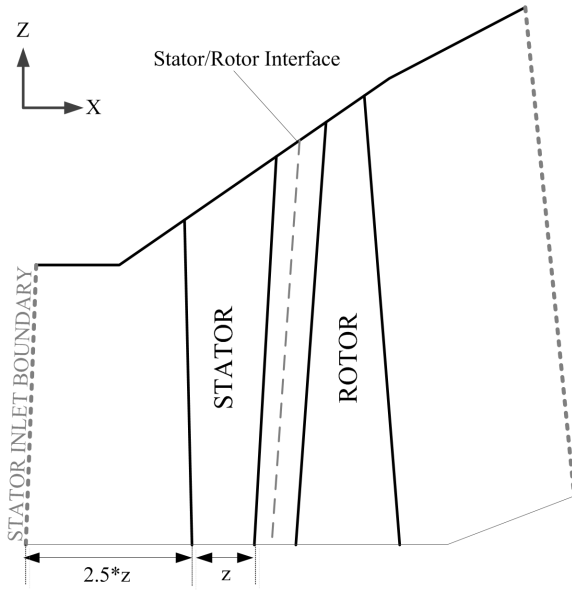
Figure 4.1: Diagram of the Stage Domains and Interfaces
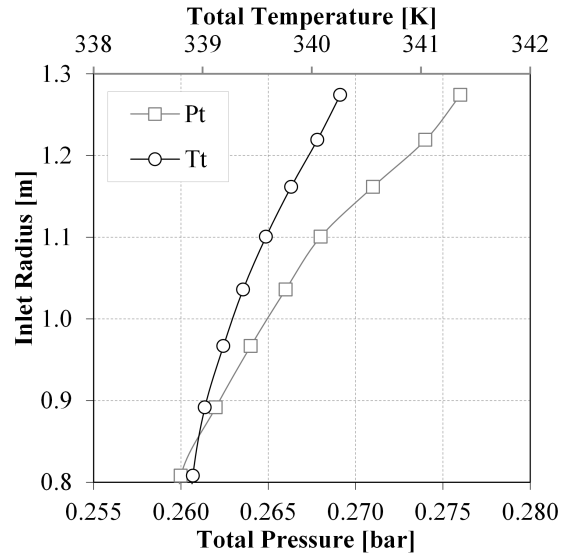
Figure 4.2: P_t and T_t Distribution at Stator Inlet [bar, K]
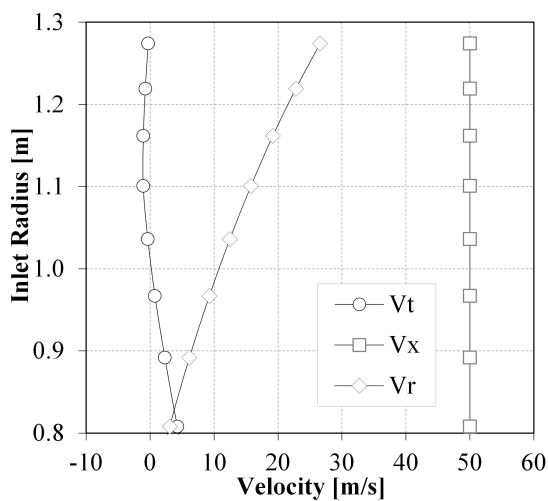
Figure 4.3: V_r, V_t and V_x Distribution at Stator Inlet [m·s^{-1}]
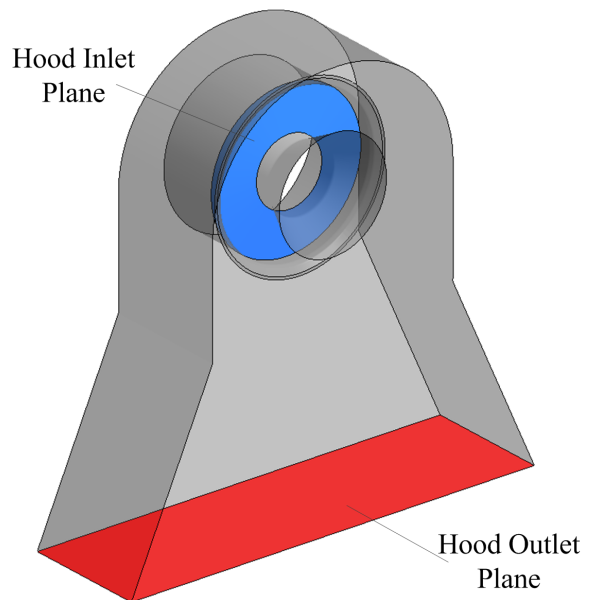
Figure 4.4: Location of the Exhaust Hood Inlet and Outlet Planes

Fluid Property	Value
C_P	4153 J/kgK
γ	1.12
Thermal Conductivity	0.061 W/mK
Dynamic Viscosity	1.032×10^{-5} Pas

Table 4.1: Fluid Properties for Case Set-up

Meridional Plane   Half-Joint Plane   Front Plane
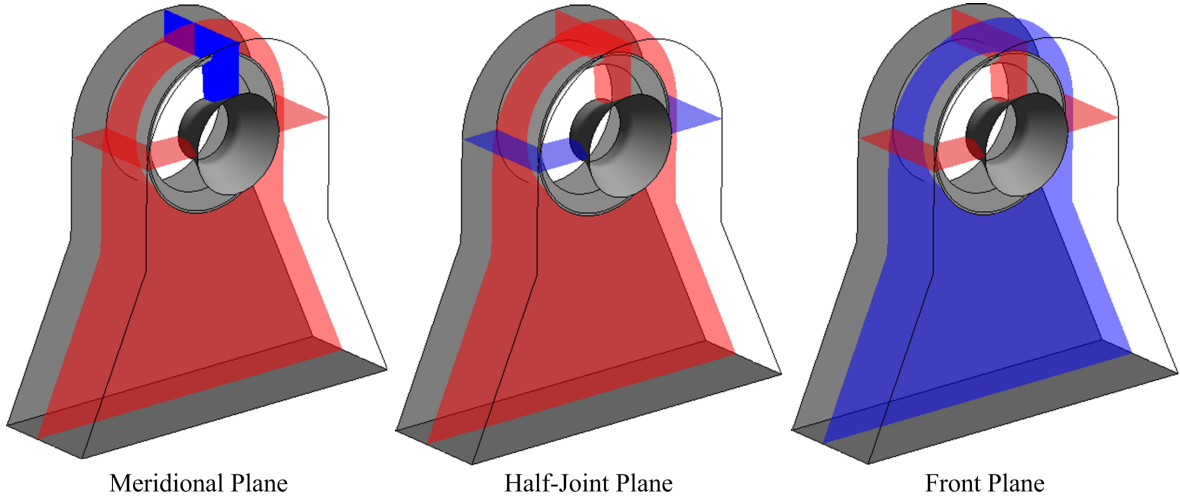
Figure 4.5: Diagram of the Three Cutplanes Considered in the Exhaust Hood Flow Structure Analysis in this Thesis

gas in all cases with flow properties corresponding to wet steam, Table 4.1. The ideal gas law assumption is a common simplification [47, 43, 52, 61] in exhaust hood calculations. To quote Tindell et al. [61]:

> "It is recognised that exhaust hood fluid in a steam turbine is usually wet steam, i.e. a two-phase fluid. Typically operation is in a pressure-temperature region where γ does not vary significant from exhaust hood inlet to exit. In fact, the maximum temperature difference between total and static conditions within the exhaust hood is 10°C"

The computational modelling of multi-phase wet steam is a research area which should be explored as a secondary effect, once a representative bulk exhaust hood flow regime has been established.

Throughout this thesis, analysis of the internal exhaust hood flow structure will be considered on three planes; meridional, half-joint and front planes, shown in Figure 4.5.

4.2   Sequential Coupling

Sequential exhaust hood calculations involve solving the exhaust hood flow structure separately from that of the last stage turbine blades. Flow profiles from an isolated LSB calculation are used at the inlet boundary condition to the exhaust hood calculation, a diagram of
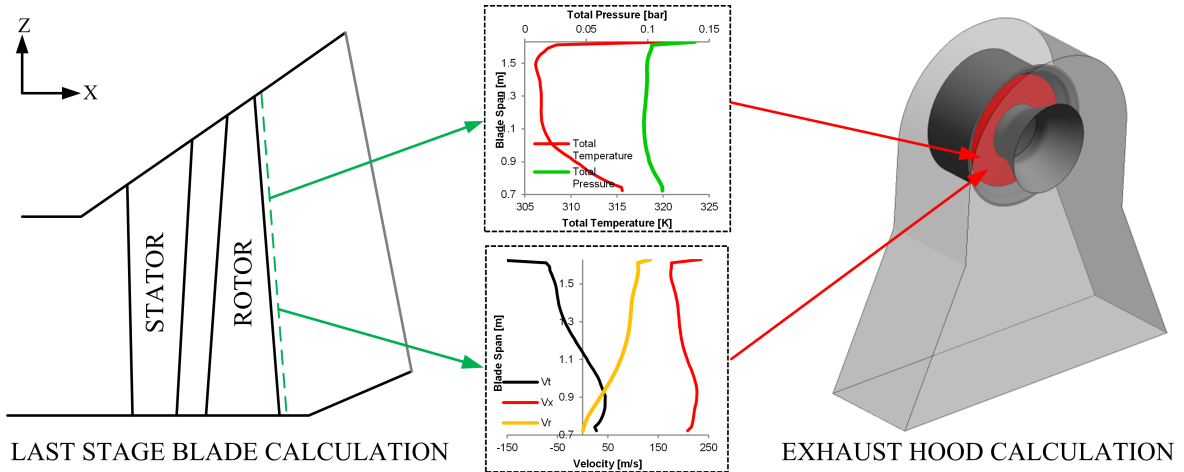
Figure 4.6: Schematic of a Sequential Calculation

which is shown in Figure 4.6. Provided the mass flow rate through the exhaust hood calculation is the same as that through the turbine calculation, the two flow fields are coupled in the stream-wise direction. The influence of the LSBs can be seen on the exhaust hood flow field, but no influence of the exhaust hood is experienced by the turbine flow.

The sequential approach to coupling the exhaust hood to the LSBs is adopted in Chapters 5 and 6. The literature has shown that a representative flow structure in the exhaust hood is only achieved when radial variations of flow profiles taken downstream of the rotor trailing edge were used at the inlet boundary condition [34, 61]. These profiles could be empirically determined or taken from a separate CFD calculation on the LSBs. In the absence of experimental data, flow profiles are extracted from a single passage stage CFD calculation of the DSTC and applied at inlet boundary condition in a separate CFD calculation of the DEDHTC.

In this thesis, all calculations using a sequentially coupled approach are carried out using the ANSYS Fluent 12.1 commercial flow solver. Details of the computational grids generated for each calculation are described in each chapter in Sections 5.1.1, 5.2.1 and 6.1.1.

4.2.1   Isolated Stage Calculation

For the isolated stage calculation on the DSTC, the stage domain in split into two computational domains; stator and rotor. These domains are coupled by a mass-averaged mixing plane, the details of which are discussed later in Section 4.3.1, which was situated equidistant between the stator trailing edge and the rotor leading edge.

The stator inlet plane and boundary condition specification are as described in Section 4.1. The rotor outlet plane was situated 2.5 rotor axial chord lengths downstream of the rotor trailing edge, shown in Figure 4.7. A static pressure outlet boundary condition was used, set at 8800Pa, as in the preliminary calculations at Alstom in Chapter 3.

The eddy viscosity two equation k-ϵ turbulence model was used to approximate the turbulent characteristics of the flow. As the most common turbulence model highlighted in the literature review [30, 71, 2, 47, 32] used for simulating exhaust hood flows this enabled a more

Fluid Property	Initial Value
Gauge Pressure	10000 Pa
Static Temperature	339.45 K
V_x	50 m/s
V_y	0 m/s
V_z	0 m/s

Table 4.2: Initialisation Values for Isolated Stage Case Set-up

Parameter	Set-Up
Solver Type	Pressure-Based
Working Fluid	Water Vapour (Table 4.1)
Density Model	Ideal Gas
Turbulence Model	Standard k-ϵ
Wall Treatment	Standard Wall Functions
Pressure-Velocity Coupling Scheme	SIMPLE
Gradient Spatial Discretisation	Green-Gauss Node Based
Spatial Discretisation (Pressure)	Standard
Spatial Discretisation	2nd Order Upwind
Under Relaxation Factors	0.1 - 0.3
Convergence Criteria	$1E-5$
Iterations	Approx. 6000

Table 4.3: Summary of Calculation Set-Up For Isolated Stage Calculation in ANSYS Fluent 12.1

representative validation comparison to be made with existing published research, discussed in Sections 5.1.3 and 5.2.4. This turbulence model requires the specification of turbulence intensity and turbulence viscosity ratio at stator inlet; set as 10% and 100 respectively, with values taken from calculations at Alstom Power described in Chapter 3. Standard wall functions were used to approximate the boundary layer flows, a common simplification to prevent excessively high cell counts in the exhaust hood [71, 68, 32].

The working fluid for the computation was as specified in Table 4.1 and the DSTC flowfield initialised as in Table 4.2. To facilitate convergence, initially the working fluid was specified as of constant density, using first order accurate discretisation and the rotational speed of the rotor much lower than the nominal load of 3000rpm at around 500rpm. As the calculation residuals dropped by around 4 orders of magnitude, ideal gas modelling was used, with second order accurate discretisation and the rotor speed was gradually increased in 500rpm increments until at 3000rpm. The convergence criteria was set to a drop in all residuals to $1E-5$. This was achieved in around 6000 iterations.

Table 4.3 defines the computation set up for the isolate stage calculation in ANSYS Fluent 12.1.

4.2.2   Isolated Exhaust Hood Calculation

Sequential calculations require artificial geometry manipulation to achieve convergence and this was applied to the DSEHTC. Typically, in coupled exhaust hood calculations, the exhaust hood inlet boundary would coincide with the outlet boundary of the rotor. This interface is likely to occur at close to the rotor trailing edge, Figure 4.8, before the sharp radial turning of the flow guide. In sequentially coupled calculations, if the exhaust hood inlet boundary coincides with the axial location of the rotor trailing edge of the stage calculation, it is situated in a region of sharp radial variation and achieving a converged solution can be challenging. Hence for all sequentially coupled calculations in this thesis, the exhaust hood inlet boundary was extended upstream of its baseline location and the LSB boundary extended downstream of its actual location to facilitate convergence, Figure 4.7. The exhaust hood calculation domains are shown in red and the stage domains in green. This approach is known as the 'far-field' method and has been successfully applied in the literature to aid the numerical stability of the calculations [36, 18, 19]. Determining the required upstream extension to facilitate convergence is an iterative process. In the calculations in this thesis, the exhaust hood was extended one rotor axial chord length upstream of the baseline location.

However, in repositioning the exhaust hood inlet and rotor outlet planes, the radial flow profiles taken downstream of the rotor trailing edge in the isolated stage calculation are applied in the exhaust hood calculation at a location upstream of where they actually occur. In this particular case, circumferentially averaged flow profiles consisting of 45 points of total pressure, total temperature, three components of velocity, and turbulent kinetic energy and dissipation rate are extracted from a measurement plane at the rotor trailing edge in the DSTC calculation, Figure 4.7 and applied at the hood inlet plane in the DEDHTC calculation. It is therefore important to verify the accuracy of the flow profiles at the location at which they would occur in the coupled calculation; at the rotor trailing edge axial location in the hood calculation, highlighted in grey in Figure 4.7. This is discussed in Section 5.2.3.

In addition, the circumferentially averaged profiles taken from the rotor trailing edge in the DSTC calculation form a single 2D span of a user specified number of points running along the z-axis which, when directly applied to the exhaust hood calculation, cannot fully define the 3D hood inlet annulus boundary, Figure 4.9. Subsequently a trigonometric transformation of the flow profile was required to apply the boundary condition around complete circumference. Figure 4.10 shows the transformation of the original flow profile, shown in red, around the exhaust hood inlet annulus in increments of 5°.

It is typical to specify a hood static pressure outlet boundary condition, shown as the outlet plane in Figure 4.4. For sequentially coupled calculations, the value of outlet static pressure must result in the same mass flow rate passing through the exhaust hood as through the LSBs to artificially couple the calculations in the stream-wise direction. Determining the outlet static pressure of the exhaust hood is an iterative process, as outlined in Figure 4.11. Typically, to stabilise convergence, the calculation is started with a higher outlet static pressure than is required for the desired mass flow rate, around 12000Pa. This calculation is run until convergence and the outlet pressure dropped and repeated until the stage mass
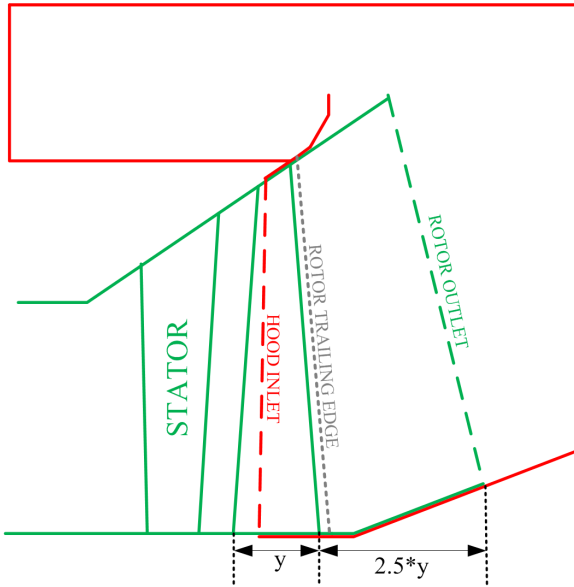
Figure 4.7: Schematic of the Sequential Coupling Boundaries
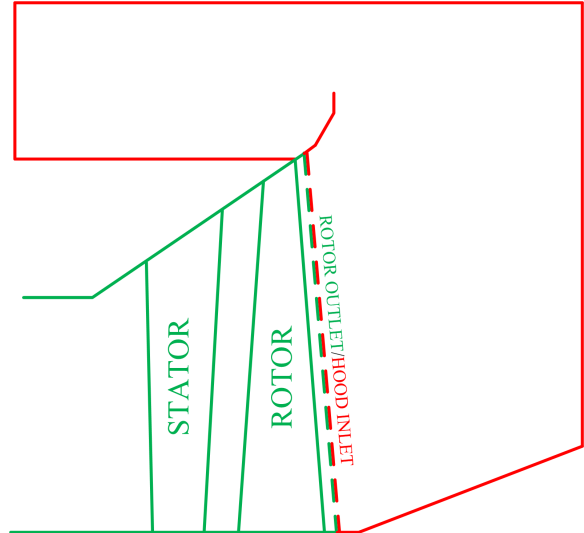
Figure 4.8: Schematic of a Coupled Calculation LSB/Hood Interface
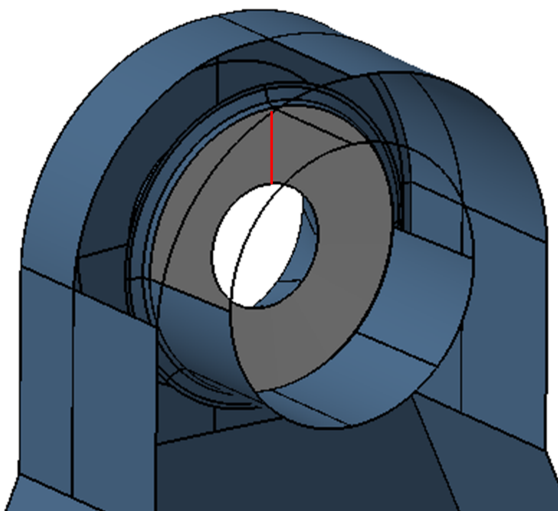
Figure 4.9: Location of Stage Outlet Profile at Hood Inlet
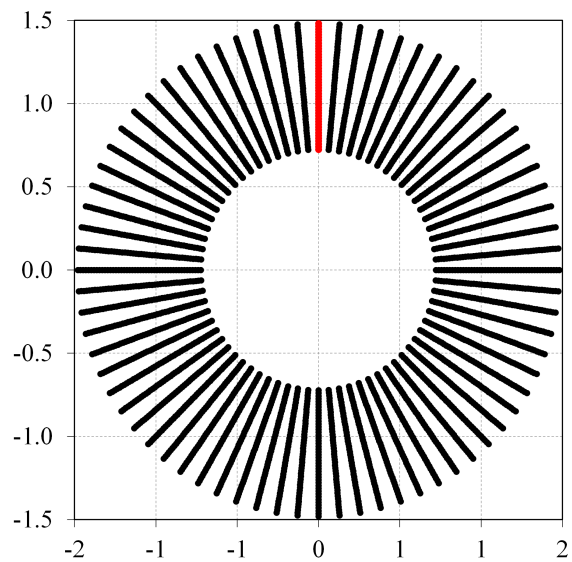
Figure 4.10: Trigonometric Transformation of Flow Profile Around Hood Inlet Annulus
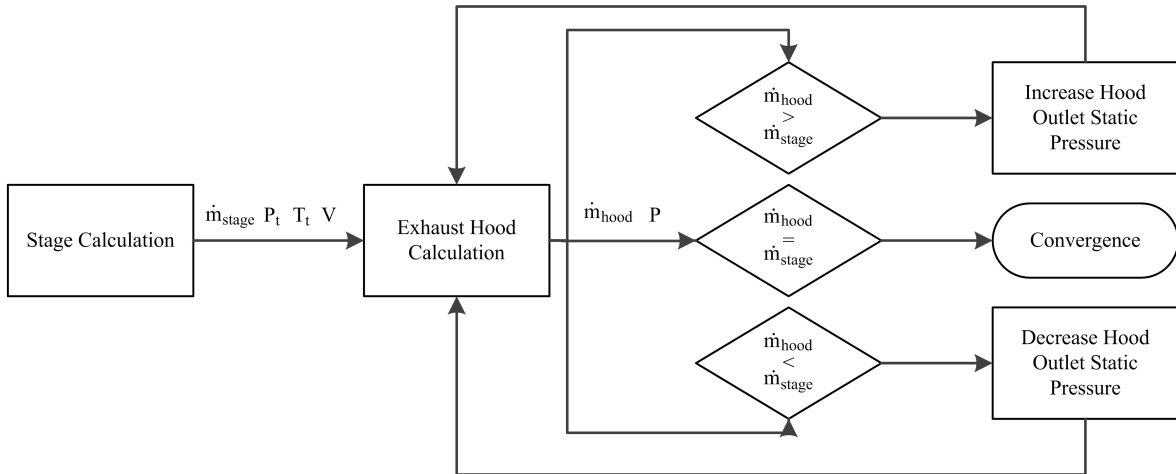
Figure 4.11: Flow Chart Determining Exhaust Hood Outlet Static Pressure

Fluid Property	Initial Value
Gauge Pressure	9000 Pa
Static Temperature	310 K
V_x	186 m/s
V_y	-44 m/s
V_z	66 m/s

Table 4.4: Initialisation Values for Isolated Exhaust Hood Case Set-up

flow rate is achieved. With the DEDHTC, an outlet static pressure of 8000Pa gave a mass flow rate of 88.2 kg/s, within 1% of the DSTC mass flow rate.

Flow calculations on the isolated exhaust hood were also carried out in ANSYS Fluent 12.1. The exhaust hood flow field was initialised as in Table 4.4, with first order accurate discretisation, constant density modelling of the working fluid and with a uniform inlet hood boundary condition, with inlet values taken as the average of the radial variations extracted from the rotor trailing edge in DSTC. After around 1000 iterations, ideal gas modelling was used and the radial variations in inlet flow introduced. After a further 1000 iterations second order accurate discretisation was used. A converged solution, was achieved in around 7000 iterations, where the convergence criteria was set as a drop in residuals of at least 4 orders of magnitude. Details of the full computation set us are tabulated in Table 4.5.

The sequential calculation method has the advantage that it enables a representative exhaust hood flow structure to be generated at a small computational cost. However, although the method enables the LSB turbine flow field to be transferred to the exhaust hood, the exhaust hood back pressure is not experienced by the turbine. More advanced computational models enable this interaction to be captured, and for this a *bi-directionally coupled* methodology is required, as discussed in 4.3.

Parameter	Set-Up
Solver Type	Pressure-Based
Working Fluid	Water Vapour (Table 4.1)
Density Model	Ideal Gas
Turbulence Model	Standard k-ϵ
Wall Treatment	Standard Wall Functions
Pressure-Velocity Coupling Scheme	Coupled
Gradient Spatial Discretisation	Green-Gauss Node Based
Spatial Discretisation (Pressure)	Standard
Spatial Discretisation	2nd Order Upwind
Under Relaxation Factors	0.1 - 0.3
Convergence Criteria	$1E-4$
Iterations	Approx. 7000

Table 4.5: Summary of Calculation Set-Up For Isolated Exhaust Hood Calculation in ANSYS Fluent 12.1

4.3   Bi-directional Coupling

Bi-directionally coupled calculation methods capture the interaction between the LSBs and the exhaust hood i.e. not only the effect the turbine has on the exhaust hood (as in sequential coupling) but also the effect the exhaust hood has on the turbine. The two flow fields are calculated simultaneously with the turbine coupled to the exhaust hood by an interface. Each method has a different treatment at this interface depending on the level of complexity of the model. The accuracy of the CFD calculation is improved when the interaction between turbine and hood is modelled, but the simultaneous solving of the two flow fields is more computationally expensive. There are four main methods of bi-directional coupling incorporated into commercial CFD software in addition to the various industry developed tools described in Chapter 2. These are listed below (in increasing order of complexity). Only methods 1-3 are considered in this thesis, the details of which are described in the following three sections.

1. Mixing Plane Approach

2. Frozen Rotor Approach

3. Non-Linear Harmonic Method

4. Full Unsteady Calculations

Throughout this thesis, all bi-directionally coupled flow calculations are carried out using NUMECA Fine/Turbo 8.10. The generation of the computational grids used to approximate the solution domain are described individually in each chapter.

In all bi-directionally coupled calculations, the computational system is divided into three separate domains; stator, rotor and exhaust hood, which are solved simultaneously. The outlet of one domain must coincide with the inlet of the adjacent domain. This means the exhaust hood and rotor geometry domains are different compared with the sequential coupling

Fluid Property	Initial Value
Static Pressure	10000 Pa
Static Temperature	305 K
V_z	150 m/s

Table 4.6: Fluid Properties for Bi-Directionally Coupled Case Set-up

approach, as shown in Figure 4.8 as the rotor trailing edge (outlet) must coincide with the axial location of the hood inlet plane. The rotor/hood interface is positioned 0.5 rotor axial chord lengths downstream of the rotor trailing edge; so the interface is not positioned in the flow guide region where the sharp axial-radial turning of the flow can cause convergence issues. The stator/rotor coupling domain is as in the isolated stage calculation, situated equidistant between stator trailing edge and rotor leading edge.

At inlet to the stator, the flow profiles were specified to a total pressure inlet boundary condition as in Figures 4.2 and 4.3. The working fluid was specified as an ideal gas with flow properties corresponding to wet steam, as in Table 4.1. The exhaust hood outlet boundary condition, in Figure 4.4, was specified as a fixed outlet static pressure of 10000Pa. The solver has an option for back-flow control at the outlet boundary, which ensures the total temperature of any recirculating flow re-entering the boundary is the same as that that exiting.

The flow field was initialised in two parts to facilitate convergence; LSB domains and exhaust hood. The turbine flow field was initialised from a converged stage calculation generated using NUMECA Fine/Turbo. The exhaust hood blocks were initialised with the flow field tabulated in Table 4.6. The convergence criteria was defined as a decreased in the global residual by at least 5 orders of magnitude. This was typically achieved for all bi-directionally coupled calculations in between 5000 and 7000 iterations.

In the sequentially coupled calculations described in the previous section, turbulence was simulated by the k-ϵ turbulence model, the most commonly applied model in the literature. For all bi-directionally coupled simulations the Spalart-Allmaras turbulence model was selected. This is the most sophisticated turbulence model available for the non-linear harmonic approach in the code used and was applied in all bi-directionally coupled flow calculations so a valid comparison could be made between them. Experimental validation of a range of annular gas turbine diffusers found that the Spalart-Allmaras turbulence model gave considerably better agreement with experimental data than with the k-ϵ model did [63].

The CFL number of all calculations was set to 3. This enables faster convergence by scaling the time-steps of the flow solver time-marching iteration scheme.

4.3.1   Mixing Plane

The mixing plane method involves circumferentially averaging flow variables at an interface between two computationally coupled domains. This interface treatment preserves radial variations in flow properties but circumferential variations are averaged out. The method was

first applied to the exhaust hood/turbine interface by Fan et al. in 2007 [15] and is the least computationally demanding method of bi-directionally coupling the turbine to the exhaust hood as only one blade passage needs to be modelled regardless of the stage periodicities. It is the most widely adopted method of solving single passage coupled flow calculations, as in the computation of the isolated DSTC in described in Section 4.2.1.

The mixing plane approach can be classified as a *multiple frame of reference* model (MFRM). Each of the three domains in the computational system (stator, rotor and exhaust hood) is treated differently. The rotating component, in this case the LSB rotor, is modelled in the rotating frame of reference and the stationary components, stator and exhaust hood, are modelled in the stationary (or absolute) frame of reference. By solving each domain's flow field in its local frame of reference, the inherently unsteady turbomachinery flow can be approximated as steady.

Each of the domains are coupled by an interface, in this case a mixing plane. Specification of the stator/rotor mixing plane equidistant between the stator trailing edge and rotor leading edge ensure that there is sufficient distance from the leading or trailing edges of the blades, so as not to artificially enforce circumferential flow uniformity. Similarly with the rotor/exhaust hood interface location downstream of the rotor trailing edge.

At each interface (stator/rotor and rotor/exhaust hood), circumferentially averaged flow profiles are determined for upstream and downstream sides of the interface. These profiles are then used to update the boundary conditions at the opposite side of the interface until convergence is achieved.

The drawback of the approach when used to couple the LSBs and exhaust hood system is seen at the rotor outlet/hood inlet interface. The exhaust hood flow field is highly circumferentially non-uniform due to the non-axisymmetric hood geometry and the high degree of flow swirl from the rotation of the turbine blades, Figure 4.12. The circumferential averaging at the interface removes this asymmetry, Figure 4.13, imposing an unrepresentative back pressure on the turbine. Coupled exhaust hood and LSB flow simulations calculated using the mixing plane approach are discussed later in Chapter 7.

4.3.2   Frozen Rotor

The frozen rotor approach is the only, currently used, quasi-steady method which captures the circumferential asymmetry at the rotor exit plane. Similar to the mixing plane approach, the frozen rotor method is also a MFRM, where each domain is solved in its local frame of reference giving an approximately steady solution; the stator and exhaust hood domains are solved in the stationary frame of reference, the rotor in the rotating frame of reference. Unlike the mixing plane approach there is no averaging at the interface between domains, instead the appropriate local frame transformation is applied, linking the stationary to the rotating domains. Subsequently, as the rotating domain does not physically rotate during the simulation, the resulting flow field is dependent upon the relative position of the stationary domains (stator and exhaust hood) to the rotor. The rotor can be said to be 'frozen' in space and time.
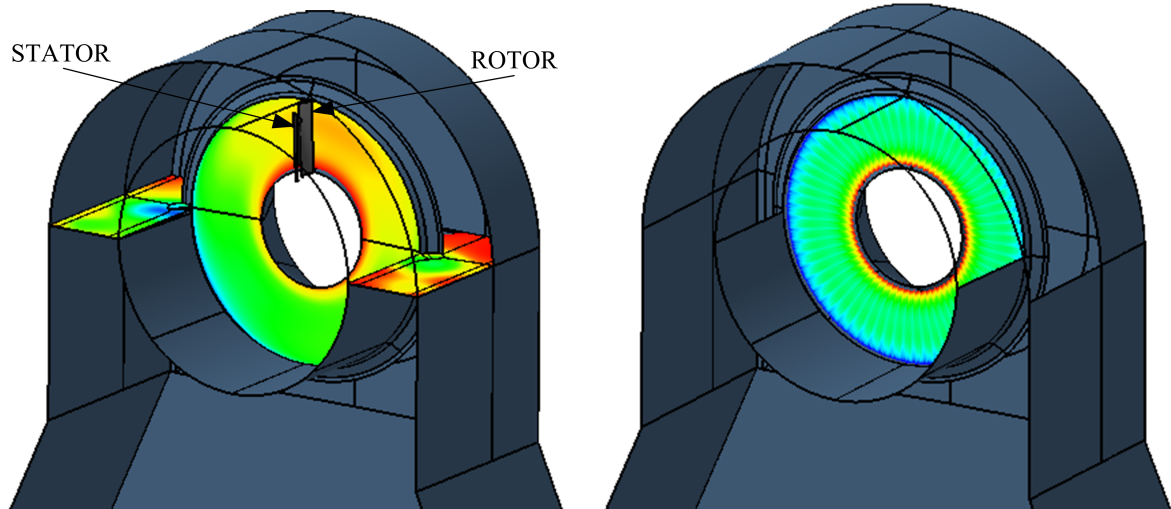
Figure 4.12: *P* Contours showing Exhaust Hood Asymmetry at Inlet and Half-Joint Plane

Figure 4.13: Circumferential Averaging of *P* at the Rotor Outlet with Mixing Plane Approach

The frozen rotor method is the industry standard for calculating rotor-volute flow fields where pitch-wise flow variations are significant. Recently, this method has become commonplace in exhaust hood simulations, where the circumferential flow field variations are prominent [64, 32]. However, in both cases, this requires the modelling of all blade passages and subsequently large computation expense, as there is no common periodicity between the rotor and the exhaust hood. In stage calculations, it is possible to reduce the computational demand by using rotational periodicity. In these cases the pitch ratio should be close to one between stator and rotor. However, with 60 stator passages and 65 rotor passages in the DSTC, the full annulus would need to be modelled even for a stage calculation, without the presence of the exhaust hood. In this thesis, full annulus frozen rotor calculations on the exhaust hood and LSB system are described in Chapter 8.

Verstraete et al. [64] suggested a method for reducing the computational demand of exhaust hood system frozen rotor calculations by modelling only one stator passage and using a mixing plane between stator and full annulus rotor. This is a viable option in LSB calculations as typically the stage is choked, and subsequently the passage to passage variations around the stator outlet annulus are small. This option of computational power reduction is explored in Section 8.2 with the flow field, loss coefficient and memory requirement compared to the full annulus frozen rotor approach.

The method by Verstraete et al. has the further advantage of eliminating the stator's sensitivity to rotor positioning by circumferentially averaging at the interface between the two. One disadvantage of the frozen rotor approach is the final calculation flow field is highly dependent on the relative position of the rotor to the stator and exhaust hood - as the calculation is carried out with the rotor in a 'frozen' fixed location. It is therefore recommended when modelling all stator and all rotor blades to carry out the calculation at a series of rotor positions to determine the sensitivity of the result [11], see Figure 4.14.

Baseline Rotor Positioning   Rotor Clocked by 0.5 Blade Pitch
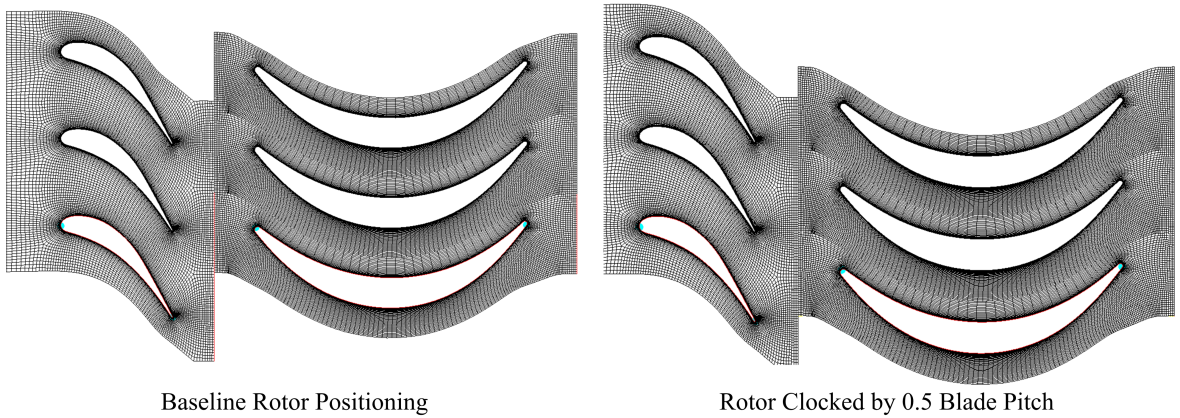
Figure 4.14: Example of Rotor Clocking Positions in Frozen Rotor Approach
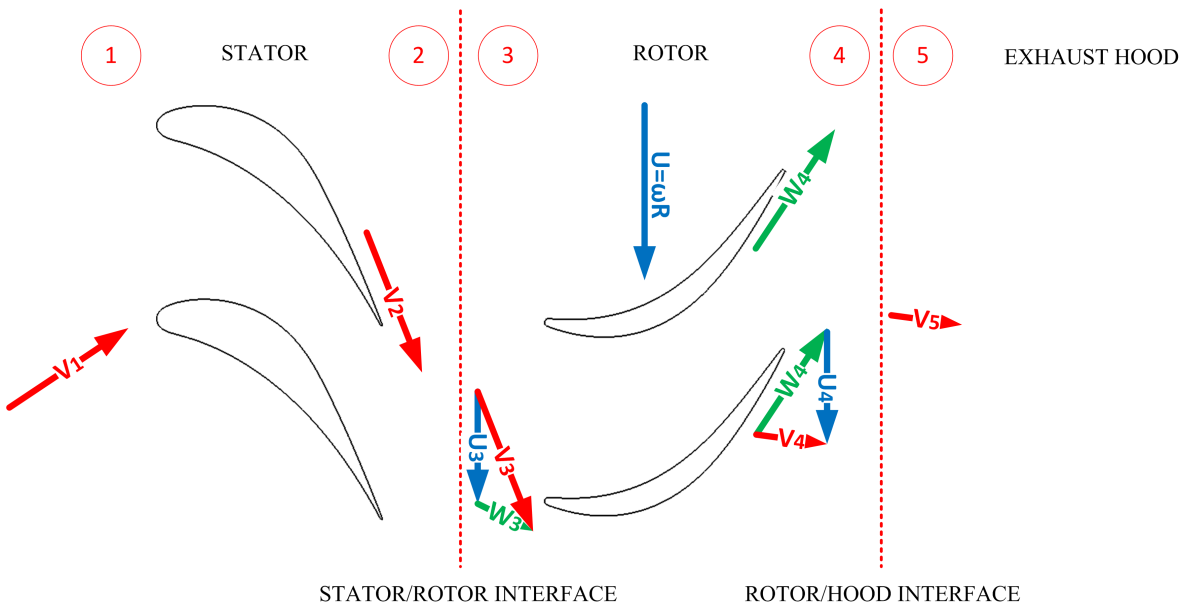
Figure 4.15: Velocity Triangles of the Frozen Rotor Approach for Exhaust Hood Calculations

The velocity triangles in Figure 4.15 detail the interface treatment in the frozen rotor approach. The stator is solved in the stationary/absolute frame of reference and as such the frame velocity ($\vec{U}$) in each of the three momentum equations reduces to zero. Conversely, the rotor is solved in the rotating/moving frame of the reference and as such includes the additional acceleration terms in the momentum equations. At the interface between stator and rotor a local frame transformation is performed, via Equation 4.1, transforming from the stationary to rotating frame of reference. The same frame transformation, but in the opposite direction, from rotating to stationary reference frames occurs at the rotor/exhaust interface.

$$\vec{V} = \vec{W} + \vec{U} \tag{4.1}$$

Although the frozen rotor method is a simple approach to modelling the circumferential asymmetry at the exhaust hood inlet, the modelling of all blade passages is very computa-

tionally demanding. Also, the sensitivity of calculation result to the fixed location of the rotor, requires the lengthy calculation to be computed for a series of clocked rotor positions. As such, researchers strive for a more computationally efficient method of computing the exhaust hood inlet's circumferential asymmetry. In this thesis, a novel application of the non-linear harmonic method to exhaust hood flows is explored to address this.

4.3.3   Non-Linear Harmonic

The non-linear harmonic (NLH) method was developed in the late 1990's by He and Ning [25] to offer a computationally efficient approach for studying the effects of unsteadiness on the aero-thermal performance and aero-elastic characteristics of turbomachinery. The NLH method has been widely used to reduce the calculation size of unsteady flows in high pressure (HP) turbine blades and in axial compressors. This thesis describes the first application of the non-linear harmonic method to steam turbine exhaust hood flows.

The fundamental assumption of the NLH method is that the most dominant unsteady disturbances are caused by the relative rotation of the blade rows i.e. the blade passing frequency (BPF) in the relative frame of reference for each blade row. With this in mind, an unsteady flow variable, $U(\vec{r}, t)$ can be decomposed by Fourier transformation into a time-averaged component, $\bar{U}(\vec{r})$, and the sum of the unsteady periodically appearing perturbations, $\sum U'(\vec{r}, t)$, shown in Equation 4.2.

$$U(\vec{r}, t) = \bar{U}(\vec{r}) + \sum U'(\vec{r}, t) \tag{4.2}$$

Each periodic perturbation can be decomposed into its fundamental frequency and N harmonics by Fourier transformation, according to Equation 4.3. This means that only one blade passage needs to be modelled as the frequencies can be reconstructed around the full annulus. The number of perturbations, M, that need to be modelled when calculating the flow through a blade passage is determined by the number of important blade passing frequencies acting at the blade row inlet and exit boundaries. The accuracy of the solution is controlled by the order of the Fourier series, i.e. modelling an infinite number of harmonics will give the equivalent result to the sliding mesh calculation. In this way, each perturbation ($U'(\vec{r}, t)$) can be modelled by a limited number of sinusoidal harmonic oscillations, which are integer multiples of the first harmonic of each blade passing frequency.

$$U'(\vec{r}, t) = A_{U,k} \cos(k\omega t) + B_{U,k} \sin(k\omega t) \tag{4.3}$$

Substitution of equation 4.3 into equation 4.2 leads to:

$$U(\vec{r}, t) = \bar{U}(\vec{r}) + \sum_{k=1}^{M} \sum^{N} A_{U,k} \cos(k\omega t) + B_{U,k} \sin(k\omega t) \tag{4.4}$$

The value of the instantaneous flow variable, U, in Equation 4.4 is a direct function of the *number of perturbations*, M, and the *number of frequencies per perturbation*, N - two user specifiable variables in the calculation set-up. Substitution of Equation 4.4 into the
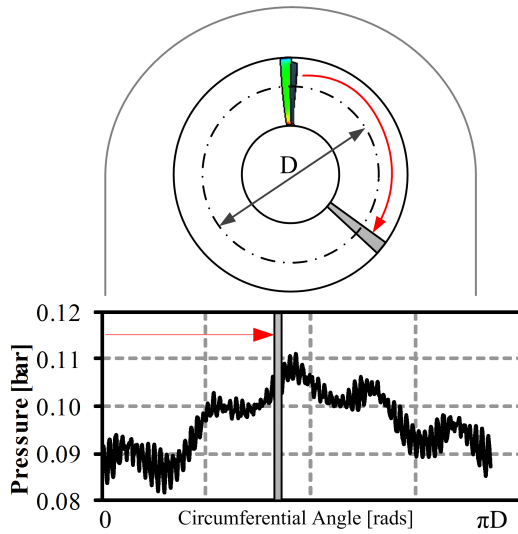
Figure 4.16: Reconstructing Frequencies Around Inlet Annulus
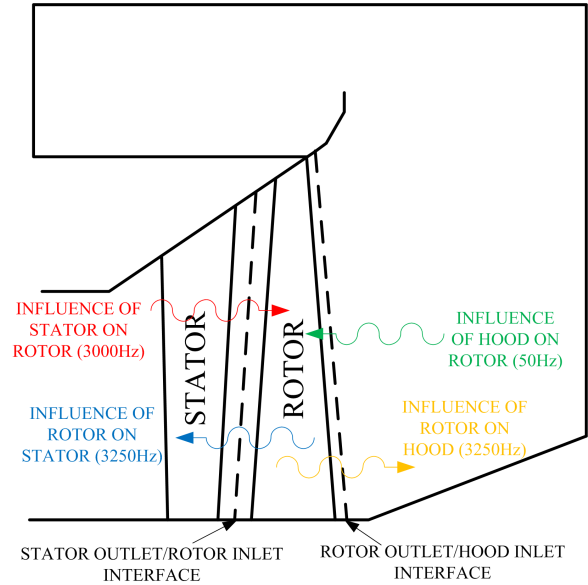
Figure 4.17: Number of Perturbations in Exhaust Hood System

Reynolds Averaged Navier-Stokes equations and collecting all same order sine and cosine terms, results in $2N$ time-invariant coupled equations being formed for each perturbation. These additional equations represent the influence of the deterministic unsteady fluctuations on the mean flow field, in an analogous manner to the way that the Reynolds Stress terms represent the influence of turbulence on the mean flow. The total number of coupled steady equations that have to be solved for each flow variable, U, including the mean flow equation, therefore becomes $2MN + 1$, where M is the number of perturbations modelled for the blade passage flow. Although the NLH approach is significantly less computationally demanding than full annulus unsteady methodologies, it is more computationally demanding than steady single passage calculations due to the additional computational power required to solve the additional $2MN$ coupled steady equations. This additional power must be balanced against the improved accuracy of modelling more harmonics.

The method used to pass flow information across the stator to rotor and the rotor to exhaust hood interface planes is described in detail by Vilmin et al. [65]. The NLH approach requires just one blade passage to be calculated for both the stator and the rotor blade rows, albeit with boundary conditions and flow equations cast in the frequency domain. The harmonic equations resulting from the Fourier decomposition are periodic in space with phase-lagged frequency components. This allows the time-averaged flow to be reconstructed around the annulus on either side of the interfaces, even though only one blade passage has been calculated, Figure 4.16. Good continuity can be achieved across the interfaces provided that a high enough number of harmonics, N, is included in the calculation. It is normally recommended that at least three harmonic frequencies are included when calculating turbomachinery stage flows. A harmonic study is required to determine the minimum number of harmonics for a particular problem, which is described in Section 7.1.1 for the exhaust hood system considered in the present study.

Chapter	Method	Application
5	Sequential Coupling	Validation of the DSEHTC
6	Sequential Coupling	Study of tip leakage modelling and condenser non-uniformity
7	Mixing Plane and NLH	Influence of inlet circumferential non-uniformity and diffuser axial length
8	Frozen Rotor and NLH	Validation of NLH as alternative to full annulus methods and off-design studies

Table 4.7: Summary of Numerical Campaign in this Thesis

The accuracy of the solution is not only governed by the number of harmonics (N) modelled, but also by the number of perturbations (or blade passing frequencies), M, considered, which is a direct function of the physical problem calculated. In the case of a single stage turbine, there is only one blade passing frequency. In the case of multi-stage calculations, the middle row experiences the wake of the upstream row *and* the potential flow field generated by the downstream row, 2 BPFs. In applying the approach to the coupled exhaust hood and LSB system, the rotor experiences the wake of stator blade upstream, and the potential flow field generated by the exhaust hood downstream, Figure 4.17. Given the periodicity of each row and the rotor speed of 3000rpm, the frequencies of perturbations associated with each harmonic are: [60; 65; 1] x 3000rpm = [3000Hz; 3250Hz, 50Hz] where 60 is the periodicity of the stator row, 65 of the rotor row and 1 of the exhaust hood [46]. The stator row sees one frequency of perturbation of 3250Hz of the downstream rotor row. The rotor row sees one frequency of perturbation of 3000Hz of the upstream stator row and one frequency of 50Hz from the downstream exhaust hood, i.e. two frequencies of perturbation. The exhaust hood sees one frequency of perturbation of the upstream rotor row of 3250Hz. So in order to capture the full frequency effects, two perturbations need to be modelled.

The convergence rate and the coupling between mean flow and harmonic equations is improved when the flow field is initialised by an existing quasi-steady solution. Subsequently, each calculation was started by running 1000 steady iterations before switching to a quasi-unsteady regime. Convergence was achieved after approximately 7000 iterations in total.

The NLH method is ideally suited to LP exhaust hood calculations including the LSBs. Flow gradients will be much larger in the radial direction compared to the circumferential direction at exit from the last stage. Capturing the circumferential variations in the time-averaged flow by calculating variations at just the fundamental passing frequencies and a limited number of their harmonics, has the potential to capture much more of the flow physics, without needing to go to the expense of full annulus 3D blade row calculations. A comprehensive study of the application of the NLH method to the steam turbine exhaust hood system is described in Chapters 7 and 8.

4.4 Concluding Remarks

This chapter describes the computational modelling strategies used in this thesis. Table 4.7 summarises the numerical campaign undertaken which includes over 30 CFD simulations and around 3000 hours of CPU time. The table indicates where the results of each stage/hood coupling method are used and the application.

5

Comparison of the Flow Structure in the Durham Stage and Exhaust Hood Test Case with Other Published Studies

The primary objective of the DSTC, the generation of which is described in Chapter 3, is for use as an inlet boundary condition to an exhaust hood CFD calculation. This chapter describes the computational analysis of the LSB design, using commercial CFD software, to determine its suitability as an exhaust hood inlet boundary condition by comparing the rotor outlet flow profiles with those published in the literature for other modern blade designs.

This chapter also describes the sequentially coupled analysis of the DSEHTC, to determine whether the exhaust hood design, described in Chapter 3, produces vortices of comparable magnitude and location with other published research. These findings, along with those in Chapter 3, were presented at the ASME Turbo Expo conference, in Copenhagen, Denmark in 2012 [4].

5.1   Last Stage Blades

The flow structure (and subsequently efficiency) of the exhaust diffuser is strongly influenced by the flow which exits the LSB. It is therefore vital to apply representative conditions at inlet to the exhaust hood in any simulation to generate results comparable with field data.

For a given operational condition, blade designers aim to minimise the kinetic energy leaving the LSBs as this equates to energy which cannot be converted to useful work by the turbine. Gray et al. [23] highlighted that an approximately uniform distribution of absolute velocity with minimum swirl is desirable to reduce the leaving energy. However, raising the reaction at the root to control separation at the hub of the rotor blade raises the axial velocity in this region, contributing towards non-uniformity in the absolute velocity profile. Hence, a compromise exists between improving the efficiency of the blading, and minimising the leaving energy. The DSTC geometry has been designed with this in mind, to provide a representative inlet flow field for an exhaust hood calculation. This chapter discusses the comparison of the outlet flow profiles for the Durham LSB compared to those published in the literature for other modern blade designs.
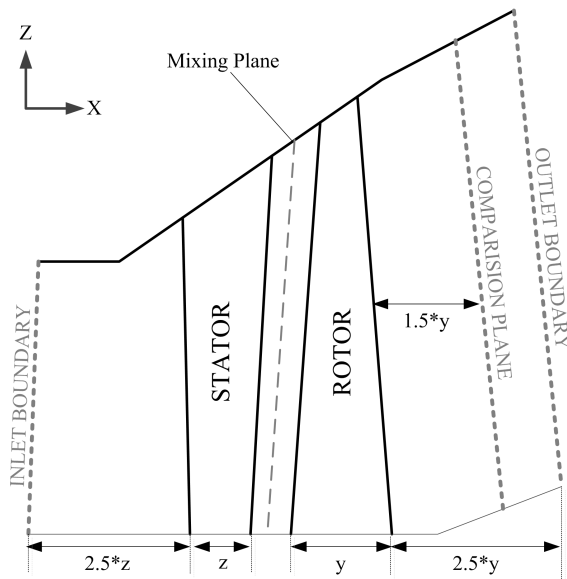
Figure 5.1: Diagram of Stage Domains
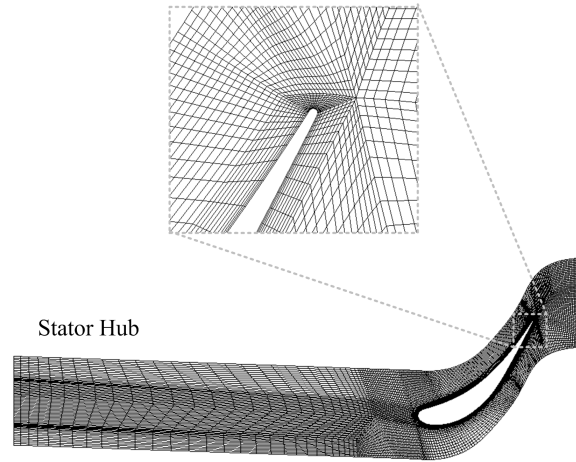
Figure 5.2: Stator Mesh at the Hub
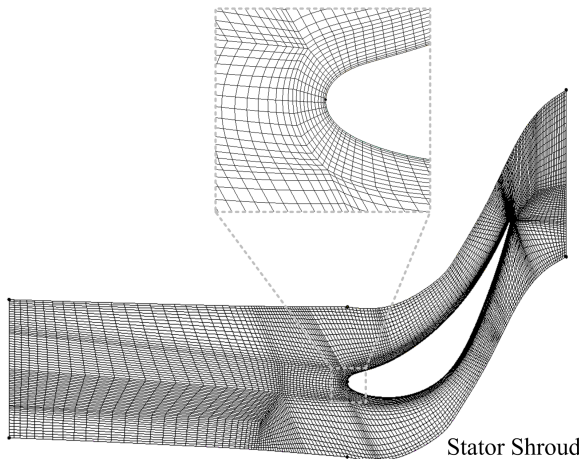
Figure 5.3: Stator Mesh at the Shroud
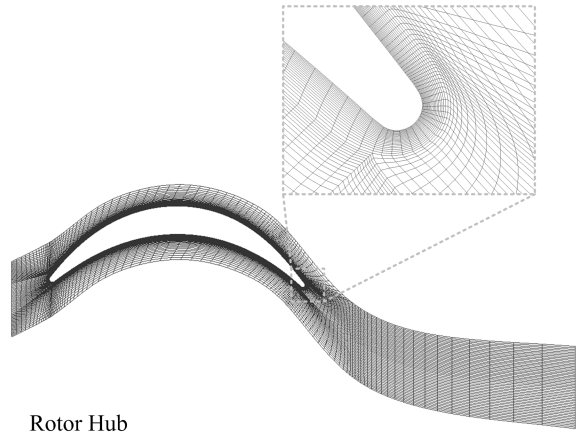
Figure 5.4: Rotor Mesh at the Hub

5.1.1   Mesh Generation

As described in Section 4.2.1, the DSTC was divided into two domains: one for the stator
and one for the rotor. The each domains inlet and outlet locations are described in Section
4.2.1 and also included again in Figure 5.1.

The commercial grid generation software ANSYS ICEM-CFD was used to generate a fully
structured hexahedral grid for the stator blade. An O-grid modelled the boundary layer at
the blade surface with a wall cell width was set to give a y^+ within the domain between 30
and 300 for the use of wall functions to resolve the boundary layer flow. The blade, hub
and shroud were set as non-slip walls with periodic boundaries situated mid passage between
adjacent blades. The final multi-block structured grid consisted of 977500 nodes. The final
grid can be seen in Figure 5.2.

The rotor mesh was generated using the Pointwise V16.04 commercial grid generation
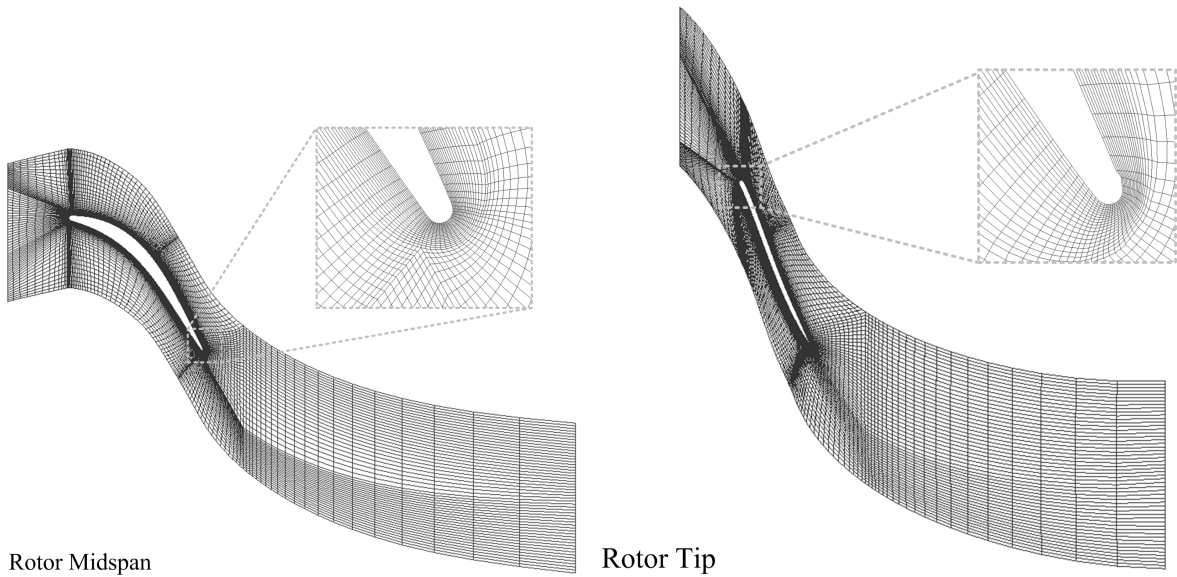
Rotor Midspan

Figure 5.5: Rotor Mesh at the Midspan

Rotor Tip

Figure 5.6: Rotor Mesh at the Shroud

software. The meshing software was changed from ANSYS ICEM-CFD used for the stator as the highly twisted rotor blade with large casing flare was very difficult to mesh and a higher quality grid was achieved using Pointwise V16.04. The final multi-block structured grid consisted of approximately 2 million cells. An O-grid modelled the boundary layer at the blade surface with a wall cell width to give a y^+ within the domain between 30 and 300 for the use of wall functions to resolve the boundary layer flow.

5.1.2   Computational Tools

The stage flow calculations were carried out with the commercial CFD software ANSYS Fluent 12.1. The computation set up is as described in depth in Section 4.2.1. Description of the mixing plane interface treatment coupling stator and rotor is described in Section 4.3.1.

5.1.3   Comparison of Results with Literature

The purpose of the DSTC was to produce a representative inlet boundary condition to an exhaust hood calculation and subsequently the results from the test case needed to be validated against those published in existing literature.

It is widely accepted that the swirl angle exiting the LSBs has a significant influence on the flow structure in the exhaust hood [54, 18, 43]. Fu and Liu's [18] computational study from 2008 showed that the swirl angle and total pressure distribution interact strongly with each other, influencing the formation of vortices within the diffuser. A high swirl angle at the hub of the blade was shown to facilitate the formation of a large vortex within the diffuser, hindering the pressure recovery potential because of the blockage caused by the vortex. A high swirl angle at the tip was shown to improve the pressure recovery and reduce the circumferential non-uniformity at the hood inlet. A negative total pressure gradient at inlet was shown to increase the pressure recovery coefficient and reduce flow non-uniformities.
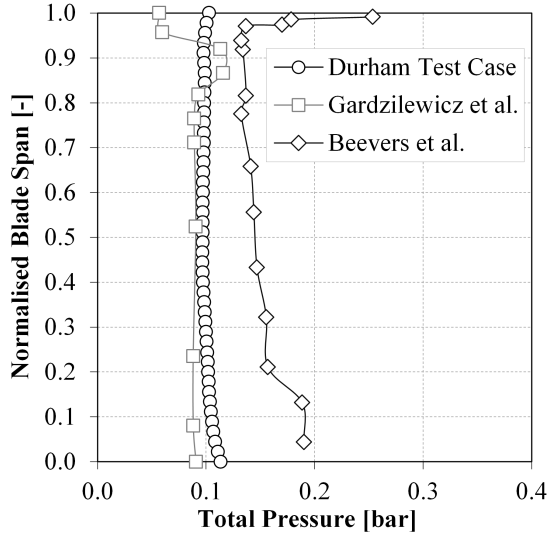
Figure 5.7: P_t Distribution at Comparison Plane [bar]
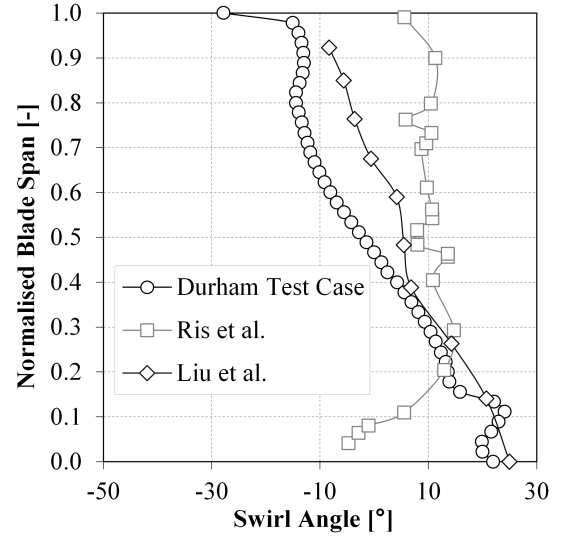
Figure 5.8: Swirl Angle (α) Distribution at Comparison Plane [°]

The reverse effect was observed with a favourable total pressure profile at inlet. These effects were shown to be consistent across a range of Reynolds Numbers, Mach Numbers and working fluids [19]. For these reasons, it is important to ensure that the total pressure and swirl angle distributions downstream of the DSTC are comparable with those published in the existing literature.

The comparison is shown in Figures 5.7 and 5.8, with swirl angle defined in Equation 5.1. Radial flow profiles are taken as a series of 45 circumferentially averaged points on a comparison plane 1.5 rotor axial chord lengths downstream of the rotor trailing edge, Figure 5.1. The flow profiles compared are for blades of a different geometry at a different operating point and are included to illustrate that the DSTC produces profiles within the scope of existing work.

$$\alpha = \arctan \frac{V_t}{V x} \tag{5.1}$$

The total pressure profile from Beevers et al. [2] in Figure 5.7 is taken from a CFD study at Alstom Power using their custom Exhaust Design System (EDS) tool, immediately downstream of the rotor trailing edge. As the published data does not include an x-axis scale, a zero point is assumed for comparison. The data from Gardzilewicz et al. are experimental test measurements taken from a 360MW industrial turbine [21]. Details of the operation point are not published.

Due to the different operating conditions the magnitude of the total pressure profiles in Figure 5.7 cannot be directly compared. The shape of the distribution is in good agreement with the literature, with an approximately uniform profile between 0.3 and 0.8 normalised blade span. A slightly elevated total pressure at the hub of the blade is due to the addition of tangential lean on the stator in the blade design process to raise the reaction at the root

of the blade. Although this comes at the price of increasing blade exit kinetic energy which cannot be recovered, it is a feature of other blades in the literature, particularly prominent in the work of Beevers et al. [2]. The major discrepancies are found in the tip region, above 0.8 normalised blade span. This is because the tip leakage effect has not been modelled in the DSTC in the calculations shown in Figure 5.7 but is present in both of the literature example calculations.

Figure 5.8 compares the swirl angle at rotor exit of the DSTC with two examples of other published work. Data from Liu et al. is extracted from a 15% scale air test facility where a screen and guide vane are used to simulate the swirl and pitch angle of a 300/600MW Westinghouse turbine from the 1980s. Profiles from Ris et al. are taken from a CFD simulation of an exhaust hood including baffles, operating at 53 kg/s with a rotor outlet static pressure of 3.52 kPa; the results of which were verified by experimental data. In all cases, the swirl angle profiles for the DSTC in Figure 5.8 show a similar swirl angle profile to those published in existing literature and are particularly comparable to work of Liu et al. The average swirl angle along the length of the blade is 0°, indicating that the blade effectively converts the kinetic energy of the flow to usable power.

Overall, the DSTC design has been shown to produce representative flow profiles when compared to those found in other published work, confirming the design's suitability for use as an inlet boundary condition to an exhaust hood CFD calculation.

5.2   Exhaust Hood

The DEDHTC was generated from an amalgamation of other published designs as described in Chapter 3, and is designed to produce a representative flow structure and loss regions compared with existing published results. As no experimental or field data exists at present for the design, the computed flow field from the validation CFD calculations has been benchmarked against those published in the literature.

5.2.1   Mesh Generation

The commercial grid generation package, Pointwise V16.04 was used to mesh the exhaust hood. A multi-block structured, hexahedral mesh was generated with approximately 2.6 million cells, Figure 5.9. The wall cell width was set to give a y^+ within the domain between 30 and 300 for the use of wall functions to resolve the boundary layer flow.

5.2.2   Computational Tools

The computation set up for the calculation of the sequentially coupled exhaust hood flow is described in full in Section 4.2.2.
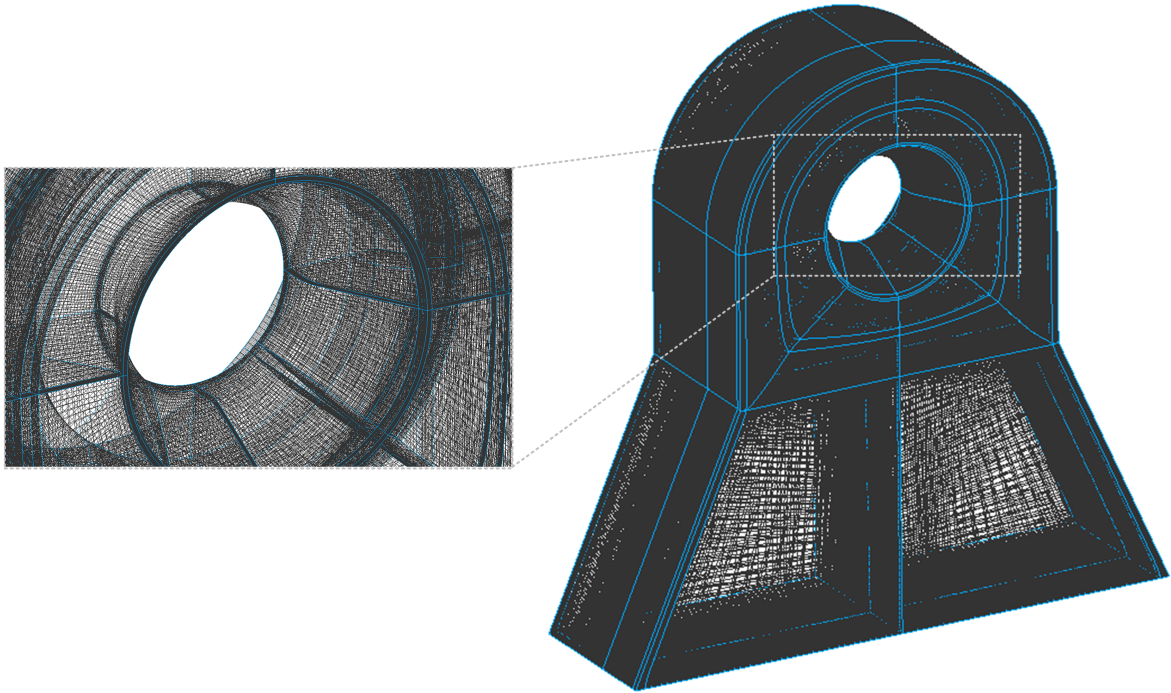
Figure 5.9: Exhaust Hood Mesh

5.2.3   Sequential Coupling Validation

The exhaust hood inlet boundary is situated one rotor axial chord length upstream of its baseline location (which typically coincides with the axial location of the rotor trailing edge in the stage calculation) and, as such, the radial flow profiles taken from downstream of the rotor trailing edge in the stage calculation are applied one axial chord length upstream of where they would occur in reality, Figure 5.10. Therefore, the flow profiles at the axial location of the rotor trailing edge in the exhaust calculation, need to be verified against those taken from the rotor trailing edge in the stage calculation.

Figures 5.11 and 5.12 compares total pressure and swirl angle distributions taken at the axial location of the rotor trailing edge (RTE) in the exhaust hood calculation with the distributions taken at the rotor trailing edge of the stage calculation.

Total pressure and swirl angle have been highlighted by Liu et al. [36] as significant influencing factors on the formation of vortices within the diffuser. Subsequently, it is important that the distributions extracted from the stage calculation are transferred to the same location in the exhaust hood calculation to ensure representative boundary conditions are maintained. Figure 5.12 shows good agreement between both the total pressure and swirl angle distributions in the stage and exhaust calculations.

5.2.4   Comparison of Results with Literature

In order to verify the validity of the DEDHTC, the flow features from CFD calculations are compared to those published in the existing literature, to ascertain that a representative flow field is produced by the test case geometry.
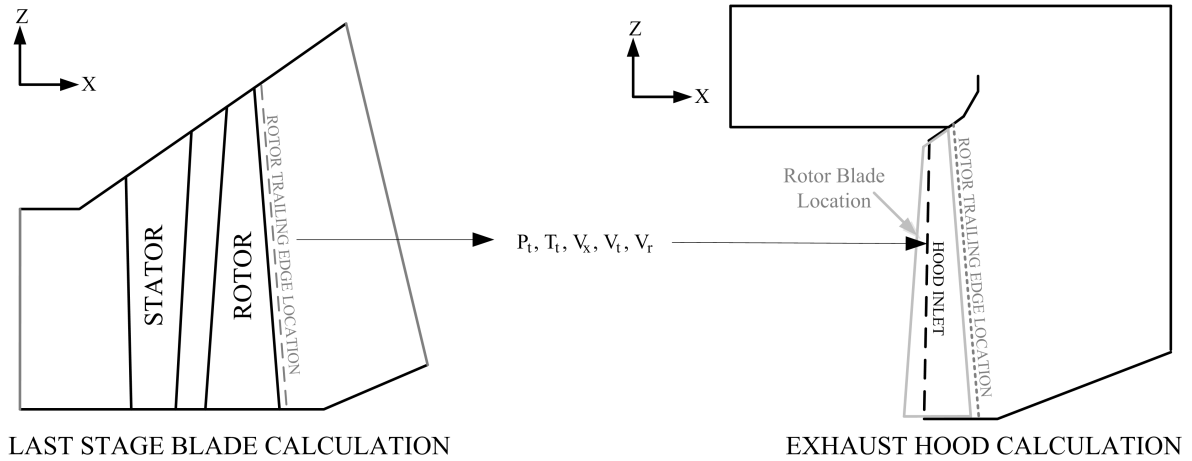
Figure 5.10: Schematic of Sequential Calculations

The exhaust hood flow can be categorised into two main regions, as highlighted in Figure 5.13:

1. Separations within the diffuser

2. Downflow to the condenser

The highly non-uniform flow downstream of the LSBs (and applied at exhaust hood inlet), combined with the compact length axial-radial diffuser results in the formation of a series of separations and vortices within the diffuser, Figure 5.14.

Previous research [61, 67, 15] has found that the primary source of loss within the exhaust hood is the separations and vortices within the diffuser. Each vortex has a blockage effect which hinders the diffuser's ability to effectively recover static pressure. The vortices can be categorised as follows:

1. Separation along the *bearing cone*

2. Separation at the *flow guide tip*

3. Separation *along the flow guide*

4. *Additional* vortices

The static pressure recovery of the exhaust hood was calculated to be C_p = -0.035 from Equation 1.1; relatively low compared with other values published in the literature, which can be as high as 0.5 [19]. However, this is not an optimised exhaust hood and there is significant scope for improvement.

Separation along the Bearing Cone

Previous research has found separation along to bearing cone to be one of the most significant source of loss in the exhaust hood [61, 67, 15]. As the static pressure increases in the stream-wise direction along the bearing cone, the adverse pressure gradient leaves the diffuser more
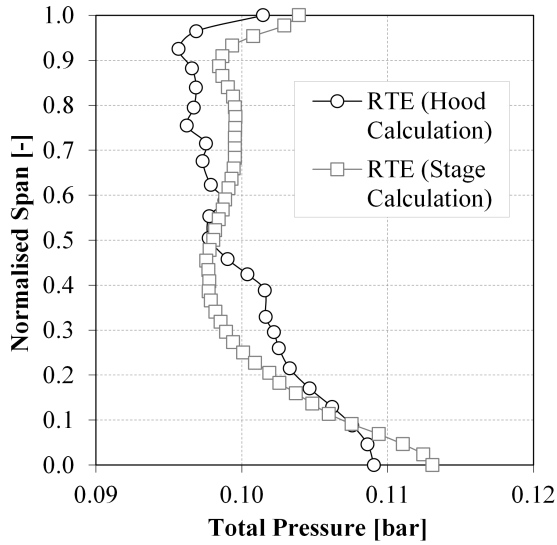
Figure 5.11: P_t Distribution at the Rotor Trailing Edge Planes in the Stage and Hood Calculations [bar]
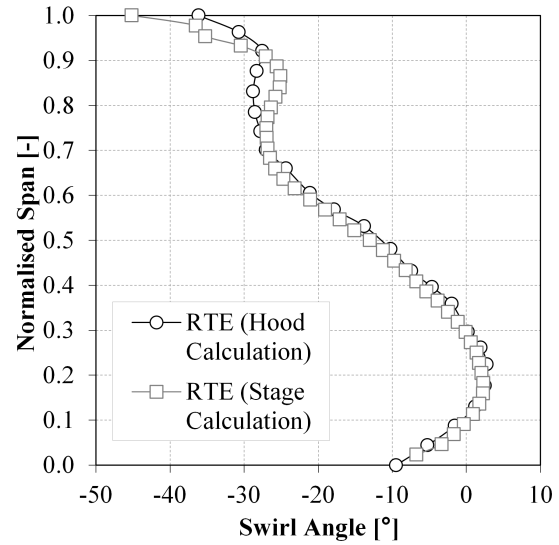
Figure 5.12: Swirl Angle Distribution (α) at the Rotor Trailing Edge Planes in the Stage and Hood Calculations [°]

susceptible to separation. This can lead to the formation of a large vortex (around $\frac{2}{3}$ of the diffuser height [67]) causing a blockage effect which reduces the diffuser's ability to recover static pressure, due to the reduction of the effective area.

However, the formation of the separation along the bearing cone has been shown in the literature to be highly dependent on the inlet total pressure profile, magnitude of swirl angle at the hub of the LSB, the operating point of the turbine and the diffuser geometry. In the case of the DEDHTC, the bearing cone separation is absent, when compared with other research. This is due to the combined total pressure profile and swirl angle profiles generated from the DSTC and used at inlet to the exhaust hood. Fu and Liu's research from 2008 [18] showed the detrimental effect of a high swirl angle at the hub of the blade, evident in the DSTC, can be reversed with the presence of an adverse total pressure gradient at inlet. The elevated total pressure at the hub of the DSTC, Figure 5.7, due to the addition of tangential lean to the stator in the blade design process, has generated a slight adverse total pressure gradient, sufficient to counteract the negative effect of the high swirl angle at the hub, Figure 5.8.

In addition, Fan et al. in 2007 [15] numerically investigated a similar straight bearing cone geometry and found the bearing cone separation to only be present when the exhaust hood was coupled to the LSBs via a mixing plane. When the exhaust hood was considered independent of the LSBs, such as in this investigation, no separation occurred. This provides scope for further work to determine whether it is the diffuser geometry or the fact the interaction between the LSBs and hood inlet has not been modelled accurately enough that is responsible for under-prediction of the separation zone along the bearing cone.

Separation at the Flow Guide Tip

The DEDHTC has successfully captured the large separation region behind the tip of the flow guide. This was found to be the most significant source of loss, echoing similar results by other researchers [18, 66]. This separation was attributed by Zhang et al. [70] to the "backward-facing step expansion" phenomena, from the flow guide tip into the collector.

As this vortex progresses in the stream-wise direction, it forms the two counter-rotating outlet vortices at inlet to the condenser, increasing in magnitude due to the decrease in pressure in the condenser neck. This increase in magnitude can be seen by the larger low static pressure region in Figure 5.15 and in the velocity vectors in Figure 5.16.

Separation along the Flow Guide

Figure 5.15 also highlights a low pressure region below the flow guide, indicating a separation. This separation is expected as the geometry is based on research by Yoon et al. [68], where a "significant separation" was found where there is a sudden change in kink angle, from axial to 30° (the flow guide geometry shown in black on both images in Figure 5.15). Yoon et al. found this separation could be suppressed by geometric optimisation, echoing findings from previous researchers [61, 68] that the flow guide separation is strongly dependant upon the geometry.

However, the primary factor governing flow guide separation is the tip leakage jet. Previous work [27, 16] has shown a favourable effect of the tip leakage jet on the flow in the guide region of the exhaust diffuser. The high adverse pressure gradient in the flow guide region can cause the flow to separate, but the leakage jet has been shown to add momentum to the boundary layer region, delaying separation. As this simulation does not incorporate the effect of the tip leakage, its beneficial effects cannot be utilised which may contribute to the low pressure recovery coefficient. The effect of tip leakage jet on the exhaust hood system is analysed in Chapter 6.

Downflow to the Condenser

The large flow guide tip vortex expands and progresses downstream to form a pair of counter-rotating vortices in the condenser neck, shown in the velocity vectors in Figure 5.17. Figure 5.18 shows velocity contours on the hood outlet plane where reverse flow (denoted as a positive velocity) at the core of each vortex is visible, as noted previously by other researchers [54]. The low energy at the core drives the main flow outwards to the walls of the condenser neck, resulting in higher velocities at the backwall and the bulk of the flow discharging down the endwalls and highly non-uniform flow. The vortices are of non-equal magnitude because of the swirl applied at hood inlet.

Flow Asymmetry

One key aspect characterising the exhaust hood flow structure is the asymmetry of the flow. This asymmetry can be seen clearly in two planes, at the half-joint plane in Figure 5.19 and
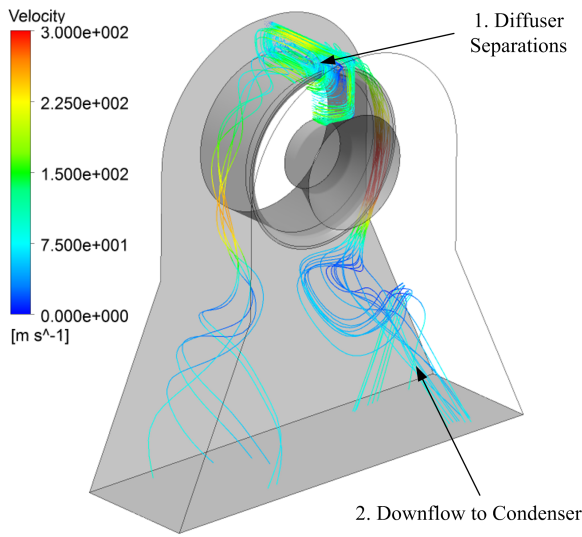
Figure 5.13: Exhaust Hood Streamtraces
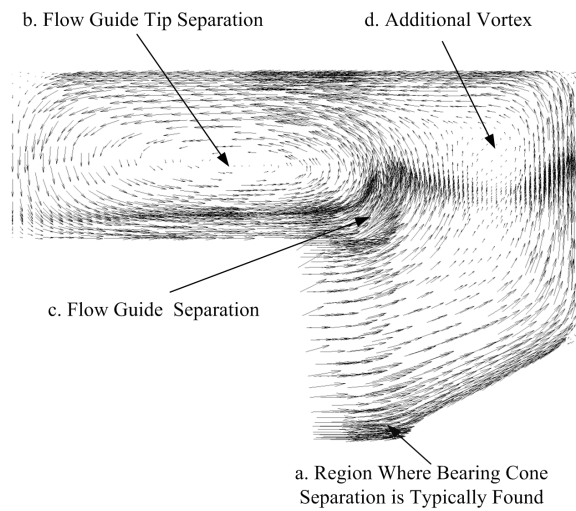
Figure 5.14: Velocity Vectors within Diffuser
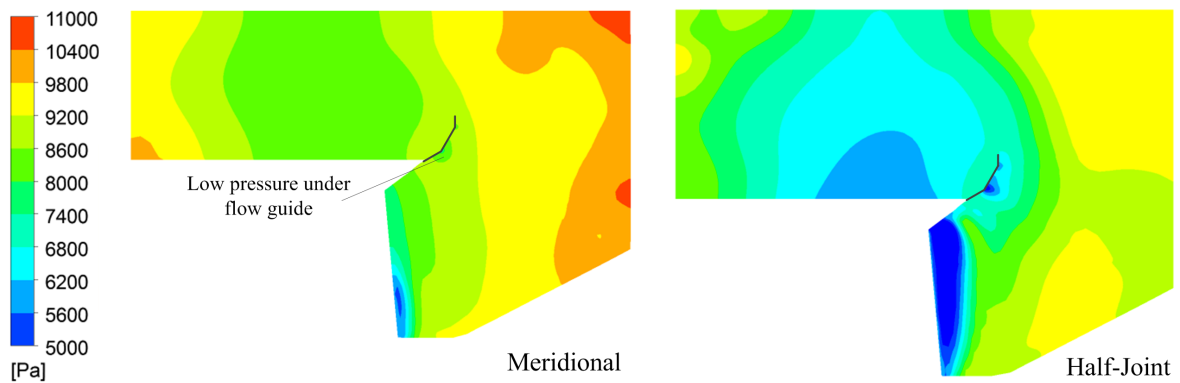
Figure 5.15: P Contours at Meridional and Half-Joint Planes [Pa]
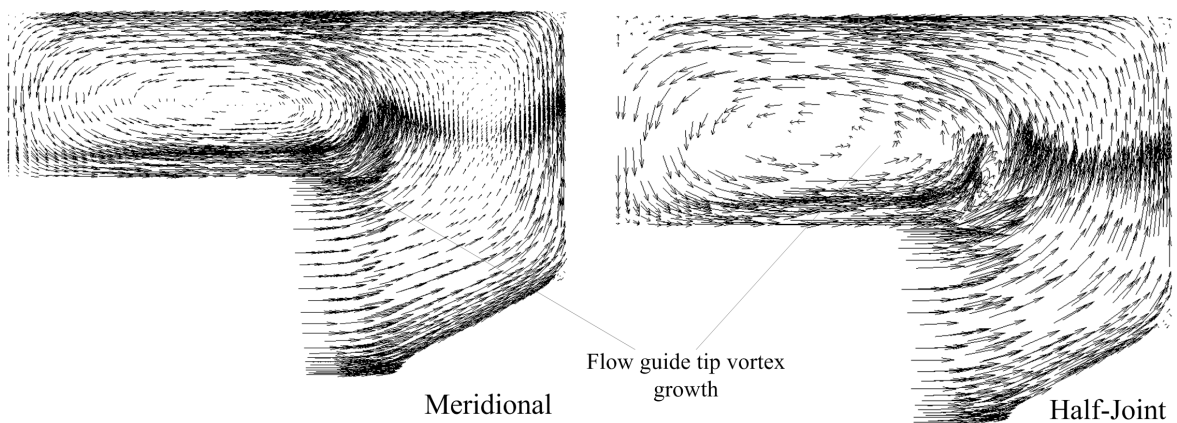
Figure 5.16: Velocity Vectors at Meridional and Half-Joint Planes
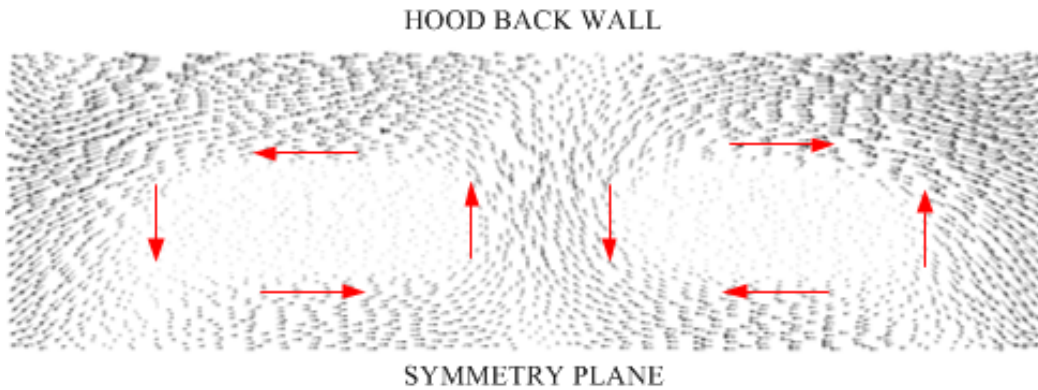
Figure 5.17: Velocity Vectors at the Exhaust Hood Outlet Plane
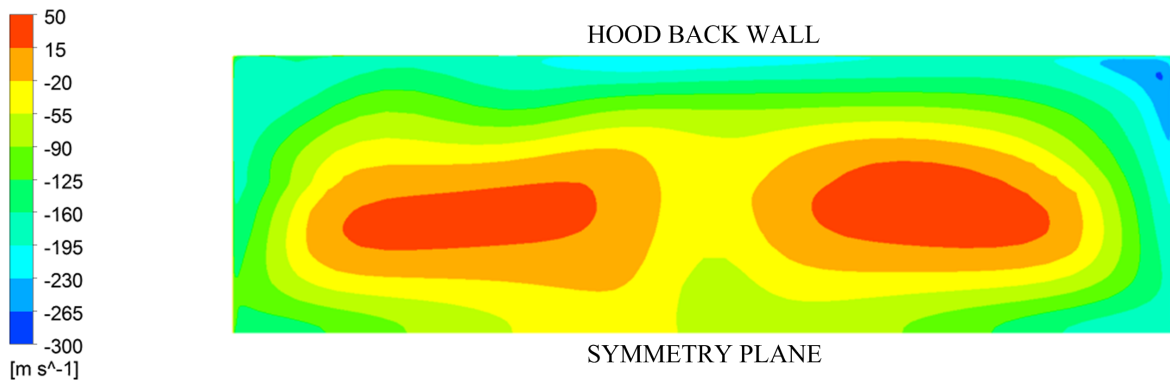
Figure 5.18: V_z Contours at the Exhaust Hood Outlet Plane [m·s^{-1}]

at the exhaust hood inlet in Figure 5.20. Researchers in the past 15 years have observed this two plane asymmetry [3, 67]. Benim et al. [3] observed the prominent asymmetry between the left and right hand sides of the exhaust hood, as seen in Figure 5.19 and this was attributed by Xu et al. [67] to be due to the swirl at inlet to the exhaust hood. The asymmetry between the top and the bottom of the exhaust hood, shown in Figure 5.20, is due to the non-axisymmetric exhaust hood geometry; a flow characteristic observed by multiple researchers including Benim et al. [3].

5.3   Concluding Remarks

A literature review highlighted an absence of any freely available LSBs or exhaust hood geometries for researchers to utilise. To address this, an open-source geometry, free of any commercial restrictions was generated as described in Chapter 3. A low pressure last stage turbine blade was developed based on an original Alstom Power design and an exhaust hood from surveying existing published geometries. In order to determine the suitability of the DSEHTC geometries, a comprehensive CFD study was carried out.

The CFD simulation described in this chapter of an isolated, single passage of the DSTC showed the design generates outlet flow profiles which are comparable to those published in the existing literature for other modern blade designs. This study confirmed the suitability
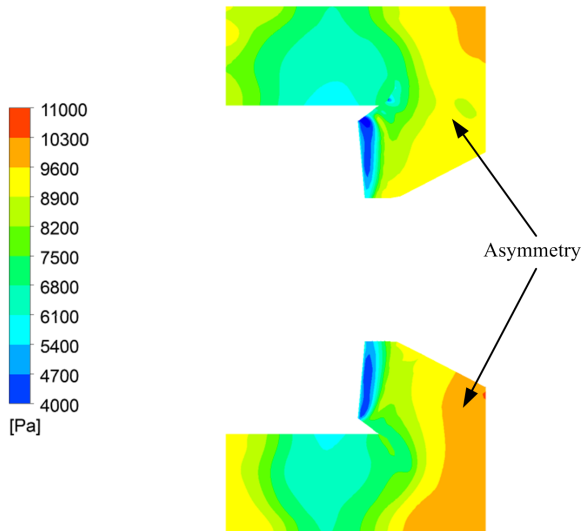
Figure 5.19: *P* Contours at the Exhaust Hood Half-Joint Plane [Pa]
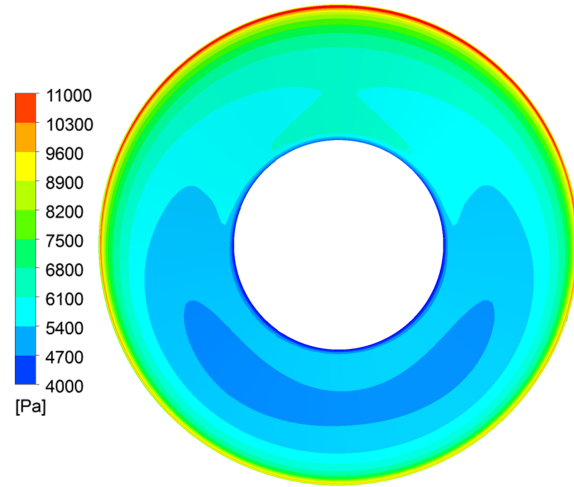
Figure 5.20: *P* Contours at the Exhaust Hood Inlet Plane [Pa]

of the DSTC for use as an inlet boundary condition to an exhaust hood CFD calculation.

In this chapter, the DSTC was used the provide an inlet boundary condition to the DEDHTC, to confirm whether the hood design produced a flow structure comparable to those found in the literature. A sequential approach, described in Section 4.2, to coupling the LSBs to the exhaust hood was adopted, in order to generate preliminary results with a low computational demand. The DEDHTC was shown in this chapter to successfully capture the main vortices, separations and flow characteristics observed by other researchers, such as:

1. Separation at the tip of the flow guide

2. Low pressure region under the flow guide

3. Counter-rotating vortices at the exit from the hood/condenser inlet plane

4. Asymmetry of the exhaust hood flow

Based on the validation results in this chapter, other researchers can be confident that the proposed geometry is a suitable test case for further, more comprehensive CFD studies. Further still, there is a need for experimental validation data, which is lacking in the field as a whole. With the DSEHTC geometry openly available, it is hoped that the geometry will go some way to facilitate the generation of additional experimental data by other workers in the field.

The preliminary DSTC geometry does not include the moving blade tip leakage and hence leakage effects were not included in any of the studies described in this chapter. The literature review has highlighted the universal acknowledgement of the importance of the tip leakage jet on the flow structure within the exhaust hood, and it is important that any future

studies include this effect to improve the accuracy of the hood inlet boundary condition. The influence of the rotor tip leakage on the flow structure, loss and vortex formation within the DEDHTC is explored next in Chapter 6.

6

Influence of Bulk Boundary Conditions on Exhaust Hood Performance

In Chapter 5, the DSTC was shown to provide a comparable inlet boundary condition to an exhaust hood calculation when validated against those published in existing literature. The DEDHTC was shown to produce a representative flow structure within the exhaust hood when the DSTC was used as its inlet boundary condition.

With the DSEHTC validated, this chapter explores the effect of increasing the boundary condition complexity: modelling the rotor tip leakage jet at hood inlet and including a condenser cooling water pressure gradient at hood outlet.

Musch et al. in 2013 [43] concluded the main effects (first-order effects) on the diffuser flow field are the tip jet and swirl of the last stage. Section 5.1.3 showed that the swirl angle produced by the DSTC is comparable with other modern blade designs published in the literature, however, the tip leakage jet was not simulated in the preliminary validation calculations. As the tip leakage jet is widely accepted as being one of the most significant factors influencing the flow structure and pressure recovery of the exhaust hood, it is important to assess its influence on the DEDHTC.

A comprehensive literature study has revealed that, to the author's knowledge, there has been no previous study of the effect of the outlet boundary condition on the exhaust hood flow structure; specifically the non-uniformity caused by the condenser cooling water pressure gradient. Currently, researchers impose a uniform static pressure outlet boundary, despite significant non-uniformities from the condenser. The absolute value of static pressure imposed in the calculation is typically dictated by the seasonal atmospheric pressure variations to be simulated (in coupled calculations) and matching the mass flow rate through the exhaust hood to the stage flow (in sequential calculations).

This chapter explores the influence of the bulk boundary conditions, tip leakage and condenser effects, on the exhaust hood flow structure in a sequential CFD calculation. This chapter is based on a publication in Part A of the IMechE Journal of Power and Energy [6].

6.1 Influence of the Tip Leakage

The accurate modelling of the last stage rotor tip leakage is widely accepted as one of the most important factors in generating a representative flow structure in the exhaust hood,

particularly in the flow guide region. The strong adverse pressure gradient along the flow guide can result in a separation forming in the upper diffuser in a region of large axial-radial turning. The high velocity jet which forms in the gap between the last stage rotor blade and the turbine shroud casing adds momentum to the boundary layer along the flow guide, and can suppress the separation. Suppressing the separation reduces the blockage effect in the diffuser, and subsequently can lead to a significant increase in static pressure recovery [32]. However, the C_p increase does not necessarily yield an increase in turbine efficiency as the benefits seen in the exhaust hood from the tip leakage flow should be balanced against the leakage loss in the turbine. Similarly, although tip jets of higher Mach number than the main flow yield a higher pressure recovery, the higher the jet Mach number the more significant the mixing losses between the tip jet and the bulk flow [16].

This section describes modifications made to the DSTC, outlined in Chapter 5, to include the effect of the rotor tip leakage and explore the effect this has on the exhaust hood flow structure.

6.1.1   Last Stage Blades with and without Rotor Tip Leakage Flows

Rotor Modifications

The DSTC geometry was modified to include the rotor tip gap. This was set at 4.2mm (approximately 0.5% of the blade height) based on discussions with Alstom Power in Rugby, from whom the original blade geometry was obtained, Figure 6.1.

As in Section 5.1.1, the DSTC was divided into two domains, coupled by a mass-averaged mixing plane, situated equidistant between stator trailing edge and rotor leading edge. The stator mesh and domain topology remained unchanged from calculations described in Chapter 5. The rotor domain tip region was re-meshed using the commercial grid generation software Pointwise V16.04 to include the tip gap, Figure 6.2. The same multi-block structured grid as described in Section 5.1.1 modelled the blade span. An unstructured block was used in the complex tip gap topology to achieve a good quality grid in a region of high blade twist and significant casing flare. The combination of a structured blade mesh and an unstructured tip gap has previously yielded successful results in the work of Verstraete et al. in 2012 [64]. The final rotor grid comprised of approximately 2.2 million cells with a y^+ between 30 and 200, meeting the y^+ criteria of the k-ϵ turbulence model with standard wall functions.

Computational Modelling

The effect of the tip leakage jet on flow structure was first explored with the LSBs considered separate to that of the exhaust hood. The calculation set-up for computing the tip leakage flows is identical to that of the stage calculations described in Section 4.2.1.

Comparison with No-Leakage Flows

As in Section 5.1.3, circumferentially averaged flow profiles downstream of the rotor trailing edge were generated for the DSTC with tip leakage modelling. The series of 45 points
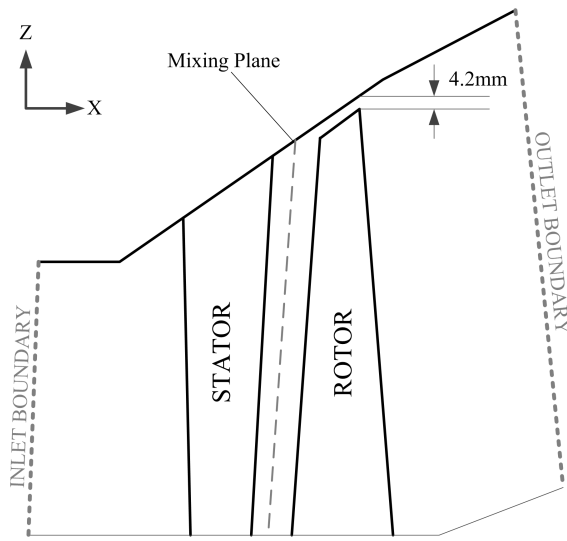
Figure 6.1: Stage Diagram with Tip Leakage
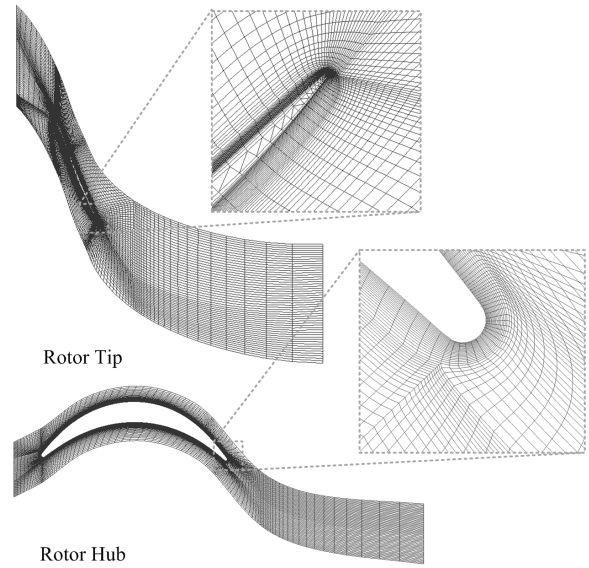
Figure 6.2: Modified Rotor Mesh with Tip Leakage

were taken at a profile 1.5 axial chord lengths downstream of the rotor trailing edge, at the Comparison Plane in Figure 5.1, to enable comparison with the non-tip leakage flow results.

Figures 6.3 and 6.4 compare the flow profiles of total pressure and swirl angle taken downstream of the rotor trailing edge, with and without tip leakage. Along the blade span, the two flow profiles are very similar. There is a small but finite reduction in swirl angle exiting the LSB when the tip gap is included. The leakage of flow from the pressure to suction surface of the blade results in a lower blade loading and a subsequently reduced axial velocity which is reflected in the lower swirl by around 2° compared with the non-leakage case.

The effect of tip leakage can predominately be seen in the top 5% of the blade. The elevated total pressure in the tip region, evident in all tip leakage flows, can be seen in Figure 6.3. A significantly higher swirl angle is observed in the tip region when tip leakage is modelled, shown in Figure 6.4; an effect also noted in the comprehensive study of tip leakage flows carried out by Li et al. in 2013 [32]. Swirl angle, as previously discussed, has been widely shown to have a significant influence on the flow structure in an exhaust hood calculation. This higher swirl angle at the outer radius of the hood inlet annulus will influence the asymmetry of the coupled exhaust hood system.

6.1.2   Exhaust Hood with and without Tip Leakage

With the effect of the rotor tip leakage captured in the flow profiles analysed in Section 6.1.1, these distributions can be used as an inlet boundary condition to a sequentially coupled exhaust hood calculation to determine the effect tip leakage flows have to on the DEDHTC. The tip leakage results will be compared with the non-tip leakage flow results generated in Chapter 5.2.4.
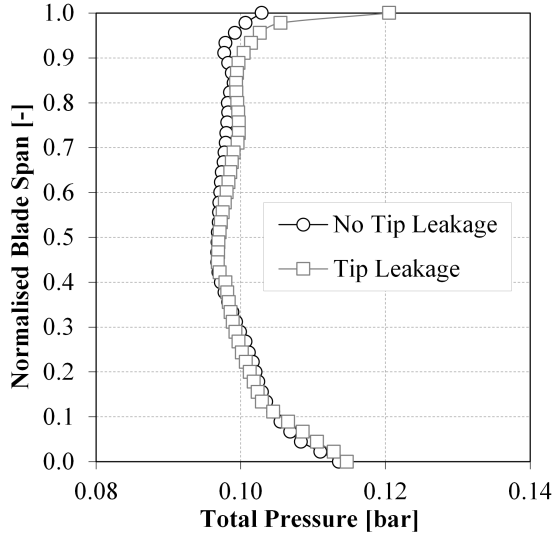
Figure 6.3: P_t Distribution at the Comparison Plane with and without Tip Leakage Included [bar]
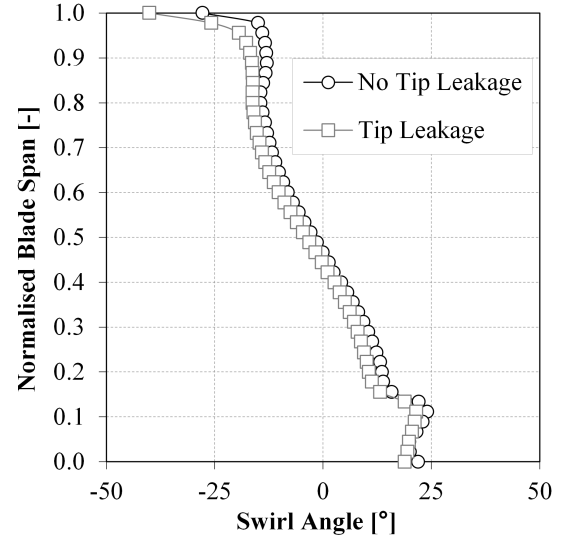
Figure 6.4: Swirl Angle (α) Distribution at the Comparison Plane with and without Tip Leakage Included [°]

Method	C_p	ΔC_p
No Tip Leakage	-0.035	-
Tip Leakage	0.236	+0.271

Table 6.1: C_p for Exhaust Hood with and without Rotor Tip Leakage Flows [-]

Computational Modelling

The computational set-up for the sequential exhaust hood calculation is identical to those detailed in Section 4.2.2 and as used in Section 5.2.2. Circumferentially averaged profiles taken at the rotor trailing edge plane of the DSTC tip leakage calculation were used as the inlet boundary condition to the isolated exhaust hood calculation. The profiles were once again scaled in axial height to be compatible with the smaller exhaust hood inlet annulus, set upstream of its baseline location to achieve convergence. The same hood outlet static pressure was used for both tip leakage and non-tip leakage exhaust hood calculations to enable a direct comparison between the static pressure recovery coefficients to be made and to ensure the same mass flow rate through the exhaust hood as through the stage.

Comparison of Hood Flow with and without Rotor Blade Tip Leakage Flows

There is a significant (+0.271) rise in the predicted value of C_p when the tip leakage jet is included in the simulations to 0.236, from -0.035 without the tip leakage jet, summarised in Table 6.1. This is a similar magnitude (0.01 to 0.398) to that observed by Li et al. [32] in a comprehensive CFD study of tip leakage flows, giving confidence in the reliability of the results.

The increase in pressure recovery is due to the high velocity jet energizing the flow along
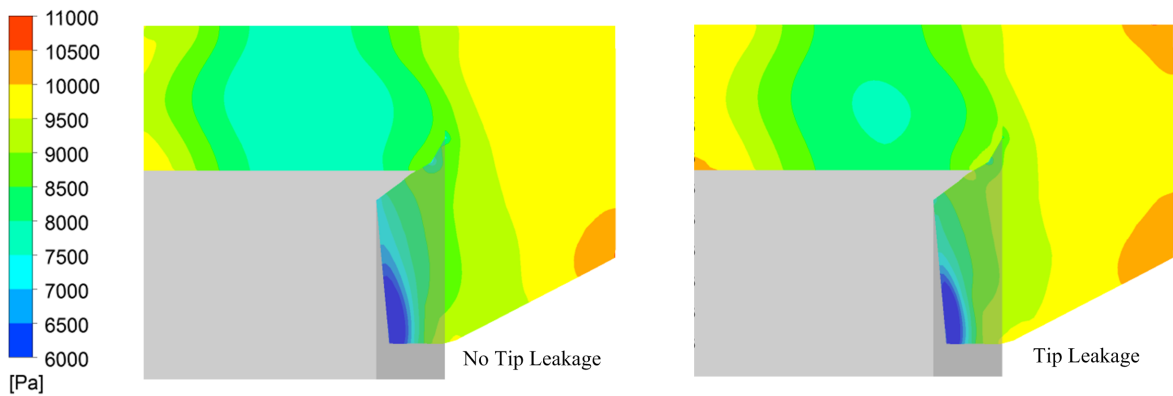
Figure 6.5: *P* Contours at the Meridional Plane [Pa]
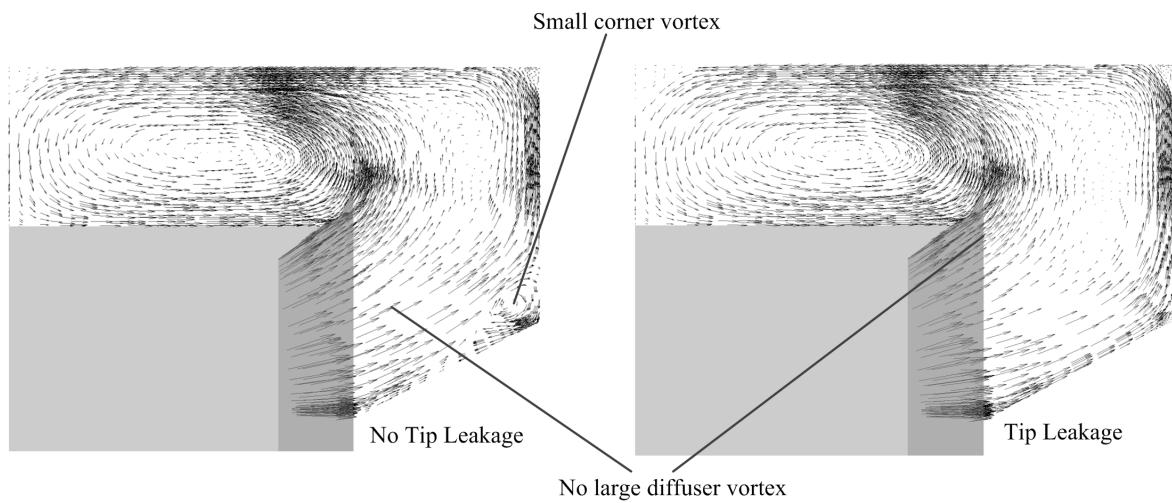
Figure 6.6: Velocity Vectors at the Meridional Plane

the flow guide, reducing the size of the low pressure region, shown in Figure 6.5. No large vortex exists in the diffuser of the DEDHTC, as shown in Figure 6.6, as observed in some other published research, and subsequently the tip leakage jet cannot suppress a vortex forming near the flow guide and reduce its blockage effect. Instead the tip leakage jet has the positive effect of increasing the static pressure in the diffuser, contributing to a higher static pressure recovery, an effect similarly observed in a study by Li et al. [32]. However, a small corner vortex has been eliminated when tip leakage is included in the model, but is not the primary contributor to loss due to its small magnitude.

The tip leakage jet primarily influences the flow field in the proximity of the flow guide, highlighted in the static pressure contours and velocity vectors in Figure 6.7. The high energy of the flow from the leakage jet reduces the low pressure region at each kink in the flow guide and additionally increases the overall static pressure in the diffuser. The positive influence of the leakage jet extends to the region behind the flow guide, where the strength of the low pressure vortex core has reduced, as shown in Figures 6.5 and 6.6. Reducing the strength of the flow guide tip vortex reduces the blockage effect in the collector and contributes to a higher pressure recovery throughout the whole exhaust hood.
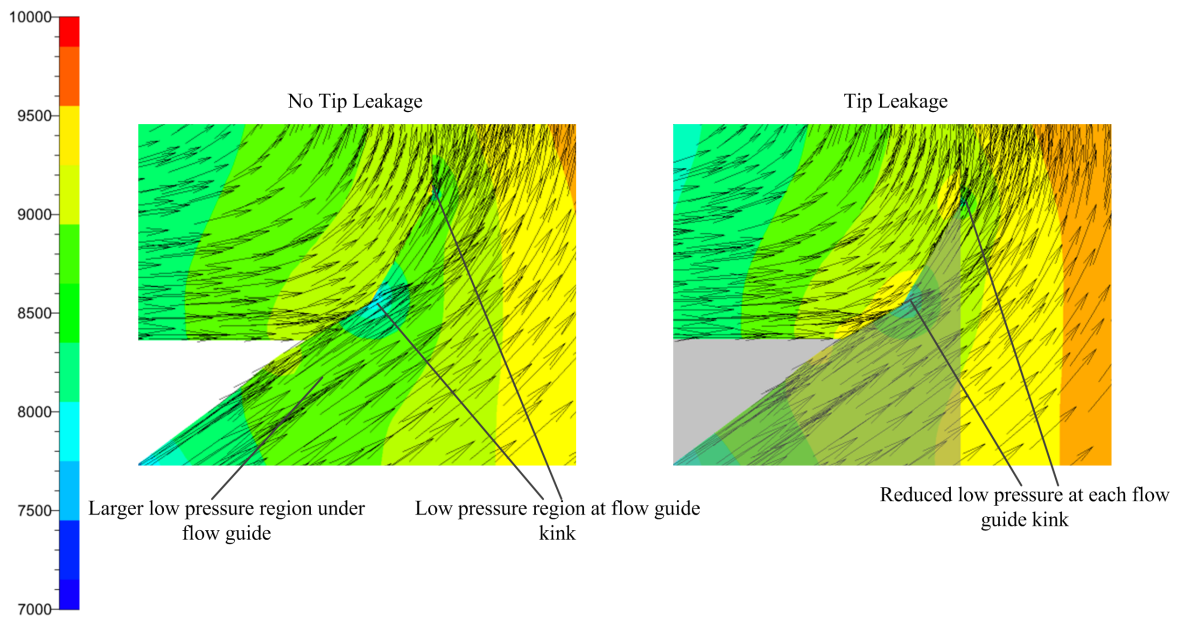
Figure 6.7: Velocity Vectors and P Contours at the Meridional Plane Flow Guide [Pa]
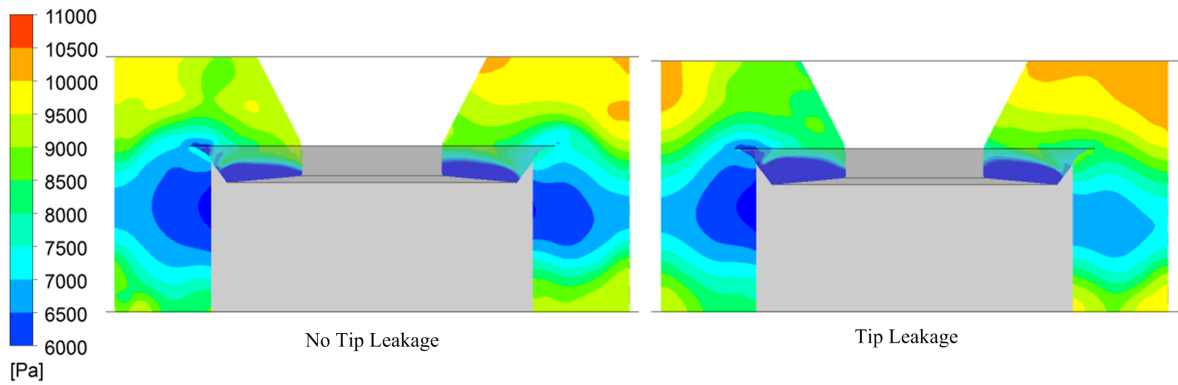
Figure 6.8: P Contours at the Half-Joint Plane [Pa]

The flow is noticeably more asymmetric with the addition of the tip leakage jet, as shown in Figure 6.8. The magnitude of the low pressure regions on both the left and right hand sides of the exhaust hood has decreased with the addition of the tip leakage jet due to the reduced vortex strength formed in the upper exhaust hood. However, the magnitude of this reduction is different for the two sides. This is due to the change in inlet tangential velocity, as the high velocity jet adds more flow at a higher radius, increasing the swirl at the tip and driving more fluid to the left hand side of the exhaust hood, as shown in Figure 6.9.

To quantify the changes in asymmetry at the exhaust hood half-joint plane, a root mean square (RMS) metric was devised. The static pressure from an array of 54 data points on the left hand side of the exhaust hood was compared with the same, mirrored array on the right, see Figure 6.10. The difference in static pressure between corresponding points on each side of the exhaust hood, $U_n - U_{-n}$, was computed and input into Equation 6.1. The ΔP at each point was compared with the average ΔP, $\bar{U}$, across the half-joint plane. The output $RMS_{\Delta P}$ gives a measure of the variation in static pressure between left and right hand side
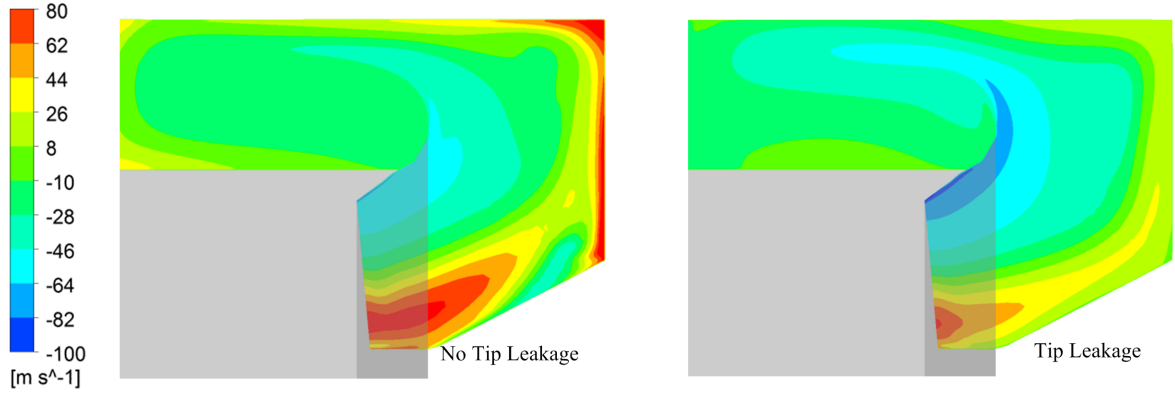
Figure 6.9: V_t Contours at the Meridional Plane [m·s^{-1}]

Method	$RMS_{\Delta P}$
No Tip Leakage	318.69
Tip Leakage	441.12

Table 6.2: $RMS_{\Delta P}$ at Exhaust Hood Half-Joint Plane [Pa]

of the exhaust hood.

$$RMS_{\Delta U} = \sqrt{\frac{((U_1 - U_{-1}) - \bar{U})^2 + ((U_2 - U_{-2}) - \bar{U})^2 + ...((U_n - U_{-n}) - \bar{U})^2}{n}} \qquad (6.1)$$

The additional inlet swirl as a result of the addition of the tip leakage jet has increased the asymmetry between the left and right hand side of the exhaust hood, as shown in Table 6.2. Although increased asymmetry is a negative characteristic of exhaust hood flows, the positive influence of the leakage flows on the flow guide region outweighs the asymmetry disadvantages.

6.2   Influence of Condenser Pressure Variations

At present, the majority of research focuses on the importance of the inlet boundary conditions and little attention is paid to ensuring representative conditions at hood outlet. Most researchers model the exhaust hood outlet as a constant static pressure boundary condition, set to give the correct mass flow rate through the exhaust hood system. The absolute value of this static pressure is governed by the condenser heat sink, which varies seasonally with the atmospheric temperature and/or sea water temperature (depending on the method of cooling). This annual variation has been shown to be as large as 0.29 bar (from 0.23 bar to 0.52 bar) for a sea water cooled plant in Finland [45].

An EDF study noted that large, potentially unsafe vibrations in the turbine shaft bearings are present at critical condenser pressures due to a shift in exhaust hood recirculations which drive water films down the bearing cone causing a thermal imbalance in the shaft [52]. This
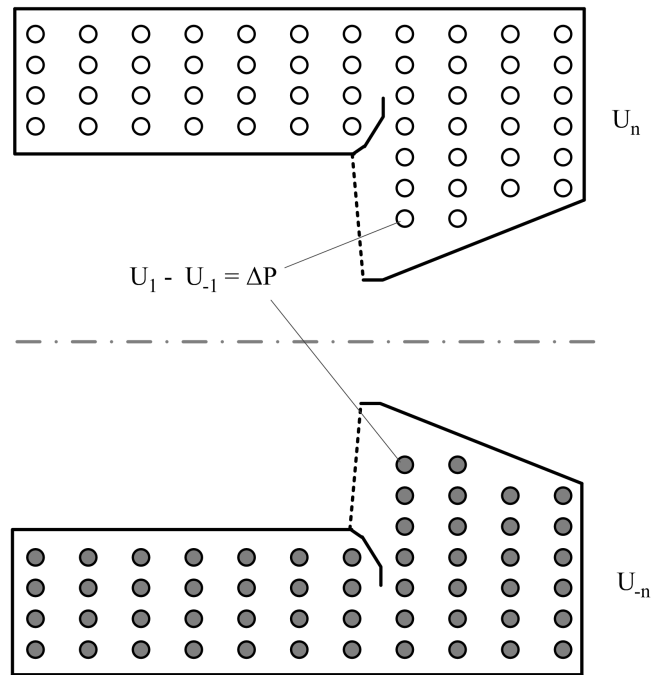
Figure 6.10: Diagram of $RMS_{\Delta P}$ Array at Exhaust Hood Half-Joint Plane

study also showed that exhaust hood flows can be clearly categorised depending on the condenser operating point. At nominal conditions, the turbine is most efficient and both sub and supersonic flows occur. At lower pressures the recirculations move upstream and the stage is choked. At higher pressures the recirculations move further upstream until reaching the LSBs. All these studies were carried out at uniform outlet pressures and no account was taken of the large pressure gradient which in reality occurs in water cooled steam turbine condensers.

6.2.1   Development of a Representative Outlet Boundary Condition

Variations in static pressure at the exhaust hood outlet are very plant specific; dictated by the individual exhaust hood geometry and the form of the condenser. To the author's knowledge, no representative field data is available for a steam turbine exhaust hood outlet or condenser inlet.

In order to address this, a representative outlet boundary condition for an exhaust hood simulation has been developed to accompany the DSEHTC. The boundary condition is based on field data taken from a 700MW steam power plant in the early 1990's. Figure 6.11 shows the normalized static pressure contours for outlet of the steam turbine plant. The exhaust hood outlet features a large variation in static pressure due to upstream, 'exhaust-specific' features, such as separations from the condenser neck walls, blockages due to internal furniture such as the bleed steam pipework and longitudinal stiffening beams and the cores of the pair of counter-rotating vortices which form from the separations generated in the exhaust diffuser that progress down through the condenser neck. This highlights the significant variation in
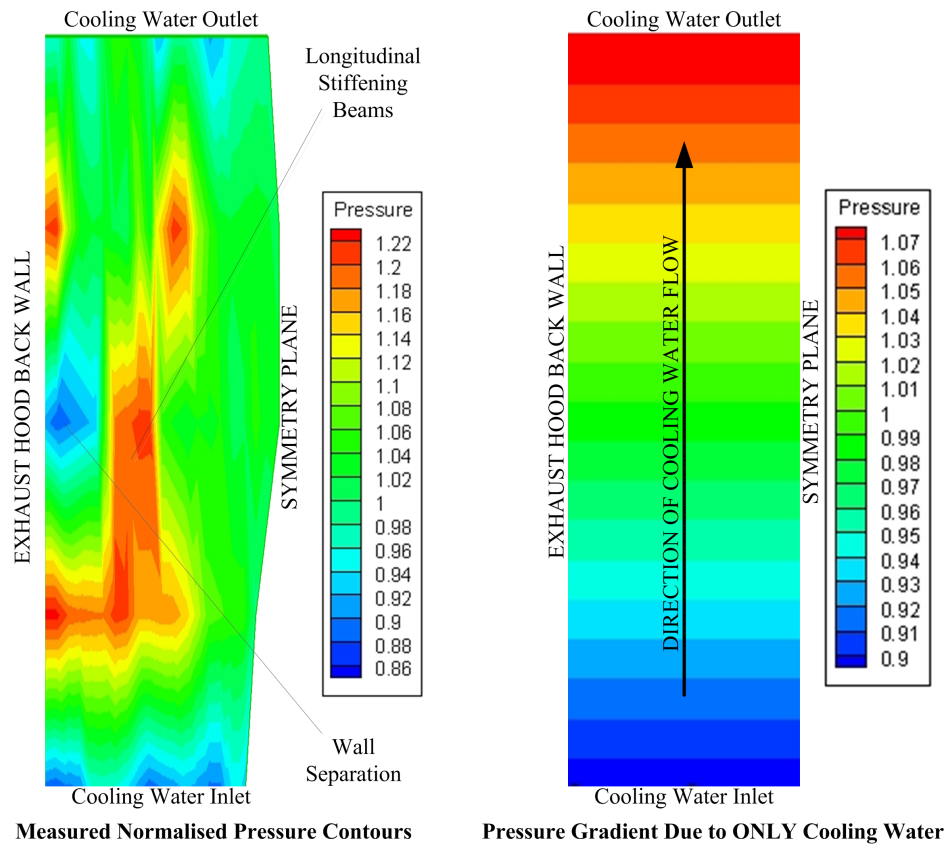
Figure 6.11: Normalised Pressure Contours Measured in the Plant and the Corresponding Generic Boundary Condition due to Only Cooling Water Flow

static pressure over the plane, from 22% above the mean to 14% below.

In order to generate a representative, but 'generic', exhaust hood outlet boundary condition, the static pressure non-uniformity was formulated based *only* on the a percentage pressure variation between left hand and right hand sides of the exhaust hood (relative to the average exhaust hood outlet static pressure) purely due to the condenser cooling water flow. Field data indicated this to be from 10% below average at the cooling water inlet, to 7% above average level at the cooling water outlet, shown in Figure 6.11. As the cooling water flows from cooling water inlet to outlet through the condenser tube nests, its temperature gradually increases giving rise to a transverse hood exit flow pressure gradient, shown diagrammatically in Figure 6.12. This pressure gradient was set at the outlet boundary condition to a sequential exhaust hood calculation with tip leakage flows modelled to assess the influence of the condenser cooling water flows on the flow structure within the exhaust hood.

6.2.2 Exhaust Hood with and without Condenser Pressure Gradient

Computational Modelling

The calculation, as described in Section 6.1.2, is used as the initial solution for the condenser pressure gradient modelling. The non-uniform outlet static pressure boundary condition was applied to the CFD model and calculation continued until convergence, roughly 2000
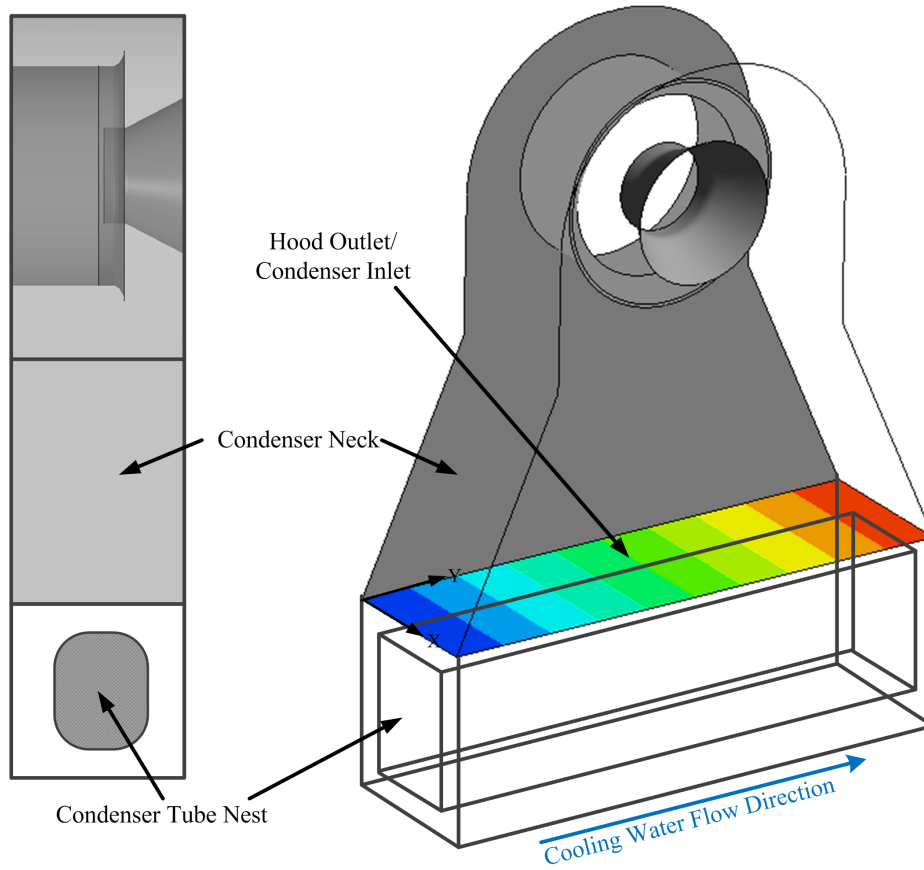
Figure 6.12: 'Generic' Outlet Boundary Condition and Condenser Diagram

iterations. This was an iterative process, as the average outlet static pressure had to be adjusted to give the same mass flow rate as in the non-tip/tip leakage stage calculations. The required average hood exit pressure was found to be 7800Pa. Calculations were carried out for cooling water pressure gradients in both directions.

Comparison with Uniform Outlet Flows

The application of a non-uniform outlet boundary condition is shown to reduce the asymmetry of the flow when the pressure gradient acts in the forwards direction, as shown the central image in Figure 6.8. The outlet pressure gradient works against the asymmetry which is inherent in the flow due to the rotation of the turbine blades, and, due to the direction of the condenser cooling water flow, reducing its effect. This is particularly noticeable at the hood half-joint plane. The asymmetry characteristic of the exhaust hood when a non-uniform outlet pressure gradient is applied is dependent on the direction of the condenser cooling water flow (or conversely the direction of rotation of the moving blades, which is not standard between power plant designs). If the pressure gradient is reversed, the opposite effect occurs and the pressure gradient contributes additionally to the asymmetry evident between the left and right hand sides of the exhaust hood, shown in Figure 6.13.

To quantify the magnitude of the influence of the condenser cooling water flow on the exhaust hood asymmetry, the $RMS_{\Delta P}$ metric, devised in Equation 6.1, is applied to the
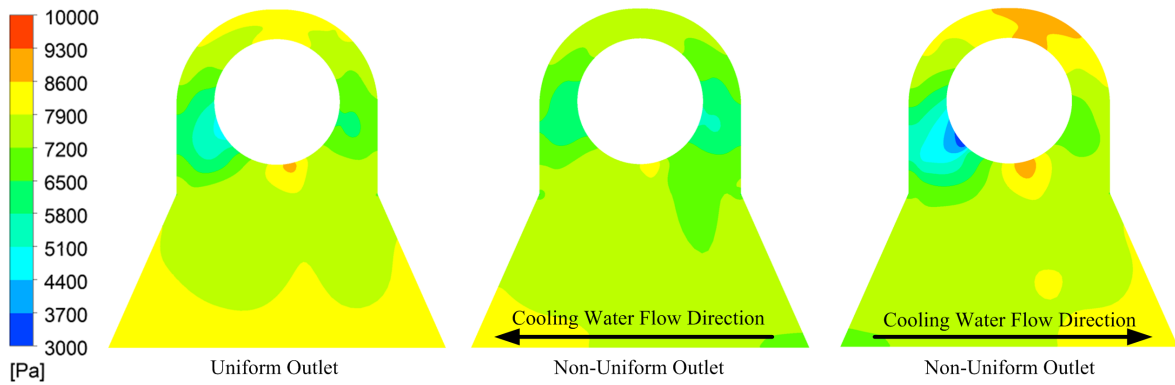
Figure 6.13: P Contours at the Hood Front Plane [Pa]

Tip Leakage	Outlet Pressure	$RMS_{\Delta P}$	$\Delta RMS_{\Delta P}$	$\Delta\%$
No Tip Leakage	Uniform	318.69	-	-
Tip Leakage	Uniform	441.12	+122.43	+38%
Tip Leakage	Forward Gradient	376.85	-64.27	-14%
Tip Leakage	Reversed Gradient	696.23	+319.38	+84%

Table 6.3: $RMS_{\Delta P}$ at the Half-Joint Plane for Different Configurations [Pa]

non-uniform outlet boundary condition test cases. The results are tabulated in Table 6.3. The inclusion of the outlet pressure gradient almost eliminates the increased variation as a result of the addition of the tip leakage jet. However, when the pressure gradient is reversed, the asymmetry level increases to over twice that of the baseline, non-tip leakage case.

Although Table 6.3 reveals the significant influence the addition of the outlet pressure gradient has on the flow structure within the exhaust hood, there is not the same level of influence on the loss coefficient. The static pressure contours in Figure 6.14 progressing through the condenser neck show the possible improvement in flow asymmetry characteristics with a non-uniform outlet boundary condition. However, the magnitude of the low pressure vortex core on the right hand side of the exhaust hood has increased due to the large low pressure volume in the condenser neck, highlighted in the velocity vectors at the top of the condenser neck in Figure 6.15. This has lead to the overall poorer predicted pressure recovery in the exhaust hood, decreasing to 0.1839 from the previous value of 0.236 calculated before the addition of the non-uniform outlet condition. This drops further to 0.167 with the reversed pressure gradient due to the increased exhaust hood flow asymmetry. However, the magnitude of this change is still only between 5% and 7% of the overall system loss.

6.3   Relative Influence of Bulk Boundary Conditions

Modelling the tip leakage jet and condenser cooling water pressure gradient increases the complexity of the computational model, resulting in a change in both observed flow structure and static pressure recovery coefficient. The changes in C_p are shown in Table 6.4.

The inclusion of the tip leakage jet has been shown to increase the static pressure recovery
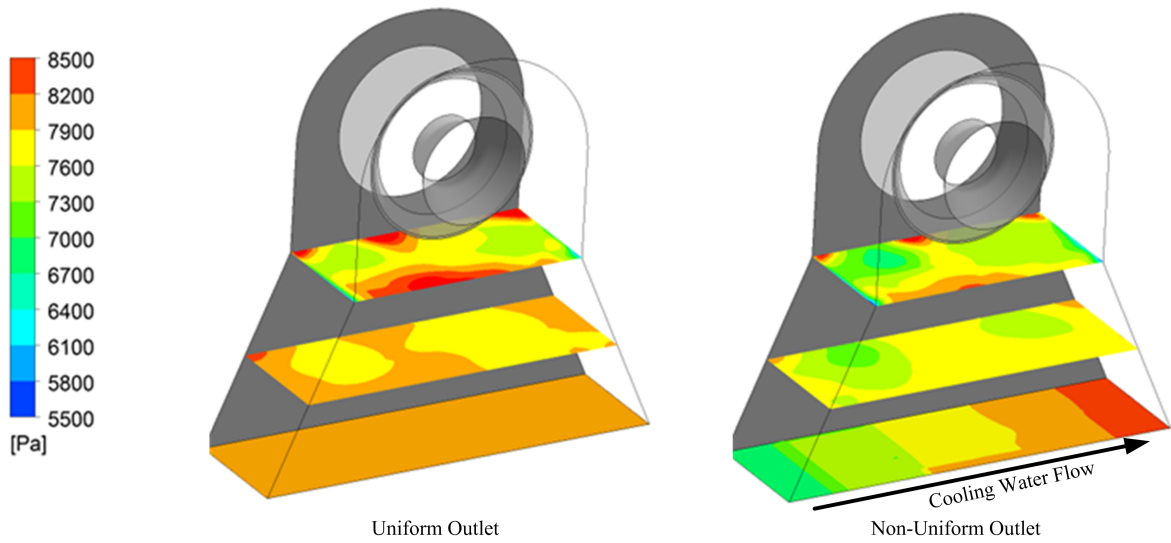
Figure 6.14: P Contours within the Condenser Neck [Pa]
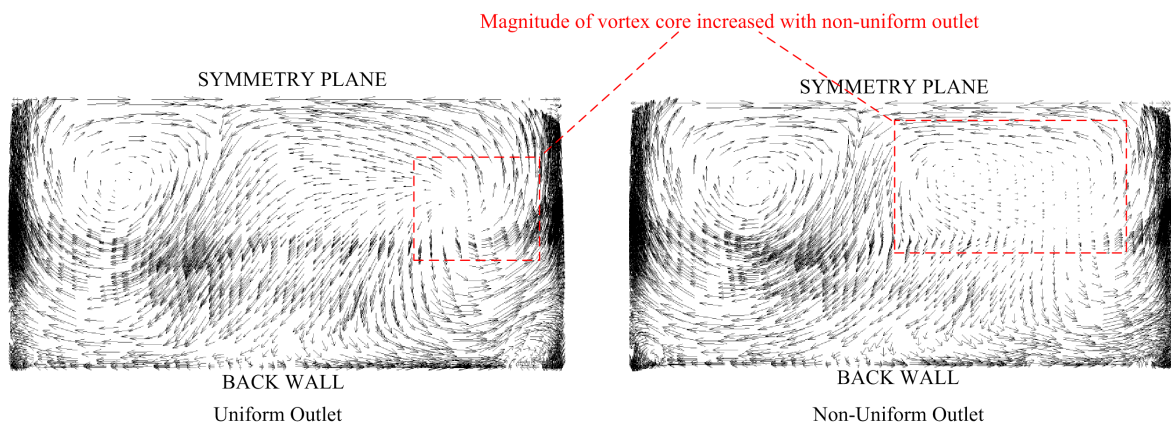
Figure 6.15: Velocity Vectors at the Top of the Condenser Neck

in the exhaust hood, consistent with findings in other published research. This is due to the additional momentum in the high velocity jet, reducing the low pressure region near the hood flow guide. However, the asymmetry of the flow increases due to the additional swirl in the tip leakage flow.

A representative condenser cooling water pressure gradient, not previously modelled in other published research, has been shown to have a large influence on the flow structure and to a lesser extent the pressure recovery inside the exhaust diffuser.

The significance of modelling these two bulk boundary conditions can be quantified from the C_p changes observed in other author's work when changing aspects such as: turbine exit conditions, the inclusion of internal reinforcements, bearing cone and other optimisations and the inclusion of circumferential non-uniformities.

An experimental study by Liu et al. in 2003 [36] showed a C_p of 0.350 when using a uniform inlet boundary condition but a C_p of -0.218 when using a non-uniform inlet boundary with a swirl and total pressure representative of a turbine exit. This leads to an ΔC_p of around 0.57.

Tip Leakage	Outlet Pressure	C_p	ΔC_p
No Tip Leakage	Uniform	-0.035	-
Tip Leakage	Uniform	0.236	+0.271
Tip Leakage	Forward Gradient	0.186	-0.05
Tip Leakage	Reversed Gradient	0.167	-0.02

Table 6.4: C_p for Different Configuration [-]

Author	Change Made	Typical ΔC_p
Liu et al.	Diffuser boundary conditions	0.57
Wang et al. or Yoon et al.	Geometrical optimisation	0.30
Tajc et al.	Exhaust reinforcements modelled	0.14
Ris et al.	Change of turbulence model	0.01
Present	Rotor Tip Leakage	0.27
Present	Condenser pressure gradient	0.05

Table 6.5: ΔC_p for Different Calculation Methods and Geometry Configurations

Typically, an exhaust diffuser flow guide and bearing cone optimisation study yields an improved C_p of around 0.3, ranging from 0.26 [66] to 0.38 [68].

Tajc et al. studied the effect of internal reinforcements on C_p on a range of hood geometries and found an average increase in loss coefficient of 0.138 when the exhaust hood furniture was modelled [56].

Table 6.5 gives a summary of the ΔC_p reported by other workers. The table also includes an estimate of the ΔC_p introduced by changing the turbulence model estimated from work by Ris et al. [47]. Although Table 6.5 is a superficial study, the results highlight the clear influence that accurate boundary condition modelling has on the predicted performance of the exhaust diffuser system. The influence of a representative condenser pressure gradient on C_p is less significant than geometrical optimisations and the addition of internal reinforcement, but is more important than turbulence model selection.

6.4   Concluding Remarks

In this chapter, tip leakage modelling was included in the DSTC calculations. As expected, when applied to the exhaust hood calculation, this had a significant influence on the pressure recovery coefficient, increasing it by 0.27. The flow structure in the exhaust hood is also affected. The large tangential velocity component in the leakage jet results in a higher inlet swirl, contributing to an increased asymmetry at the exhaust hood half-joint plane. These results highlight the importance of tip leakage modelling to generate an exhaust hood flow structure of increased accuracy and should consequently be considered a modelling effect of first-order importance. In addition, comparison with loss coefficient trends and asymmetry levels published in the literature for similar designs, gives confidence in the results for the DEDHTC design.

An asymmetric exhaust hood outlet boundary condition, representative of transverse cooling water flow in the condenser, was applied to exhaust hood calculations for the first time. A 'generic' outlet boundary condition was developed from field data. This generic condition is freely available to other researchers to include in their studies. The increased asymmetry at the half-joint plane as a result of the inclusion of tip leakage is halved by the addition of the condenser pressure gradient in one direction. This is because the direction of the outlet pressure gradient works against the left to right asymmetry of the hood due to the rotor direction, reducing its effect. This consequently means the *direction* of the condenser cooing water pressure gradient strongly influences the level of asymmetry within the hood. Reversing the direction of the hood exit pressure gradient doubles the asymmetry at the half-joint plane.

Despite the strong influence of outlet boundary gradient on flow structure, the effect on static pressure recovery coefficient is small, with a maximum change of around 0.05. To contextualise, this change is smaller than other authors have observed when adding exhaust reinforcements or conducting optimisation studies of bearing cones and flow guides. The asymmetric condenser cooling water boundary condition should be considered as a second-order effect on loss as more significant influencing factors should be prioritised in state of the art exhaust design calculations. However, for a representative prediction of flow structure, the hood exit non-uniformities should be included. As the state of the art in diffuser design advances and smaller gains are achievable, this boundary condition will need to be included to extract the best performance.

All of the studies in this chapter were conducted using a sequential approach to coupling the exhaust hood to the turbine. This computationally efficient process is ideal for the preliminary studies on the DSEHTC conducted in the previous chapters; but for advanced studies of both the flow structure and loss coefficient, it is important to capture the full *interaction* between the turbine and exhaust hood. Chapter 7 studies the influence of bi-directional, fully coupled approaches, on predictions of the exhaust hood system.

7

Single Passage Coupled Calculations

In previous chapters, flow calculations on the DSEHTC have only been described using a sequential coupling method. Although this method is computationally efficient and useful for producing indicative flow field predictions (such as those required in Chapters 5 and 6 for validating the geometry and bulk boundary condition trends) it only partially captures the interaction between stage and exhaust hood. It has been widely recognized for some decades that it is essential to accurately represent the strong coupling between the last stage blades and the diffuser/hood inlet, in order to correctly capture the flow through the exhaust hood of steam turbine low pressure cylinders.

As described in the literature review in Chapter 2, the most computationally efficient method of bi-directionally coupling the exhaust hood to the turbine is by means of a mixing plane. The low cell count and simple circumferential averaging at the interface results in fast convergence times, however, the interface treatment means that the non-axisymmetric exhaust hood flow field is mixed out.

The non-linear harmonic (NLH) method has been successfully applied to model asymmetric inlet fan flow fields in gas turbines and was recognised as a potential method for asymmetric coupling of the turbine stage and exhaust hood flow field. As only one blade passage has to be modelled with the NLH method, the low cell count means this approach is more computationally efficient than full annulus methods which are, at present, the current industry standard for capturing the exhaust hood inlet asymmetry. The NLH interface treatment, described in depth in Section 4.3.3, is more complex than the mixing plane approach, and the computational savings to not scale directly with cell count because a greater number of transport equations have to solved with the NLH method.

This chapter presents the first application of the non-linear harmonic approach for modelling a coupled steam turbine and exhaust hood system. This NLH approach is compared with results obtained using a mixing plane. This chapter is based on a publication in the ASME Journal of Engineering for Gas Turbines and Power, [7]

7.1 Computational Modelling

In order to simultaneously model the turbine and exhaust hood flow field, modifications were required to the meshes described in earlier chapters for calculating the DSEHTC. The rotor outlet plane and exhaust hood inlet plane were repositioned to lie at the same axial location,

Figure 7.1. The treatment of the rotor outlet/exhaust hood inlet interface by, in this case, either a mixing plane or the non-linear harmonic approach, defines the complexity of the flow calculation.

A new commercial mesh generation package and flow solver were adopted for the bi-directionally coupled flow calculations; NUMECA AutoGrid5 and Fine/Turbo 8.10, respectively. This decision was taken as the NLH approach (and mixing plane) were already integrated into the commercial CFD software.

7.1.1   Grid Generation

It was required to re-mesh the LSBs as the software requires a structured hexahedral grid with a cell count which enables a *multi-grid* approach. The multi-grid approach works by initialising the whole calculation domain on a coarse grid, interpolating onto a finer grid once a desired level of convergence is reached. This reduces the number of iterations required for convergence and subsequently the computational time. Figure 7.2 illustrates the multi-grid approach. During each computation, high frequency errors are rapidly damped out on a fine grid but low frequency errors can require many iterations to be removed. As the low frequency errors on a fine grid appear as high frequency errors on a coarser grid, the progression from a coarse grid to a fine grid means the high frequency errors are damped out faster. This accelerates convergence time and is the underlying principle behind the multi-grid approach. Each multi-grid requires the cell counts in the I, J and K directions of each block to have $(constant + 2)^m + 1$ cells, where m is the number of multigrid levels. This is simple and quick to implement as the software incorporates an automatic mesh generation package.

As a new mesh was required to be compatible with the new software, the opportunity was taken to refine the boundary layer simulation. It is widely accepted that in the highly separated flows, such at those in the exhaust hood system, wall functions should be used with caution as the size of the separation region can be poorly captured with a coarse boundary layer grid [63]. Subsequently the mesh was modified so that y^+ values were kept below 10 everywhere in the domain.

Following recommendations from literature and the confirmed findings in Chapter 6, it was important to include the rotor tip leakage. 17 cells spanned the 4.2mm tip gap, so that the tip flow was accurately captured in the simulations.

The preliminary stator and rotor grids were further modified in accordance with recommendations from Vilmin et al. [65]. Results from a set of 2D experiments described in the paper have shown that at least 30N cells are needed in the tangential (Θ) direction, where N is the number of harmonic frequencies that are to be calculated. The reason for this number of Θ cells is as follows.

In a turbine stage calculation, if the number of blades in stator and rotor blade rows are equal then at least 30N cells must be used in the Θ-direction in the meshes on either side of the blade row interface, as shown in Figure 7.3. If, however, there are more rotor blades than there are stator blades, the pitch of the rotor blades will be less than that of the stator blades. So, the minimum number of cells needed in the mesh on the stator side of the interface has to
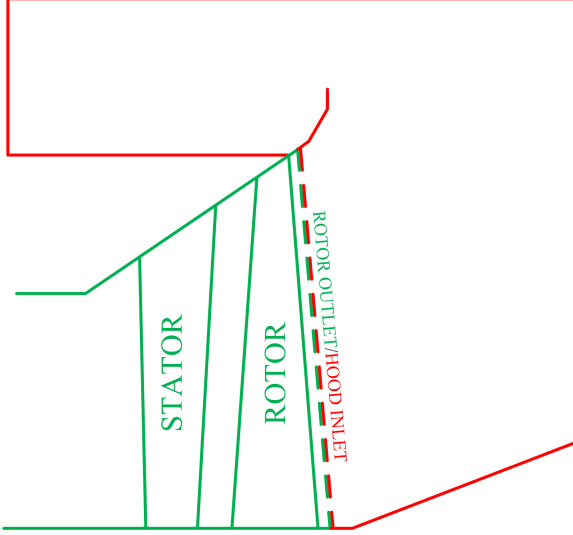
Figure 7.1: Schematic of a Coupled Calculation LSB/Hood Interface
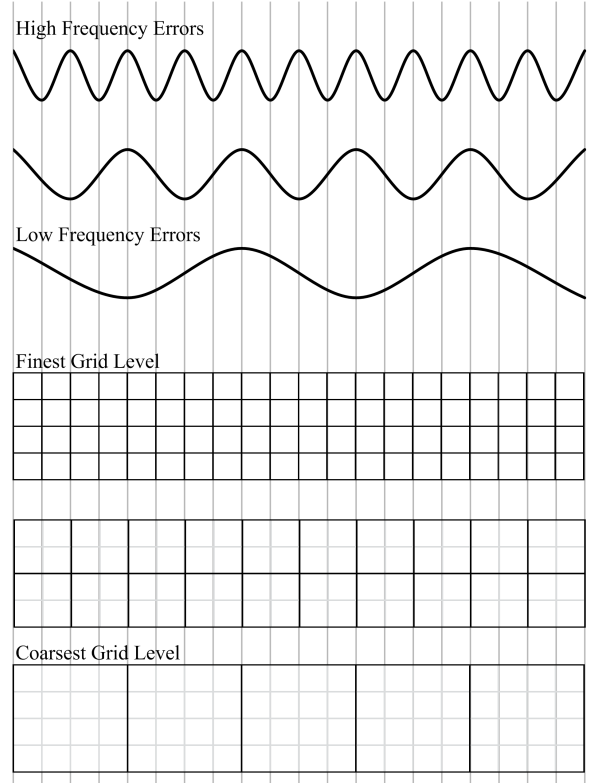
Figure 7.2: Frequency Error Spectrum and Corresponding Grids

be increased, to ensure that at least 30N cells are maintained across a rotor pitch distance in the stator blade row mesh. Conversely, the minimum number of Θ-cells needed in the rotor blade row mesh will reduce, because of the circumferential length the rotor blade row passage is less than the stator blade pitch and 30N Θ-cells per stator blade pitch can be achieved with less than this number of cells in the rotor mesh. The reverse argument is true for turbine stage calculations that feature more stator blades than rotor blades. In general, the number of cells needed in the Θ-direction on either side of the stator-rotor interface will be weighted by the number of blades in the stator and rotor blade rows according to Equations 7.1 and 7.2. These guidelines are obtained from 2D compressor experiments by Vilmin et al. [65]. This must also be applied at the interface between rotor and exhaust hood.

$$\Theta_{\text{cells upstream}} = 30N\frac{n_d}{n_u} \tag{7.1}$$

$$\Theta_{\text{cells downstream}} = 30N\frac{n_u}{n_d} \tag{7.2}$$

where n_u and n_d are the number of blades in the upstream and downstream blade rows, 60 and 65 respectively.

As described in Section 4.3.3, the number of harmonics to model (N) is a user defined variable in the NLH approach, which should be explored in order to determine the balance between solution accuracy and computational expense. To determine this compromise, four

Number of Harmonics	$\Theta_{upstream}$	$\Theta_{downstream}$	LSB Cell Count
N=1	35	31	812832
N=2	67	59	980464
N=3	99	83	1447148
N=4	131	111	1540848

Table 7.1: Last Stage Blade Cell Counts Scaled for Harmonics
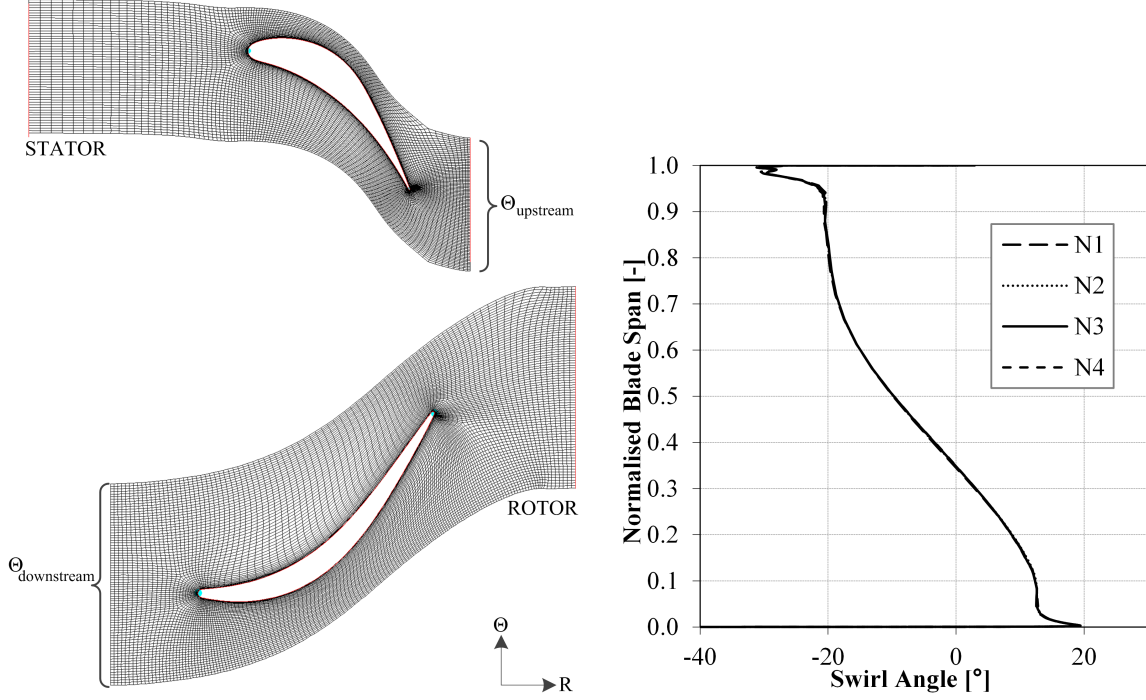
Figure 7.3: Diagram of Θ Cell Count Requirements

Figure 7.4: Swirl Angle (α) Variations at Rotor Outlet with Cell Count [°]

LSB grids were produced with Θ-direction cell counts appropriate for modelling between 1 and 4 harmonics. The cell counts are tabulated in Table 7.1.

As the Θ cell count is different for each grid tabulated in 7.1 the mesh independency of the solution needs to be shown to verify that changes between results obtained with different numbers of harmonics, were principally caused by the change in the number of harmonics used and not by the accompanying change in the mesh used. This was done by carrying out steady-state calculations with a mixing plane coupling the rotor blade passage to the stator blade passage, for each of the grids in Table 7.1. The exhaust hood was not included in these simulations. These calculations were carried out using the NUMECA Fine/Turbo 8.10 solver with the Low-Re Spalart-Allmaras turbulence model. The same pitch-averaged stator inlet boundary conditions for total pressure, total temperature and three velocity components, were used as applied in the previous sequential simulations, (see Figures 4.2 and 4.3). The rotor exit static pressure was set to 8800Pa in all of the calculations with working fluid properties as listed previously in Table 4.1. Convergence was achieved in less than 2000 iterations with a 3-level multi-grid and a CFL number equal to 3.
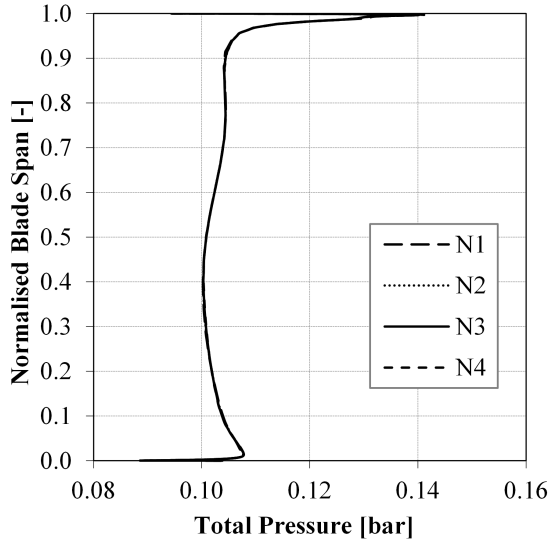
Figure 7.5: P_t Variations at Rotor Outlet with Cell Count [Pa]
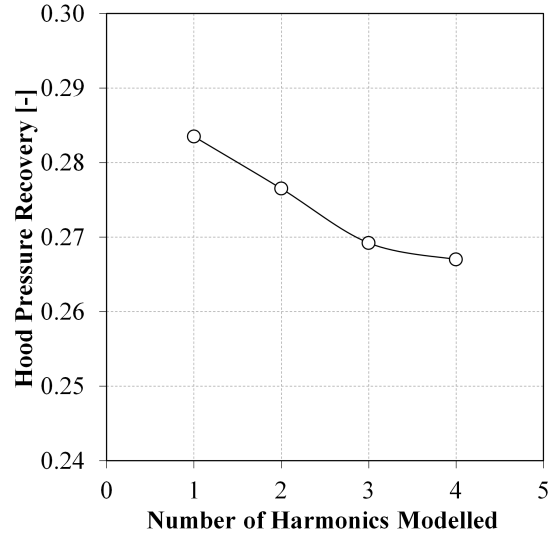
Figure 7.6: C_p Variations with Number of Harmonics Modelled

Figures 7.4 and 7.5 show the swirl angle and total pressure radial variations downstream of the rotor trailing edge. The last stage blade meshes generated for modelling between 1 and 4 harmonics yield essentially identical results confirming that any differences observed in the NLH calculations to follow can only be due to the number of harmonics modelled. The effect of number of harmonics is explored in Section 7.1.2.

The exhaust hood grid was not re-meshed in NUMECA AutoGrid5 as it was possible to import the mesh already generated in Pointwise V16.04 as described previously in Section 5.2.1. This mesh, however, did require some modification to match the Low-Re requirements of the turbulence model. The mesh topology was unchanged but the cell count was increased to include a finer boundary layer grid so a y^+ of less than 10 could be achieved everywhere in the domain. It was not possible to generate a multi-block grid automatically with the meshing software used, but manual adjustment of the cell counts allowed the requirements for a 3 level multi-grid to be satisfied to accelerate convergence. The final exhaust hood cell count was 4.26 million cells.

7.1.2   Calculation Set-up

The common calculation parameters between the mixing plane and NLH approaches are described in Section 4.3; namely the same inlet and outlet boundary conditions, initialisation, working fluid and turbulence model. The differences between the two calculations come only from the treatment of the stator/rotor and rotor/hood interfaces. The specific characteristics of the mixing plane interface treatment is described in Section 4.3.1. The details of the NLH approach are described in Section 4.3.3.

Method Name	No. Stator Blade Passages Modelled	Stator/Rotor Interface	No. Rotor Blade Passages Modelled	Rotor/Hood Interface
Mixing Plane	1	Mixing Plane	1	Mixing Plane
NLH Method	1	NLH	1	NLH

Table 7.2: Summary of Computational Set Up

Non-Linear Harmonic Approach

There are two main user selectable control variables which are specific to the non-linear harmonic approach; number of perturbations modelled (M) and number of harmonics used per perturbation (N). The number of perturbations required to model the turbine and exhaust hood system is 2 as already explained in Section 4.3.3.

The number of harmonics per perturbation (N) directly affects the flow structure in the computation. A balance must be struck between solution accuracy from modelling a large number of harmonics and the additional computational power required to solve them. Continuity over the domain interfaces improves with increasing number of harmonics [24]; capturing one harmonic (associated with the BPF) results in significant discontinuity whereas continuity is near perfect at N=4. For engineering applications, satisfactory continuity should be achieved with at least three harmonics [26]. In order to examine this fully, the exhaust hood and coupled LSB calculation was run for between 1 and 4 harmonics, with the LSB cell count appropriate for the number of harmonics modelled, as specified in Table 7.1.

The specifics of the calculation set up are described in Section 4.3.3. Plotting the pressure recovery of the exhaust hood against the number of harmonics modelled in Figure 7.6 confirms that it is sufficient to model 3 harmonics per perturbation.

Mixing Plane Approach

The single LSB passage was coupled to the exhaust hood by a mixing plane. This was also applied at the interface between the stator and rotor. The specifics of the calculation set up is described in Section 4.3.1.

Table 7.2 summarises the interface treatments and set-up of computational domains in the stator, rotor and exhaust hood, for the non-linear harmonic and mixing plane calculations.

7.2 Results Comparing the Mixing Plane with the NLH Method for Coupling Stage and Exhaust Hood

In this section, results are compared for fully coupled exhaust hood and last stage blade row flow predictions, that have been calculated using the mixing plane and NLH methods. This comparison allows the importance of modelling the circumferential asymmetry in the flow across the interface between stationary and rotating reference frames to be assessed.
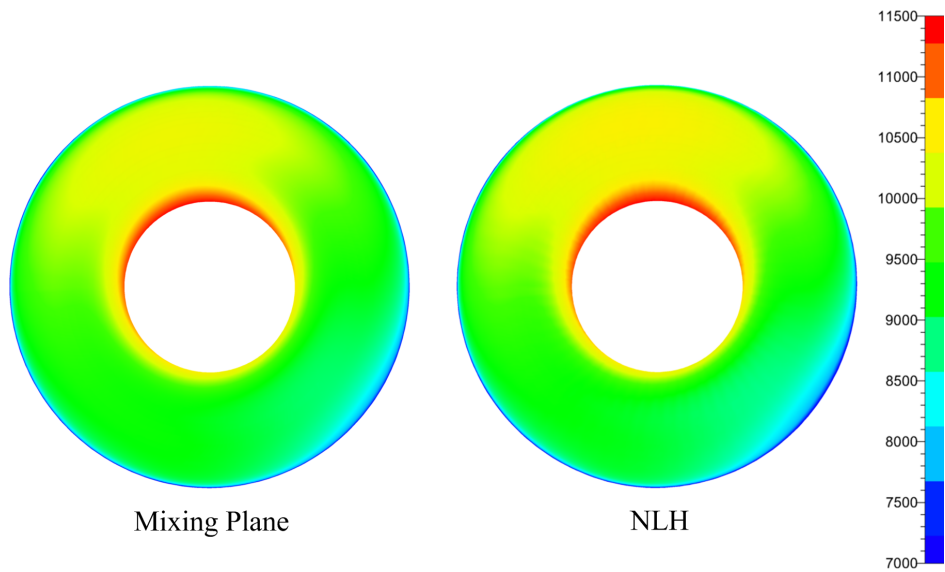
Figure 7.7: P Contours on the Hood Inlet side of the Rotor/Hood Interface [Pa]

The mixing plane approach allows the exhaust hood to be coupled to the last stage blades bi-directionally with a manageable computational demand. However, the exhaust hood's non-axisymmetric geometry and high swirl generates a circumferentially non-uniform back pressure from the exhaust hood onto the rotor. This is mixed out using the mixing plane approach due to the circumferential averaging at the rotor-exhaust interface, resulting in unrepresentative conditions applied at rotor outlet.

Until now, the only known method to model this circumferential asymmetry was to model the full rotor annulus in a frozen rotor or sliding mesh calculation, in order to achieve a periodic solution. The innovative treatment of the interface with the NLH approach enables the asymmetric flow to be reconstructed either side of the interface from the time-averaged flow and its harmonics even though only one blade passage has been calculated, provided that at least three harmonics are modelled.

7.2.1   Effect of Inlet Circumferential Asymmetry on the Exhaust Hood Flow Structure

Asymmetry in the flow due to the 3D nature of the exhaust hood can be seen in the static pressure contours on the downstream side of the rotor-hood interface, for both the mixing plane and NLH predictions in Figure 7.7.

Static pressure contours on the upstream side of the rotor-hood interface are shown in Figure 7.8 for flow calculations obtained using the NLH and mixing plane methods. The figure illustrates how circumferential non-uniformity is strongly coupled across the interface in the NLH calculations, and the impact of mixing out the non-uniformity in the mixing plane calculation. The novel treatment of the interface with the NLH method enables the non-uniformity present in the exhaust hood flow to be transferred to the stage flow. This can clearly be seen from the circumferential flow variations spanning several blade passages in
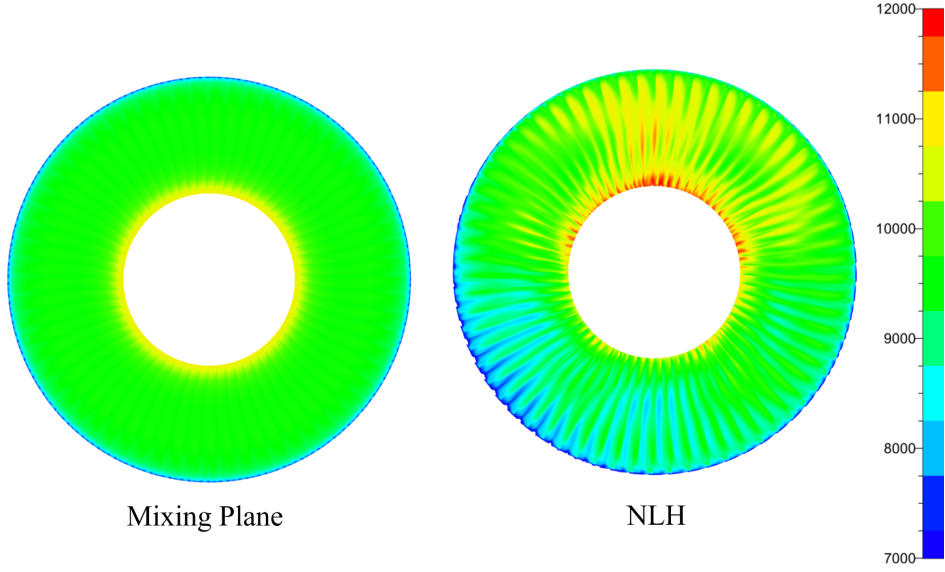
Figure 7.8: P Contours on the Rotor Outlet side the of Rotor/Hood Interface [Pa]

Method	RMS_{P_t}	RMS_P
Mixing Plane Approach	140	41
Non-Linear Harmonic	776	645

Table 7.3: Rotor Outlet Plane RMS_P and RMS_{Pt} Values [Pa]

7.8, denoting a more representative boundary condition at the rotor outlet/hood inlet plane.

In order to quantify the level of non-uniformity present in the interface flow structure, a root mean square metric was calculated according to Equation 7.3 where U_i is the variable value (static or total pressure) calculated at the ith node on the interface plane, and n is the total number of interface nodes. The static and total pressure RMS values, RMS_P and RMS_{Pt} respectively, were computed around three circumferential locations on the rotor outlet plane, shown in Figure 7.9, and averaged to give an overall variation over the rotor outlet/hood inlet interface plane. The same process was applied at the diffuser outlet plane to measure the variation in dynamic pressure, $RMS_{P_{dyn}}$, described later in this chapter in Section 7.2.3. The analysis locations are shown by the dotted lines in Figure 7.10.

$$RMS_U = \sqrt{\frac{(U_1 - \bar{U})^2 + (U_2 - \bar{U})^2 + ...(U_n - \bar{U})^2}{n}} \tag{7.3}$$

The total and static pressure RMS values at the rotor outlet plane are tabulated in Table 7.3. The total pressure variation using the NLH approach is approximately 5 times that captured with the mixing plane method. The difference in static pressure variation between calculations is even more pronounced. Only radial variations in the flow are captured using the mixing plane method and so the higher values for the NLH calculation are a direct result of the additional circumferential variation in flow structure, captured at the interface place using this method.
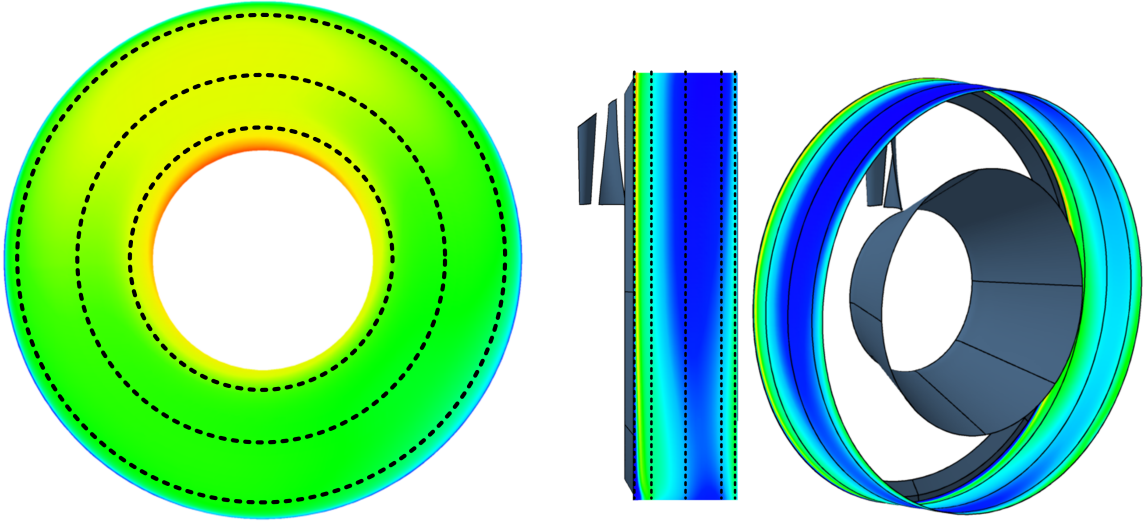
Figure 7.9: RMS_U Inlet Circumferential Asymmetry Analysis Points

Figure 7.10: RMS_U Diffuser Outlet Circumferential Asymmetry Analysis Points

Method	$RMS_{\Delta P}$
Mixing Plane Approach	243.57
Non-Linear Harmonic	343.26

Table 7.4: $RMS_{\Delta P}$ at the Exhaust Hood Half-Joint Plane [Pa]

When comparing the flow structure within the exhaust hood, it is clear that both methods have captured the high loss vortices, specifically the flow guide tip separation. The modelling of the inlet circumferential asymmetry has a noticeable affect on the flow structure within the hood itself. Figure 7.11 show the static pressure contours at the exhaust hood half-joint plane. Computing the static pressure variation between the left and right hand half-joint sides of the exhaust hood using the $RMS_{\Delta P}$ metric described in Section 6.1.2 shows that the asymmetry of the flow within the hood has been increased when applying the NLH approach (see Table 7.3).

The increase in asymmetry is due to the increased complexity of the swirl angle distribution at inlet to the exhaust hood. The circumferential asymmetry of the swirl angle produced with the NLH approach works with the asymmetry in the exhaust hood, increasing its effect. Figure 7.12 shows that there is a positive swirl angle on the underside of the hood inlet and a high negative swirl angle in the upper portion, in the calculations with the NLH method. This combination acts to increase the asymmetry in the flow structure at the half-joint plane.

7.2.2   Effect of Inlet Circumferential Asymmetry on the Exhaust Hood C_p

The most widely used parameter in determining the performance of the steam turbine exhaust hood is the static pressure recovery coefficient, C_p, Equation 1.1.

Table 7.5 compares the C_p predictions obtained with the mixing plane approach and
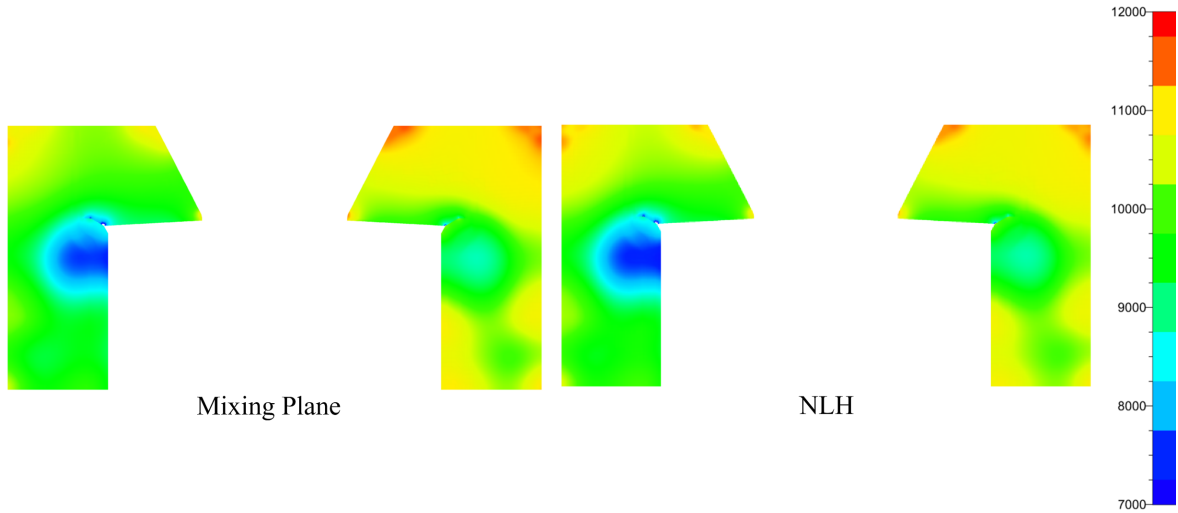
Figure 7.11: *P* Contours at Exhaust Hood Half-Joint Plane [Pa]
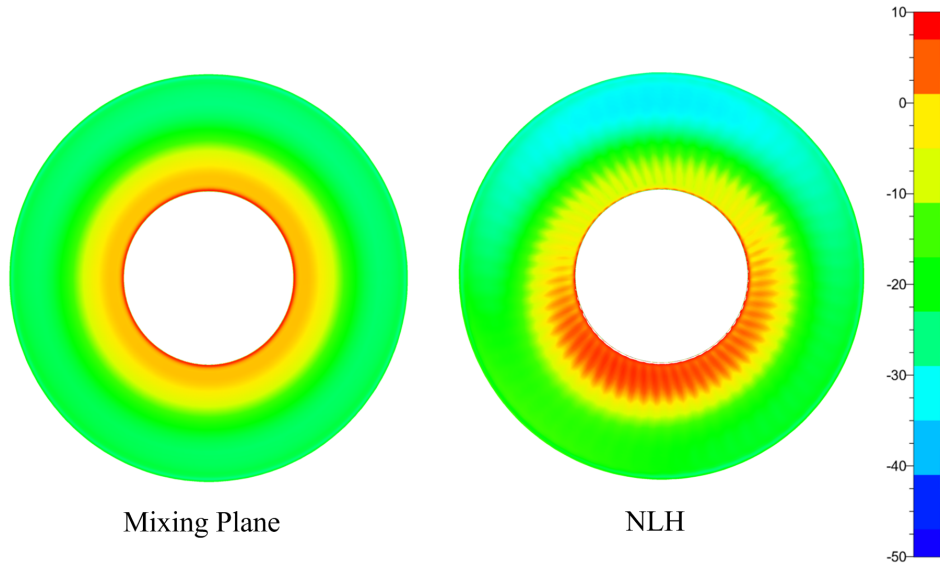
Figure 7.12: Swirl Angle (α) Contours at Rotor Outlet of Rotor/Hood Interface [°]

the NLH method. Despite the significantly different flow structure at the rotor outlet plane calculated using the two methods, the static pressure recovery coefficients are surprisingly similar. This was an unexpected result as the literature always stresses the importance of capturing the full blade row to exhaust hood coupling in calculations and experiment, when investigating exhaust hood performance. In this case, using the NLH method results in a predicted pressure recovery that is just 3.3% lower than the value predicted using the mixing plane method, relative to the ideal case, $C_p = 1.0$.

The value of C_p depends upon three plane-averaged quantities i.e. total and static pressure on the rotor outlet plane and the static pressure on the hood outlet plane. The exhaust hood outlet static pressure was a fixed boundary condition of 10000Pa in both sets of calculations. Hence, any change in C_p between the two methods must result from changes in the total and static pressure fields at the hood inlet/rotor outlet boundary. As Table 7.3 showed the rotor

Method	C_p
Mixing Plane Approach	0.2725
Non-Linear Harmonic	0.2479

Table 7.5: Exhaust Hood Static Pressure Recovery Coefficients [-]

-	Mixing Plane Approach	Non-Linear Harmonic	Δ
P_t [Pa]	11217	11297	80
P [Pa]	9552	9588	32

Table 7.6: Rotor Outlet Average P and ΔP [Pa]

outlet static and total RMS pressure variation differ by the order of 100s Pa between the calculations with different interface treatments. Table 7.6 shows the difference between the mean pressure levels on the interface plane with the two approaches. The difference in mean total and static pressure is much smaller than the RMS levels, and is only of order of 10s Pa. It can therefore be concluded that even through the circumferential variations around the hood inlet plane are significant compared to the radial flow variations, they do not have a large impact on the losses calculated within the DEDHTC.

It should be noted that predicting an accurate flow distribution is likely to be more important in design calculations of real exhaust hoods, which include the internal structure of the hood. Local variations in the flow are important for the placement of internal support struts, splitter plates, bled-steam pipework etc. Large losses can potentially result if any of these features are poorly designed with respect to the flow surrounding them. The idealised test case, calculated in the present study, does not feature any internal structure of this nature. It is therefore likely that a greater difference in C_p values would result from calculations with the different interface approaches, for real exhaust hood designs, when the internal hood structure is included.

7.2.3 Effect of Diffuser Axial Length

A series of calculations were carried out in which the exhaust hood back wall was moved, as shown in Figure 7.13. The aim of the calculations were to determine whether a tighter exhaust diffuser exit has any impact on the importance of circumferential variations in the hood inlet flow, on the value predicted for the exhaust hood pressure recovery coefficient, C_p. The back wall of the hood was moved to locations 50% and 75% of the distance from the diffuser outlet plane in the baseline hood design, for the calculations.

Additional mixing plane and NLH calculations were run with the back wall at the two new positions. The calculated pressure recovery coefficients are plotted against the diffuser axial position in Figure 7.14. 100% denotes the baseline diffuser position as defined in the DEDHTC outlined in Chapter 3.
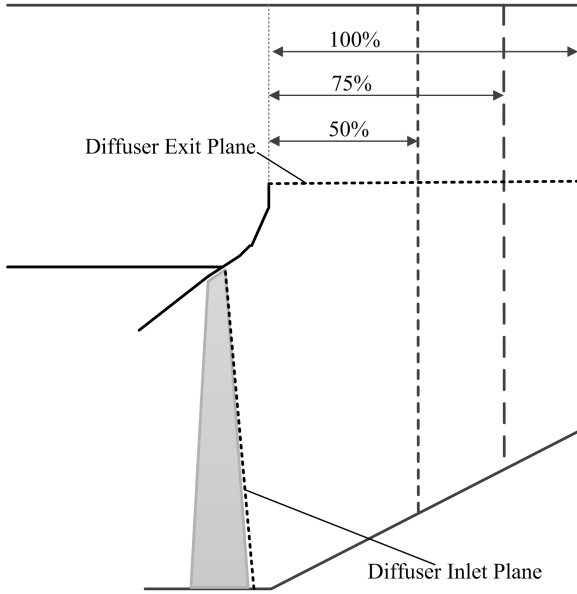
Figure 7.13: Diagram of Exhaust Hood Back Wall Locations
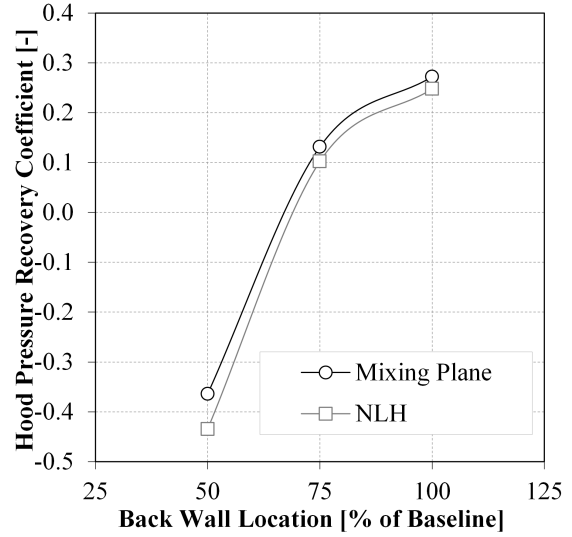
Figure 7.14: C_p Variations with Exhaust Hood Back Wall Location [-]
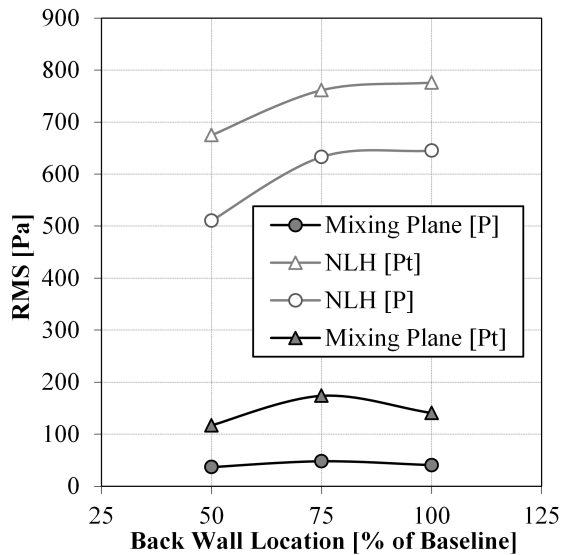
Figure 7.15: Average RMS_P and RMS_{P_T} at the Rotor Outlet Plane [Pa]
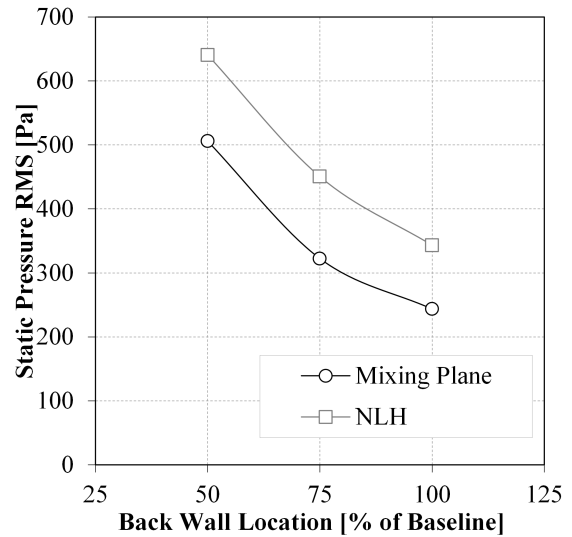
Figure 7.16: $RMS_{\Delta P}$ at the Exhaust Hood Half-Joint Plane [Pa]
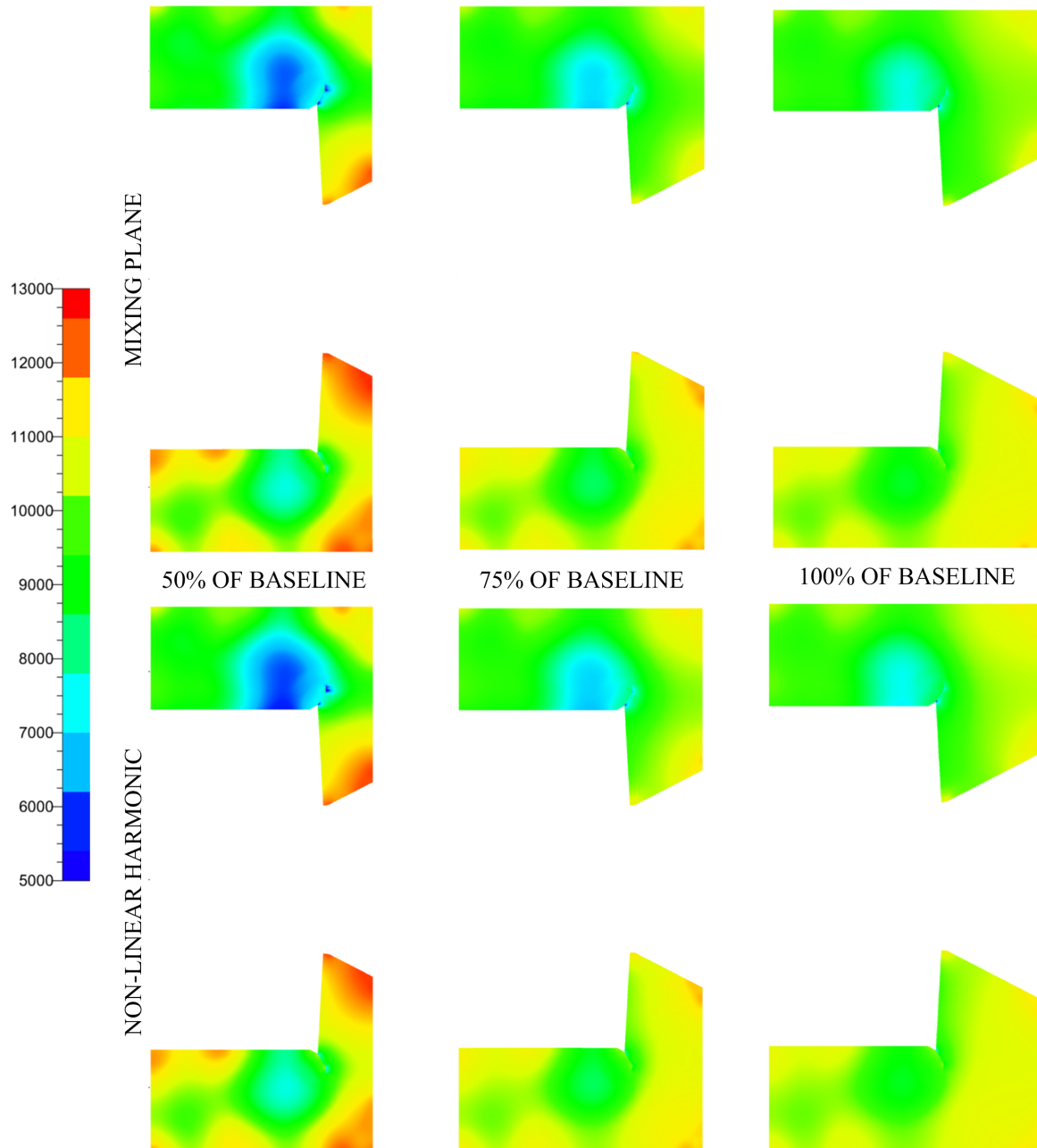
Figure 7.17: *P* Contours at the Exhaust Hood Half Joint Plane for a Range of Diffuser Axial Lengths using the Mixing Plane and NLH Approaches [Pa]

Both methods show the same trend of C_p with movement of the hood back wall position. As the diffuser exit becomes more constrained, the ability of the exhaust hood to recover pressure drops rapidly. At the 75% position, some pressure recovery is still predicted, but at the 50% position the losses in the hood are much greater than any kinetic energy recovery in the diffuser. This results in an overall exhaust hood net loss ($C_p \leq 0$), causing the average static pressure at rotor exit to increase to a level above that in the condenser. Hoznedl et al. [27] showed experimentally the exhaust hood losses decrease with increasing axial length. Also an extensive experimental study by Finzel et al. [16] showed that exhaust hood losses are relatively insensitive above a certain diffuser size, but below a critical level, losses increase significantly for more compact hoods, similar to the results shown in Figure 7.14.

The NLH method consistently predicts a lower pressure recovery potential than the mixing plane approach. As loss is a function of flow velocity squared, any increase in flow non-uniformity (in this case the introduction of circumferential variations at the rotor outlet plane with the NLH model) will be expected to result in higher predicted losses, as seen in Figure 7.14.

As the exhaust hood becomes more compact, the difference between the absolute values of pressure recovery predicted by the mixing plane approach and the NLH method can be seen to increase in Figure 7.14. However, the difference remains relatively small compared to the absolute value.

Figure 7.15 shows RMS_{P_T} and RMS_P around the rotor outlet plane for each back wall location. These results show how the circumferential variations in flow properties present in the NLH calculations, give rise to RMS variations that are an order of magnitude greater than for the mixing plane calculations, for all of the exhaust hood lengths calculated. This results in the lower values of C_p in the NLH predictions shown in Figure 7.14, for the reasons already discussed.

The asymmetry of the flow at the exhaust hood half-joint plane can also be evaluated by using the $RMS_{\Delta P}$ metric defined in Equation 6.1. Figure 7.16 shows the increased asymmetry between the left and right hand side of the exhaust hood at the half-joint plane. The magnitude of the asymmetry increases as the diffuser axial length decreases. This is also evident in the static pressure contours in Figure 7.17. This is due to increased average swirl angle of the inlet flow, tabulated in Table 7.7. All test are conducted at the same mass flow rate, so the axial velocity remains consistent. However, the tangential velocity component increases as the more compact diffuser length constricts the flow, causing the rotation to occur in a shorter axial length.

Figure 7.17 shows the static pressure contours at the exhaust hood half-joint plane for each back wall location using both the non-linear harmonic method and the mixing plane approach. A lower static pressure is evident at the core of the flow guide tip vortex when using the non-linear harmonic approach, resulting in a poorer static pressure recovery and a lower C_p compared with the mixing plane approach. In addition the increased asymmetry calculated in Figure 7.16 can also be seen.

The level of asymmetry at the half-joint plane is higher, across a range of diffuser axial

Back Wall Location [% of Baseline]	Mixing Plane	NLH
100	-16.3	-16.7
75	-19.5	-19.7
50	-27.4	-27.8

Table 7.7: Average Hood Inlet Swirl Angle [°]
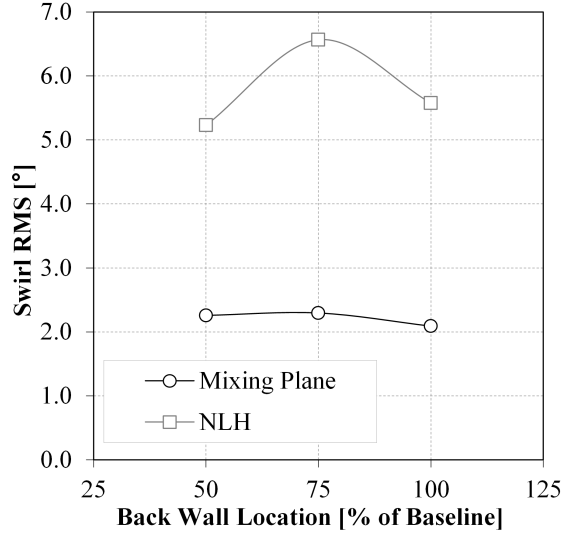
Figure 7.18: Average RMS_{Swirl} at Exhaust Hood Inlet Plane [°]
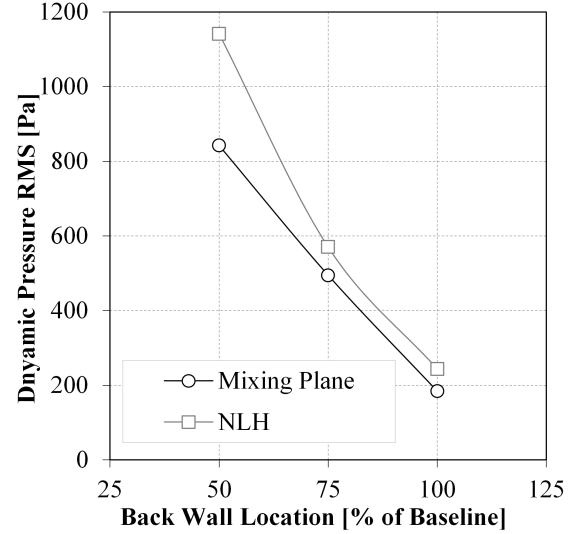
Figure 7.19: Average $RMS_{P_{dyn}}$ at Exhaust Diffuser Outlet Plane [Pa]

lengths, when using the NLH approach than the mixing plane method for the reasons previously discussed. The magnitude of the difference between approaches remains consistent as the level of the asymmetry of the swirl of the inlet flow remains similar. Figure 7.18 shows the circumferential swirl angle variations around the exhaust hood inlet annulus, calculated using the method described in Section 7.2.1. Although the average swirl angle over the exhaust hood inlet increases, the circumferential variations around the annulus do not change significantly, leading to the relatively consistent RMS_{Swirl} in Figure 7.18.

Figure 7.19 shows that $RMS_{P_{dyn}}$ at the diffuser exit plane is several times greater at 50% back wall location, compared to the result for the 100% position. Dynamic head is plotted as this essentially shows the velocity distribution at the diffuser outlet and it is this velocity field which is important for the placement of internal exhaust 'furniture', as discussed earlier in Section 7.2.1. The tighter diffuser exit at the 50% location leads to much larger gradients in the flow at this location, compared to the more generous 100% position. It can be seen that the greater variation in the flow structure due to the inclusion of circumferential variations at diffuser inlet with the NLH approach, is carried downstream and effects the diffuser exit plane flow, at all back wall locations. This confirms that adopting the NLH method in place of a mixing plane approach will have an impact on the flow in the exhaust hood downstream of the diffuser, and supports the statements made previously concerning the potential for the

NLH method to produce results more representative of real exhaust hood flows, compared to the mixing plane method.

7.3   Concluding Remarks

The first application of the non-linear harmonic approach to coupled steam turbine LP last stage blade and exhaust hood calculations has shown to be an effective method for transmitting information on flow asymmetry across the interface plane, without the need to model to full rotor annulus. The interface treatment with the NLH method enables both the radial *and circumferential* variations in flow field to be transferred between the turbine and the exhaust hood. This has not previously been achieved without modelling all rotor passages.

The NLH method has been shown to predict consistently higher exhaust losses, than the current standard single passage approach, the mixing plane method. The difference in the predicted losses between the two methods increases for more compact axial length exhaust hoods but still remains relatively small compared to the absolute levels of loss. This was a surprising result as the literature universally states the importance of modelling the circumferential asymmetry in exhaust hood flows. However, the predicted velocity flow field between the two methods was shown to be significantly affected; with distinctly asymmetric flow noted at the diffuser outlet and exhaust hood half-joint plane when circumferential variations are modelled at the inlet by the NLH method. This is argued to be particularly important when modelling real exhaust hoods with internal 'furniture'. The performance of these designs will depend strongly on the predicted velocity flow field. Misalignment of the flow with features such as splitter plates and reinforcing elements is likely to have a large impact on hood loss. As the DSEHTC does not include any internal structure, this provides scope for additional work.

The NLH method's ability to capture the circumferential variations around the exhaust hood inlet annulus can only be truly verified when compared with the full annulus frozen rotor calculations. This will be the subject of Chapter 8.

8

Multiple Passage Coupled Calculations

The most representative exhaust hood CFD simulations capture not only the radial but also the circumferential variations of flow properties at the exhaust hood inlet. This is regarded in the literature as influential in the formation of vortices within the diffuser [3]. At present, it is only possible to model the circumferential asymmetry at the rotor outlet/hood inlet interface by modelling all the rotor passages and coupling to the hood by means of a frozen rotor or full unsteady interface. The high cell counts which arises from modelling the full last stage annulus means that, at present, modelling the circumferential variations around the exhaust hood inlet annulus is prohibitively computationally expensive for use in design calculations (for example: 267 hours on 3 parallel computers, each with 8GB of memory and 4 CPU [33]).

In Chapter 7, the non-linear harmonic method was shown to capture the circumferentially non-uniform flow variations from the exhaust hood and transfer them to the last stage whilst only modelling a single LSB passage. This was shown to be of particular importance in compact axial length exhaust hoods. The NLH approach has been compared to the current standard single passage approach, the mixing plane method, which circumferentially averages at the rotor/hood interface and hence only preserves radial variations of flow structure. As such, the validity of the NLH approach as a technique for capturing circumferential flow variations can only be confirmed when compared against a full annulus method.

In this chapter, the NLH method is directly compared with the frozen rotor approach as a method of modelling the circumferential asymmetry at inlet to the exhaust hood.

8.1   Frozen Rotor vs. NLH

The interface between the rotor outlet and the exhaust hood inlet governs the complexity of any fully coupled CFD calculation. This chapter compares two methods of interface treatment: the full annulus quasi-steady frozen rotor approach and the single passage quasi-unsteady non-linear harmonic approach. Each method's ability to capture the circumferential asymmetry of the exhaust hood inlet and transfer it to the rotor outlet plane has been evaluated, as well as the relative hood performance predicted by each method.

8.1.1   Computational Set-up

The frozen rotor approach is as described in Section 4.3.2. The computational set up is identical to that described for all bi-directionally coupled calculations in Section 4.3. The frozen rotor full annulus computation has the same inlet and outlet boundary condition turbulence model and exhaust hood grid to that described for the NLH approach, to enable a valid comparison to be made.

The number of blade passages modelled, the treatment of the stator/rotor interfaces and the rotor/hood interface are the only differences between calculations and are the subject of the study discussed in this chapter. The Frozen Rotor (Full Annulus) computation involves modelling all 60 stator passages and all 65 rotor passages. At the interface between each domain (stator and rotor, rotor and exhaust hood) a frozen rotor interface is applied. This applies a local frame transformation linking the stationary (stator and exhaust hood domains) to the rotating rotor domain. As no averaging takes place at the interface the circumferential variations around the inlet annulus are preserved. Full details of the method can be found in Section 4.3.2.

With any frozen rotor full annulus method, the primary drawback is the high cell counts which arise from modelling the full stator and rotor annulus. In this application, the baseline stator single blade passage mesh consisted of 0.48 million cells and the baseline single rotor of 0.86 million (described in Section 7.1.1) leading to a cell count in excess of 80 million for a full annulus calculation. With this prohibitively high cell count it was important to carry out a thorough mesh dependency study to reduce the cell count as far as possible without compromising the rotor outlet flow profiles. This was done by running the stage calculation in NUMECA Fine/Turbo 8.10, isolated from the exhaust hood. The cell count of each block in the stage mesh topology was individually reduced, independent of the other blocks, ensuring the cell count enabled a 3 level multi-grid approach to be maintained. The stage calculation was rerun to determine the minimum cell count for each block in the topology independently. The individual block reductions were applied over the whole stage topology and the calculation rerun.

As previously discussed in Section 5.1.3, total pressure and swirl angle profiles at inlet to the exhaust hood are the most influential at determining the flow structure and vortices. As the overall focus of this chapter is the exhaust hood aerodynamics and performance, provided the profiles at outlet of the rotor were not compromised in the mesh dependency study, any effect the cell count reduction has on the predicted stage efficiency is considered unimportant and has been neglected in the present study. Figures 8.1 and 8.2 show the total pressure and swirl angle profiles for the baseline cell counts compared with those with the reduced mesh. The profiles are essentially unaffected by the cell count reduction and the resolution of the rotor tip leakage jet in the upper 5% of the blade span has been maintained. This study successfully reduced the cell count for the full turbine annulus and exhaust hood calculation by almost 50%, to a more manageable 48.28 million. The full results of the mesh dependency study are summarised in Table 8.1.

With a reduced cell count of 48.28M cells, the new mesh was coupled to the exhaust
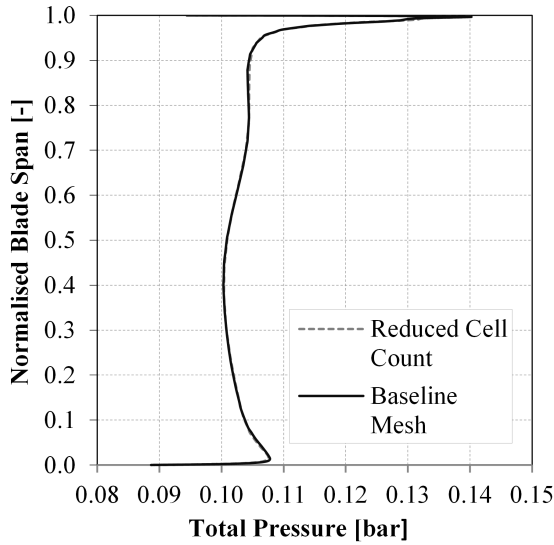
Figure 8.1: P_t Variation at the Rotor Outlet Plane [Pa]
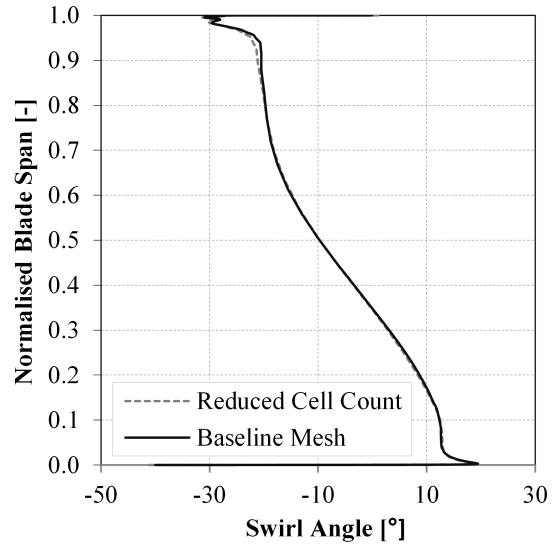
Figure 8.2: Swirl Angle (α) Variation at the Rotor Outlet Plane [°]

-	Cell Count Baseline	Cell Count Reduced
Stator Blade	480863	236447
Rotor Blade	861853	461789
Full Annulus	84.87M	48.28M

Table 8.1: Cell Count Reduction for Stator and Rotor Domains for Full Annulus Frozen Rotor Calculations

hood. The fully coupled frozen rotor exhaust hood system calculation was initialised using a constant pressure, temperature and axial velocity, the values of which are tabulated in Table 4.6. Convergence was achieved in approximately 5000 iterations. The set-up of the two methods to be compared is summarised in Table 8.2.

8.1.2   Results Comparing the Frozen Rotor with the NLH Method for Coupling Stage and Exhaust Hood

The non-linear harmonic method is compared with the frozen rotor (full annulus) approach. The circumferential asymmetry predicted by the two methods at the rotor outlet plane has been compared and quantified. The exhaust hood pressure recovery coefficient and the relative memory requirement of each method have also been evaluated.

Circumferential Asymmetry Comparison

Figure 8.3 compares the static pressure contour plots at the rotor outlet plane for the frozen rotor and NLH approaches. Both plots are similar and the circumferential asymmetry seen

Method Name	No. Stator Blade Passages Modelled	Stator/Rotor Interface	No. Rotor Blade Passages Modelled	Rotor/Hood Interface
Frozen Rotor [Full Annulus]	60	Frozen Rotor	65	Frozen Rotor
Non-Linear Harmonic	1	NLH	1	NLH

Table 8.2: Summary of Computational Set-up
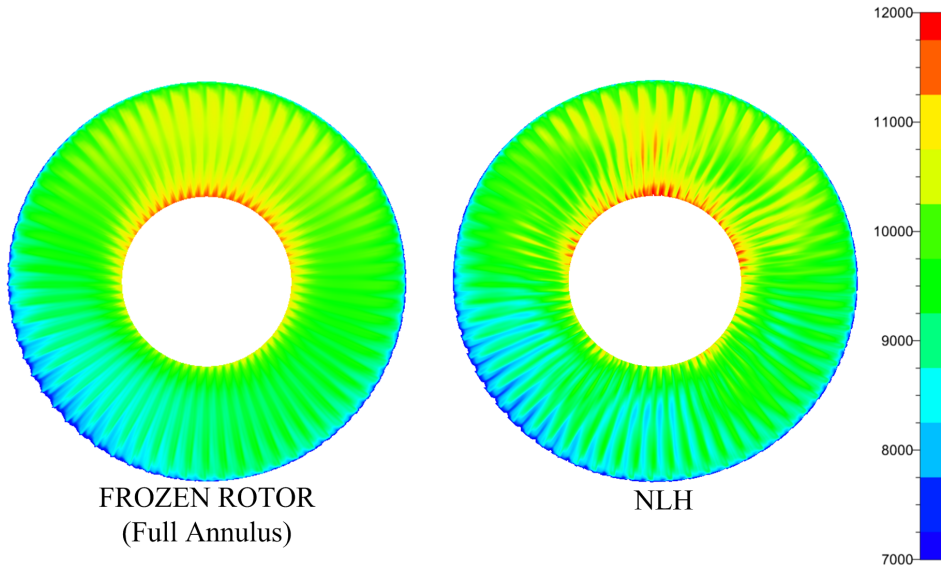
Figure 8.3: P Contours at the Rotor Outlet Plane [Pa]

in the full annulus frozen rotor approach is also captured by the single passage NLH method.

When static pressure is plotted against circumferential distance around the annulus at midspan in Figure 8.4, the NLH result is shown to produce a more asymmetric flow field than the full annulus frozen rotor approach. For both the frozen rotor and NLH approaches a high frequency is evident in the static pressure plots which is the BPF. A low frequency is also evident, the wavelength of which is the same as the normalised circumferential distance, which is due to the interaction with non-axisymmetric geometry of the exhaust hood. With the non-linear harmonic approach, an additional frequency is present which form 5 'beats', not evident in the frozen rotor calculations. This is due to the unsteady interaction between the stator and rotor captured by the NLH approach and is a function of the difference between the number of stator and rotor blades. A simple study in Figures 8.5 and 8.6 demonstrate this. Two simple sinusoidal frequencies are generated of different amplitudes with arbitrary defined lag between them; the blue plot shows the frequency generated with 60 stator blades and the green with 65 rotor blades. The red plot shows the the frequency formed when these two waveforms are added together and interact, and 5 'beats' are clearly present in Figure 8.5, as in Figure 8.4. When the number of rotor blades is increased 66 in Figure 8.6, an additional frequency with 6 'beats' is now present.

In order to evaluate this circumferential asymmetry a root mean square (RMS) metric, used previously to quantify the level of inlet fluctuation relative to the average, defined in Equation 7.3 was used. This was applied at 3 circumferential locations (10%, 50% and 90% of
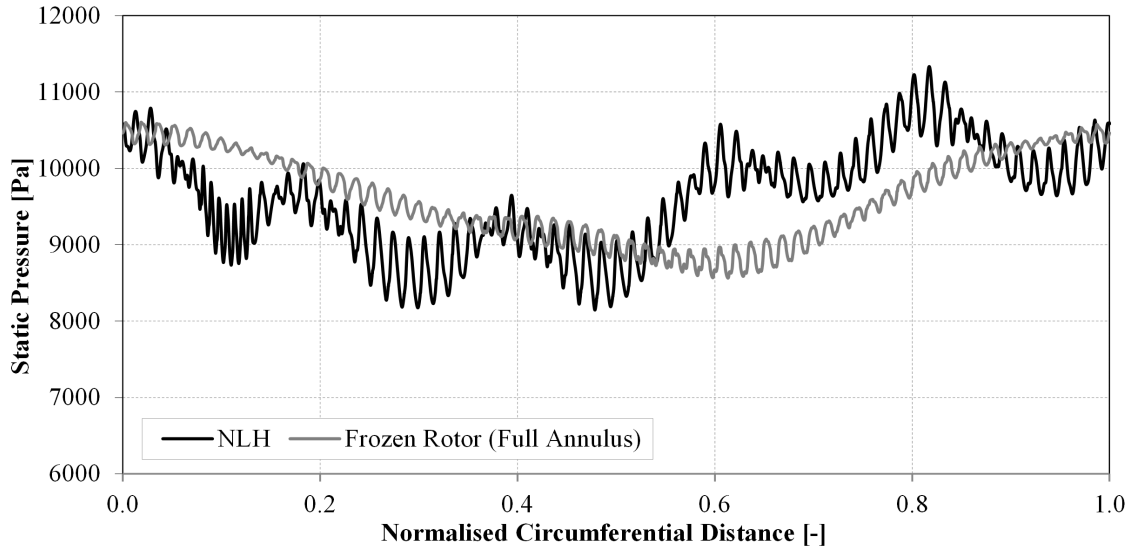
Figure 8.4: Circumferential Variations of P at Rotor Outlet at Midspan [Pa]

blade span) around the rotor outlet annulus for static pressure and total pressures variations. These plots are shown in Figure 8.7 and 8.8 respectively.

At the rotor hub, the circumferential asymmetry predicted by both the frozen rotor and NLH approaches is similar. However, further along the blade span the circumferential asymmetry predicted by the NLH is higher than that of the frozen rotor approach, a trend which increases with increasing radius.

This trend can be explained by considering the blade-to-blade static pressure contours at the rotor midspan, shown in Figure 8.9. For this comparison, 3 blade passages have been reconstructed when representing the single passage NLH approach. The relative peaks and troughs of the rotor wake and shock structures are significantly more visible with the NLH approach than with the frozen rotor. This is due to the NLH method superimposing the sinusoidal harmonic oscillations of the BPF onto the existing steady flow solution, which is also evident in Figure 8.4. These peaks and troughs due to the rotor wake and shocks at outlet lead to circumferential variations which are captured in the RMS calculation. As the flow structure becomes more complex with increasing blade span, the circumferential variations become more prominent.

Without experimental validation or a full unsteady computation it is difficult to definitively determine which of the two methods produces the flow field more comparable with that found in reality. Multiple papers exist for other applications comparing the quasi-unsteady NLH approach with full unsteady computations [26, 65, 46]. All have shown that the unsteady flow field can be reproduced with good accuracy using the NLH approach, provided a sufficient number of harmonics are modelled. The harmonic study carried out in Section 7.1.2 has shown the results to be almost independent of number of harmonics modelled. In order to advance the state of the art computational tools some experimental test cases are required.
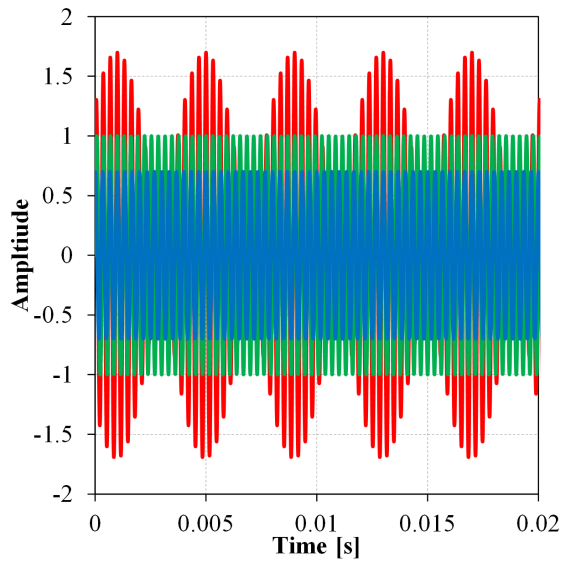
Figure 8.5: Simple Sinusoidal Frequencies Representing 60 Stator Blades, 65 Rotor Blades and their Interaction
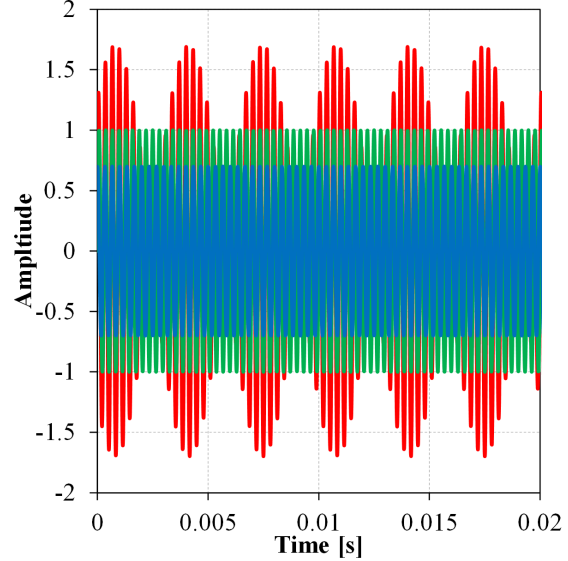
Figure 8.6: Simple Sinusoidal Frequencies Representing 60 Stator Blades, 66 Rotor Blades and their Interaction

Method	C_p	Memory Requirement [Mb]
Frozen Rotor (Full Annulus)	0.2411	9537
NLH	0.2479	4966

Table 8.3: Comparison of C_p and Memory Requirements of the Frozen Rotor and NLH Approaches

Pressure Recovery Coefficient and Memory Requirement

Although there are noticeable differences in the predicted circumferential asymmetry variations between the frozen rotor and NLH methods, the performance of the diffuser predicted by the two methods was similar. Table 8.3 shows the static pressure recovery coefficients and memory requirements for the frozen rotor and NLH calculations.

The difference between the two approaches is less than 1% of the average total system loss. Although the circumferential asymmetry is noticeably different towards the tip of the rotor blade, when averaged, these variations are around 20Pa for total pressure and zero for static pressure and hence the predicted losses are almost identical.

As the primary purpose of the proposed use of the NLH approach is to capture the circumferential asymmetry at hood inlet/rotor outlet in a reduced computational demand compared with full annulus frozen rotor methods, the comparative memory requirements for each approach, is also shown in Table 8.3. The NLH method offers an almost 50% reduction in memory requirement compared with the full annulus frozen rotor method, whilst still producing comparable static pressure recovery coefficients and circumferential asymmetry variations.
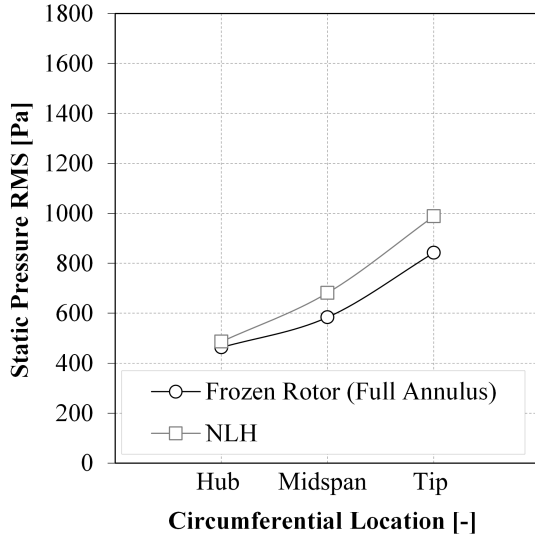
Figure 8.7: RMS_P at 3 Circumferential Locations on the Rotor Outlet Plane [Pa]
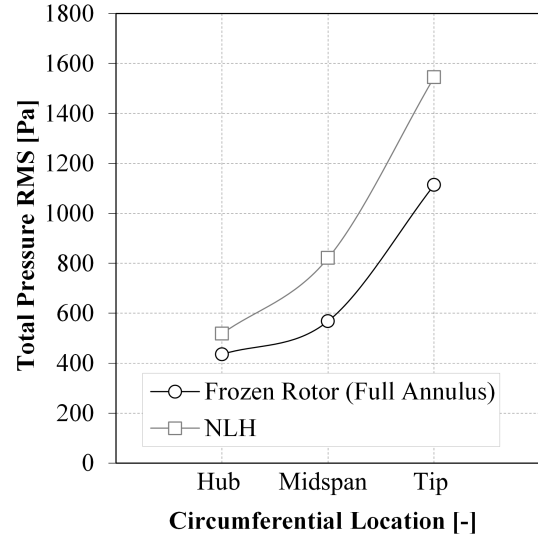
Figure 8.8: RMS_{P_t} at 3 Circumferential Locations on the Rotor Outlet Plane [Pa]

8.2   Reducing the Demand of Full Annulus Calculations

In some cases when applying the frozen rotor to stage calculations (without the exhaust hood), it is possible to reduce the computational demand by using rotational periodicity. However, there is no common periodicity between rotor and exhaust hood and as such the full rotor annulus has to be modelled.

Verstraete et al. [64] suggested a method of reducing the computational demand of exhaust hood system frozen rotor calculations by modelling only one stator passage, and using a mixing plane between the stator and a full annulus rotor calculation. This was suggested as a viable option for LP LSB calculations as typically the stage is choked, and consequently the passage to passage variations at the rotor inlet plane are small around the annulus. The merits of this approach compared to a full annulus stator calculation has not been evaluated or discussed in any paper to date.

For the stator to be choked, Equation 8.1 must be satisfied. The pressure ratio for the DSTC at nominal load is 0.5035, and so the stage is choked, (for the γ used in this study of 1.1152). This option for reducing the frozen rotor computational demand by the use of a mixing plane between stator and full annulus rotor, can therefore be explored. Results obtained in this way are compared against the previous full annulus stator and rotor frozen rotor method results in the previous section.

$$\frac{P_{statordownstream}}{P_{statorupstream}} \leq \left[\frac{2}{\gamma+1}\right]^{\frac{\gamma}{\gamma-1}} = 0.582 \qquad (8.1)$$
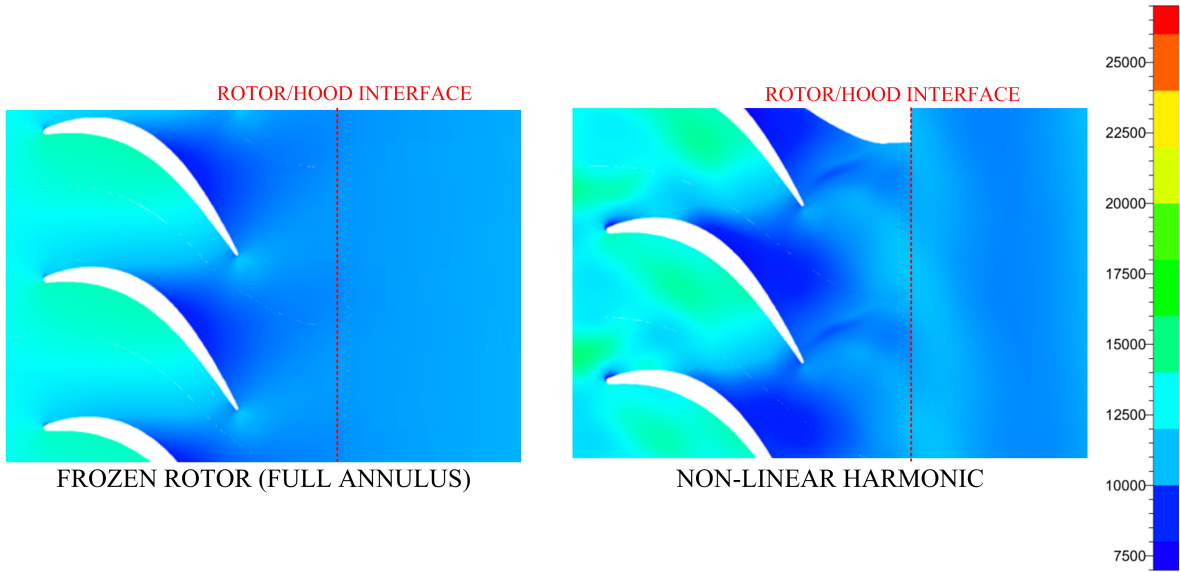
Figure 8.9: Blade to Blade View of Static Pressure Contours at Midspan [Pa]

8.2.1   Computational Set-up

The frozen rotor (single passage) calculation is set-up using the same mesh (reduced cell count for stator and rotor), initialisation, boundary conditions, turbulence model and rotor/hood interface as used for the frozen rotor (full annulus) calculations described earlier. This is as described in Section 4.3 and 4.3.2. The difference between the two approaches comes from the set-up of the interface between the stator and rotor. The full annulus 60 stator blades are reduced to a single passage which is coupled to the full annulus rotor domain by a mass averaged mixing plane situated equidistant from stator trailing edge and rotor leading edge. This reduces the cell count from just over 48 million cells (see Table 8.1) to 34.3 million. The treatment of the mixing plane interface is described in depth in Section 4.3.1. A summary of the two approaches compared in this section is tabulated in Table 8.4.

Method Name	No. Stator Blade Passages Modelled	Stator/Rotor Interface	No. Rotor Blade Passages Modelled	Rotor/Hood Interface
Frozen Rotor [Full Annulus]	60	Frozen Rotor	65	Frozen Rotor
Frozen Rotor [Single Passage]	1	Mixing Plane	65	Frozen Rotor

Table 8.4: Summary of the Computational Set-up for Full Annulus and Single Stator Passage Frozen Rotor Calculations

8.2.2   Results for Reducing Computational Demand of Frozen Rotor Calculations

Figure 8.10 shows the static pressure variations around the stator outlet for frozen rotor (full annulus) calculation and the frozen rotor (single passage) results. As anticipated, the rotor
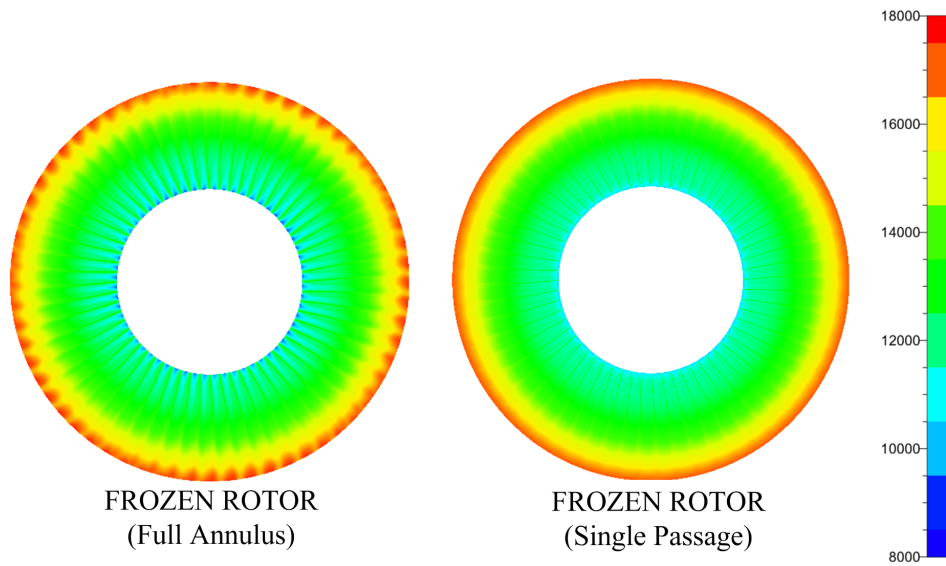
Figure 8.10: P Contours at the Stator Outlet Plane [Pa]

wakes are clearly visible with the full annulus method, particularly at the hub and tip region. These have been circumferentially averaged and mixed out when the single passage mixing plane approach is used. However, the bulk flow field between mixing plane and full annulus methods are similar. Although the mixing plane averages the wakes out, the circumferential variations around the annulus, between individual blade passages are small. By calculating the average static pressure at rotor outlet plane for two approaches, the difference predicted by the two approaches is only 15Pa.

It is more important, however, to consider the rotor outlet plane downstream, as the output here affects the exhaust hood flow structure and static pressure recovery. Figure 8.11 compares the static pressure variations around the rotor outlet for the frozen rotor (full annulus) method and the frozen rotor (single passage) approach. The distributions are essentially identical with little difference between the two results.

The RMS metric described in Equation 7.3 was applied to the static and total pressure variations around the rotor outlet annulus, to further explore the effect of modelling only one stator passage. Figures 8.12 and 8.13 shows the static and total pressure circumferential RMS variations predicted by the single stator passage frozen rotor approach and with the full annulus method. The predicted circumferential asymmetry between the two methods is almost identical, a very positive result as the single stator frozen rotor method therefore produces a comparable non-uniformity but using 30% less cells than a full annulus calculation.

To evaluate how the predicted performance of the exhaust hood varies with frozen rotor computational set-up, the static pressure recovery coefficient was calculated for both approaches. This is shown in Table 8.5. The static pressure recovery coefficients predicted by the two methods vary by only 0.5% of the total average loss of the system.

Table 8.5 also shows the memory requirement to solve each calculation. As the NLH calculation was carried out on a desktop PC with 16GB of RAM using 4 processors and the frozen rotor calculation on a high-performance cluster with 8 cores, a direct comparison of
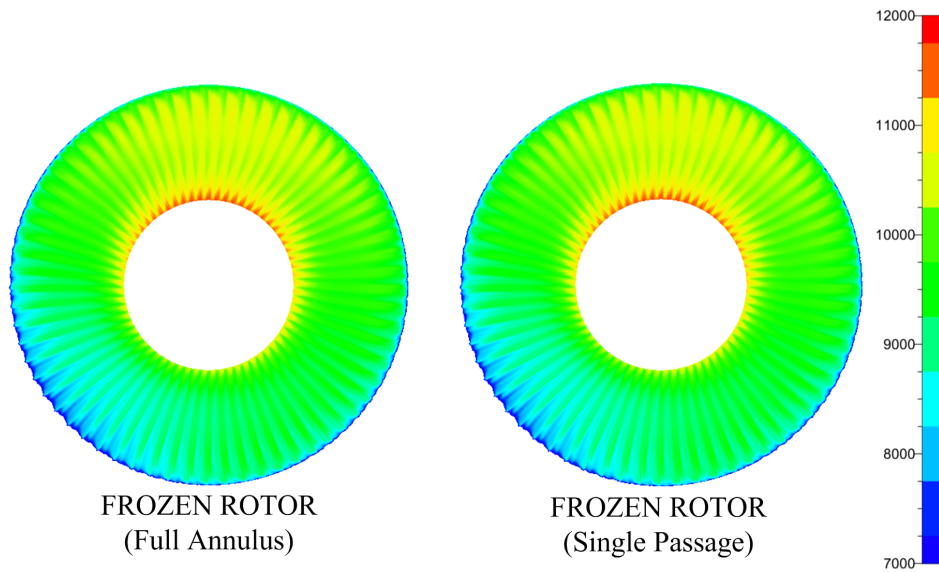
Figure 8.11: P Contours at the Rotor Outlet Plane [Pa]

Method	C_p	Memory Requirement [Mb]
Frozen Rotor [Full Annulus]	0.2411	9537
Frozen Rotor [Single Passage]	0.2453	5099

Table 8.5: Comparison of C_p and Memory Requirements for both Frozen Rotor Methods

computational effort by a standard measure (such as CPU hours) is not straightforward; so a comparison between the memory requirement for each calculation is used instead. Modelling only one stator passage reduces the cell count for the turbine and exhaust hood system by almost 30% (to 34.3 million cells) compared with the full annulus method. This equates to a 46% decrease in computational power requirement, from Table 8.5, so the memory required to carry out the computation is now almost equivalent to that of the NLH method. This study highlights that both the frozen rotor (single passage) approach *and* the non-linear harmonic method are viable alternatives to the full annulus frozen rotor calculation method. The NLH is advantageous over the frozen rotor (single passage) approach in situations where the stator is unchoked.

8.3   Effect of Running Off-Design

This study has so far shown that the predicted static pressure recovery coefficient from a range of coupling methods is very similar at nominal load. However, industry is increasingly moving towards investigating the effects of running at off-design conditions and exploring the effects of a more flexible plant operation. With the use of renewables predicted to rise significantly over the next few decades, a more flexible operation of traditional coal and nuclear power plants will be required to meet the variable grid demand. With this in mind, LP turbines
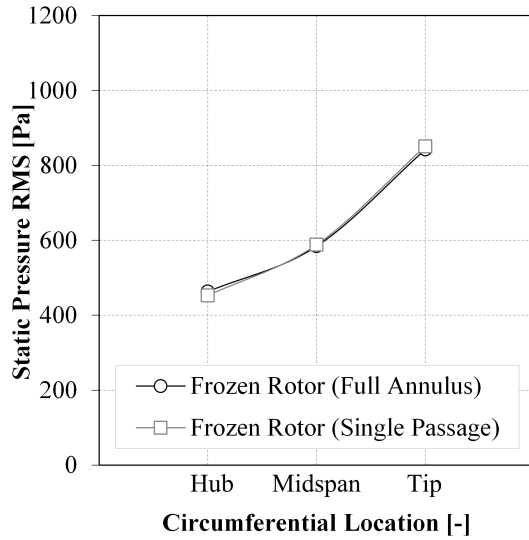
Figure 8.12: RMS_P at 3 Circumferential Locations on the Rotor Outlet Plane [Pa]
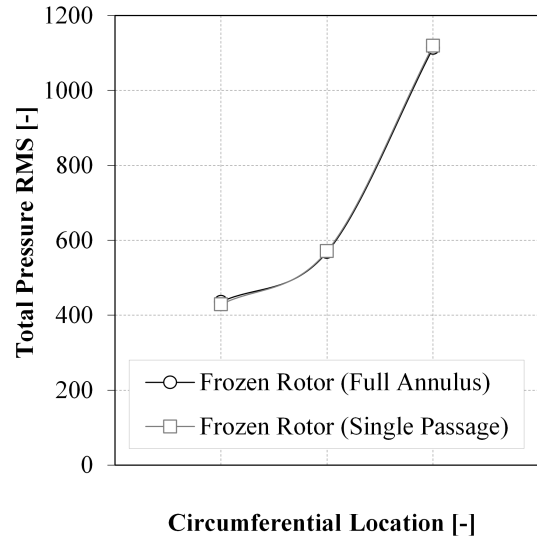
Figure 8.13: RMS_{P_t} at 3 Circumferential Locations on the Rotor Outlet Plane [Pa]

are likely to be run at off-design conditions for a significant proportion of generating time. Accurate prediction of performance at off-design conditions is therefore becoming increasingly important. This section explores the effect of the different stage to hood coupling methods on the prediction of off-design flows.

8.3.1   Computational Set-up

For frozen rotor and NLH calculations, the computational set-up is as described in previous sections, but instead of a total pressure boundary condition at inlet to the stator, a mass flow rate boundary has been applied, to allow the flow structure for a range of mass flow rates to be computed. The computation was rerun at nominal load (a mass flow rate of 88.6kg/s) and then repeated with each coupling method with reduced inlet mass flow rates of 70 kg/s, 65kg/s and 50 kg/s to study the effects of running at off-design conditions. This process was repeated with a mixing plane applied to the interface between turbine outlet and exhaust hood inlet. The circumferential averaging in the mixing plane method means only radial flow variations from the exhaust hood are transferred to the turbine, and the circumferential asymmetry is mixed out. The mixing plane set-up is as described in Section 7.1.2.

8.3.2   Results Running of Off-Design Conditions

Pressure Recovery

Figure 8.14 shows the pressure recovery for the full exhaust hood system, including both the exhaust diffuser and hood. As discussed previously, at nominal load the three methods of coupling predicted a similar level of exhaust performance, point 1 on Figure 8.14. As anticipated, the pressure recovery in the exhaust system decreases with decreasing mass flow

rate, highlighted by a black arrow in Figure 8.14. However, unexpectedly, the performance of the exhaust hood improves at very low mass flow rates, around 50% of nominal load, shown by the grey arrow in Figure 8.14. To investigate the trends shown in Figure 8.14, the exhaust system pressure recovery is considered in two sections; the diffuser element in Figure 8.16, and the exhaust hood outer casing part in Figure 8.17, shown diagrammatically in Figure 8.15.

Considering first the pressure recovery within only the diffuser, Figure 8.16, lower mass flow rates result in a poorer diffuser performance, the trend highlighted by the black arrow in Figure 8.14. As the mass flow decreases, the inlet flow velocity is lower leading to a higher static pressure at the rotor outlet (diffuser inlet) plane. The low velocity within the diffuser causes the additional vortex in the upper exhaust casing to grow, spreading down into the diffuser itself, shown in the streamlines in Figure 8.18. At nominal load, the majority of the inlet flow passes into the volute, forming the flow guide tip vortex. A portion of the flow forms an additional vortex in the upper diffuser, with the division of flow direction highlighted by the red dashed line. At off design condition, this additional vortex grows in both size and intensity with decreasing mass flow rate, until it dominates the diffuser passage, causing a blockage which hinders the pressure recovery potential, as shown in the total pressure contours in Figure 8.19. At very low mass flow rates this leads to a lower static pressure at the diffuser outlet compared with the inlet, Figure 8.20, and a negative C_p. The vortex expansion within the diffuser at low mass flow rates is also observed in the work of Shao et al. [48]. However, this study used a mixing plane at the rotor hood interface and so the effect of circumferential asymmetry was not included in the calculations.

Figure 8.16 shows predicted C_p within the diffuser is lower with methods which model the inlet circumferential asymmetry (NLH and frozen rotor) than it is with the mixing plane approach; an important observation, indicating the importance of the stage to hood coupling method at off-design. This is also highlighted in region 2 in Figure 8.14. This is consistent with the trend discussed in Chapter 7; as loss is a function of velocity squared, a large circumferential velocity variation at inlet leads to a higher loss within the system. Figure 8.16 also shows that the performance predicted by the NLH approach is within 1% of the total system loss predicted by the frozen rotor approach, across a range of operational conditions. This is particularly important as it reinforces that the NLH is a viable, computationally efficient alternative to the frozen rotor approach for capturing inlet circumferential flow variations. At very low mass low rates, around 50% of the design point, all three methods predict a similar level of diffuser performance. This is because the additional vortex has grown so large that its affect dominates over the inlet modelling method. This offers an explanation as to the effect seen in region 3 of Figure 8.14.

When considering the static pressure recovery within the hood (from the diffuser outlet plane to the condenser, see Figure 8.15), shown in Figure 8.17, the opposite trend is observed to that within the diffuser; a lower mass flow rate results in a significantly improved hood pressure recovery. This is an interesting result as the condenser pressure is fixed at 10000Pa in the calculation set-up. The decreasing diffuser outlet (hood casing inlet) static pressure
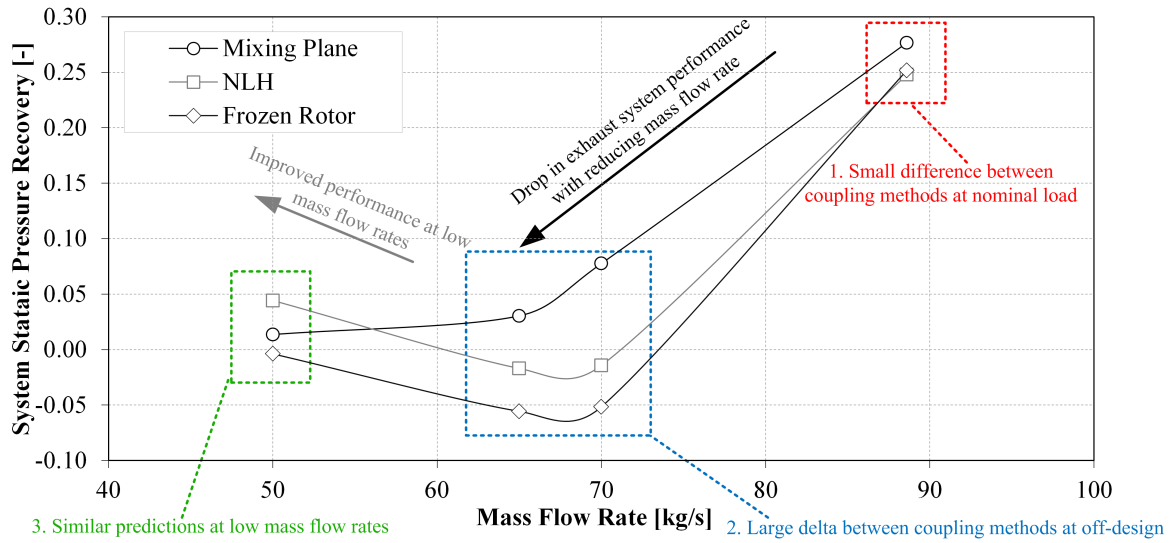
Figure 8.14: C_p for the Exhaust Hood System (Diffuser and Hood) [-]
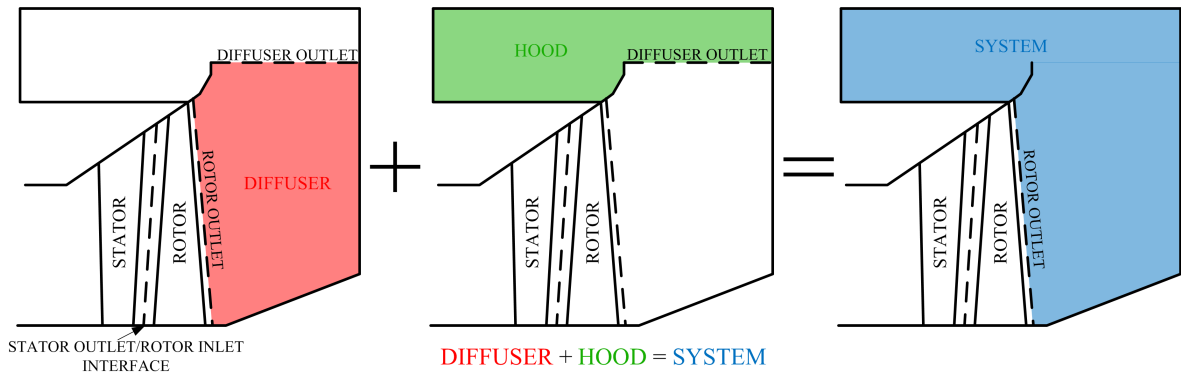
Figure 8.15: Diffuser/Hood Diagram of Analysis Planes
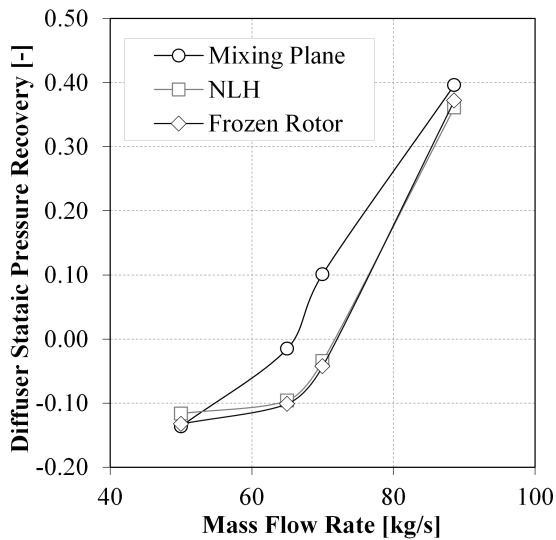
Figure 8.16: C_p for the Exhaust Diffuser [-]   Figure 8.17: C_p for the Exhaust Hood [-]
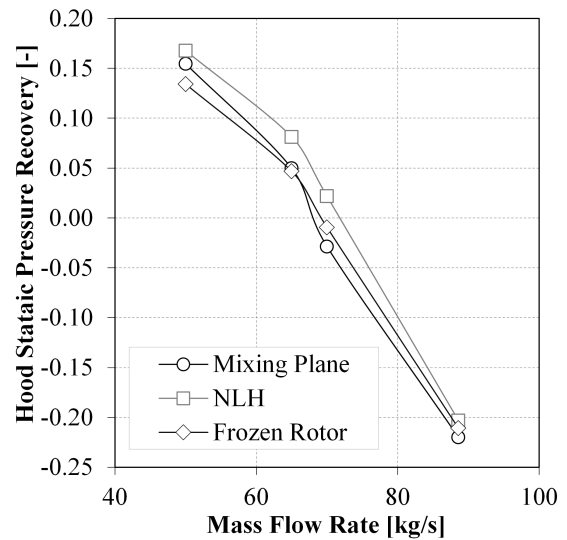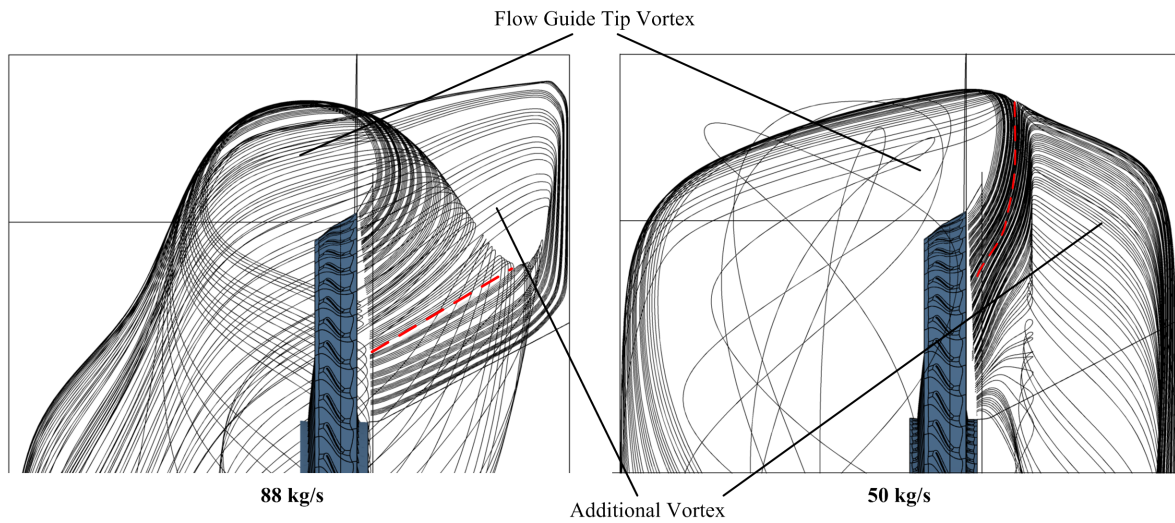
Figure 8.18: Streamlines at the Meridional Plane for Nominal Load and 50 kg/s using Frozen Rotor Approach

should lead to a poorer pressure recovery, shown in Figure 8.21. However, the performance of the exhaust hood casing is dominated by the flow guide tip vortex. As the mass flow through the system decreases, the velocity decreases, which results in the strength of the vortex decreasing and a subsequently improved hood performance. This is shown by the higher total pressure at the core of the flow guide tip vortex in Figure 8.19.

Combining the increased losses in the diffuser, Figure 8.16, and the improved performance within the exhaust hood, Figure 8.17, results in the overall system pressure recovery variation shown in Figure 8.14. The benefits of the decreased flow guide tip vortex intensity outweighs the increased diffuser losses at very low mass flow rates (50 kg/s), leading to the overall improved performance compared to the intermediate mass flow rates investigated, denoted by the grey arrow in Figure 8.14.

Inlet Swirl and Flow Asymmetry

It is widely stated in the literature that at low mass flow rates, the swirl angle at exit to the LSBs increases. This is shown diagrammatically in Figure 8.22 adapted from Gray et al. [23].

Results from this study confirm the findings of the literature. The average swirl angle magnitude at inlet to the exhaust hood increases, as anticipated, with decreasing mass flow rate, Figure 8.23. Positive swirl is denoted as in the same direction of the turbine rotation. This is consistent across all methods, where the *average* swirl angle prediction varies by less than 1%, regardless of computational approach.

Although each interface treatment produces very similar *average* swirl angle prediction, the swirl angle *distribution* around the exhaust hood inlet annulus varies significantly, as shown in Figure 8.25. For methods which capture the inlet circumferential asymmetry (frozen rotor and NLH), the inlet swirl angle distribution is highly non-uniform around the inlet annulus. With the mixing plane approach, the circumferential averaging at the interface
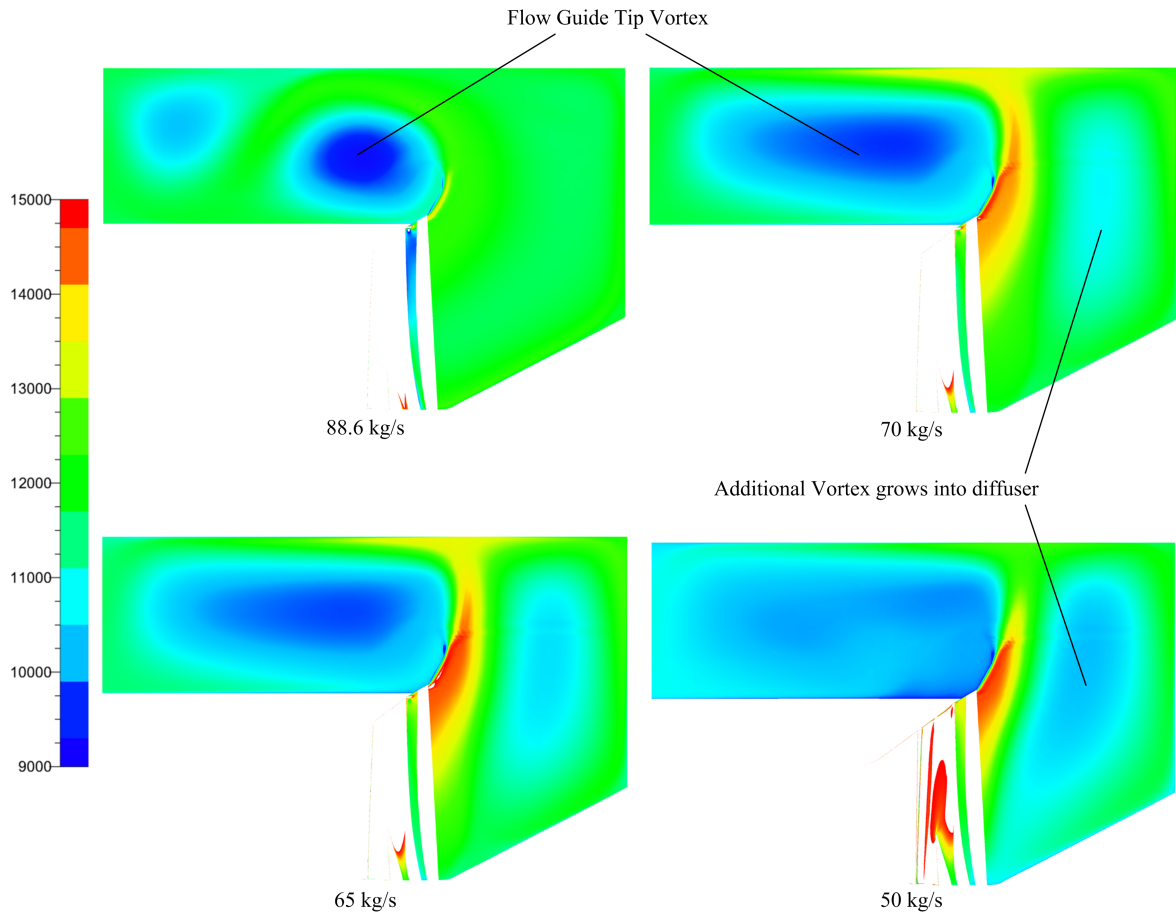
Figure 8.19: P_t Contours at the Meridional Plane at a Range of Mass Flow Rates [Pa]
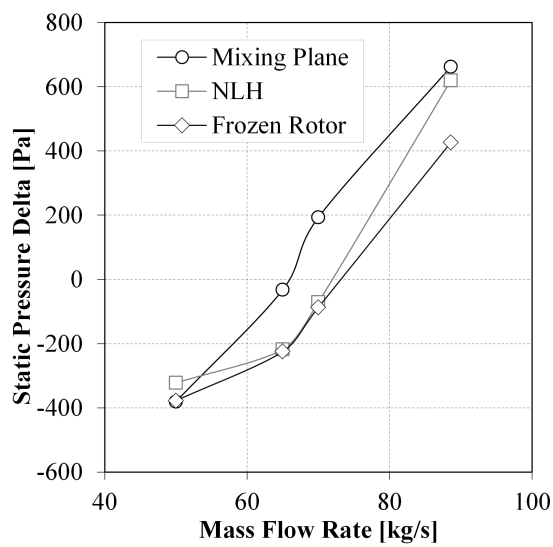
Figure 8.20: Delta Between Rotor Outlet P and Diffuser Outlet P [Pa]
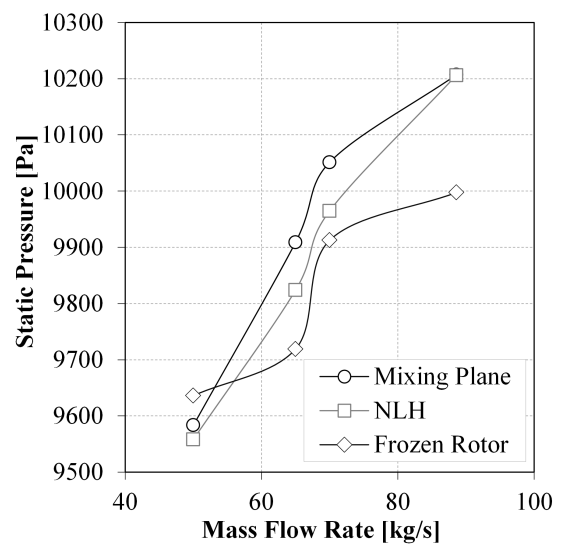
Figure 8.21: Average P at the Diffuser Outlet Plane [Pa]
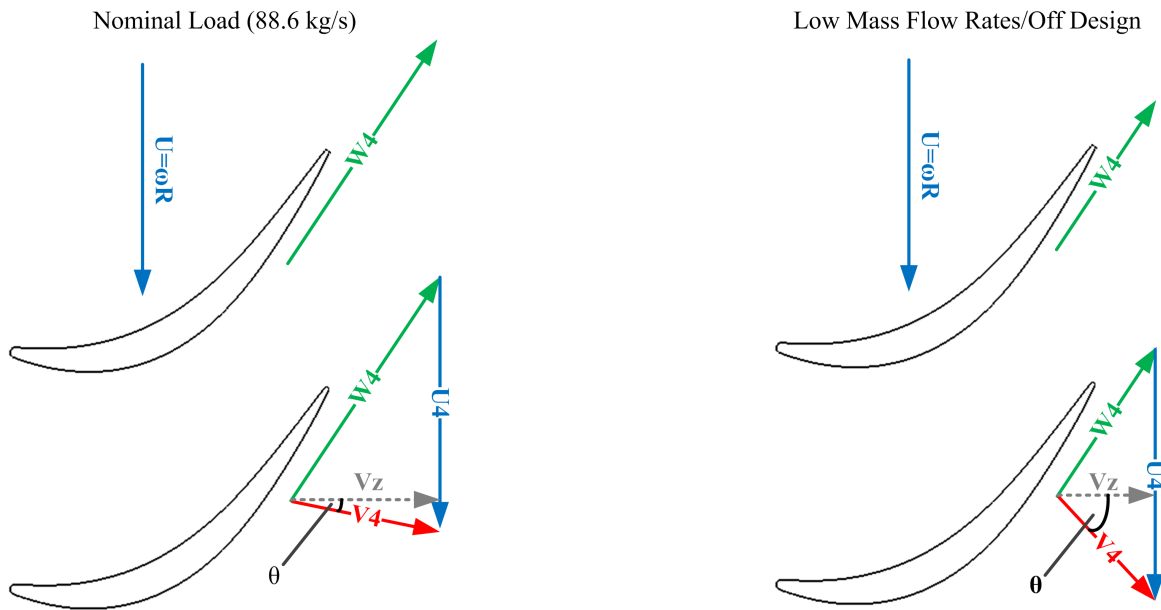
Figure 8.22: Rotor Outlet Swirl Angle at Off-Design Conditions from Gray et al. [23]
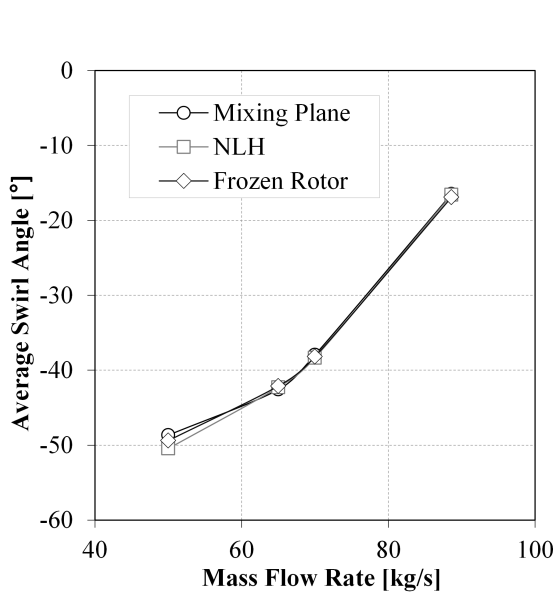
Figure 8.23: Average Swirl Angle (α) at Exhaust Hood Inlet Plane [°]
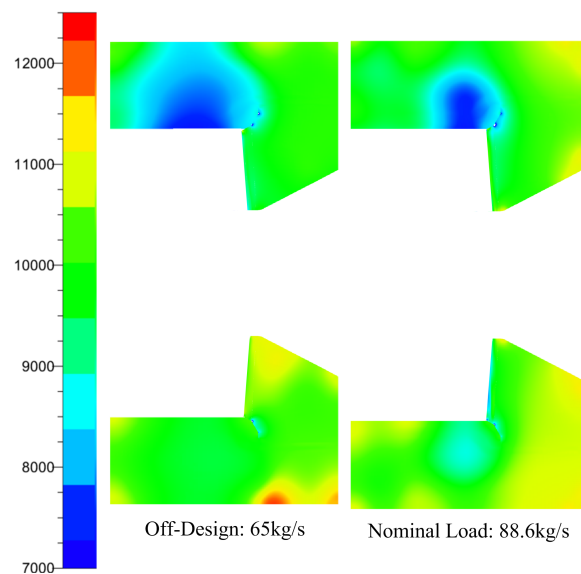
Figure 8.24: P Contours at the Half-Joint Plane at Nominal and Low Load using Frozen Rotor Approach [Pa]
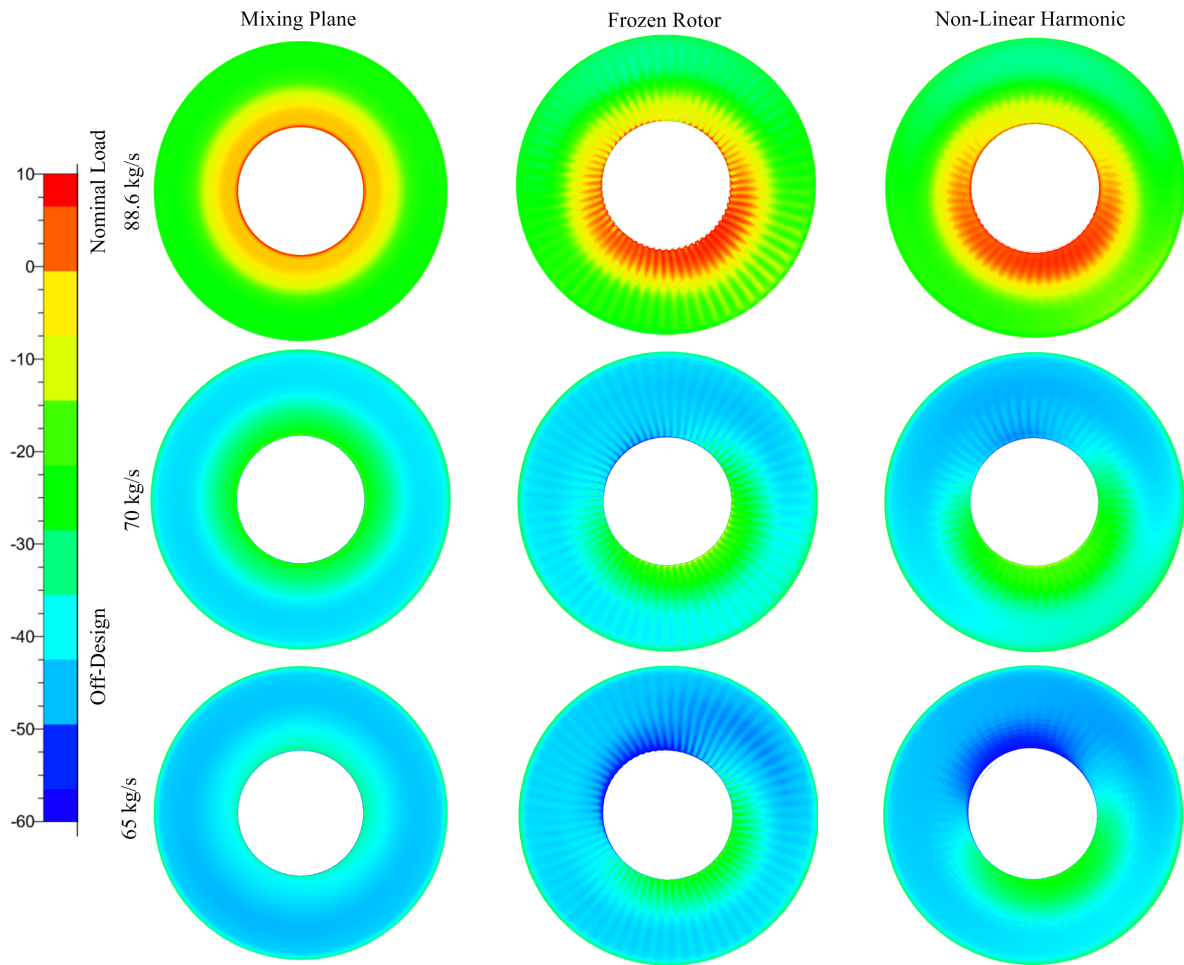
Figure 8.25: Swirl Angle Contours at the Exhaust Hood Inlet Plane at Three Mass Flow Rates [°]

results in only radial variations around the annulus.

In Section 7.2.1, the inlet swirl angle is shown to have a detrimental effect on the exhaust hood flow structure, increasing the asymmetry at the exhaust hood half-joint plane. Figure 8.24 shows the static pressure contours computed using the frozen rotor approach at the exhaust hood half-joint plane for nominal load (88.6kg/s) and at off-design (65 kg/s). The difference in flow structure between the left hand side and the right hand side of the exhaust hood is more noticeable at off-design conditions. To quantify this increase in asymmetry, the variation between the left and right hand sides of the exhaust hood is computed as an RMS, as described in Section 6.1.2 and plotted in Figure 8.26. As the mass flow rate decreases, the asymmetry increases. This trend is noticeable in both the mixing plane approach and the higher order frozen rotor and NLH methods due to the increased average inlet swirl at off-design, as shown in Figure 8.23. Higher order methods, which capture the hood inlet circumferential asymmetry, predict a higher level of asymmetry at the exhaust hood half-joint plane than the mixing plane approach to mass flow rates around 65 kg/s. This is because the circumferential asymmetry of the swirl angle distributions in Figure 8.25 naturally contribute to the 3D nature of the exhaust hood flow. The swirl non-uniformity is particularly noticeable
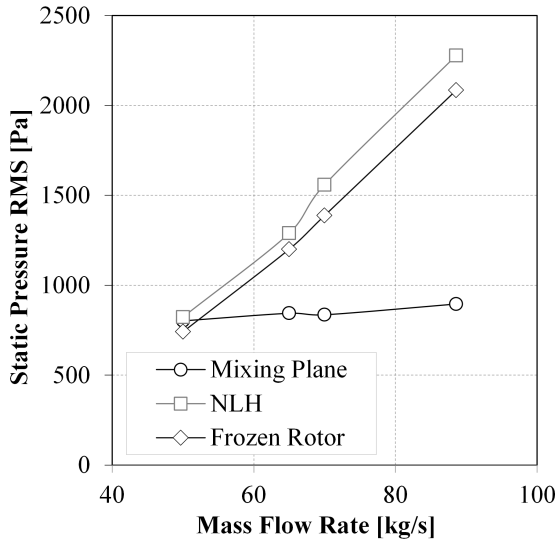
Figure 8.26: RMS_P at the Exhaust Hood Half-Joint Plane [Pa]
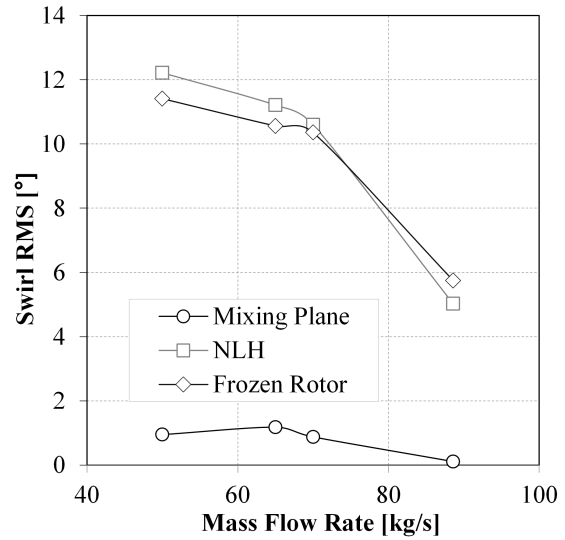
Figure 8.27: RMS_{Swirl} at the Rotor Hub on Exhaust Hood Inlet Plane [°]

at the blade hub at the inlet annulus, shown in Figure 8.27, where the RMS_{swirl} is computed by applying Equation 7.3 from Section 7.2.1.

8.4   Concluding Remarks

In Chapter 7, the non-linear harmonic approach was shown to capture circumferential variations around the hood inlet annulus when modelling only one blade passage, compared to the current industry standard single passage approach using a mixing plane. The most widely adopted method of capturing the exhaust hood circumferential non-uniformity is the full annulus frozen rotor approach.

This chapter has shown that the NLH approach and frozen rotor methods both predict a similar level of non-uniformity at the turbine outlet plane. This is a very positive result as the NLH results were achievable using approximately half of the memory requirement for the frozen rotor calculations. In addition, the static pressure recovery coefficient predicted by the NLH is within 1% of the total loss predicted with the frozen rotor method. This comprehensive study has shown the NLH approach to be a viable, computationally efficient alternative to the current standard frozen rotor method.

A method of reducing the computational demand of frozen rotor calculations has also been suggested. As the stator stage is choked, the passage to passage variations around the stator outlet annulus are small. Hence it is possible to use a mixing plane interface between stator and rotor and approximate the circumferential variations as being negligible. This means that cell count can be reduced by around 35% by modelling only one stator passage, whilst still modelling the full rotor annulus. The approach was shown to produce near identical C_p and circumferential asymmetry predictions compared to the full stator annulus frozen rotor approach, whilst reducing the computational demand by around 46%.
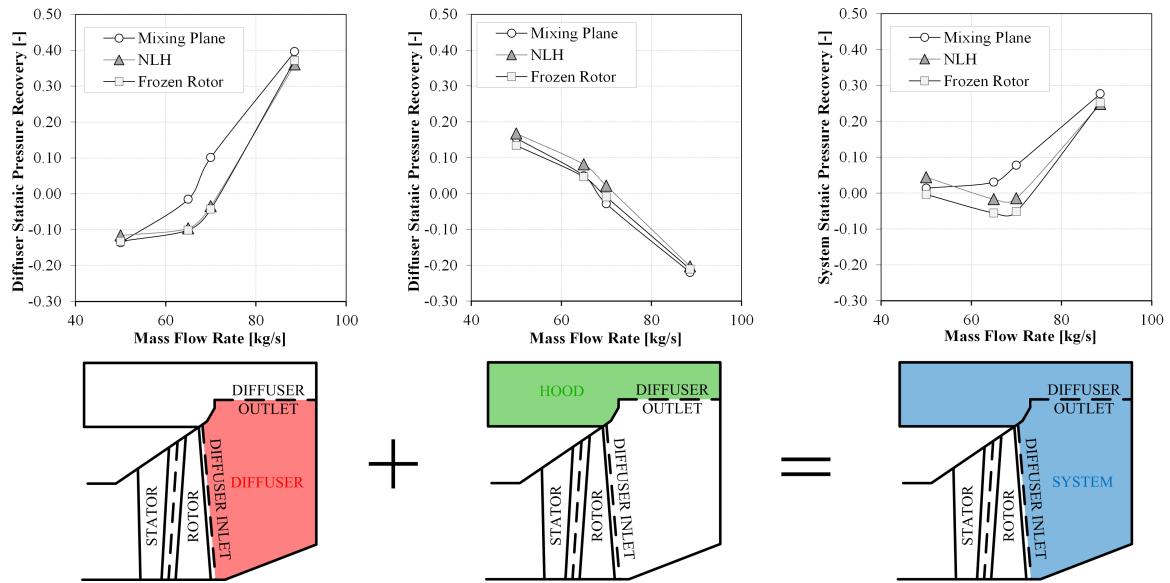
Figure 8.28: Diagram of C_p within the Exhaust Hood System [-]

Comparing results to that in the previous chapter, mixing plane, non-linear harmonic and frozen rotor approaches have all shown to produce very similar predictions of loss at nominal design load conditions. At off-design mass flow rate conditions, the interface modelling strategy has been shown to have a significant impact on the predicted performance and flow structure within the exhaust hood. Figure 8.28 summarises the loss within the diffuser, hood and full exhaust hood system discussed earlier in the chapter. Neglecting to model the circumferential variations around the hood inlet annulus with the mixing plane approach, results in an under-prediction of the asymmetry within the hood itself. Also the loss within the diffuser is under-predicted, leading to an over-prediction of pressure recovery. For improved modelling at off-design conditions the interface treatment between rotor and hood has been shown to have a significant influence on the flow prediction; and as such it is recommended that circumferential variations at the inlet annulus are captured.

Either the NLH approach or the single stator passage frozen rotor method is recommended for modelling inlet circumferential flow variations as results are achievable in around half the computational demand of the full annulus frozen rotor method. As the frozen rotor (single passage) method is dependent upon the stage being choked, for cases when the stator stage is unchoked the non-linear harmonic method is preferable.

9

Recommendations, Conclusions and Future Work

This thesis explores the following three aspects of the computational modelling of low pressure steam turbine exhaust hood flows:

1. The development of a generic, open-source test geometry of the LSBs of an LP turbine and an accompanying exhaust diffuser and outer casing.

2. The influence of the bulk inlet and outlet boundary conditions (tip leakage and condenser cooling water pressure gradient) on the flow structure and pressure recovery within the exhaust hood system.

3. The effect of the interface treatment between rotor outlet and exhaust hood inlet on the flow structure and loss predicted by the system for a range of geometries and operational conditions.

This chapter summarises and contextualises the findings from this work, offering recommendations for computational modelling approaches for a range of cases and considers which effects should be considered of primary importance to include in a steam turbine exhaust hood CFD simulation. Overall conclusions are drawn and recommendations for future work are suggested.

9.1   Recommendations

The relative importance of CFD modelling strategy, boundary conditions and interface treatment on simulating steam turbine LP exhaust hood flows can be broadly considered from two perspectives; those which have the greatest influence on the predicted loss coefficient and those which have a greater influence on flow structure. Of course the two are not mutually independent, however, computing the loss of the full exhaust hood system by considering the averaged total and static pressures from rotor outlet to hood outlet, in some cases the effects of flow asymmetry changes at the diffuser outlet and half joint plane can be masked.

Table 9.1 summarises the influence the parameters studied in this thesis have on the pressure recovery predicted in the exhaust hood.

Effect Considered	C_p			ΔC_p Effect	ΔC_p Method
No Tip Leakage	-0.35			-	-
Tip Leakage	0.236			+0.271	-
Condenser Pressure Gradient	0.186			+0.05	-
Condenser Pressure Gradient [Reversed]	0.167			-0.02	-
-	Mixing Plane	NLH	Frozen Rotor	-	-
Bi-Directional Coupling	0.2725	0.2749	-	+0.01	+0.03
Modelling Circumferential Inlet Variations	-	0.2749	0.2411	-0.03	+0.01
Compact Diffuser Axial Length [50%]	-0.3639	-0.4584	-	-0.73	+0.10
Off-Design Running [65kg/s]	0.050	0.081	0.047	-0.17	0.03

Table 9.1: Summary of C_p for Computational Modelling Methods Considered in this Thesis

Table 9.2 details the flow asymmetry predicted at the exhaust hood half-joint plane for a range of computational approaches.

Considering Tables 9.1 and 9.2, tip leakage modelling is shown to be a first-order effect as its influence on loss coefficient is the most significant of any boundary condition considered, and the changes of asymmetry present within the exhaust hood highlight the important effect of tip leakage on flow structure.

The inclusion of the condenser cooling water gradient resulted in the largest influence on exhaust hood flow structure of any modelling aspect considered and where possible this effect should be incorporated into any exhaust hood model. However, a C_p change of between only 0.05 and 0.02 was predicted in the exhaust hood system. This may again be due to the fact that C_p values are calculated using averaged values at the hood inlet plane and the hood outlet plane, the latter of which is fixed in the calculation set up. Subsequently, only the changes in inlet flow structure as a result of the addition of a non-uniform outlet pressure are reflected in the calculation of C_p, which may mask boundary conditions true influence on loss.

The major contribution in this thesis is the exploration of the effect of LSB/exhaust coupling method on the flow structure and loss coefficient predicted by a CFD model of the system. Recommendations for modelling this interface, based on the comprehensive study in this thesis, are included in the forthcoming two sections.

9.1.1   Sequential Coupling

In a sequentially coupled calculation, imposing radial variations of turbine outlet flow at the exhaust hood inlet couples the calculation in *only* the stream-wise direction, meaning the effect of the exhaust hood is not seen by the stage. This has two negative drawbacks. Firstly, from the perspective of the modelling the flow physics, the strong interaction which exists in reality between the stage and hood is only partially captured. Secondly, from a

Effect Considered	RMS_P			ΔRMS_P Effect	ΔRMS_P Method
No Tip Leakage	319			-	-
Tip Leakage	441			+122	-
Condenser Pressure Gradient	377			-64	-
Condenser Pressure Gradient [Reversed]	696			+319	-
-	Mixing Plane	NLH	Frozen Rotor	-	-
Bi-Directional Coupling	243	343	-	-98	-100
Modelling Circumferential Inlet Variations	-	343	309	+100	+34
Compact Diffuser Axial Length [50%]	506	641	-	+398	-135
Off-Design Running [65kg/s]	0.025	499	633	560	+73 to +134

Table 9.2: Summary of RMS_P at the Half-Joint Plane for Computational Modelling Methods Considered in this Thesis

practical implementation perspective, the communication between stage and exhaust hood improves the stability of the flow calculation. Artificially imposing the turbine outlet flow at the exhaust hood inlet can destabilise the calculation and can make convergence difficult to achieve. To address this, a manual modification was made to the exhaust hood geometry, to extend the hood inlet one rotor axial chord length upstream of its baseline location. However, determining the extension required to procure convergence is a time consuming, iterative process. Although this modification results in a more stable calculation, the so called "far-field" approach results in the rotor outlet flow profile boundary condition being applied far upstream from where it would occur in reality, requiring further post-processing to verify the flow profile has not been distorted.

With this in mind, and the fact that modern computing power means that fully coupled approaches are now readily achievable, the preference should be to run a bi-directionally coupled calculation.

9.1.2   Bi-Directional Coupling

Bi-directionally coupled methods can be broadly categorised into those that do, and do not, model the circumferential asymmetry at the exhaust hood inlet. As discussed in previous chapters, this circumferential asymmetry develops as a result of the non-axisymmetric exhaust hood geometry and the swirl from the rotation of the turbine blades.

At present, the most widely adopted method of capturing the exhaust hood inlet asymmetry is with the frozen rotor approach, which requires the modelling of all rotor blade passages, resulting in a very large cell count and subsequently leads to high computational demand and long convergence times. This has largely made this approach impractical for routine design

Method Name	No. Stator Passages Modelled	Stator/Rotor Interface	No. Rotor Passages Modelled	Rotor/Hood Interface
Mixing Plane	1	Mixing Plane	1	Mixing Plane
Non-Linear Harmonic (NLH)	1	NLH	1	NLH
Frozen Rotor [Full Annulus]	60	Frozen Rotor	65	Frozen Rotor
Frozen Rotor [Single Passage]	1	Mixing Plane	65	Frozen Rotor

Table 9.3: Summary of Computational Set-ups Used in this Thesis

exercises. This leaves workers with two options; neglect circumferential variations around the inlet annulus in favour of a computationally efficient single passage calculation with a mixing plane rotor/hood interface, or commit to a highly computationally intensive full annulus calculation which retains the complexity of the inlet boundary condition.

This thesis also explores the effect the bi-directional coupling methodology has on the loss coefficient and flow structure within the steam turbine exhaust hood; the first time such a study has been carried out. The summary of the computational set-ups used to carry of this study is included in Table 9.3.

The interesting, and unexpected, outcome of this study was to reveal that at design conditions, for a typical exhaust hood geometry, the method of interface treatment has only a small effect on predicted pressure recovery coefficient, shown in Table 9.1. Even more surprising was that including the circumferential asymmetry at inlet to the exhaust hood only has a small effect on loss coefficient. Comparing the mixing plane method (which retains only radial flow variations) with both the NLH and frozen rotor approaches, the difference in loss in less than 3% of the total system loss. Although methods which model circumferential variations consistently predict a higher loss than the mixing plane approach, an effect which stems from loss as a function of V^2.

Subsequently, if a reasonable estimate of *only* loss is required, representative results can be achieved neglecting the inlet circumferential non-uniformity and using the less computationally demanding mixing plane interface between rotor and exhaust hood, in the following cases:

- Studies conducted at nominal load

- Geometries where the diffuser axial length is greater than or equal to the blade height

However, the inclusion of the circumferential non-uniform coupling between LSB and exhaust hood is shown to have a significant influence on the flow structure in the exhaust hood, particularly the asymmetry between the left and right hand side of the exhaust hood at the half-joint plane, as shown in Table 9.2. The circumferential swirl angle variations at inlet influence the flow structure in the exhaust hood, the effects of which are particularly important in the following cases:

- Studies conducted at off-design conditions

- Cases which include the internal furniture

- Geometries of very compact axial length, less than the blade height

Increasingly, the exhaust hood flow structure is studied at off-design as renewable energy is contributing more to power generation, a more variable operation of traditional coal and nuclear plants will be required to cope with the flexible demand. The inlet swirl angle, which determines the half-joint asymmetry, is a function of mass flow rate. As the half-joint asymmetry becomes increasingly pronounced at off-design conditions due to the increased swirl, using a higher order bi-directionally coupled model captures the true complexity of the inlet swirl, leading to improved flow structure predictions.

Similarly, as the non-uniformity in the exhaust hood flow is particularly important when considering the design and placement of the exhaust hood internal 'furniture', capturing the circumferential variations of inlet swirl improves the prediction of diffuser asymmetry and subsequently reinforcement design. The reinforcements within the exhaust hood cause blockages which generate additional vortices and loss. As significant performance gains can be achieved by optimisation of the internal furniture, inaccurate prediction of the flow distribution within the exhaust hood may produce misleading results.

The large scale of the turbine low pressure cylinders (30-40m [57]) results in industry designing increasingly compact down-flow type diffusers which reduces the size, and subsequently cost, of the plant. Although the literature has shown that the more compact the diffuser, the poorer the pressure recovery [27], diffuser axial lengths are typically less than twice the LSB height [64]. In diffusers of generous axial length, the short length scale of the radial variations (such as the tip leakage) are dominant. However, in compact axial length diffusers, the circumferential variations (which are of a much larger length scale) become more prominent. Although capturing the inlet circumferential non-uniformity is shown in Table 9.1 not to have a large influence on the loss predicted, Table 9.2 shows that halving the diffuser axial length approximately doubles the level of asymmetry in the hood. As the inlet circumferential variations influence the asymmetry in the hood, it is important these are captured by a higher order interface treatment.

As the frozen rotor (single passage) method and the NLH approach enable the inlet circumferential non-uniformity to be captured in around half the computational demand of the annulus frozen rotor approach (see Tables 8.3 and 8.5), these methods are both recommended for numerical modelling of the above three cases. However, when using the frozen rotor (single passage) approach, workers should first determine whether the stator is choked. The validity of the method is dependent on this condition to minimise passage to passage variations at the rotor inlet. In cases where the stator is unchoked, the NLH method should be selected instead.

9.2   Conclusions

This thesis explores the effect of CFD modelling strategy and boundary conditions on the loss coefficient and flow structure of an open-source, low pressure steam turbine and exhaust

hood test case and offers recommendations as to the first and second-order modelling effects on the flow.

The Durham Stage and Exhaust Hood Test Case (DSEHTC) is the first open-source geometry available to researchers and was developed to facilitate research in this highly commercially sensitive field. Over 80% of the conference and journal papers published in the field in the last 5 years have an industrial partner on the list of co-authors. Despite the heightened research interest in the steam turbine exhaust hood sector in recent years, it is difficult to produce meaningful results without an industrial backer, as the high commercial sensitivity of production exhaust hoods and turbine designs, means that at present there are no designs freely available in the literature. The DSEHTC is freely available in .IGS format in addition to a set of guidelines for its computational modelling both of which are included in a technical report at [5].

The last stage blade (LSB) design was produced in conjunction with Alstom Power where an old blade was modified sufficiently to remove IP restrictions and ensure the outlet flow profiles were representative of modern blading designs for use as an inlet boundary condition in an exhaust hood simulation. The freely available geometry for the LSB is particularly important as the majority of exhaust hood computations are carried out using a bi-directionally coupled approach, where the turbine and exhaust hood flow fields are simultaneously calculated and interaction between the two systems captured. For this, a full LSB geometry is needed, which, until now, there were no published blade profiles.

The exhaust hood was generated from an amalgamation of designs published in the literature. Preliminary studies in this thesis using a sequentially coupled approach showed the Durham Exhaust Diffuser and Hood Test Case (DEDHTC) produced vortices of comparable location and magnitude to those found in other published research. The design was analysed using different commercial software codes, a more refined calculation method and a finer mesh which showed the predicted C_p changed by only 0.04 and the vortex size and positioning were similar. Additionally, when tested across a range of operational conditions the exhaust hood has reflected trends in swirl angle and performance documented in the literature. Specifically, the vortex growth into the diffuser at off design conditions explored by Shao et al. is also observed in this work [48]. The versatility of the system design across a range of computational platforms, operational points, boundary conditions, turbulence models and grids highlights the design's potential as a significant contribution to facilitating additional research in this rapidly developing field.

The effect of the inlet rotor tip leakage jet has been widely documented and comprehensively explored in the literature. When added to simulations of DSEHTC, an improvement in performance of the diffuser due to its energising the boundary layer in the flow guide region resulted in an increase in C_p of 0.271. This was a similar magnitude improvement as observed in the literature, giving confidence in the trends predicted by the DSEHTC [32].

A literature review revealed that, to the author's knowledge, no study of the effect of hood outlet boundary condition on the exhaust hood flow structure has been conducted. The outlet static pressure is typically set to a uniform value to give the correct operational point of the

turbine and exhaust hood system studied. In reality, the hood outlet/condenser inlet flow is highly non-uniform, due to both the upstream variations induced by the exhaust hood vortices and complex flow structure and the downstream non-uniformity due to the condenser cooling water flow. The commercial sensitivity surrounding condenser design and the difficulty of instrumentation access means there is no openly accessible, representative field data on condenser inlet flows. In this thesis a generic, open source, outlet boundary condition has been developed from field data which represents the percentage pressure variation across the condenser due to the flow of cooling water. The boundary condition is accessible to any worker and is expressed as a percentage variation from the average flow. Addition of this pressure gradient to a calculation DSEHTC showed the cooling water flow direction significantly influenced the asymmetry in the exhaust hood flow (the largest of any aspect studied) but had only a small influence on overall system loss.

Although it has been widely recognised for some decades that it is essential to accurately represent the strong interaction between the LSBs and the hood inlet, no comprehensive study analysing the effect of coupling the two systems has previously been carried out. As the exhaust hood flow structure is highly three-dimensional, the most sophisticated models enable the circumferential non-uniformities which develop in the exhaust hood to be transferred to the rotor. Until now, this has typically been done by modelling the full rotor annulus, causing the calculation size to grow rapidly which makes the method impractical for routine design calculations. This thesis proposes the first alternative to full annulus methods, incorporated into commercial CFD software, by applying the non-linear harmonic (NLH) approach to exhaust hood flows. Results have demonstrated that through this novel application of the NLH method, circumferential hood asymmetry can be successfully transferred to the turbine; producing a similar flow field to that produced with the frozen rotor method but at only half of the computational cost.

This thesis also proposes a modification to the full annulus frozen rotor approach, modelling only a single stator passage and coupling to the rotor using a mixing plane. Provided the passage to passage variations around the stator outlet annulus are small, this is a viable option to reduce the cell count and subsequently the computational demand of the calculation. Analysis showed that for choked stage flow (where blade to blade variations are small), the single stator frozen rotor method produces a near identical flow structure to full annulus frozen rotor calculations, but at a memory requirement similar to that of the NLH approach.

Despite wide acceptance of the importance of reproducing the circumferential hood variations in computational models, no previous study has comprehensively evaluated the magnitude of their influence. Interestingly, results from this thesis have shown that the additional computational effort of coupling the circumferential variations to the turbine, does not influence significantly the hood loss coefficient predicted. However, the flow structure is changed markedly. Additional studies in this thesis have shown that the accurate modelling of circumferential non-uniformities should be considered of first-order importance when studying off-design conditions, diffusers of a compact axial length and when optimising internal reinforcements.

9.3   Future Work

Three general topics for further work have arisen from the investigations presented in this thesis:

1. Experimental Validation

2. Modelling Internal Reinforcements

3. Full Unsteady Simulations

9.3.1   Experimental Validation

As with any CFD study, it is important to verify the results experimentally. It is intended that this thesis explores *trends* in exhaust hood behaviour across a range of computational set-ups, operational conditions and design geometries. The prediction of the raw values of loss coefficient included in this thesis cannot be confirmed without experimental validation.

Where possible in this work, results have been verified against other published computational results, preferably those for which experimental data is available. However, experimental validation results are rare for exhaust hood studies due to the difficulty of instrumentation access and high cost and complexity of scaled test rigs, particularly those which model the rotation of the turbine blades. As the Durham Stage Test Case (DSTC) was designed purely aerodynamically, no mechanical evaluation has been conducted on the blade. It is therefore inadvisable for any future researcher to conduct scaled experimental working using the test case without first modifying the design to ensure its mechanical integrity. The literature states that it is of primary importance to capture the radial variations of total pressure and swirl angle at inlet to the exhaust hood test rig. This has previously been achieved without the need for rotational apparatus, using swirl generators and layered gauze to achieve the desired profiles. This method is recommended for carrying out future experimental studies on the DSEHTC.

9.3.2   Modelling Internal Reinforcement

In Chapter 8, the effect of modelling the inlet circumferential non-uniformities on the exhaust hood flow structure was discussed. The inlet circumferential variations influence the downstream flow, resulting in a more asymmetric distribution. It is hypothesised that due to the different level of flow asymmetry within the casing this is likely to influence the placement and design of the exhaust hood internal furniture. It is thought the optimisation of the reinforcements could not be carried out unless the inlet circumferential flow variations are full modelled.

This hypothesis is not tested in this thesis and an interesting aspect of additional research would be to model basic exhaust hood internal furniture, such as struts, and splitters, and explore how the magnitude of the predicted static pressure recovery changes with and without

inlet circumferential variations simulated. It would also be of interest to explore how results of reinforcement optimisation studies change dependent on the rotor/hood interface treatment.

At present studies which consider internal reinforcements are relatively rare but are becoming more common. The cell counts required to accurately resolve the boundary layer on each structural element become prohibitively large even with minimal reinforcements, particularly if an advanced rotor/hood interface treatment is to be used. As there are comparatively few studies available, there are few representative geometries published which could be modified and incorporated into the DSEHTC.

9.3.3   Full Unsteady Simulations

The non-linear harmonic approach is a quasi-unsteady methodology which was originally conceived to produce approximate unsteady results at a fraction of the computational cost. The method has been exploited in this thesis to reconstruct the full annulus circumferential variations whilst only modelling a single blade passage; however, the ability of the method to approximate unsteady flows has not been explored.

With increases in computational power, full unsteady exhaust hood and LSB simulations are becoming increasingly common (4 in the last 3 years [20, 51, 52, 39]). The primary drawback with each simulation is the high computational cost and large times to achieve a converged solution. If the non-linear harmonic approach could be shown to produce representative unsteady results at a significantly reduced computational demand, as it has already been shown to do for fan noise studies and axial compressors [46, 26], then this would be of major benefit to the field.

References

[1] F. Angel, J. Kubiak, C. Marino, S. Marcinkowski, and A. Gardzilewicz. Experimental investigation of exhaust losses of a low pressure steam turbine. In *Joint Power Generation Conference*, volume 32, pages 367–372, New York, USA, 2011.

[2] A. Beevers, F. Congiu, F. Pengue, and T. Mokulys. An analysis of the merits of CFD for the performance prediction of a low pressure steam turbine radial diffuser. In *ASME Turbo Expo, Glasgow, UK*. GT2010-22107, 2010.

[3] A. C. Benim, M. Geiger, S. Doehler, M. Schoenenberger, and H. Roemer. Modelling the flow in the exhaust hood of steam turbines under consideration of turbine-exhaust hood interaction. *VDI BERICHTE*, 1185:343–357, 1995.

[4] Z. Burton, G. L. Ingram, and S. Hogg. A generic low pressure exhaust diffuser for steam turbine research. In *ASME Turbo Expo, Copenhagen, Denmark*, Copenhagen, Denmark, 2012. GT2012-68485.

[5] Z. Burton, G. L. Ingram, and S. Hogg. Durham stage and exhaust hood test case technical report. `https://www.dur.ac.uk/ecs/research/techreports/`, 2013.

[6] Z. Burton, G. L. Ingram, and S. Hogg. The influence of condenser pressure variation and tip leakage on lp steam turbine exhaust hood flows. *IMechE Part A: Journal of Power and Energy*, 2013.

[7] Z. Burton, G. L. Ingram, and S. Hogg. The influence of inlet asymmetry on steam turbine exhaust hood flow. *Journal of Engineering for Gas Turbines and Power*, 136(4):042602, 2013.

[8] Z. Burton, G. L. Ingram, and S. Hogg. A literature review of low pressure steam turbine exhaust hood and diffuser studies. *Journal of Engineering for Gas Turbines and Power*, 135(6):1–10, 2013.

[9] Z. Burton, G. L. Ingram, and S. Hogg. A novel method of coupling the steam turbine exhaust hood and the last stage blades using the non-linear harmonic method. In *ASME Turbo Expo, San Antonio, Texas*, San Antonio, Texas, 2013. GT2013-94184.

[10] M. Cordova and B. Stoffel. Comparison of various turbulence models in respect to their suitability for CFD calculations of diffuser flows. In *ASME Turbo Expo, Barcelona, Spain*. GT2006-90524, 2006.

[11] F. Cottier and E. Lutum. CFD investigation on flow and heat transfer for an advanced shrouded rotor tip concept. In *9th European Turbomachinery Conference, Istanbul, Turkey*, 2011.

[12] F. Dejean, L. Bourdonneau, and J. Duplex. Three-dimensional coupled flow calculations in a low pressure steam turbine last stage and exhaust hood. In *2nd European Conference in Turbomachinery: Fluid Dynamics and Thermodynamics*, Antwerpt, Belgium, 1997.

[13] J. D. Denton. Some limitation of turbomachinery CFD. In *ASME Turbo Expo, Glasgow, UK*. GT2010-22540, 2010.

[14] J. D. Denton and U. K. Singh. Time marching methods for turbomachinery flow calculation. *Von Karman Institute for Fluid Dynamics Lecture Series*, 1:1–47, 1979.

[15] T. Fan, Y. Xie, D. Zhang, and B. Sun. A combined numerical model and optimization for low pressure exhaust system in steam turbine. In *ASME Power Conference, San Antonio, Texas*. POWER2007-22147, 2007.

[16] C. Finzel, M. Schatz, M. V. Casey, and D. Gloss. Experimental investigation of geometrical parameters on the pressure recovery of low pressure steam turbine exhaust hoods. In *ASME Turbo Expo, Vancouver, Canada*. GT2011-45302, 2011.

[17] T. F. Fric, R. Villarreal, R. O. Auer, M. L. James, D. Ozgur, and T. K. Staley. Vortex shedding from struts in an annular exhaust diffuser. *Journal of Turbomachinery*, 120(1):186–192, 1998.

[18] J. L. Fu and J. J. Liu. Influences of inflow condition on non-axisymmetric flows in turbine exhaust hoods. *Journal of Thermal Science*, 17(4):305–313, 2008.

[19] J. L. Fu and J. J. Liu. Investigation of influential factors on the aerodynamic performance of a steam turbine exhaust system. In *ASME Turbo Expo, Glasgow, UK*. GT2010-22316, 2010.

[20] J. L. Fu, J. J. Liu, and J. S. Zhou. Unsteady interactions between axial turbine and non-axisymmetric exhaust hood under different operational conditions. *Journal of Turbomachinery*, 134(4):041002, 2012.

[21] A. Gardzilewicz, J. Swirydczuk, J. Badur, M. Karcz, R. Werner, and C. Szyrejko. Methodology of CFD computations applied for analysing flow through steam turbine exhaust hoods. *Transactions of the Institute of Fluid-Flow Machinery*, 113:157–168, 2003.

[22] GE. Powering industries. `http://www.ge.com/stories/powering-industries/`, 2014.

[23] L. Gray, S. S. Sandhu, J. Davids, and L. R. Southall. Technical considerations in optimizing blade-exhaust hood performance for low pressure steam turbines. *ASME RI17*, 1989.

[24] L. He, T. Chen, R. G. Wells, Y. S. Li, and W. Ning. Analysis of rotor-rotor and stator-stator interferences in multi-stage turbomachines. *J Turbomach*, 124(4):564–571, 2002.

[25] W. He, L. Ning. Efficient approach for analysis of unsteady viscous flows in turbomachines. *American Institute of Aeronautics and Astronautics*, 36(11):2005–2012, 1998.

[26] M. Hembera, A. Loos, A. Kahrmann, F. Danner, H. Kau, and E. Johann. Validation of the non-linear harmonic approach for quasi-unsteady simulations in turbomachinery. In *ASME Turbo Expo, Orlando, USA*. GT2009-59933, 2006.

[27] M. Hoznedl, L. Tajc, J. Krejcik, L. Bednar, K. Sedlak, and J. Linhart. Exhaust hood for steam turbines-single-flow arrangement. *Frontiers of Energy and Power Engineering in China*, 3(3):321–329, 2009.

[28] T. P. Hynes and W. G. Joo. The simulation of turbomachinery blade rows in asymmetric flow using actuator disks. *Journal of Turbomachinery*, 119:723–732, 1997.

[29] V. F. Kasilov and A. V. Sharkov. Evaluating the effect of steam wetness on the efficiency of the exhaust hoods of the low-pressure cylinders of steam turbines. *Thermal Engineering*, 51(5):378–383, 2004.

[30] F. Kreitmeier and R. Greim. Optimization of blade-diffuser interaction for improved turbine performance. *Proceedings of the Institution of Mechanical Engineers, Part A: Journal of Power and Energy*, 217(4):443–451, 2003.

[31] D. S. Kumar and K. L. Kumar. Effect of swirl on pressure recovery in annular diffusers. *Journal of Mechanical Engineering Science*, 22(6):305–313, 1980.

[32] J. Li, Z. Li, and Z. Feng. Effects of the last stage rotor tip leakage flow on the aerodynamic performance of the exhaust hood for steam turbines. In *ASME Turbo Expo, San Antonio, Texas*, San Antonio, Texas, 2013. GT2013-94377.

[33] Z. Li, J. Li, X. Yan, Z. Feng, H. Ohyama, and M. Zhang. Investigations on the flow pattern and aerodynamic performance of last stage and exhaust hood for large power steam turbines. In *ASME Turbo Expo, Copenhagen, Denmark*. GT2012-69291, 2012.

[34] J. Liu and T. P. Hynes. The investigation of turbine and exhaust interactions in asymmetric flows: Part 1 - blade row models applied. In *ASME Turbo Expo, Amsterdam, Netherlands*. GT2002-30342, 2002.

[35] J. Liu and T. P. Hynes. The investigation of turbine and exhaust interactions in asymmetric flows: Part 2 - turbine-diffuser-collector interactions. In *ASME Turbo Expo, Amsterdam, Netherlands*. GT2002-30343, 2002.

[36] J. J. Liu, Y. Q. Cui, and H. D. Jiang. Investigation of flow in a steam turbine exhaust hood with/without turbine exit conditions simulated. *Journal of Engineering for Gas Turbines and Power*, 125(1):292–299, 2003.

[37] R. Maier and J. Wachter. Shock-induced flow oscillations in steam turbine diffusers. *Journal of Turbomachinery*, 110(2):173–180, 1988.

[38] A. T. McDonald, R. W. Fox, and R. V. Van Dewoestine. Effect of swirling inlet flow on pressure recovery in conical diffusers. *AIAA Journal*, 9(10):2014–2018, 1971.

[39] B. Megerle, I. McBean, T. S. Rice, and P. Ott. Unsteady aerodynamics of low-pressure steam turbines operating under low volume flow. In *ASME Turbo Expo, San Antonio, Texas*, San Antonio, Texas, 2013. GT2013-95409.

[40] S. Mizumi and K. Ishibashi. Design philosophy and methodology of a low pressure exhaust hood for a large power steam turbine. In *ASME Turbo Expo, San Antonio, Texas*, San Antonio, Texas, 2013. GT2013-94303.

[41] S. Mizumi, K. Ishibashi, and Y. Sawamura. Steam turbine exhaust hood with swirl flow separtion ducts. In *ASME Turbo Expo*, Copenhagen, Denmark, 2012. GT2012-68315.

[42] C. Musch, H. Stuer, and G. Hermle. Optimization strategy for a coupled design of the last stage and the successive diffuser in a low pressure steam turbine. In *ASME Turbo Expo*, Vancouver, Cananda, 2011. GT2011-46237.

[43] C. Musch, H. Stuer, and G. Hermle. Optimization strategy for a coupled design of the last stage and the successive diffuser in a low pressure steam turbine. *Journal of Turbomachinery*, 135(1):011013, 2013.

[44] J. A. Owczarek, A. S. Warnock, E. Bulanowski, V. Polignano, and V. Rusak. Improvement of the exhaust flow of a low-pressure turbine. Technical report, Electric Power Research Inst., Palo Alto, CA (USA), 1990.

[45] P. Punnonen, J. Kaikko, J. Backman, and S. Savolainen. Modelling of nuclear power plant steam turbines. In *10th European Turbomachinery Conference*, Lappeenranta, Finland, 2013.

[46] A. Purwanto, T. Deconinck, S. Vilmin, E. Lorrain, and C. Hirsch. Efficient prediction of nacelle installation effects at take-off conditions. In *9th European Turbomachinery Conference*, 2011.

[47] V. V. Ris, L. L. Simoyu, S. A. Galaev, N. N. Gudkov, V. I. Kirillov, E. M. Smirnov, A. I. Kirillov, and V. V. Ermolaev. Numerical simulation of flow in a steam turbine exhaust hood: Comparison results of calculations and data from a full-scale experiment. *Journal of Thermal Engineering*, 56(4):277–283, 2009.

[48] S. Shao, Q. Deng, H. Shi, Z. Feng, K. Cheng, and Z. Peng. Numerical investigation on flow characteristics of low pressure exhaust hood under off-design conditions for steam turbines. In *ASME Turbo Expo*, San Antonio, Texas, 2013. GT2013-95259.

[49] O. Sieker and J. R. Seume. Influence of rotating wakes on separation in turbine exhaust diffusers. *Journal of Thermal Science*, 17(1):42–49, 2008.

[50] V. Solodov and V. Gnesin. Three-dimensional simulation of non-stationary flow phenomena in last stage exhaust hood compartment. *Journal of Thermal Science*, 6(4):231–236, 1997.

[51] M. Stanciu, Y. Fendler, and J.-M. Dorey. Unsteady stator-rotor interaction coupled with exhaust hood effect for last stage steam turbines. In *9th European Turbomachinery Conference*, Istanbul, Turkey, 2011. B035.

[52] M. Stanciu, M. Marcelet, and J.-M. Dorey. Numerical investigation of condenser pressure effect on last stage operation of low pressure wet steam turbines. In *ASME Turbo Expo, San Antonio, Texas*, San Antonio, Texas, 2013. GT2013-94070.

[53] M. Stastny, P. Kolar, and A. Tucek. 3D flow in the axial-radial exahust hood of a steam turbine. *Journal of Thermal Science*, 6(4):237–240, 1997.

[54] M. Stastny, T. Ladislav, P. Kolar, and A. Tucek. Effect of inlet swirl on the flow in a steam turbine exhaust hood. *Journal of Thermal Science*, 9(4):327–333, 2000.

[55] L. Tajc, L. Bednar, J. Polansky, and E. I. Gudkov. Exhaust hoods of double-flow arrangement. In *4th European Conference on Turbomachinery*, pages 1–8.

[56] L. Tajc, L. Bednar, I. Sikova, L. A. Feldberg, and E. I. Goudkov. The experimental investigation of the influence of the flow swirl and tip clearance jet on aerodynamic characteristics of exhaust hoods. In *Engineering Mechanics*, pages 1–10, Svratka, Czech Republic, 2006. SKODA Power.

[57] T. Tanuma, Y. Sasao, S. Yamamoto, Y. Niizeki, N. Shibukawa, and H. Saeki. Numerical investigation of three-dimensional wet steam flow in an exhaust diffuser with non-uniform inlet flows from the turbine stages in a steam turbine. In *ASME Turbo Expo*, Copenhagen, Denmark, 2012. GT2012-69496.

[58] T. Tanuma, Y. Sasao, S. Yamamoto, Y. Niizeki, N. Shibukawa, and H. Saeki. Aerodynamic interaction effects from upstream and downstream on the down-flow type exhaust diffuser performance in a low pressure steam turbine. In *ASME Turbo Expo*, San Antonio, Texas, 2013. GT2013-95901.

[59] T. Tanuma, Y. Sasao, S. Yamamoto, S. Takada, Y. Niizeki, N. Shibukawa, and H. Saeki. Numerical investigation of exhaust diffuser performances in low pressure turbine casings. In *ASME Turbo Expo, Vancouver, Canada*, San Antonio, Texas, 2011. GT2011-45677.

[60] R. H. Tindell and T. M. Alston. A comparison of two methods for utilizing steam turbine exhaust hood flow field data. *Journal of Turbomachinery*, 114(2):398–401, 1992.

[61] R. H. Tindell, T. M. Alston, C. A. Sarro, G. C. Stegmann, L. Gray, and J. Davids. Computational fluid dynamics analysis of a steam power plant low-pressure turbine downward exhaust hood. *Journal of Engineering for Gas Turbines and Power*, 118:214–224, 1996.

[62] V. Uvarov, I. Shkurikhin, and V. Molyakov. Investigation of joint operation of turbine stages and of a radial-annular diffuser with a controlled boundary layer. *Thermal Engineering*, 23(5):18–20, 1976.

[63] V. Vassiliev, S. Irmisch, and S. Florjancic. CFD analysis of industrial gas turbine exhaust diffusers. In *ASME Turbo Expo*, pages 1–19, Amsterdam, The Netherlands, 2002. GT2002-30597.

[64] T. Verstraete, J. Prinsier, A. Di Sante, S. Della Gatta, and L. Cosi. Design optimization of a low pressure steam turbine radial diffuser using an evolutionary algorithm and 3D CFD. In *ASME Turbo Expo*, Copenhagen, Denmark, 2011. GT2012-69515.

[65] S. Vilmin, E. Lorrain, C. Hirsch, and M. Swoboda. Unsteady flow modeling across the rotor/stator interface using the non-linear harmonic method. In *ASME Turbo Expo, Barcelona, Spain*, Barcelona, Spain, 2006. GT2006-90210.

[66] H. Wang, X. Zhu, and Z. Du. Aerodynamic optimization for low pressure turbine exhaust hood using kriging surrogate model. *International Communications in Heat and Mass Transfer*, 37(8):998–1003, 2010.

[67] X. Xu, S. Kang, and C. Hirsch. Numerical simulation of the 3D viscous flow in the exhaust casing of a low-pressure steam turbine. In *ASME Turbo Expo*, New Orleans, Louisiana, 2001. GT2001-0487.

[68] S. Yoon, F. J. Stanislaus, T. Mokulys, G. Singh, and C. M. A three-dimensional diffuser design for the retrofit of a low pressure turbine using in-house exhaust design system. In *ASME Turbo Expo, Vancouver, Canada*, Vancouver, Canada, 2011. GT2011-45366.

[69] A. E. Zaryankin and E. N. Myslitskii. Study of exhaust hood in combination with a wheel of a radial-axial turbine. In *MEI*, Moscow, Russia, 1969.

[70] W. Zhang, B. Paik, Y. Jang, S. Lee, and J. Kim. Particle image velocimetry measurements of the three-dimensional flow in an exhaust hood model of a low-pressure steam turbine. *Journal of Engineering for Gas Turbines and Power*, 129(2):411–419, 2007.

[71] S. Zhou, J. Liu, and J. Fu. Experimental and numerical investigation of interaction between turbine stage and exhaust hood. *Proceedings of the Institution of Mechanical Engineers, Part A: Journal of Power and Energy*, 221(7):991–999, 2007.